Modelling and Analysis of Electric Arc Loads Using Harmonic Domain Techniques

by

Jose Enrique Ortega-Calderon

A thesis submitted to the
Department of Electronics and Electrical Engineering
of
The University of Glasgow
For the degree of
Doctor of Philosophy

October 2008

A Adriana, Isaac, Franco y Olivia

Abstract

It has been reported that as much as 12% of global electricity production goes into producing artificial light using arc discharge lamps and that global annual production of these lamps may be as much as 1.2 billion units. In the liquid steel production industry, one metric tone of steel demands, on average, 400 kW-hr and in the year 2007, the crude steel output reached 1,343.5 million metric tons. In both instances, engineered electric arcs are present and represent major loads in electrical power systems which require the utmost attention. They observe a highly non-linear behaviour with the capacity to export harmonic distortion and flicker into the power system. Electric arc furnace installations, in particular, are well-known to be sources of dynamic disturbances affecting neighbouring loads. Arc discharge lamps, on aggregate, may exhibit the same perturbing effect. Over the years, the non-linear nature of these loads and their ubiquitous nature have caught the interest of researchers in all corners of the world and from different backgrounds, including this author.

The research work reported in this thesis advances current knowledge in the modelling and simulation of electric arcs with particular reference to arc discharge lamps with electromagnetic ballasts and electric arc furnaces with particular reference to operational unbalances and the impact in the installation of ancillary power electronics equipment. In these two quite distinct applications, linked by the presence of engineered electric arcs, the fundamental modelling item is a non-linear differential equation which encapsulates the physic of the electric arc by applying power balance principles. The non-linear differential equation uses the arc conductance as state variable and adapts well to model a wide range of characteristics for which a set of experimental coefficients are available. A fact of perhaps equal relevance is that the non-linear differential equation is amenable to algebraic representations using operational matrices and suitable for carrying out periodic steady-state solutions of electric circuits and systems. The modelling and numerical solution takes place in the harmonic space where all harmonics and cross-couplings between harmonics are explicitly represented. Good application examples are the harmonic domain solution of arc discharge lamps with electromagnetic ballasts and the harmonic domain solution of electric arc furnaces with ancillary power electronics equipment. Building on the experience gained with the representation of the arc discharge lamps with electromagnetic ballasts, the research

turns to the representation of the electric arc furnace installation with provisions for reactive power compensation using power electronic control and harmonic filters. This is a three-phase application which comprises several nodes, giving rise a large-scale model of a non-linear system which is solved in the direct frequency domain using a blend of the Newton-Raphson method and the Gauss-Seidel method, achieving robust iterative solution to a very tight tolerance. Both algorithms are implemented in MATLAB code and the raw simulation results which are the harmonic complex conjugated vectors of nodal voltages are used to assess in a rather comprehensive manner the harmonic interactions involved in both kinds of applications.

Acknowledgements

I would like to thank my beloved wife Adriana and my sons Isaac and Franco for their love, support and understanding in this journey, and to my mother Olivia for her unreserved support and prays to God.

Thank go to my supervisor Professor Enrique Acha who invited me to come to Glasgow to carry out my PhD in the Department of Electronics and Electrical Engineering of the University of Glasgow, his help and directions have been invaluable from beginning to end, and I wish to extend my gratitude to his wife Monica who helped us to get established in Milngavie.

I would like to thank my friend and colleague Damian Vilchis and his wife Eva Palacios. They have given us help and support throughout this time. We have shared knowledge and I have learnt from him interesting ways of solving problems.

I wish to thank my friend Jose Castillo (Pepe) who has given me his support and help whenever I have requested it. I would like at this point in time to remember his brother, my dear friend Benito Castillo (Manolo), whose untimely death nineteen years ago, gave me inspiration and strength for living each day of my life as if it were to be the last one.

I would like to thank my friend, Professor Armando Llamas, the Director of the Centre for Energy at ITESM, who has always lent me his help and support. He is an example of high professional standards, hard work and good will.

I would like to thank my next-door neighbour and friends Kenneth, Elaine, Amy and Zoë; since our coming to Scotland, back in 2003, they have always shown their hospitality and given us continuous friendship, making us feel at home.

I would like to thank Peter Miller, who always found time to assist me with all kinds of experiments in the laboratory. I shall always remember his insightful points of view and

the many conversations about electrical regulations and the development of electrical engineering in the United Kingdom

This journey could not have been possible without my sponsor, CONACYT, the Mexican organization who funded this PhD research. I would like to thank every one who works for such a noble institution, for their support and professionalism. I would like to thank my direct contact in the organization, Mrs. Georgina Mendez Reyes, who has always given me sound advice.

I wish to acknowledge the supplementary financial assistance provided by ITESM through its PEX programme. In particular, I would like to thank the Principal, Dr. Alfredo Bustani, the PEX Director, Dr. Fernando Jaimes, and Professors Graciano Dieck and Sergio Martinez from the Department of Electrical and Electronics Engineering.

I feel that I have ran out of space to thank all the colleagues and researchers whose work has been used as the basis on which the research reported in this thesis has been built on; I very much hope that using this work, further research finding can be generated.

Contents

List of Figures

List of Tables

List of Symbols

$\varepsilon_1, \varepsilon_2$	Error tolerances
Θ	Kernel of the Hilbert transform
Λ	Kirchhoff's linear current operator
ρ	Specific electrical resistance
$\varphi(t)$	Instantaneous angle
$\psi(t)$	Analytical signal
ψ	Linkage flux
ω_0	Base angular frequency
Ω	Instantaneous angular frequency
$A(t)$	Instantaneous amplitude
A	Area
$B_{\beta\alpha}$	Loop matrix
d	Geometric mean distance between conductors
ds	Geometric mean radius
$\mathbf{D}$	Derivative operator vector
f	Base frequency
g	Arc conductance
g_a	Arc conductance?
Gm	Arc conductance matrix of discharge lamp
$\mathbf{G}$	Arc furnace conductance vector
$\mathbf{G_A}$	Lamp arc conductance vector
$\mathbf{G_B}$	Ballast conductance vector
h	Number of harmonics
$i(t)$	Instantaneous current
I_{Arc}	Arc current vector of discharge lamp
I_e	Effective current
I_{e1}	Fundamental effective current
I_{eH}	Harmonic effective current
rms	Root Mean Square
I_{rms}	*rms* current
I_{rms1}	Fundamental *rms* current
I_{rmsH}	Harmonic *rms* current
$\mathbf{I}$	Identity matrix
$\mathbf{I}$	Harmonic current vector
$\mathbf{I_h}$	Hilbert harmonic current vector
$\mathbf{I_A}$	Analytical current vector
$\mathbf{I_{NB}}$	Norton current in the ballast
j	Imaginary operator
J_β	Independent current vector
k_1, k_2, k_3	Lamp and arc furnace specific parameters
ki	Ratio of currents in the original lamp and a new lamp
l	Length
m	Arc radius factor
N	Number of lamps

n	Arc cooling factor
p	Instantaneous power
p_{avg}	Average power
pf_e	Effective power factor
$\mathbf{p}_{inst}$	Instantaneous power vector
P_e	Effective active power
$\mathbf{q}_{inst}$	Instantaneous quadrature power vector
r	Arc radius
$\mathbf{R}$	Arc radius vector
R	Resistance
s	Instantaneous complex power
$\mathbf{s}_{\text{inst}}$	Instantaneous complex power vector
$\text{sgn}(\omega)$	Signum function
S	Conductor length
S_e	Effective apparent power
T	Time period
u	Real signal
v	Hilbert Transform
$v(t)$	Instantaneous voltage
V_{Arc}	Vector of arc voltage of the discharge lamp
V_e	Effective voltage
V_{e1}	Fundamental effective voltage
V_{eH}	Harmonic effective voltage
V_{rms}	*rms* voltage
$V_{rms\text{H}}$	*rms* harmonic voltage
V_{rms1}	*rms* fundamental voltage
$\mathbf{V}$	Harmonic voltage vector
$\mathbf{V_A}$	Analytical voltage vector
$\mathbf{V_h}$	Hilbert harmonic voltage vector
$\mathbf{Y_B}$	Harmonic matrix of inductive effects in the ballast core
$\mathbf{G_B}$	Harmonic matrix of resistive effects (losses) in the ballast core
$\mathbf{Y_{NB}}$	Admittance matrix of the ballast's Norton equivalent

List of Acronyms

CELMA	Federation of National Manufacturers Associations for Luminaries and Electrotechnical Components for Luminaries in the European Union
IAEEL	International Association for Energy Efficient Lighting
IEE	Institute of Electrical Engineers
IEEE	Institute of Electrical and Electronic Engineers
IET	Institute of Engineering and Technology
IISI	International Iron and Steel Institute
DFT	Discrete Fourier Transform
FFT	Fast Fourier Transform
IDFT	Inverse Discrete Fourier Transform
IFFT	Inverse Fast Fourier Transform
ODE	Ordinary Differential Equations
AC	Alternating Current
PCC	Point of Common Coupling
p.u.	Per-unit
rms	Root Mean Square
TDDI	Total Demand Distortion of Current
TDDV	Total Demand Distortion of Voltage
THDI	Total Harmonic Distortion of Current
THDV	Total Harmonic Distortion of Voltage
EAF	Electric Arc Furnace
EMTP	Electro-Magnetic Transient Program
IGBT	Insulated Gate Bipolar Transistor
SPLC	Smart Predictive Line Controller
STATCOM	Static Compensator
SVC	Static Var Compensator
TCR	Thyristor Controlled Reactor
TSRC	Thyristor Series Reactor Compensator
TCSR	Thyristor Controlled Series Reactor
TSSR	Thyristor Switched Series Reactor
UHP	Ultra High Power

1 Introduction

1.1 Background

Whether at home, the office, shopping, or while walking in the street, in each situation, more often than not, we are regular users of artificial light. Artificial light represents a important kind of electric load whose global consumption has been put at ten to fifteen percent of all the electrical power generated in the world [Zissis 2000], this is more than 2000 T-W-hr of electricity which, incidentally, translates into 2900 millions metric tons of carbon dioxide emissions per year [IAEEL 2000]. It is estimated that 10-15% of the overall electricity consumption is used to produce electrical light, of which 85% corresponds to electrical light generated with arc discharge lamps [J. Vaclavik *et al.* 2004]. At the same time, society's appetite for steel manufactured products is on the increase. Steel is a ubiquitous material found in transport vehicles, domestic appliances and building installations. Its demand has grown up steadily as confirmed by the world steel production's trend of the last few years. A recent media release of the International Iron and Steel Institute [2008] announced that world crude steel output reached 1,343.5 million metric tons in the year 2007. This represents the highest level of crude steel output in history. Incidentally, one kind of steel production method, the electric arc furnace, has increased its presence in the world; it is referred that Europe alone, produces 45 percent of its steel in electric arc furnaces. In this type of installations the amount of energy required to produce one metric ton of steel is between 300 and 500 kW-hr, each installation of electric arc furnace operates typically at power levels of 30 to 100 MW. Hence, electrical arc furnace installations are very large loads that consume huge quantities of electricity and, more often than not, impact very considerably on the electrical network which they are attached to, affecting negatively the operation of neighbouring loads.

The forgoing discussion remarks on the importance of electric arcs, as loads, that requires a great deal of engineering attention and study; this applies to both arc discharge lamps and electric arc furnace installations.

1.2 Electric Arc Models

Arc discharge lamps and electric arc furnaces which at first sight may look as too dissimilar, have in fact a common key characteristic; the electrical arc as a physical phenomenon. This is the subject of plasma physics where extensive research has been carried out for both fields of application, aiming at establishing the theory which permits the development of mathematical models to characterise the arc behaviour. Comprehensive research surveys can be found for arc discharge lamps in [Lister *et al.* 2004], and for the electric arc furnace in [Jones and Fang 1980] and [Bakken *et al.* 1997].

Over the years, several electric arc discharge lamp models have been put forward employing varying degrees of complexity in the characterisation of the physical phenomena. The development of the most comprehensive models requires the solution of non-linear partial differential equations based on the mass, momentum and energy conservation principle, making use of the state equation of ideal gases and Ohm's law. The formulation of such differential equations requires boundary conditions techniques in conjunction with the conservation of local charge neutrality, chemical and equilibrium equations [Troudi 2002]. Less elaborated models have also been used, with the drawback that constants used in the formulation have no clear physical meaning. Recently a dynamic conductance model for the discharge lamp was developed starting from the principle of power balance [Blanco 2007], which yields a clearer physical meaning. However, close scrutiny reveals that such equation does not differ much from a well-established equation found in [Acha *et al* 1990], which is the one used in this work.

Concerning electric arc furnace models, these may be classified into simple and complex. The latter requires the solution of mass, momentum and energy conservation equations, which can be realised into two or three dimensions. On the other hand, simple models exist where the arc column is assumed to be a uniform cylinder [Edels and Fenlon 1965] and [Phillips 1967]. These models have been derived from the equations that satisfy the integral energy balance of the arc [Bakken *et al* 1997]. These models are useful for estimating the current-voltage characteristics of electric arcs with

good approximation. The one-dimensional power balance model used in this work to characterise the electric arc can be considered to belong to the latter kinds of models.

1.3 Harmonic Models of Electric Arcs

Interest in the development of electric arc load models which can be integrated with models of the electrical power network have been high on the agenda of many researchers for quite some time. The goal has been to carry out comprehensive studies of the impact that the arc load has on the complete electrical system. The testing of new ancillary equipment such as electronic power devices or magnetic core based equipment to enhance the operation of arc loads has also provided a strong motivation for research work in this area. Quite substantial negative effects have been attributed to these kinds of non-linear loads. In the case of arc discharge lamp installations, waveform harmonic distortions are well documented [Liew 1989] and [Václavík *et al.* 2004], with concerns expressed in electrical installations with half-neutral wires. In the case of the electric arc furnace, some of the adverse power quality effects are more widespread, encompassing harmonic distortion, imbalances, sags, swells, angle jumps, inter-harmonics, flicker [Mayordomo *et al.* 2000] and sub-synchronous resonances [Tsao and Tsai 2004].

1.3.1 Harmonic domain

The widespread use of power electronics and non-linear loads has brought the importance of harmonic studies to the fore. As stated by the IEEE Task Force on Harmonics Modelling and Simulation [2004], harmonic studies are used to quantify the distortion in voltage and current waveforms and their effect in the electrical power network. Power engineering researchers have developed simulation models in both frames of reference; time and frequency domains. The advantages and disadvantages of different techniques for harmonic studies have been well dissected by the IEEE Task Force on Harmonics Modelling and Simulation [1996]. One key characteristic of the harmonic domain as a framework is that it yields physical insight in to the interaction that takes place between the various elements of the electrical power network, quantifying directly their dominant harmonic components and their adverse impact on neighbouring equipment for steady or quasi-steady state conditions. Moreover,

references [Acha 1986] and [Xu *et al.*1991] remark on the fact that the electrical power network always possesses some degree of imbalance and that due to the marked effect that imbalance has on harmonic behaviour, realistic power system harmonic studies call for all harmonic representation of power plant components to be carried out in the phase frame of reference.

1.3.2 Harmonic domain models of arc discharge lamps

In electrical power engineering applications the time domain framework has dominated the development of simulation models for the electric arc discharge lamps, mostly aimed at electronic ballast design. A small number of frequency models exist in the open literature; one of the most prominent [Carrillo *et al.* 1996], [Carrillo and Cidras 1998] is based on a piece-wise linear approximation of the arc current-voltage characteristic obtained at a given frequency (e.g. 50 Hz). It lacks model flexibility due to its inability to incorporate crucial physical characteristics of the arc plasma, among other things, its frequency dependency. An alternative approach, which also lack frequency dependency, has been adopted by [Chang 2003], where the arc is modelled as a harmonic voltage source with the help of a FFT procedure, converted into a Norton equivalent. A fundamentally different modelling solution based on the power balance equation of the arc was put forward by [Acha *et al.* 1990]. This model accomplishes good results for the electric arc but it has, so far, not been integrated with any element of the external electrical network. This is in fact a full harmonic domain model well able to reproduce the non-linear frequency dynamic effects found in electric arc loads. It should be remarked that this might be the only worthwhile available model of the electric arc in frequency domain, with the potential for direct merging with the electrical parameters of the external electrical network since its state variable is the arc conductance as opposed to the arc radius. The harmonic domain framework enables to assess the periodic steady state of arc discharge lamp circuits in quite a comprehensive manner such as harmonic current flows and network resonances [Madrigal 2001]. Developing further the harmonic domain model of the electric arc is very timely because of current interest in the development of low-losses magnetic ballast designs to comply with new European directives 2000/55/EC [CELMA 2000] which aims at reducing the energy consumption of ballast for fluorescent lighting. At the prototype stage, low-losses iron core ballasts have been used to replace electronic ballasts [Kim

and Nam 1998]; experimental work that has been complemented with the use of a power electronic central dimming system [Chun *et al.* 2007]. Hence, harmonic domain models of electric arc discharge lamps which can be integrated with other non-linear devices such as magnetic core ballasts and power electronics circuits are urgently needed for the development of improved energy efficiency solutions.

1.3.3 Harmonic domain models of electric arc furnaces

Several electric arc furnace load models have been presented in the open literature using the time domain frame of reference. As stated in the document presented by the Task Force on Harmonics Modeling and Simulation [2004], so far the electric arc has mainly been characterised by black box models, which are mathematical approximations fitted to the shape of the current-voltage characteristic of the electric arc with no regards to physical meaning. Moreover, the electric arc furnace installation has usually been represented by only its positive sequence model instead of the more realistic three-phase representation. This applies to both, time and frequency domain solutions. Furthermore, on the rare occasions when three-phase models have in fact been used, non-linear elements such as transformer magnetising branches are not considered. The secondary circuit of the electric arc furnace and the series reactor are frequently combined into a single equivalent circuit and the electrodes are not often included. A small number of electric arc furnace models have been developed in harmonic domain; in one of such works [Ting 1997], the electric arc furnace load uses the model developed in [Acha *et al.* 1990] but the electric arc furnace installation is reduced to a single-phase equivalent circuit. Another model [Mayordomo *et al.* 1997] and [Beites *et al.* 2001] uses a hard to justified equivalence between the non-linear equation that describes a diode circuit and the current-voltage characteristic of the arc; such analogy bears little relationship to the physical phenomena actually taking place in the electric arc. The Task Force on Harmonics Modeling and Simulation [2001, 2004] states that the power balance models are a new way of arc furnace modelling. Current research interest in electric arc furnace modelling is in the integration of power electronic device models for the study of reactive power compensation and harmonic elimination. Even though well developed harmonic domain models of high-power, high-current semiconductor equipment are available no reference seem to exist in the open literature on the harmonic interaction of

electric arc loads with other power system non-linearities such as saturated transformers and power electronic MVAR compensation. This is a challenging area open to research, where comprehensive models of three-phase electric arc furnace installations should be extended to include the non-linear effects of other power plant components in the installation and their full integration into the harmonic domain framework.

In this research project the electric arc discharge lamp and the electric arc furnace system are both modelled in the harmonic domain. The aim is to develop a comprehensive harmonic analysis method with which to assess the impact of arc loads in the external electrical circuit, focusing on the harmonic interaction of devices of various kinds exhibiting different non-linear phenomena. In the case of arc discharge lamps the interaction with saturated magnetic ballast is analysed, and in the case of electric arc furnace installations interaction with the non-linear characteristic of transformer magnetic cores and the periodic switching of power electronics devices is analysed. Comprehensive simulations are carried out to assess complete systems, quantifying the amount of harmonic distortion and power quantities that exist in typical test networks under both balanced and unbalanced conditions.

1.4 Main Aims

(i) To research comprehensively on accepted definitions of electrical power quality quantities, with the aim of conducting meaningful harmonic analyses of three-phase electrical systems comprising non-linear plant components of various kinds. Classification of electrical powers in to conservative and non-conservative ones aids the understanding of the powers emanating from the Hilbert Transform, using Tellegen's theorem, and those defined in IEEE Standard 1459. The various power terms selected to be used in this research work have been derived using vector and matrix operations in the complex conjugated harmonic domain. Their application goes right through all the chapters of this work.

(ii) It is an aim of this research to integrate an isolated arc discharge lamp model which is based on a power balance equation into a fuller electric circuit using the dynamic arc conductance as a state variable. This would ensure a seamless coupling with the non-linear inductance of the magnetic ballast which is well

represented by a saturated conductance. This would be the first time that the combined models of the electric arc tube and the ballast's iron core have been solved together in harmonic domain. Indeed it would be appropriate to compare simulation results with experimental data obtained in the laboratory. This would imply the integration of two different non-linear models, one represented by the non-linear differential equation of the electric arc and the other by the polynomial characteristic of the electromagnetic ballast. It is envisaged that these models could be extended to form an aggregated model, able to represent a number of arc discharge lamps, in the harmonic domain. These aggregated models should prove useful in assessing non-linear effects in the network due to a large number of lamps of mixed capacities. Moreover, the single lamp-ballast system and the aggregated model should be integrated into the harmonic frame of reference alongside the models of transformers and power electronic devices.

(iii) It is also an aim of this research to develop the harmonic model of a conventional three-phase electric arc furnace installation where the Thevenin equivalent circuit representing the power supply is combined with the step-down transformer, series reactor, furnace transformer, secondary circuit, graphite electrodes and the electric arc. It is important that this combined model includes the non-linear characteristics of the magnetising branches of the step-down and furnace transformers. Each individual plant component would be represented by either a linear or a non-linear (linearised) admittance model, an approach conducive to the formation of a global nodal admittance representation of the whole arc furnace installation, enabling the use of iterative solutions using harmonic domain techniques. This would be the first time that the combined models of three-phase electric arcs, transformer's iron cores and the other elements of the electric arc furnace installation are represented together in the harmonic domain framework.

(iv) High-current, high-power semiconductor equipment is beginning to be more pervasive in electric arc furnace installations and this research would be a good focal point for investigating the harmonic impact of the power electronics technology on these installations. Examples of popular power electronics equipment the Static Var Compensator and the Thyristor Controlled Series Reactor. This would be the first time that their modelling representation would be

integrated not only with those of the electric arc but also with models of banks of transformers, both of which act as non-linear loads in the arc furnace installation. The three different non-linear models would be integrated and solved together in the harmonic domain for direct frequency solutions where the time dimension is not involved; the power balance non-linear differential equation of the electric arc, the polynomial characterisation of power transformer saturation, and the periodical switching function of the Thyristor Controlled Reactor.

1.5 Main Research Achievements

Research work by the author on power system harmonic analysis has led to the following key contributions in the area of harmonic modelling of electric arcs:

(i) It has been found in this research that Tellegen's theorem is a useful tool to classify various forms of electrical power into conservative and non-conservative. The Tellegen's theorem support the set of conservative powers develop using the Hilbert Transform and the analytic functions, this association is useful to develop power-based models of electrical power equipment and systems

(ii) The development of an advanced model of the arc discharge lamp circuit in the harmonic domain, with provisions for the saturated iron core of the lamp ballast and the power factor corrector capacitor alongside the electric arc model. The model exhibits two kinds of non-linearity and its solution is carried out using iterations for the fundamental and harmonic state variables, with linear convergence. The simulation results have been experimentally validated. This model is quite general, applicable to any kind of electric arc discharge lamp that possesses a continuous, dynamic current-voltage characteristic whether linear or non-linear. It is suitable for conducting further research into the area of arc discharge lamps including laminated iron core ballasts and electronic ballasts for increased energy efficiency lamp systems. Moreover, the aggregated model of the arc discharge lamp-ballast system makes practical the harmonic study of complete installations with hundreds of lamps of different kinds and ratings, assessing the impact in the in-feed transformer and neutral wire of the installation.

(iii) A comprehensive model of a conventional electric arc furnace installation representing its three-phase nature has been established. In addition to developing the harmonic domain model of the electric arc furnace using the dynamic conductance as state variable, the following plant components have been modelled and integrated within the overall harmonic domain model of the installation: the Thevenin equivalent circuit representing the power supply, the step-down transformer, series reactor, furnace transformer, secondary circuits and graphite electrodes. It should be remarked that the non-linear characteristics of the magnetising branches of the step-down and furnace transformers should be included correctly. The model exhibits two kinds of non-linearity and several linear components; its solution is carried out using iterations for the fundamental and harmonic state variables, with linear convergence. The model of the electric arc furnace installation is quite flexible, suitable for incorporating additional models of power plant components that may already exist in the industrial installation or that may exist in future as a result of expansion plans, whether linear or non-linear.

(iv) Electric arc furnace installations may require harmonic filtering and reactive power compensation. Moreover, as power electronics-based reactive power compensators continue to evolve, their use in electric arc furnace installations is becoming more widespread. Models of both passive filters and shunt and series thyristor-controlled reactors are incorporated into the overall model of the arc furnace installation and comprehensive studies have been carried out to assess the harmonic interaction of the electric arc and the power electronics-based equipment. These simulation studies have taken account of a small of distortion contributed by the magnetizing branches of both transformers in the installation and unbalanced operation. The overall algorithm was tested for robustness towards the convergence with extreme unbalanced conditions showing to be in each case to be linear or around an operating point.

1.6 Publications

The following publications were generated during the course of this research:

JOURNAL PUBLICATIONS

1. P.L. Roncero, E. Acha, J. E. Ortega-Calderon, V. Feliu, A. Garcia-Cerrada, A Versatile Control Scheme for a Dynamic Voltage Restorer for Power Quality Improvement, accepted for publication in IEEE Transactions on Power Delivery

2. J.E. Ortega-Calderon and E. Acha: 'Three-phase Modelling of Electric Arc Furnace Installations in Harmonic Domain', to be submitted to IEEE Transactions on Power Delivery.

3. J.E. Ortega-Calderon and E. Acha: 'Modelling of Electric Arc Furnace Installations with VAR Compensation Using a SVC System', to be submitted to IEEE Transactions on Power Systems.

4. J.E. Ortega-Calderon and E. Acha: 'An Assessment of the Impact of a Series TCR in the Operation of an Electric Arc Furnace Installations', to be submitted to IEEE Transactions on Power Delivery.

CONFERENCE PUBLICATIONS

J.F. Petit-Suarez, J. E. Ortega-Calderon, E. Acha, G. Robles, H. Amaris, Harmonic Domain Modelling of an Arc Discharge Lamp System, IEEE Power Tech 2007, Lausanne, Switzerland, July, 2007.

1.7 Chapter Presentation

Chapter two re-examines fundamental electrical power theory relevant to this work. The chapter starts by outlining Tellegen's theorem, a powerful analytical tool that enables a clear distinction between conservative powers and quasi-powers. A practical approach of the Hilbert Transform is used to prove the conservative property of the quasi-instantaneous quadrature power. Moreover, starting from the original real signal and its Hilbert Transform, analytic signals are made up, and these serve the purpose of establishing a set of conservative powers i.e. quasi-instantaneous active and reactive power. Both definitions are well represented in either time or frequency domains. In addition, three-phase analytic signals are used to define the quasi-instantaneous analytic symmetrical components which will, in turn, be the basis for obtaining a quasi-instantaneous frequency definition for positive sequence. Furthermore, definitions

presented in IEEE Standard 1459 [2001] are revisited for their direct application to harmonic domain simulation results.

Chapter three presents a newly integrated arc discharge lamp-ballast system model in the harmonic domain, where the non-linear characteristics of the fluorescent lamp and the electromagnetic ballast are combined into a single overall model. The arc discharge lamp model intrinsically incorporates frequency dependence. The non-linear differential equation whose formulation is based on power balance principles is solved in harmonic domain using the Newton-Raphson method. The electric arc dynamic conductance is taken to be the state variable, enabling a seamless integration with the harmonic nodal admittances of the external circuit. To such end, the magnetic ballast is modelled as a Harmonic Norton equivalent using a polynomial characterisation of the magnetic core saturation. The whole harmonic nodal admittance equation is solved by successive iteration using an efficient combination of the Newton-Raphson method and the Gauss method, using a sequential procedure. This algorithm is implemented in MATLAB code, showing linear convergence. Simulation results are compared with experimental readings obtained in the laboratory and show a fairly close agreement between them. Towards the end of the chapter, the ballast model is extended to develop an aggregated ballast model aiming at representing a large number of lamps.

Chapter four presents the harmonic domain three-phase model of a complete electric arc furnace system. The nonlinearity of the electric arc plasma is represented by a non-linear power balance equation that is solved in the harmonic domain using the Newton-Raphson method. The original non-linear differential equation which uses the arc radius as state variable is transformed into an alternative differential equation towards to use the dynamic conductance as state variable that is a more amenable formulation for the robust solution of the complete harmonic nodal admittance equation representing the whole electrical arc furnace installation, comprising: (i) power supply's Thevenin equivalent; (ii) step-down transformer; (iii) series reactor; (iv) furnace transformer; (v) secondary circuit (bus and flexible cables); (vi) electrodes; (vii) electric arc conductance. For the step-down and furnace transformers, the non-linear magnetising branches are modelled using harmonic Norton equivalents. Integration of the complete system is carried out and the iterative algorithm is coded in MATLAB, showing linear convergence. Simulation studies are carried out for the test system considering balanced

and unbalanced operation, followed by a comprehensive analysis of the power quality data associated with each node of the arc furnace installation.

Chapter five deals with the modelling of high-power, high current semiconductor equipment used for the provision of VARS in modern electric arc furnace installations. A Static VAR Compensator is taken to be connected to the secondary winding of the step-down transformer and assuming balanced operating conditions, simulation studies are carried out for the full range of Thyristor Controlled Reactor (TCR) firing angle values. Harmonic voltages, currents, powers and other key power quality parameters are calculated at each node of the electric arc furnace installation. In a follow up study, the SVC performance is studied for a fixed value of TCR firing angle, operating under a wide range of unbalanced loading conditions. The effectiveness of including passive filters in the electric arc furnace installation is assessed. The chapter closes with an assessment of the impact of a Thyristor Controlled Series Reactor (TCSR) in the electric arc furnace installation; a study carried out assuming balanced loading conditions and a range of TCR firing angles.

Chapter six draws the overall conclusions of the PhD research project and suggests possible avenues of research in this challenging area of electrical power systems.

2 Power Theories

2.1 Basic Theory

Modern electrical systems contain a high level of interconnection and large quantities of energy are exchanged between generator buses and loads; a problem that can be suitably studied by resorting to the solution of non-linear simultaneous algebraic and differential equations. Since the mid fifties the use of digital computers for the solution of the classical power flow problem has been on the increase and different methods of solution for cases of sinusoidal steady state operation have been developed [Stott 1974]; [Heydt 1986]; [Acha *et al.* 2004]. In essence, all power flow methods have their basis on electrical circuit theory, in particular, Kirchhoff's voltage and current laws in conjunction with the principle of conservation of energy. Evidently the fulfilments of the same laws are necessary for power flow analysis under non-sinusoidal conditions. However, so far, no general definitions for non-active powers exist for all applications. This is synthesized in the introduction of the IEEE Standard 1459; Trial-Use Standard Definitions for the Measurement of Electric Power Quantities Under Sinusoidal, Non-sinusoidal, Balanced, or Unbalanced Conditions [PSIMC 2000]:

"There is not yet available a generalized power theory that can provide a simultaneous common base for; energy billing, evaluation of electric energy quality, detection of the major sources of waveform distortion and theoretical calculations for the design of mitigation equipment such as active filters or dynamic-compensators"

Basic research on power definitions under non-sinusoidal conditions has been carried out from the beginning of the twentieth century up to the present day [Steinmetz 1900; Curtis *et al.* 1935; Lyon, 1935; Shepherd, 1972; Sharon, 1973, Kusters, 1980, Page, 1980, Miller; 1982, Akagi, 1984; Czarnecki, 1987]. Different power theories under non-sinusoidal conditions intended mainly at reactive (non-active) power compensation have been put forward. The various theories use different power and quasi-power definitions which can be classified in the first instance into conservatives and non-conservatives. Definitions for single-phase systems can be extended to multi-

phase systems. The majority of powers and quasi-powers definitions have been given some form of physical interpretation.

The first issue to be addressed in the area of power theories is to establish the difference between the terms power and quasi-power. The former is reserved for powers that have a clear physical meaning and can be represented in both time and frequency domain; e.g. instantaneous power and active power. Quasi-powers do not have a complete physical meaning; e.g. apparent power and reactive power.

The various powers and quasi-powers can be divided into conservative and non-conservative; characteristics which can be validated with the use of Tellegen's theorem [Penfield 1970]. Conservative powers can be used in mathematical relationships describing an electrical system: the algebraic sum of inputs and outputs at a given node of the system yields zero. Hence, conservative powers are used in electrical power flow algorithms which rely on the classical definitions of active power and reactive power. Non-conservative powers such as apparent power can only be used at a point in the circuit where the optimisation of energy transfer is required.

Single-phase and multiphase power definitions find application in the solution of non-active compensation. The power flow under sinusoidal conditions is a particular case of the use of extracted conservative powers and quasi-powers using the Hilbert Transform. This tool is quite general and covers the concepts of complex power, active power and reactive power in electrical systems operating under non-sinusoidal conditions [Hahn 1996]. The various powers definitions can be formulated in either the time domain or the frequency domain. Both domains are fully equivalent; each one having advantages and disadvantages in the application of power flow algorithms. Table 2-1 shows a classification of power and quasi-powers

	Conservative	**Non-conservative**
Power	Active power Instantaneous power Instantaneous Active power	
Quasi-powers	Reactive Power Instantaneous Reactive Power Instantaneous complex power	Apparent power Instantaneous apparent power

Table 2-1 Powers classification

2.2 Conservative Powers and Quasi-powers

The solution methods of sinusoidal power flows have their basis in the use of conservative powers and conservative quasi-powers definitions: concepts that can be extended with some care to power flows in non-sinusoidal regimes. The instantaneous power is an example of conservative power. It is the product of voltage and current in the time domain and the result of discrete convolutions in frequency domain. In each instant of time, the instantaneous power is conservative since Kirchhoff's laws apply. Another important characteristic, from the frequency domain point of view, is that the resultant power at each frequency component is also conservative. For instance, active power (zero frequency term of the Fourier series) is a good example.

Arguably Kirchhoff's laws form the basis of electric circuit theory. If a network is defined with no ports, *b* branches, *n* nodes, and *s* separate parts, Kirchhoff's current law places *n-s* constraints on the currents, so that only *b-n+s* currents may be specified independently, after which all remaining branch current may be found by means of the following linear relations [Penfield 1970]

$$i_\alpha = \sum_\beta B_{\beta\alpha} J_\beta \tag{2.1}$$

here J_β is the *b-n+s* independent currents, and $B_{\beta\alpha}$ is the rectangular matrix, *(b-n+s)b* known as the Loop Matrix or tie-set schedule of the network.
Kirchhoff's voltage law may be expressed in terms of $B_{\beta\alpha}$. For each arbitrary current there is one closed path within the remainder of the network not including other independent currents. Thus, there are *b-n +s* such loops, for each of which Kirchhoff's law voltage equations may be written. The result is

$$\sum_\alpha B_{\beta\alpha} j_\alpha = 0 \tag{2.2}$$

The form of the Kirchhoff's equations given above is convenient for the proof of Tellegen theorem; the set of equations corresponding to a network with no ports. If ports do exist then it is necessary to include a change of sign.

From equations (2.1) and (2.2) we can derive a simple power theorem as follows:
The following expression is the instantaneous power definition at a node of a network where the power flows in the α branches add up to zero.

$$\sum_{\alpha} i_{\alpha} v_{\alpha} = 0 \tag{2.3}$$

If the network elements are represented in terms of ports, a similar expression can be used, where at each point in time, the power that enters a network at its ports is distributed in each element of the network.

$$\sum_{p} i_{p} v_{p} = \sum_{\alpha} i_{\alpha} v_{\alpha} \tag{2.4}$$

A more general statement of instantaneous powers can be made with reference to an electrical network having two states. This situation may arise when the voltages and current of each state belong to different excitations, or different elements or different initial conditions but the same topology.

From the equation (2.5) to (2.15) the prime and double prime superscripts refer to two such states,

$$\sum_{p} i'_{p} v''_{p} = \sum_{\alpha} i'_{\alpha} v''_{\alpha} \tag{2.5}$$

$$\sum_{p} i''_{p} v'_{p} = \sum_{\alpha} i''_{\alpha} v'_{\alpha} \tag{2.6}$$

Tellegen's theorem applies to currents and voltages that are not necessarily in the same network, or at least, not in the same network at the same time. Products between prime and double prime elements are termed "quasi-powers" in [Penfield 1970], where extensive work on the application of Tellegen's theorem has been carried out.

Reference [Penfield 1970] presents a generalisation of Tellegen's theorem by using Kirchoff's operators; these can be linear or non-linear. If we have a set of branch currents termed $\{i_\alpha\}$ that obeys Kirchoff's current law:

$$i_\alpha = \sum_\beta B_{\beta\alpha} j_\beta \tag{2.7}$$

Then an expression using the Kirchoff's linear current operator Λ can be written:

$$\Lambda i_\alpha = \sum_\beta B_{\beta\alpha} \left(\Lambda j_\beta \right) \tag{2.8}$$

The operator Λ is independent of topology and applies only to the current where it is used, i.e., it can be used in each independent current j_β of the branch.
A simple substitution of equation (2.7) in (2.8) yields:

$$\Lambda \sum_\beta B_{\beta\alpha} j_\beta = \sum_\beta B_{\beta\alpha} \left(\Lambda j_\beta \right) \tag{2.9}$$

If Λ' and Λ'' are two different Kirchoff operators it is possible to define a current set that obeys Kirchoff currents laws:

$$\Lambda' i_\alpha = \sum_\beta B_{\beta\alpha} \left(\Lambda' j_\beta \right) \tag{2.10}$$

and a set of voltages that obeys Kirchoff voltage laws can be expressed:

$$\sum_\beta B_{\beta\alpha} \left(\Lambda'' v_\alpha \right) = 0 \tag{2.11}$$

From these we can obtain a general expression of Tellegen's theorem:

$$\sum_p \Lambda' i_p \Lambda'' v_p = \sum_\alpha \Lambda' i_\alpha \Lambda'' v_\alpha \tag{2.12}$$

and its counterpart:

$$\sum_p \Lambda'' i_p \Lambda' v_p = \sum_\alpha \Lambda'' i_\alpha \Lambda' v_\alpha \tag{2.13}$$

Subtraction of the previous two equations yields the difference form of Tellegen's theorem:

$$\sum_p \left(\Lambda' i_p \Lambda'' v_p - \Lambda'' i_p \Lambda' v_p \right) = \sum_\alpha \left(\Lambda' i_\alpha \Lambda'' v_\alpha - \Lambda'' i_a \Lambda' v_\alpha \right) \tag{2.14}$$

and their addition enables the additive form:

$$\sum_p \left(\Lambda' i_p \Lambda'' v_p + \Lambda'' i_p \Lambda' v_p \right) = \sum_\alpha \left(\Lambda' i_\alpha \Lambda'' v_\alpha + \Lambda'' i_a \Lambda' v_\alpha \right) \tag{2.15}$$

The pair formed by equations (2.14) and (2.15) is known as the weak form of Tellegen's theorem.

The different forms of Tellegen's theorem are the basis for power and quasi-power definitions that yield conservative properties. All these forms of Tellegen's theorem conservation properties were tested [Penfield 1970], and so are the instantaneous power and active power definitions. Moreover, new power and quasi-power definitions can be created by combining different forms of Tellegen's theorems and Kirchoff's operators.

2.3 The Hilbert Transform and Analytical Signals in Electrical Power System

The Hilbert Transform was first used in the area of signal theory by Denis Gabor [1946]. He defined a complex analytic signal which is a generalisation of the well-known Euler's formula. The concept of analytical signal has been used ever since in signal theory, control systems and circuit analysis. For the construction of a complex analytical signal it is necessary to use the original signal as the real part and the Hilbert Transform as the imaginary part. The application of the Hilbert Transform for

modelling and analysis of electric machinery can be found in the work of Yamamura [1991], who has termed this application of Hilbert Transform and analytical signals, "spiral vector theory". It can also be found in the work of Nowomiejski [1981] who set about to develop a general electric power theory where active, reactive and apparent powers are all defined using the Hilbert Transform. In addition, the Hilbert Transform has been adopted as the fundamental part of the Hilbert-Huang Transform [Huang 1998]; a relatively recent development carried out by NASA for the analysis of non-linear phenomena.

2.3.1 The Hilbert Transform basic definitions

The Hilbert Transform of a one-dimensional real signal *u(t)* is defined by the integral [Hahn 1996]:

$$v(t) = \frac{-1}{\pi} P\int_{-\infty}^{\infty} \frac{u(\eta)}{\eta} d\eta = \frac{-1}{\pi} P\int_{-\infty}^{\infty} \frac{u(\eta)}{1-\eta} d\eta \tag{2.16}$$

and the inverse Hilbert Transform is:

$$u(t) = \frac{-1}{\pi} P\int_{-\infty}^{\infty} \frac{v(\eta)}{\eta} d\eta = \frac{-1}{\pi} P\int_{-\infty}^{\infty} \frac{v(\eta)}{1-\eta} d\eta \tag{2.17}$$

where *P* stands for principal value of the integral. The above equations can be written in a simpler form using the convolution symbol:

$$v(t) = u(t) \otimes \frac{1}{\pi t} \tag{2.18}$$

$$u(t) = -v(t) \otimes \frac{1}{\pi t} \tag{2.19}$$

Then the kernel of the Hilbert Transformation is identified by:

$$\Theta(t) = \frac{1}{\pi t} \tag{2.20}$$

Application of the Fourier transform to the kernel function gives:

$$\Theta(\omega) = -\mathrm{j}\,\mathrm{sgn}(\omega) \tag{2.21}$$

with the signum function (distribution) defined as:

$$\mathrm{sgn}(\omega) = \begin{cases} +1 & \omega > 0 \\ 0 & \omega = 0 \\ -1 & \omega < 0 \end{cases} \tag{2.22}$$

Furthermore, using the convolution theorem, the spectrum of the Hilbert Transform is obtained:

$$u(t) \Leftarrow F \Rightarrow U(\omega) \tag{2.23}$$

$$v(t) \Leftarrow F \Rightarrow V(\omega) = \mathrm{j}\,\mathrm{sgn}(\omega) U(\omega) \tag{2.24}$$

Periodical real signals are those which, if incremented by a constant period of time *T*, will keep the same value. Hence:

$$u(t) = u(t + T) \tag{2.25}$$

Then a series Fourier decomposition of a periodical real signal in the complex conjugate space can be represented as:

$$u(t) = \sum_{n=-\infty}^{n=\infty} U_n \, e^{\mathrm{j}n\omega_0 t} \tag{2.26}$$

The Hilbert Transform of this signal is expressed as:

$$v(t) = \sum_{n=-\infty}^{n=\infty} -\mathrm{j}\,\mathrm{sgn}(n) U_n e^{\mathrm{j}n\omega_0 t} \tag{2.27}$$

Real signals and its Hilbert Transform have been defined in the time and the frequency domain.

2.3.2 The analytic complex signals

Analytic signals have been studied in great depth and applied in the areas of communications. The reason for the term analytic is that these signals satisfy Cauchy-Riemann conditions [Hahn 1996]. Indeed, because of their valuable mathematical properties, analytical signals are information rich, having instantaneous module and instantaneous angle values. An extensive documentation of analytical signals and their applications in signal processing can be found in [Cohen 1995].

An analytical signal can be represented in the time domain as a complex signal of the form:

$$\psi(t) = u(t) + \mathrm{j}v(t) \tag{2.28}$$

where *u(t)* is the real signal and *v(t)* is the Hilbert Transform of *u(t)*. If the analytical signal construction is carried out in the harmonic domain all the positive frequency elements are multiplied by two, the zero element multiplied by one and the negative frequency elements multiplied by zero.

$$u(t) \Leftarrow H \Rightarrow v(t) \tag{2.29}$$

$$u(t) \Leftarrow F \Rightarrow U(\omega) \tag{2.30}$$

$$v(t) \Leftarrow F \Rightarrow -\mathrm{j}\,\mathrm{sgn}(\omega) U(\omega) \tag{2.31}$$

Therefore:

$$\psi(t) \Leftarrow F \Rightarrow U(\omega) + \mathrm{j}\left[-\mathrm{jsgn}(\omega)U(\omega)\right] = \left[1+\mathrm{sgn}(\omega)\right]U(\omega) \tag{2.32}$$

where

$$1+\mathrm{sgn}(\omega) = \begin{cases} +2 & \omega > 0 \\ 1 & \omega = 0 \\ 0 & \omega < 0 \end{cases} \tag{2.33}$$

Using Fourier series for a periodical signal:

$$\psi(t) = \sum_{n=-\infty}^{n=\infty} U_n e^{\mathrm{j}n\omega_0 t} + j\sum_{n=-\infty}^{n=\infty} -\mathrm{jsgn}(n)U_n e^{\mathrm{j}n\omega_0 t} = \sum_{n=-\infty}^{n=\infty} \left[1+\mathrm{sgn}(n)\right]U_n e^{\mathrm{j}n\omega_0 t} \tag{2.34}$$

where

$$1+\mathrm{sgn}(n) = \begin{cases} +2 & n > 0 \\ 1 & n = 0 \\ 0 & n < 0 \end{cases} \tag{2.35}$$

A complex analytical signal in rectangular representation can be transported to a polar representation:

$$u(t) = A(t)\cos\left[\varphi(t)\right] \tag{2.36}$$

$$v(t) = A(t)\sin\left[\varphi(t)\right] \tag{2.37}$$

$$\psi(t) = A(t)e^{\mathrm{j}\varphi(t)} \tag{2.38}$$

The instantaneous amplitude is calculated from

$$A(t) = \sqrt{u^2(t) + v^2(t)} \tag{2.39}$$

and the instantaneous angle

$$\varphi(t) = \tan^{-1} \frac{v(t)}{u(t)} \tag{2.40}$$

Then the instantaneous angular frequency can be defined by

$$\Omega(t) = \dot{\varphi}(t) = \frac{d}{dt} \tan^{-1} \frac{v(t)}{u(t)} = \frac{u(t)\dot{v}(t) - v(t)\dot{u}(t)}{u^2(t) + v^2(t)} \tag{2.41}$$

From the relationship between instantaneous angular frequency and instantaneous frequency:

$$F(t) = \frac{\Omega(t)}{2\pi} = \frac{\dot{\varphi}(t)}{2\pi} \tag{2.42}$$

It should be mentioned that the validity of the instantaneous frequency definition has been questioned [Huang 1998] because under some conditions the instantaneous frequency takes negative values. This issue has received a great deal of attention and as result the Hilbert-Huang transform has emerged. This tool is used for the time frequency analysis of complex signals of different non-linear phenomena. Its basis is the utilisation of an empirical method for extracting the intrinsic mode functions [Huang 1998] with the salient characteristic that no negative frequencies are present. In the research carried out by this author it has been found that when applied to symmetrical components, and using the positive sequence signal information, no negative frequencies are present.

2.4 Powers and Quasi-Powers Using the Hilbert Transform

The Hilbert Transform and the application of Tellegen's Theorem have given rise to a set of power and quasi-power definitions. The Hilbert Transform can be considered as a result of the application of one Kirchoff linear operator, in this case convolution. If a network exists for a given state, and a second state is established by Hilbert transforming the first state, then it can be considered that the network is using different operators in each state. The utilisation of Hilbert Transform in the development of power definitions was put forward by authors such as Nowomiejski [1981] and Hahn [1996]. These definitions are fundamentally different from the instantaneous reactive power theory put forward by Akagi, Kanazawa and Nabae [1984] and successive modification such as the generalised instantaneous power theory of Feng Zhang Peng [1996]. This work, however, has been criticised by some authors, claiming that even in cases of sinusoidal operation but unbalanced conditions it yields misleading results [Czarnecki 2006].

There is one important point to be clarified when using the Hilbert Transform concerning the difference that exists between instantaneous and quasi-instantaneous definition. Hilbert transformation of a signal in real time is not possible [Hahn 1996], but good approximations have been achieved. However, for off-line processing of data it is quite straightforward to apply. Then, the utilisation of Hilbert Transform in electric power theory widens the existent instantaneous and quasi-instantaneous powers and quasi-powers definitions, where the most important characteristic is that they are conservative quantities. Hence, energy balances can be carried out in the entire electrical network. Another important characteristic of the Hilbert Transform, when applied to the set of power and quasi-power definitions, is that it can be used in single-phase and multi-phase multi-wire electrical systems.

A set of different conservative powers and quasi-powers can be obtained if the voltage and current values are transformed using the Hilbert Transform. The use of the complex Fourier transform and discrete convolutions simplifies all operations in harmonic domain.

A periodical, non-sinusoidal real signal voltage can be approximated by a finite set of complex Fourier terms:

$$v(t) = \sum_{n=-h}^{n=h} V_n e^{jn\omega_0 t} \tag{2.43}$$

$$v(t) = \left[V_{-h} e^{-jh\omega_0 t} + \quad \cdots \quad + V_{-1} e^{-j1\omega_0 t} + \quad V_0 e^{j0\omega_0 t} + \quad V_1 e^{j1\omega_0 t} + \quad \cdots \quad + V e^{jh\omega_0 t} \right] \tag{2.44}$$

This can be expressed as the product of two vectors:

$$v(t) = \begin{bmatrix} V_{-h} & \cdots & V_{-1} & V_0 & V_1 & \cdots & V_h \end{bmatrix} \begin{bmatrix} e^{-jh\omega_0 t} \\ \vdots \\ e^{-j1\omega_0 t} \\ e^{j0\omega_0 t} \\ e^{j1\omega_0 t} \\ \vdots \\ e^{jh\omega_0 t} \end{bmatrix}^T \tag{2.45}$$

where the first vector is the complex term of each frequency and the second vector is the corresponding time frequency value term.

Similarly, the Hilbert Transform of *v(t)* can be expressed as:

$$v_H(t) = \sum_{n=-h}^{n=h} -j\,\mathrm{sgn}(n) V_n e^{jn\omega_0 t} \tag{2.46}$$

And in vector form:

$$v_H(t) = \begin{bmatrix} jV_{-h} & \cdots & jV_{-1} & 0V_0 & -jV_1 & \cdots & -jV_h \end{bmatrix} \begin{bmatrix} e^{-jh\omega_0 t} \\ \vdots \\ e^{-j1\omega_0 t} \\ e^{j0\omega_0 t} \\ e^{j1\omega_0 t} \\ \vdots \\ e^{jh\omega_0 t} \end{bmatrix} \tag{2.47}$$

If the periodical non-sinusoidal voltage and currents are approximated by a finite set of complex Fourier terms, the voltage and current coefficients in these series can be used as entries in harmonic vectors **V** and **I,** respectively. Moreover, $\mathbf{V_h}$, $\mathbf{I_h}$ are Hilbert harmonic vectors:

$$\mathbf{V} = \begin{bmatrix} V_{-h} \\ \vdots \\ V_{-1} \\ V_0 \\ V_1 \\ \vdots \\ V_h \end{bmatrix} = \begin{bmatrix} V_{real+h} + \mathrm{j}V_{imag+h} \\ \vdots \\ V_{real+1} + \mathrm{j}V_{imag+1} \\ V_{real\,0} \\ V_{real+1} - \mathrm{j}V_{imag+1} \\ \vdots \\ V_{real+h} - \mathrm{j}V_{imag+h} \end{bmatrix} \tag{2.48}$$

$$\mathbf{I} = \begin{bmatrix} I_{-h} \\ \vdots \\ I_{-1} \\ I_0 \\ I_1 \\ \vdots \\ I_h \end{bmatrix} = \begin{bmatrix} I_{real+h} + \mathrm{j}I_{imag+h} \\ \vdots \\ I_{real+1} + \mathrm{j}I_{imag+1} \\ I_{real\,0} \\ I_{real+1} - \mathrm{j}I_{imag+1} \\ \vdots \\ I_{real+h} - \mathrm{j}I_{imag+h} \end{bmatrix} \tag{2.49}$$

$$\mathbf{Vh} = -\mathrm{j}\mathrm{sgn}(n) \begin{bmatrix} V_{-h} \\ \vdots \\ V_{-1} \\ V_0 \\ V_1 \\ \vdots \\ V_h \end{bmatrix} = \begin{bmatrix} \mathrm{j}V_{real+h} + \mathrm{jj}V_{imag+h} \\ \vdots \\ \mathrm{j}V_{real+1} + \mathrm{jj}V_{imag+1} \\ 0 \\ -\mathrm{j}V_{real+1} - (-\mathrm{j})\,\mathrm{j}V_{imag+1} \\ \vdots \\ -\mathrm{j}V_{real+h} - (-\mathrm{j})\,\mathrm{j}V_{imag+h} \end{bmatrix} = \begin{bmatrix} \mathrm{j}V_{real+h} - V_{imag+h} \\ \vdots \\ \mathrm{j}V_{real+1} - V_{imag+1} \\ 0 \\ -\mathrm{j}V_{real+1} - V_{imag+1} \\ \vdots \\ -\mathrm{j}V_{real+h} - V_{imag+h} \end{bmatrix} \tag{2.50}$$

$$\mathbf{Ih} = -\mathrm{j}\,\mathrm{sgn}(h)\begin{bmatrix} I_{-h} \\ \vdots \\ I_{-1} \\ I_0 \\ I_1 \\ \vdots \\ I_h \end{bmatrix} = \begin{bmatrix} \mathrm{j}I_{real+h} + \mathrm{jj}I_{imag+h} \\ \vdots \\ \mathrm{j}I_{real+1} + \mathrm{jj}I_{imag+1} \\ 0 \\ -\mathrm{j}I_{real+1} - (-\mathrm{j})\,\mathrm{j}I_{imag+1} \\ \vdots \\ -\mathrm{j}I_{real+h} - (-\mathrm{j})\,\mathrm{j}I_{imag+h} \end{bmatrix} = \begin{bmatrix} \mathrm{j}I_{real+h} - I_{imag+h} \\ \vdots \\ \mathrm{j}I_{real+1} - I_{imag+1} \\ 0 \\ -\mathrm{j}I_{real+1} - I_{imag+1} \\ \vdots \\ -\mathrm{j}I_{real+h} - I_{imag+h} \end{bmatrix} \tag{2.51}$$

2.4.1 Instantaneous power, active power and quadrature instantaneous power

The product of the real signals of voltage and currents waveforms yields the well known instantaneous power. Multiplication of signals in time domain means discrete convolutions in the frequency domain, an operation which may be carried out with the product of the Toeplitz matrix form [Acha and Madrigal 2001] of one signal and the vector form of the second signal. The main characteristic of the instantaneous power is its conservative property.

$$p = v(t)i(t) \tag{2.52}$$

$$\mathbf{p}_{inst} = \mathbf{v} \otimes \mathbf{i} = \mathbf{v}^{\mathbf{Tpz}}\mathbf{i} \tag{2.53}$$

$$\mathbf{p}_{\mathbf{inst}} = \mathbf{v} \otimes \mathbf{i} = \begin{bmatrix} V_0 & V_{-1} & \cdots & V_{-h} & 0 & 0 & 0 \\ V_1 & V_0 & V_{-1} & \cdots & V_{-h} & 0 & 0 \\ \cdots & V_1 & V_0 & V_{-1} & \cdots & V_{-h} & 0 \\ V_h & \cdots & V_1 & V_0 & V_{-1} & \cdots & V_{-h} \\ 0 & V_h & \cdots & V_1 & V_0 & V_{-1} & \cdots \\ 0 & 0 & V_h & \cdots & V_1 & V_0 & V_{-1} \\ 0 & 0 & 0 & V_h & \cdots & V_1 & V_0 \end{bmatrix} \begin{bmatrix} I_{-h} \\ \vdots \\ I_{-1} \\ I_0 \\ I_1 \\ \vdots \\ I_h \end{bmatrix} \tag{2.54}$$

$$\mathbf{p_{inst}} = \begin{bmatrix} V_0 I_{-h} + & V_{-1} I_{-h+1} + & \cdots & +V_{-h} I_0 & 0 & 0 & 0 \\ V_1 I_{-h} + & V_0 I_{-h+1} + & V_{-1} I_{-h+2} + & \cdots & +V_{-h} I_1 & 0 & 0 \\ \cdots & V_1 I_{-2} & V_0 I_{-1} & V_{-1} I_0 & \cdots & V_{-h} I_{h-1} & 0 \\ V_h I_{-h} + & \cdots & +V_1 I_{-1} & +V_0 I_0 & +V_{-1} I_1 + & \cdots & +V_{-h} I_h \\ 0 & V_h I_{-h+1} & \cdots & V_1 I_0 & V_0 I_1 & V_{-1} I_2 & \cdots \\ 0 & 0 & V_h & \cdots & V_1 & V_0 & V_{-1} \\ 0 & 0 & 0 & V_h & \cdots & V_1 & V_0 \end{bmatrix} \tag{2.55}$$

where the superscript Tpz means Toeplitz matrix.

Moreover, the active or average power is defined as:

$$p_{avg} = \frac{1}{T} \int_0^T v(t) i(t) dt \tag{2.56}$$

From which the average value in the harmonic domain of instantaneous power can be calculated (which is the addition of the zero frequency components)

$$p_{avg} = V_h I_{-h} + \cdots + V_1 I_{-1} + V_0 I_0 + V_{-1} I_1 + \cdots + V_{-h} I \tag{2.57}$$

In the quest for the generalisation of electric power theory, Nowomiejski [1981], arrived at the same power definition as Budeanu [1927] using the Hilbert Transform. More specifically, the product of voltage with the Hilbert Transform of the current yields the quadrature instantaneous power, which in the frequency domain is given by the equation:

$$\mathbf{q}_{inst} = \mathbf{v} \otimes \mathbf{i_H} = \mathbf{v}^{\mathbf{Tpz}} \mathbf{i_H} \tag{2.58}$$

where the superscript Tpz is used to signify Toeplitz matrix. The quadrature instantaneous power can also be expressed by the product:

$$\mathbf{q}_{inst} = \mathbf{-v_H} \otimes \mathbf{i} = \mathbf{-v_H}^{\mathbf{Tpz}} \mathbf{i} \tag{2.59}$$

In these equations two states in different times can be observed and their discrete convolution is termed instantaneous quadrature power.
If we substitute the operators from the original equation (2.13) by the Hilbert Transform operator

$$\sum_p \Lambda'' i_p \Lambda' v_p = \sum_\alpha \Lambda'' i_\alpha \Lambda' v_\alpha \tag{2.60}$$

to

$$\sum_p \frac{1}{\pi t} \otimes i_p v_p = \sum_\alpha \frac{1}{\pi t} \otimes i_\alpha v_\alpha \tag{2.61}$$

where the transform operator is convolved with the current. Therefore, it is clear that this quasi-power definition is conservative by the application of Tellegen's Theorem. This instantaneous quasi-power has been used for compensation in single-phase systems where the instantaneous reactive theory of Akagi and the generalised instantaneous reactive theory of Zhang are not applicable [Czarnecki 2002]. The importance of this definition is that it has conservative properties and it can be used in conjunction with the instantaneous power for the calculation of power and quasi-power flows in electrical systems.

2.5 The Instantaneous Complex Power

The construction of analytical signals has enabled alternative power definitions. For instance the concepts used in sinusoidal circuits have been extended to non-sinusoidal situations, giving the generalisation of the classical complex power definition applicable in sinusoidal cases to the instantaneous complex power definition applicable in both sinusoidal and non-sinusoidal cases.
The new power definition can be realised by constructing the analytical signals, in the field of complex numbers using the original signal in the real part and its Hilbert Transform in the imaginary part. Then the analytical voltage is expressed as follows:

$$v_A(t) = \sum_{n=-h}^{n=h} V_n e^{\mathrm{j}n\omega_0 t} + \mathrm{j}\left(\sum_{n=-h}^{n=h} -\mathrm{jsgn}(n) V_n e^{\mathrm{j}n\omega_0 t} \right) = \sum_{n=-h}^{n=h} \left[1 + \mathrm{jsgn}(n)\right] V_n e^{\mathrm{j}n\omega_0 t} \tag{2.62}$$

The analytical function of the current *i(t)* is obtained in a similar manner:

$$i_A(t) = \sum_{n=-h}^{n=h} I_n e^{\mathrm{j}n\omega_0 t} + \mathrm{j}\left(\sum_{n=-h}^{n=h} -\mathrm{jsgn}(n) I_n e^{\mathrm{j}n\omega_0 t} \right) = \sum_{n=-h}^{n=h} \left[1 + \mathrm{jsgn}(n)\right] I_n e^{\mathrm{j}n\omega_0 t} \tag{2.63}$$

An analytical signal can be formed in the frequency domain with the sum of the vector voltage plus the operator j multiplied by its Hilbert Transform:

$$\mathbf{v_A} = \mathbf{v} + \mathrm{j}\mathbf{v_H} \tag{2.64}$$

The analytical current is constructed in the same form:

$$\mathbf{i_A} = \mathbf{i} + \mathrm{j}\mathbf{i_H} \tag{2.65}$$

If voltages and currents are represented in vector form:

$$\mathbf{V_A} = \begin{bmatrix} V_{-h} \\ \vdots \\ V_{-1} \\ V_0 \\ V_1 \\ \vdots \\ V_h \end{bmatrix} + j \left(-\mathrm{jsgn}(n) \begin{bmatrix} V_{-h} \\ \vdots \\ V_{-1} \\ V_0 \\ V_1 \\ \vdots \\ V_h \end{bmatrix} \right) = \begin{bmatrix} 0 \\ \vdots \\ 0 \\ V_{real\,0} \\ 2\left(V_{real+1} - \mathrm{j}V_{imag+1}\right) \\ \vdots \\ 2\left(V_{real+h} - \mathrm{j}V_{imag+h}\right) \end{bmatrix} \tag{2.66}$$

$$\mathbf{I_A} = \begin{bmatrix} I_{-h} \\ \vdots \\ I_{-1} \\ I_0 \\ I_1 \\ \vdots \\ I_h \end{bmatrix} + \mathrm{j} \left(-\mathrm{jsgn}(n) \begin{bmatrix} I_{-h} \\ \vdots \\ I_{-1} \\ I_0 \\ I_1 \\ \vdots \\ I_h \end{bmatrix} \right) = \begin{bmatrix} 0 \\ \vdots \\ 0 \\ V_{real\,0} \\ 2\left(I_{real+1} - \mathrm{j}I_{imag+1}\right) \\ \vdots \\ 2\left(I_{real+h} - \mathrm{j}I_{imag+h}\right) \end{bmatrix} \tag{2.67}$$

One definition of instantaneous complex power (Hahn, 1996) in time domain is given by:

$$s = \frac{1}{2} v_A(t) i_A^*(t) = \frac{1}{2}\left(v(t) + \mathrm{j} v_H(t)\right)\left(i(t) + \mathrm{j} i_H(t)\right)^* \tag{2.68}$$

The instantaneous complex power [Hahn 1996] in the frequency domain can be defined by the convolution of the analytical voltage vector and the conjugate of the analytical current vector divided by two

$$\mathbf{s}_{inst} = \frac{1}{2}\left(\mathbf{v} + j\mathbf{v}_\mathbf{H}\right) \otimes \left(\mathbf{i} + j\mathbf{i}_\mathbf{H}\right)^* \tag{2.69}$$

$$\mathbf{s}_{inst} = \frac{1}{2}\left(\left(\mathbf{v} \otimes \mathbf{i}^* - \mathbf{v}_\mathbf{H} \otimes \mathbf{i}_\mathbf{H}^*\right) + j\left(\mathbf{v} \otimes \mathbf{i}_\mathbf{H}^* + \mathbf{v}_\mathbf{H} \otimes \mathbf{i}^*\right)\right) \tag{2.70}$$

The time domain product of the analytical voltage and the conjugate of the analytical current divided by two is known as “instantaneous complex power”. The real term is termed “instantaneous active power”, the imaginary term is termed “instantaneous reactive power” and the absolute value is termed “instantaneous apparent power”. Each sub-term of the real and imaginary terms of the instantaneous complex power is a conservative power or a conservative quasi-power. In this case the product of the real term of the analytical voltage and the real term of the analytical current is the well-known instantaneous power. The description of each term and sub-term in the time domain has its counterpart in the frequency domain, where convolutions are used. In the frequency domain, each frequency component possesses the conservation attribute in the entire electrical network.

The instantaneous complex power definition is the classical definition of power under sinusoidal conditions which directly gives the instantaneous values of voltage and current.

2.6 Three-phase System Power Definitions

If we have a voltage vector *v(t)* and a vector current *i(t)*:

$$\vec{v} = \begin{bmatrix} v_a(t) & v_b(t) & v_c(t) \end{bmatrix}^T \tag{2.71}$$

$$\vec{i} = \begin{bmatrix} i_a(t) & i_b(t) & i_c(t) \end{bmatrix}^T \tag{2.72}$$

Their Hilbert Transform is given by:

$$\vec{v} = \begin{bmatrix} v_a(t) \\ v_b(t) \\ v_c(t) \end{bmatrix} \Leftarrow H \Rightarrow \begin{bmatrix} v_{aH}(t) \\ v_{bH}(t) \\ v_{cH}(t) \end{bmatrix} = \vec{v}_H \tag{2.73}$$

and

$$\vec{i} = \begin{bmatrix} i_a(t) \\ i_b(t) \\ i_c(t) \end{bmatrix} \Leftarrow H \Rightarrow \begin{bmatrix} i_{aH}(t) \\ i_{bH}(t) \\ i_{cH}(t) \end{bmatrix} = \vec{i}_H \tag{2.74}$$

The analytical signals of voltage and current can be defined by:

$$\vec{v}_{Aabc} = \begin{bmatrix} v_a(t) + jv_{aH}(t) \\ v_b(t) + jv_{bH}(t) \\ v_c(t) + jv_{cH}(t) \end{bmatrix} = \begin{bmatrix} v_{aA}(t) \\ v_{bA}(t) \\ v_{cA}(t) \end{bmatrix} \tag{2.75}$$

$$\vec{i}_{Aabc} = \begin{bmatrix} i_a(t) + ji_{aH}(t) \\ i_b(t) + ji_{bH}(t) \\ i_c(t) + ji_{cH}(t) \end{bmatrix} = \begin{bmatrix} i_{aA}(t) \\ i_{bA}(t) \\ i_{cA}(t) \end{bmatrix} \tag{2.76}$$

And the three-phase instantaneous complex power can be defined by:

$$s = \frac{1}{2}\vec{v}_{Aabc}\vec{i}^{*}_{Aabc} = \frac{1}{2}\begin{bmatrix} v_{aA}(t) & v_{bA}(t) & v_{cA}(t) \end{bmatrix}\begin{bmatrix} i_{aA}(t) \\ i_{bA}(t) \\ i_{cA}(t) \end{bmatrix}^{*} \tag{2.77}$$

The instantaneous power of each phase can be represented by:

$$s = \frac{1}{2}\vec{v}_{Aabc}\vec{i}^{*}_{Aabc} = \frac{1}{2}\begin{bmatrix} v_{aA}(t) & 0 & 0 \\ 0 & v_{bA}(t) & 0 \\ 0 & 0 & v_{cA}(t) \end{bmatrix}\begin{bmatrix} i_{aA}(t) \\ i_{bA}(t) \\ i_{cA}(t) \end{bmatrix}^{*} \tag{2.78}$$

If the analytical voltage and current signals of each phase are periodic then they can be represented in the frequency domain as a set of vectors of harmonic coefficients:

$$\vec{\mathbf{v}}_{\mathbf{A}abc} = \begin{bmatrix} \mathbf{v_{aA}} & \mathbf{v_{bA}} & \mathbf{v_{cA}} \end{bmatrix}^{T} \tag{2.79}$$

$$\vec{\mathbf{i}}_{\mathbf{A}abc} = \begin{bmatrix} \mathbf{i_{aA}} & \mathbf{i_{bA}} & \mathbf{i_{cA}} \end{bmatrix}^{T} \tag{2.80}$$

Then the three-phase analytical instantaneous complex power calculated in the frequency can be calculated in a three-phase system by:

$$\vec{\mathbf{s}} = \frac{1}{2}\vec{\mathbf{v}}^{T}_{\mathbf{A}abc} \otimes \vec{\mathbf{i}}^{*}_{\mathbf{A}abc} = \frac{1}{2}\begin{bmatrix} \mathbf{v_{aA}} & \mathbf{v_{bA}} & \mathbf{v_{cA}} \end{bmatrix} \otimes \begin{bmatrix} \mathbf{i_{aA}} \\ \mathbf{i_{bA}} \\ \mathbf{i_{cA}} \end{bmatrix}^{*} \tag{2.81}$$

$$\vec{\mathbf{s}} = \frac{1}{2}\left(\mathbf{v_{aA}} \otimes \mathbf{i}^{*}_{\mathbf{aA}} + \mathbf{v_{bA}} \otimes \mathbf{i}^{*}_{\mathbf{bA}} + \mathbf{v_{cA}} \otimes \mathbf{i}^{*}_{\mathbf{cA}} \right) \tag{2.82}$$

If the complex power of each phase is calculated separately then:

$$\mathbf{s} = \frac{1}{2}\begin{bmatrix} \mathbf{V}_{\mathbf{aA}}^{\mathbf{Tpz}} & \mathbf{0} & \mathbf{0} \\ \mathbf{0} & \mathbf{V}_{\mathbf{bA}}^{\mathbf{Tpz}} & \mathbf{0} \\ \mathbf{0} & \mathbf{0} & \mathbf{V}_{\mathbf{bA}}^{\mathbf{Tpz}} \end{bmatrix}\begin{bmatrix} \mathbf{I}_{\mathbf{aA}}^{*} \\ \mathbf{I}_{\mathbf{bA}}^{*} \\ \mathbf{I}_{\mathbf{cA}}^{*} \end{bmatrix} = \begin{bmatrix} \mathbf{s}_{\mathbf{aA}} \\ \mathbf{s}_{\mathbf{bA}} \\ \mathbf{s}_{\mathbf{cA}} \end{bmatrix} \tag{2.83}$$

The total or individual powers of each phase give the values required for power compensation or the optimisation of energy transfers in the network.

2.7 The Analytical Symmetrical Components

The first direct application of symmetrical components in the frequency domain is due to Fortescue [1918] encouraging the use of other transformations with the goal of simplifying calculation and facilitate the modelling. The extension of this method to time domain for the calculation of transients in electrical machinery is well presented by Lyon [1954], but the real developer of the tool was T. Bekku [1927], who termed the method instantaneous symmetrical components.

The construction of analytical signals using the Hilbert Transform from real signals of three-phase voltages and currents permits the correct application of symmetrical components in time domain, as mentioned by Yamamura in his spiral vector theory book [Yamamura 1991] from which the instantaneous positive, negative and zero sequence components can be obtained. Contrary to Lyon's symmetrical components [Lyon 1954], the utilisation of "instantaneous analytical symmetrical components" yields positive and negative sequences which are independent from one another. The instantaneous symmetrical components obtained from analytical signals are the basis for the definitions of instantaneous negative and positive sequence impedances, negative and positive sequence admittances, and instantaneous negative and positive sequence frequencies.

In a three-phase electrical system the voltage in each phase can be decomposed into a set of three components as shown in equation (2.84):

$$\vec{v}_{ASy}=\begin{bmatrix} v_{aA}(t) \\ v_{bA}(t) \\ v_{cA}(t) \end{bmatrix}=\begin{bmatrix} v_{aA}^{(0)}(t) & + & v_{aA}^{(1)}(t) & + & v_{aA}^{(2)}(t) \\ v_{bA}^{(0)}(t) & + & v_{bA}^{(1)}(t) & + & v_{bA}^{(2)}(t) \\ v_{cA}^{(0)}(t) & + & v_{cA}^{(1)}(t) & + & v_{cA}^{(1)}(t) \end{bmatrix} \tag{2.84}$$

If each sequence set is balanced, with the three quantities in the first set having the same magnitude and holding the same direction; the three quantities in the second set having equal magnitudes and displaced from each other by 120 degrees and rotating in a given direction; and the three quantities in the third set having equal magnitudes and displaced from each other by 120 degrees and rotating in the backward direction, then this set can be presented as

$$\vec{v}_{ASy}=\begin{bmatrix} v_{aA}(t) \\ v_{bA}(t) \\ v_{cA}(t) \end{bmatrix}=\begin{bmatrix} v_{aA}^{0}(t) & + & v_{aA}^{1}(t) & + & v_{aA}^{2}(t) \\ v_{aA}^{0}(t) & + & a^2 v_{aA}^{1}(t) & + & a v_{aA}^{2}(t) \\ v_{aA}^{0}(t) & + & a v_{aA}^{1}(t) & + & a^2 v_{aA}^{1}(t) \end{bmatrix}=\begin{bmatrix} 1 & 1 & 1 \\ 1 & a^2 & a \\ 1 & a & a^2 \end{bmatrix}\begin{bmatrix} v_{aA}^{0}(t) \\ v_{aA}^{1}(t) \\ v_{aA}^{2}(t) \end{bmatrix} \tag{2.85}$$

The same result can be extended to the currents

$$\vec{i}_{ASy}=\begin{bmatrix} i_{aA}(t) \\ i_{bA}(t) \\ i_{cA}(t) \end{bmatrix}=\begin{bmatrix} i_{aA}^{0}(t) & + & i_{aA}^{1}(t) & + & i_{aA}^{2}(t) \\ i_{aA}^{0}(t) & + & a^2 i_{aA}^{1}(t) & + & a i_{aA}^{2}(t) \\ i_{aA}^{0}(t) & + & a i_{aA}^{1}(t) & + & a^2 i_{aA}^{1}(t) \end{bmatrix}=\begin{bmatrix} 1 & 1 & 1 \\ 1 & a^2 & a \\ 1 & a & a^2 \end{bmatrix}\begin{bmatrix} i_{aA}^{0}(t) \\ i_{aA}^{1}(t) \\ i_{aA}^{2}(t) \end{bmatrix} \tag{2.86}$$

If the equations (2.85) and (2.86) are solved for symmetrical components values then the so-called analytical instantaneous symmetrical components are:

$$\vec{v}_{ASy}=\begin{bmatrix} v_{A}^{0}(t) \\ v_{A}^{1}(t) \\ v_{A}^{2}(t) \end{bmatrix}=C\vec{v}_{A}=\frac{1}{3}\begin{bmatrix} 1 & 1 & 1 \\ 1 & a & a^2 \\ 1 & a^2 & a \end{bmatrix}\begin{bmatrix} v_{aA}(t) \\ v_{bA}(t) \\ v_{cA}(t) \end{bmatrix} \tag{2.87}$$

and

$$\vec{i}_{ASy}=\begin{bmatrix} i_{A}^{0}(t) \\ i_{A}^{1}(t) \\ i_{A}^{2}(t) \end{bmatrix}=C\vec{v}_{A}=\frac{1}{3}\begin{bmatrix} 1 & 1 & 1 \\ 1 & a & a^2 \\ 1 & a^2 & a \end{bmatrix}\begin{bmatrix} i_{aA}(t) \\ i_{bA}(t) \\ i_{cA}(t) \end{bmatrix} \tag{2.88}$$

Construction of the analytical instantaneous symmetrical components from analytical signals permits a new set of decoupled variables to be created which incorporate all the system characteristics and with no loss of information. The importance of the application of analytical symmetrical components in condition monitoring of electrical machinery cannot be underestimated. As matter of fact, each sequence component of voltage and current gives information about the status of equipment or system. With these values the impedance sequence components can be calculated, powers and instantaneous frequency extracted from the positive sequences.

The three-phase instantaneous complex power in the time domain can be calculated by:

$$s_{ASy} = \frac{1}{2}\begin{bmatrix} v_{aA}(t) \\ v_{bA}(t) \\ v_{cA}(t) \end{bmatrix}^T \begin{bmatrix} i_{aA}(t) \\ i_{bA}(t) \\ i_{cA}(t) \end{bmatrix}^* = \frac{1}{2}\left[\begin{bmatrix} 1 & 1 & 1 \\ 1 & a^2 & a \\ 1 & a & a^2 \end{bmatrix}\begin{bmatrix} v_{aA}^0(t) \\ v_{aA}^1(t) \\ v_{aA}^2(t) \end{bmatrix}\right]^T \left[\begin{bmatrix} 1 & 1 & 1 \\ 1 & a^2 & a \\ 1 & a & a^2 \end{bmatrix}\begin{bmatrix} i_{aA}^0(t) \\ i_{aA}^1(t) \\ i_{aA}^2(t) \end{bmatrix}\right]^* \quad (2.89)$$

The reversal rule of matrix algebra states that the transpose of the product of two matrices is equal to the product of the transpose of the matrices in reverse order, then:

$$s_{ASy} = \frac{1}{2}\begin{bmatrix} v_{aA}^0(t) & v_{aA}^1(t) & v_{aA}^2(t) \end{bmatrix}\begin{bmatrix} 1 & 1 & 1 \\ 1 & a^2 & a \\ 1 & a & a^2 \end{bmatrix}\begin{bmatrix} 1 & 1 & 1 \\ 1 & a & a \\ 1 & a^2 & a \end{bmatrix}\begin{bmatrix} i_{aA}^0(t) \\ i_{aA}^1(t) \\ i_{aA}^2(t) \end{bmatrix}^* \quad (2.90)$$

and

$$s_{ASy} = \frac{3}{2}\begin{bmatrix} v_{aA}^0(t) & v_{aA}^1(t) & v_{aA}^2 \end{bmatrix}\begin{bmatrix} i_{aA}^0(t) \\ i_{aA}^1(t) \\ i_{aA}^2(t) \end{bmatrix}^* \quad (2.91)$$

Then the calculation of symmetrical components in the frequency domain can be carried out by:

$$\vec{\mathbf{v}}_{\mathbf{ASy}} = \begin{bmatrix} \mathbf{v}_{\mathbf{A}}^{\mathbf{0}} \\ \mathbf{v}_{\mathbf{A}}^{\mathbf{1}} \\ \mathbf{v}_{\mathbf{A}}^{\mathbf{2}} \end{bmatrix} = \mathbf{C}\vec{\mathbf{v}}_{\mathbf{A}} = \frac{1}{3}\begin{bmatrix} \mathbf{I} & \mathbf{I} & \mathbf{I} \\ \mathbf{I} & a\mathbf{I} & a^2\mathbf{I} \\ \mathbf{I} & a^2\mathbf{I} & a\mathbf{I} \end{bmatrix}\begin{bmatrix} \mathbf{v}_{\mathbf{aA}} \\ \mathbf{v}_{\mathbf{bA}} \\ \mathbf{v}_{\mathbf{cA}} \end{bmatrix} \tag{2.92}$$

$$\vec{\mathbf{i}}_{\mathbf{ASy}} = \begin{bmatrix} \mathbf{i}_{\mathbf{A}}^{\mathbf{0}} \\ \mathbf{i}_{\mathbf{A}}^{\mathbf{1}} \\ \mathbf{i}_{\mathbf{A}}^{\mathbf{2}} \end{bmatrix} = \mathbf{C}\vec{\mathbf{i}}_{\mathbf{A}} = \frac{\mathbf{1}}{\mathbf{3}}\begin{bmatrix} \mathbf{I} & \mathbf{I} & \mathbf{I} \\ \mathbf{I} & a\mathbf{I} & a^2\mathbf{I} \\ \mathbf{I} & a^2\mathbf{I} & a\mathbf{I} \end{bmatrix}\begin{bmatrix} \mathbf{i}_{\mathbf{aA}} \\ \mathbf{i}_{\mathbf{bA}} \\ \mathbf{i}_{\mathbf{cA}} \end{bmatrix} \tag{2.93}$$

Where in equations (2.92) and (2.93), **I** is the identity matrix of *(h+1,h+1)* elements
The instantaneous complex power using symmetrical components can be defined in the frequency domain by;

$$\mathbf{s}_{\mathbf{ASy}} = \frac{3}{2}\begin{bmatrix} \mathbf{v}_{\mathbf{aA}}^{\mathbf{0}} & \mathbf{v}_{\mathbf{aA}}^{\mathbf{1}} & \mathbf{v}_{\mathbf{aA}}^{\mathbf{2}} \end{bmatrix} \otimes \begin{bmatrix} \mathbf{i}_{\mathbf{aA}}^{\mathbf{0}} \\ \mathbf{i}_{\mathbf{aA}}^{\mathbf{1}} \\ \mathbf{i}_{\mathbf{aA}}^{\mathbf{2}} \end{bmatrix}^{*} \tag{2.94}$$

$$\mathbf{s}_{\mathbf{ASy}} = \frac{3}{2}\mathbf{v}_{\mathbf{aA}}^{\mathbf{0}} \otimes \left(\mathbf{i}_{\mathbf{aA}}^{\mathbf{0}}\right)^{*} + \frac{3}{2}\mathbf{v}_{\mathbf{aA}}^{\mathbf{1}} \otimes \left(\mathbf{i}_{\mathbf{aA}}^{\mathbf{1}}\right)^{*} + \frac{3}{2}\mathbf{v}_{\mathbf{aA}}^{\mathbf{2}} \otimes \left(\mathbf{i}_{\mathbf{aA}}^{\mathbf{2}}\right)^{*} \tag{2.95}$$

If the voltages and currents are given in the per unit system the positive and negative ratio with respect to the base values are calculated directly. The analytical instantaneous zero, positive and negative sequence impedances can be defined by:

$$\vec{z}_{ASy} = \begin{bmatrix} z_A^0(t) \\ z_A^1(t) \\ z_A^2(t) \end{bmatrix} == \begin{bmatrix} v_A^0(t)/i_A^0(t) \\ v_A^1(t)/i_A^1(t) \\ v_A^2(t)/i_A^2(t) \end{bmatrix} \tag{2.96}$$

and the analytical instantaneous zero, positive and negative sequence admittances can be defined by:

$$\vec{y}_{ASy} = \begin{bmatrix} y_A^0(t) \\ y_A^1(t) \\ y_A^2(t) \end{bmatrix} == \begin{bmatrix} i_A^0(t)/v_A^0(t) \\ i_A^1(t)/v_A^1(t) \\ i_A^2(t)/v_A^2(t) \end{bmatrix} \tag{2.97}$$

The instantaneous frequency definition has been a point of much discussion concerning its validity since negative frequencies appear when the analytical signal is constructed from a real signal that contains negative frequency terms, i.e., the presence of negative sequences harmonic components (fifth harmonic) in a periodical signal. If the frequency of positive sequence voltages and currents are used, the frequency values will give information about the system evicting negative frequency values, further research is required for their use for frequency measurement and condition monitoring.

2.8 Non-conservative Powers and Quasi-powers Definitions

The apparent power and the active power have been the basis for several reactive and non-active power definitions aims at compensation at a point of the system. If the average active power is subtracted from the apparent power then the result is termed non-active power. However, for apparent power diverse definitions have been put forward; all of them being referred as non-conservatives. This work will take the definition given by the IEEE Standard 1459 [PSIMC 2000] which was created to deal with three-phase unbalanced systems with harmonic distortion.

2.8.1 Root mean square values

The root mean square values of voltage and current are the starting point for the apparent power definition. For periodic voltage and current signals in time domain, the following definitions apply

$$V_{rms} = \sqrt{\frac{1}{T}\int_0^T v(t)^2 dt} \tag{2.98}$$

and

$$I_{rms} = \sqrt{\frac{1}{T}\int_0^T i(t)^2 dt} \tag{2.99}$$

If these signals are transformed in to the complex frequency domain then the root mean square values are calculated from the fundamental and harmonic components

$$V_{rms} = \sqrt{\sum_{n=-h}^{n=h} \mathrm{V}_n \mathrm{V}_{-n}} = \sqrt{\sum_{n=-h}^{n=h} |V_n|^2} \tag{2.100}$$

and

$$I_{rms} = \sqrt{\sum_{n=-h}^{n=h} \mathrm{I}_n \mathrm{I}_{-n}} = \sqrt{\sum_{n=-h}^{n-h} |I_n|^2} \tag{2.101}$$

The equation (2.100) can be applied for both phase voltage and line-to line voltages. From the above equations (2.100) and (2.101) the effective root mean square voltage and current definitions are established. These are in turn used to construct the apparent power definition of three-phase electrical systems operating under non-sinusoidal and unbalanced conditions.

The effective root mean square voltage for three-phase four-wire systems is in accord with IEEE Standard 1459

$$V_e = \sqrt{\frac{1}{18}\left[3\left(V_a^2 + V_b^2 + V_c^2\right) + V_{ab}^2 + V_{bc}^2 + V_{ca}^2\right]} \tag{2.102}$$

where phase voltages are denoted by subscripts *a*, *b* and *c* and line-to-line voltages by sub indexes *ab*, *bc* and *ca*.

The effective root mean square current for three-phase four-wire systems are defined by:

$$I_e = \sqrt{\frac{I_a^2 + I_b^2 + I_c^2 + I_n^2}{3}} \tag{2.103}$$

These expressions simplify themselves when applied to three-phase, three-wire electrical systems,

$$V_e = \sqrt{\frac{V_{ab}^2 + V_{bc}^2 + V_{ca}^2}{9}} \tag{2.104}$$

and

$$I_e = \sqrt{\frac{I_a^2 + I_b^2 + I_c^2}{3}} \tag{2.105}$$

2.8.2 Power quality indices

The IEEE Standard 1459 [PSIMC 2000] determines two distinctive voltage and current components of root mean square values. They are:

$$V_{rms}^2 = V_{rms1}^2 + V_{rmsH}^2 \tag{2.106}$$

$$I_{rms}^2 = I_{rms1}^2 + I_{rmsH}^2 \tag{2.107}$$

with the fundamental components calculated as:

$$V_{rms1} = \sqrt{\sum_{n=-1}^{n=1} \mathrm{V}_n \mathrm{V}_{-n}} = \sqrt{\sum_{n=-1}^{n=1} |V_n|^2} \tag{2.108}$$

where it is considered that the zero components yield to zero. The harmonic root mean square voltages are:

$$V_{rmsH} = \sqrt{\sum_{n=-h}^{n=-2} \mathrm{V}_n \mathrm{V}_{-n} + \sum_{n=2}^{n=h} \mathrm{V}_n \mathrm{V}_{-n} +} = \sqrt{\sum_{n=-h}^{n=-2} |V_n|^2 + \sum_{n=2}^{n=h} |V_n|^2} \tag{2.109}$$

Equivalent expressions are used for the fundamental and harmonic root mean square currents:

$$I_{rms1} = \sqrt{\sum_{n=-1}^{n=1} \mathrm{I}_n \mathrm{I}_{-n}} = \sqrt{\sum_{n=-1}^{n=1} |I_n|^2} \tag{2.110}$$

and

$$I_{rmsH} = \sqrt{\sum_{n=-h}^{n=-2} \mathrm{I}_n \mathrm{I}_{-n} + \sum_{n=2}^{n=h} \mathrm{I}_n \mathrm{I}_{-n} +} = \sqrt{\sum_{n=-h}^{n=-2} |I_n|^2 + \sum_{n=2}^{n=h} |I_n|^2} \tag{2.111}$$

These definitions can be extended to three-phase electrical systems using effective voltages and currents:

$$V_e^2 = V_{e1}^2 + V_{eH}^2 \tag{2.112}$$

$$I_e^2 = I_{e1}^2 + I_{eH}^2 \tag{2.113}$$

where the fundamental and harmonic effective voltages for three-phase, four-wire systems are calculated by using:

$$V_{e1} = \sqrt{\frac{1}{18}\left[3\left(V_{a1}^2 + V_{b1}^2 + V_{c1}^2\right) + V_{ab1}^2 + V_{bc1}^2 + V_{ca1}^2\right]} \tag{2.114}$$

$$V_{eH} = \sqrt{\frac{1}{18}\left[3\left(V_{aH}^2 + V_{bH}^2 + V_{cH}^2\right) + V_{abH}^2 + V_{bcH}^2 + V_{caH}^2\right]} \tag{2.115}$$

and for fundamental and harmonic effective currents:

$$I_{e1} = \sqrt{\frac{I_{a1}^2 + I_{b1}^2 + I_{c1}^2 + I_{n1}^2}{3}} \tag{2.116}$$

$$I_{eH} = \sqrt{\frac{I_{aH}^2 + I_{bH}^2 + I_{cH}^2 + I_{nH}^2}{3}} \tag{2.117}$$

Moreover, for three-phase, three-wire systems these equations reduce to:

$$V_{e1} = \sqrt{\frac{V_{ab1}^2 + V_{bc1}^2 + V_{ca1}^2}{9}} \tag{2.118}$$

$$V_{eH} = \sqrt{\frac{V_{abH}^2 + V_{bcH}^2 + V_{caH}^2}{9}} \tag{2.119}$$

$$I_{e1} = \sqrt{\frac{I_{a1}^2 + I_{b1}^2 + I_{c1}^2}{3}} \tag{2.120}$$

$$I_{eH} = \sqrt{\frac{I_{aH}^2 + I_{bH}^2 + I_{cH}^2}{3}} \tag{2.121}$$

From expressions where the fundamental and harmonic components have been separated, quality indexes for both voltage and currents have been defined.

For single-phase systems, the voltage Total Harmonic Distortion (THD_V) is the ratio of the root mean square harmonic voltage to the fundamental root mean square voltage:

$$THD_V = \frac{V_{rmsH}}{V_{rms1}} \tag{2.122}$$

Similarly the current Total Harmonic Distortion (THD_I) is:

$$THD_I = \frac{I_{rmsH}}{I_{rms1}} \tag{2.123}$$

These definitions can be extrapolated to three-phase systems using effective voltages and currents for the calculation of equivalent total harmonics, as follows:

$$THD_{eV} = \frac{V_{eH}}{V_{e1}} \tag{2.124}$$

$$THD_{eI} = \frac{I_{eH}}{I_{e1}} \tag{2.125}$$

When the root mean square values are calculated using a per unit system the harmonic root mean square values give directly a quality index in relation with the base voltage and current values. In the case of current this values will be equal to Total Demand Distortion (TDD) and in the case of voltage, this quality index will be in relation to the base voltage value instead the voltage fundamental value. These quality indices will be used in the next chapters (3, 4 and 5) of this work.

2.8.3 Apparent and Non-active Power definitions

Using equations (2.100) and (2.101), the apparent power for single-phase systems can be defined as the product of the root mean square voltage and current values:

$$S_{1\phi} = V_{rms} I_{rms} \tag{2.126}$$

and the non-active power as the difference of the average active power and the apparent power

$$N_{1\phi}^2 = S_{1\phi}^2 - P_{1\phi}^2 \tag{2.127}$$

The effective apparent power definition, applied to a three-phase system, is given by:

$$S_e = V_e I_e \tag{2.128}$$

Then the non-active power is defined by:

$$N_e^2 = S_e^2 - P_e^2 \tag{2.129}$$

and the effective power factor as:

$$pf_e = \frac{P_e}{S_e} \tag{2.130}$$

2.9 Conclusions

Research work on harmonic power flows is a challenging research exercise. Fundamental work pursuing different lines of study has been carried out; laying a solid theoretical foundation for the analysis of non-linear circuits in the next chapters. The use of conservative powers and quasi-powers, resting on the foundation afforded by Tellegen's theorem, is central to this endeavour. In particular, the use of the Hilbert Transform, analytical signals and the use of analytical instantaneous symmetrical components will be expanded to be able to analyse multi-frequency, three-phase power systems. The association between the Tellegen's theorem and Hilbert Transform is the contribution of this chapter.

In particular, the analytical instantaneous representation of voltage and current enables a seamless exchange between the time and frequency domains. In fact the frequency domain representation is simplified when a real signal is converted in to an analytical signal. The analytical signal representation makes possible the mathematically correct application of quasi-instantaneous symmetrical components and then time and frequency domain symmetrical components yield a true equivalence. From analytical quasi-instantaneous symmetrical components a set of different parameters can be extracted: impedance, admittance, power and quasi-power. The utilisation of this information for condition monitoring of electrical machinery is relevant. One of these parameters, the instantaneous frequency extracted from analytical instantaneous positive sequence, apparently overcomes the problem of the existence of negative frequency values, but further research is required in this point.

In addition the IEEE Standard 1459 [2000] definitions such as root mean square values, total harmonic distortion, apparent and non-active powers have been revisited. These can be obtained directly from harmonic conjugate components which will be the raw data of simulation results of further chapters, establishing guidelines for its use in single and three-phase electrical systems under non-sinusoidal and unbalanced condition.

3 Modelling of Arc Discharge Lamps

3.1 Introduction

Most of today's lighting needs are being met with the use of electric arc discharge lamps. Owing to their high efficiency and relatively low cost, the market for arc discharge lamps is quite buoyant and poised to remain so for many years to come; it has been reported that in 2005 alone the annual worldwide production of these lamps stood at 1.2 billion units [Zissis 2000]. These devices are of very low rating but their nature is a highly non-linear one and, on aggregate, they form an important component of the load system that requires attention. Indeed, the total energy consumption of arc discharge lamps has been put at almost twenty percent of all the electrical power generated [Zissis 2000].

The voltage-current characteristic of the electric arc in discharge lamps operating at power frequencies, i.e. 50 and 60 Hz, is non-linear and acts as a harmonic voltage source. Moreover, a ballast element, in the form of an iron core reactor, is connected in series with the tube to enable proper working of the lamp circuit [Francis 1948]. The adverse characteristic of these lamps may be overcome by operating the lamp circuit at high frequencies, in the region of kilohertz. This, however, is at the expense of replacing the iron core reactor by a solid-state frequency converter into the lamp circuit, shifting the non-linearity from the arc plasma to the silicon rectifier-inverter circuit and adding extra cost. However, this may be justified on grounds of energy savings as arc discharge lamps with electronic ballasts of the frequency conversion type consume lower watts than the traditional arc discharge lamps operating at power frequencies and using a series reactor as ballast. Nevertheless, iron core ballasts have been used for more than six decades and will continue to be used for as long as there is a marked differential price between the two kinds of lamp systems; those that use electromagnetic ballasts and operate at power frequencies and those that use an electronic ballast to act as a frequency converter.

Over the years, theoretical and practical approaches have been taken to study the arc in discharge lamps, with some of the early work relying on the use of measured instantaneous voltage-current characteristics to gain an understanding of arc behaviour [Campbell *et al.* 1953]. Qualitative and experimental work on arc discharge lamps has

gone hand-in-hand with the development of differential equations for the analysis and design of operating circuits [Peak and Spencer 1968], [Lowke and Zollweg, 1975] and [Bo and Masumi 1976]. These formulations model the electric arc with varying degrees of approximation and, with the exception of [Bo and Masumi 1976], use the electron density as their state variable. Notably, the dynamic model in [Bo and Masumi 1976] uses the arc conductance as state variable; enabling a seamless interfacing with the ballast circuit model. These dynamic models of the arc discharge lamp are calculated using numerical integration for direct time domain solutions. Alternatively, a reliable and accurate dynamic model of the arc discharge tube that also uses the arc conductance as state variable is well established, with the solution carried out in the frequency domain using iterations and harmonically related phasors [Acha *et al.* 1990]. It should be noted that non-dynamic models of the electric arc based on the use of the signum function [Gluskin 1999] and empirical relations [Chang 2003] have also been developed, these models produce fair results. Moreover, the latter reference [Chang 2003] successfully combines an empirical model of the electric arc with a harmonic domain model of an iron core [Semlyen *et al.* 1988], as ballast, for an iterative solution using harmonic domain techniques.

3.2 Modelling

The traditional fluorescent lamp circuit shown in Figure 3-1 comprises the lamp tube, the iron core ballast, a power factor correction capacitor and a starter capacitor. The first two components exhibit non-linear behaviours whereas the power factor correction capacitor may be assumed to perform linearly and it is an optional element. The starter capacitor is of low rating and it is neglected for the purpose of periodic steady state analysis.

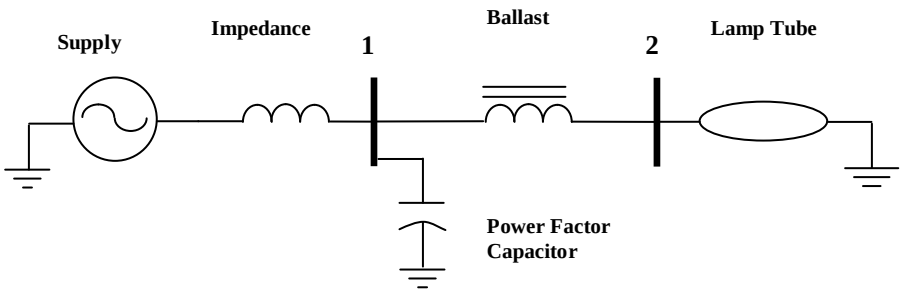

Figure 3-1 Fluorescent lamp circuit

Harmonic domain modelling and simulation techniques enable the assessment of the periodic steady state behaviour of fluorescent lamp circuits in a comprehensive manner. The key point in the characterisation of these kinds of circuits is the use of a non-linear differential equation representing the dynamics of the electric arc tube [Acha *et al.* 1990]. If the aim is to study the periodic steady state behaviour of the circuit then the differential equation may be converted into an algebraic equation using well established harmonic domain operations such as harmonic phasor vector representation of state variables, discrete convolutions, polynomial evaluations, Newton-Raphson iterative solutions and harmonic Thevenin and Norton equivalent circuits [Acha and Madrigal 2000].

3.2.1 Lamp tube model

An instantaneous power balance equation for an electric arc forms the basis of a dynamic model for the electric arc tube, where conductance g_a replaces the arc radius r as state variable in the original differential equation [Acha *et al.* 1990]. Hence,

$$g_a = \frac{i}{v} \tag{3.1}$$

where v is the voltage across the lamp tube and i is the current through it.

The dynamic equation of the electric arc tube is:

$$k_1 g_a \frac{\mathrm{d}g_a}{\mathrm{d}t} + k_2 g_a^2 = k_3 i^2 \tag{3.2}$$

where coefficients k_1, k_2 and k_3 are lamp-specific parameters, adjusted by experimentation to reproduce the measured characteristic of the lamp at the power frequency. For instance, for a 30 W, 240 V lamp the values of constants k_1, k_2 and k_3 are 1, 0.0625 and 2500, respectively.

A number of mathematical transforms applicable to the analysis of periodic waveforms exist for converting the differential equation of the arc discharge tube into an algebraic dynamic equation suitable for direct calculation of the periodic steady state solution using harmonic phasorial methods. The non-linear differential equation (3.2) transforms into the following algebraic equation:

$$\mathbf{F} = k_1 \mathbf{G_A} \mathbf{D}\left(\mathrm{j}h\omega_0\right)\mathbf{G_A} + k_2 \mathbf{G_A}^2 - k_3 \mathbf{I}^2 \tag{3.3}$$

Likewise, the algebraic equation (3.1) becomes:

$$\mathbf{G_A} = \mathbf{V}^{-1}\mathbf{I} \tag{3.4}$$

If the analysis is conducted on the complex conjugate multi harmonic space of Fourier [Semlyen *et al.* 1988] then the arc conductance $\mathbf{G_A}$, the voltage **V** across the arc and the current **I** all become harmonic vectors of dimensions $2h+1$, where h is the harmonic order. **D** is a derivative operator vector which takes the form of a diagonal matrix of entries $\mathrm{j}h\omega_0$, where $\omega_0=2\pi f$ and f is the base operating frequency. It should be noted that the $\mathbf{G_A}$ term to the left of the derivative operator **D** has the structure of a Toeplitz matrix as opposed to a vector to comply with matrix algebra rules. Also, in eq. (3.4), the harmonic vector **V** becomes a Toeplitz matrix to be able to perform the operation $\mathbf{V}^{-1}$.

The non-linear algebraic equation (3.3) and its derivative with respect to conductance $\mathbf{G_A}$ are used to determine the periodic steady state solution of the arc discharge tube using a harmonic Newton-Raphson method. The harmonic vector **F**, of dimensions $2h+1$, acts as a mismatch function, which upon convergence of the iterative solution becomes smaller than a pre-specified tolerance.

3.2.2 Electromagnetic ballast model

The electromagnetic ballast is an essential component of the lamp system, whose function is to stabilize the arc tube current which otherwise would consume a large amount of current due to an intrinsic negative resistance of arcs operating at power frequencies of 50 or 60 Hz.

The ballast is essentially an iron core inductor which incurs losses and has the capacity to saturate and, hence, to act as a lossy non-linear inductor. In this particular application the ballast is series connected and the driving voltage is the voltage difference across it, which waveform is fairly distorted because it is a function of the arc lamp voltage.

A simple but quite general model to represent a lossless magnetic non-linearity in harmonic domain is available [Semlyen *et al.* 1988]; it takes the form of a harmonic Norton equivalent, derived from the following basic iron core relations:

$$i = f(\psi) \tag{3.5}$$

$$\frac{\mathrm{d}\psi}{\mathrm{d}t} = v \tag{3.6}$$

where i is the magnetizing current of the iron core inductor, ψ is the linkage flux produced in the core, determined by integration of (3.6), and v is the induced voltage. Moreover, the non-linear relationship (3.5) may correspond to a fitted polynomial [Acha and Madrigal 2001] of a measured characteristic, of the form:

$$f(\psi) = i = a\psi + b\psi^n \tag{3.7}$$

Harmonic domain modelling of relations (3.5) and (3.6)) works on the basis that incremental linearisation around a base operating point (V_b, I_b) is a valid method, leading to the following set of relations in the harmonic domain

$$\mathbf{\Delta I} = \mathbf{F}\mathbf{\Delta \Psi} \tag{3.8}$$

$$\mathbf{D}(\mathrm{j}h\omega_0)\mathbf{\Delta \Psi} = \mathbf{\Delta V} \tag{3.9}$$

These may then be expressed in a form more suitable for interfacing with other linear and linearised, non-linear elements in the electric circuit,

$$\mathbf{I} = \mathbf{Y_B V} + \mathbf{I_N} \tag{3.10}$$

where

$$\mathbf{Y_B} = \mathbf{F}\mathbf{D}^{-1}(\mathrm{j}h\omega_0) \tag{3.11}$$

$$\mathbf{I_N} = \mathbf{I_b} - \mathbf{Y_B V_b} \tag{3.12}$$

The instantaneous flux-current characteristic of the non-linear inductor (3.5), with hysteresis and eddy current effects neglected, is suitably approximated by a polynomial expression which, in turn, is amenable to harmonic domain computations

using discrete convolutions to evaluate $\mathbf{I_b}$, corresponding to a given value of $\mathbf{V_b}$ (or $\mathbf{\Psi_b}$). If complex conjugate Fourier series is used to conduct the harmonic analysis, the dimensions of vector $\mathbf{I_b}$, $\mathbf{\Psi_b}$, and $\mathbf{V_b}$ are $2h+1$, where h is the harmonic order considered. $\mathbf{F}$ is a harmonic domain vector of dimensions $2h+1$ resulting from the flux derivative of the polynomial magnetizing characteristic, which is then expressed as a Toeplitz matrix to enable the product operation in (3.11).

A more realistic model of the ballast is achieved by incorporating the resistive effects of the iron core losses due to hysteresis and eddy currents in equation (3.10). It may take the form of a harmonic conductance $\mathbf{G_B}$ which is connected in parallel with the harmonic admittance of the Norton equivalent $\mathbf{Y_B}$ representing the loss-less magnetic core. It should be noted that $\mathbf{Y_B}$ has the form of a band-diagonal matrix whose diagonal width is a function of non-linearity and $\mathbf{G_B}$ is a diagonal matrix if it is assumed that hysteresis and eddy currents are both linear effects.

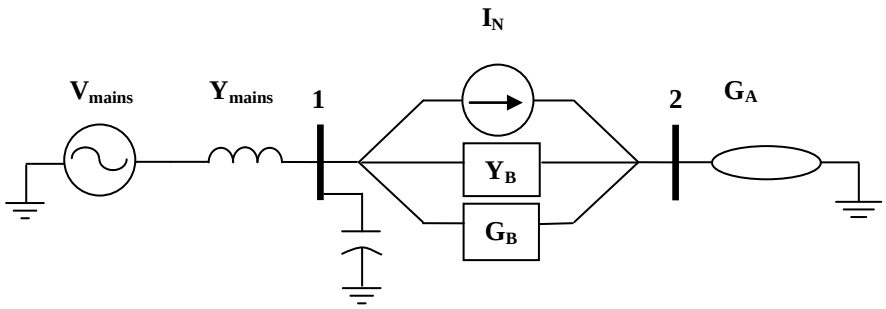

Figure 3-2 Lamp-ballast system model

As shown in Figure 3-2, in this application the harmonic Norton equivalent representing the iron core ballast, is series-connected, hence equations (3.10) and (3.12) become:

$$\mathbf{I} = \left(\mathbf{Y_B} + \mathbf{G_B}\right)\left(\mathbf{V}_1 - \mathbf{V}_2\right) + \mathbf{I_N} \tag{3.13}$$

where

$$\mathbf{I_N} = \mathbf{I_b} - \left(\mathbf{Y_B} + \mathbf{G_B}\right)\left(\mathbf{V}_{1\mathbf{b}} - \mathbf{V}_{2\mathbf{b}}\right) \tag{3.14}$$

3.2.3 Lamp-ballast system model

The combined harmonic domain model of the lamp-ballast system shown in Figure 3-2 is assembled by resorting to nodal analysis. To this end, it is useful to represent the harmonic Norton equivalent representing the ballast as a harmonic Thevenin equivalent,

$$\mathbf{V}_1 = \mathbf{V}_2 + \mathbf{Z_B I} + \mathbf{V_T} \tag{3.15}$$

where

$$\mathbf{Z_B} = \left(\mathbf{Y_B} + \mathbf{G_B}\right)^{-1} = \mathbf{F}^{-1}\mathbf{D}\left(\mathrm{j}h\omega_0\right) + \mathbf{G_B^{-1}} \tag{3.16}$$

and

$$\mathbf{V_T} = \mathbf{V_{1b}} - \mathbf{V_{2b}} - \mathbf{Z_B I_b} \tag{3.17}$$

This is then combined with the harmonic impedance $\mathbf{Z_A}$ representing the arc lamp,

$$\mathbf{V}_1 = \left(\mathbf{Z_A} + \mathbf{Z_B}\right)\mathbf{I} + \mathbf{V_T} \tag{3.18}$$

where

$$\mathbf{V}_2 = \mathbf{Z_A I} \tag{3.19}$$

and

$$\mathbf{Z_A} = \mathbf{G_A^{-1}} \tag{3.20}$$

This combined expression is more conveniently written down as a harmonic Norton equivalent:

$$\mathbf{I} = \left(\mathbf{Z_B} + \mathbf{Z_A}\right)^{-1}\mathbf{V}_1 + \mathbf{I_{BA\,N}} \tag{3.21}$$

where

$$\mathbf{I_{BA\,N}} = \left(\mathbf{Z_B} + \mathbf{Z_A}\right)^{-1}\left(\mathbf{Y_B} + \mathbf{G_B}\right)^{-1}\mathbf{I_N} \tag{3.22}$$

The conductance of the arc lamp model and the Norton equivalent representing the magnetic ballast are solved separately. Equations (3.21) and (3.22) are assembled to carry out an iteration of the combined lamp-ballast system. The iterative procedure is halted when the voltage mismatch at all nodes become smaller than a pre-specified tolerance. This is explained in more detail in Section 3.3.

3.3 Lamp-Ballast Algorithm

The solution of the lamp-ballast system requires the following basic information: the voltage and equivalent reactance (impedance) of the supply system used to feed the lamp-ballast circuit. The latter may comprise the transformer's short-circuit reactance, together with the equivalent resistance and reactance of wires. The reactance of the power factor corrector capacitor is given in cases when this element forms part of the circuit. The ballast is a non-linear inductor, which for the purpose of this application is represented by a polynomial expression; coefficients *a*, *b*, and exponent *n* are derived from the ψ-*i* experimental characteristic. A family of electric arc tube characteristics are obtained by simulations, for different values of coefficients k_1, k_2 and k_3; the best match between the simulated and measured characteristic is selected. The corresponding coefficient set k_1, k_2, k_3, *a* and *b*, and exponent *n* are fed into the data set for generic studies of the lamp system.

As shown in the flow diagram in Figure 3-3, the data system and initial conditions for carrying out the iterative solution of the lamp-ballast system are provided and the iteration counters *k* and *l* are set to 1. With the assumed initial arc current and an assumed non-distorted arc tube voltage, eq. (3.3) is solved and checked for convergence. If the function norm is smaller than a pre-specified tolerance, $\varepsilon_1 < 10^{-12}$, the inner iterative loop is abandoned. Otherwise, a new value of arc conductance is calculated using a Newton-Raphson solution of eq. (3.3). This involves evaluation of the harmonic Jacobian of eq. (3.3), calculation of the harmonic conductance increments and the updating of harmonic conductances at iteration *l* [Acha and Madrigal 2000]. Upon convergence of eq. (3.3), the arc tube voltage is calculated using eq. (3.4) with which the voltage difference across the ballast is determined to derive all the constituent elements of eq. (3.10).

It should be noted that when k=1, i.e. first global iteration, the voltage at node 1 in Figure 3-2 is sinusoidal. The combined system comprising the arc tube conductance, the Norton equivalent representing the linearised ballast and linear representations of the power factor corrector capacitor and Thevenin equivalent of the power supply is solved in the form of a supply current represented by eq. (3.21). This current which has a sinusoidal form at the beginning of the iterative process, e.g. k=1 and l=1, become non-sinusoidal at the end of the global iterative solution; a process that is halted when the difference between the harmonic currents in two successive iterations is smaller than a pre-specified tolerance, $\varepsilon_2<10^{-12}$. This tight tolerance is used for testing the algorithm, generally power flow programs which used Newton Rahpson method use a tolerance, $\varepsilon_2<10^{-12}$, [Acha *et al.* 2004] but the mismatch is with power values, using current or voltages a tolerance, $\varepsilon_2<10^{-6}$, would be adequate.

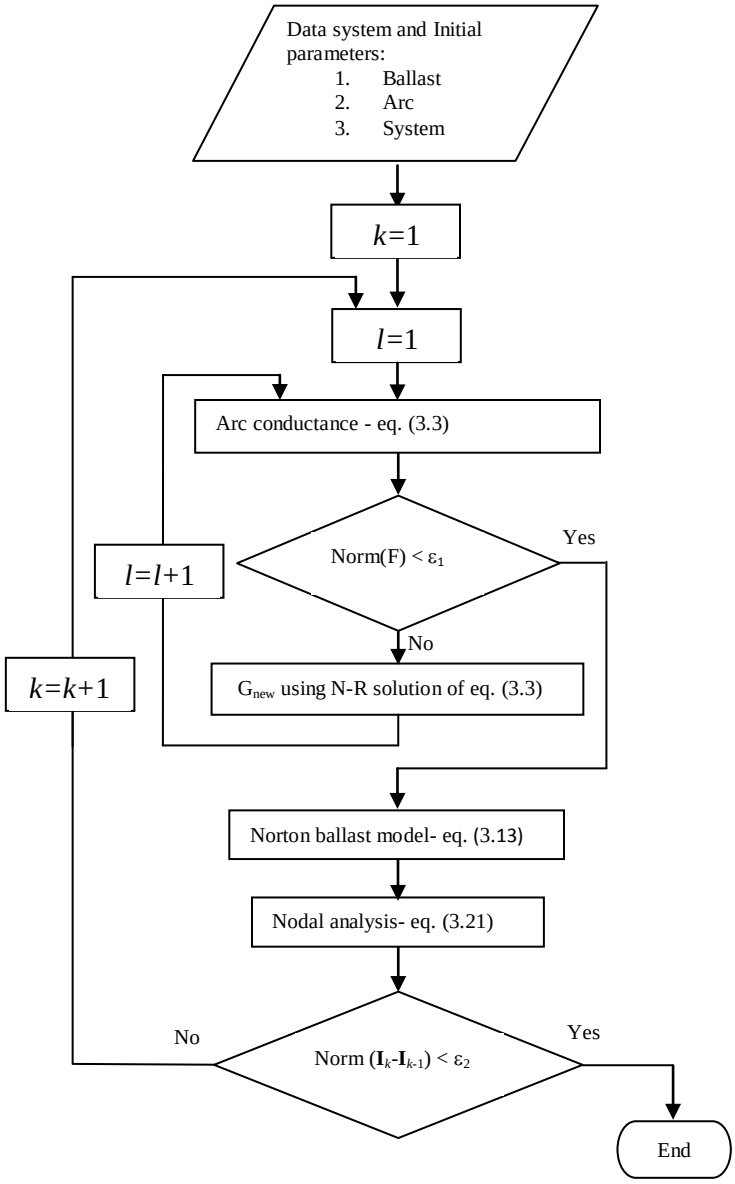

Figure 3-3 Flow diagram of the lamp-ballast system

3.4 Simulation Results and Laboratory Measurements

The proposed algorithm of Figure 3-3 has been coded in Matlab and applied to solve several test cases, some of which have been compared with actual measurements in the laboratory

The experimental setup for the individual lamp comprises a variable power supply (0-260V), a lamp tube of 65 W, 240 V, an electromagnetic ballast, a starter capacitor, an oscilloscope (Tektronic TDS3034) and a power analyser (PM100-Voltech). The variable power supply regulates the network voltage, which is found to contain

distortion. The RMS voltage and THD_V values are 244 V and 2.6735%, respectively.

The electromagnetic ballast used in the laboratory was measured; the core loss was 21.2 Ω and the top-half of its instantaneous flux-current characteristic is shown in Figure 3-4

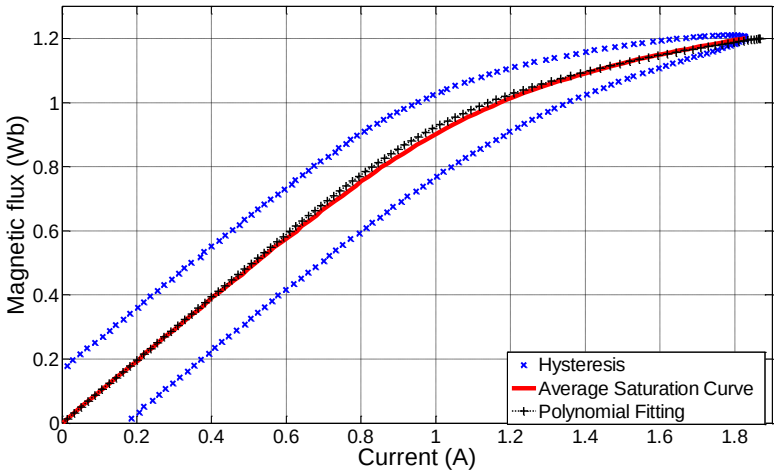

Figure 3-4 Flux-current characteristic

The average characteristic, representing the "lossless" core, is also shown in Figure 3-4 together with a fitted characteristic given by the following polynomial equation:

$$i = 0.9849\psi + 0.125\psi^9 \qquad (3.23)$$

The dynamic characteristic of the lamp tube was also measured in the laboratory, from which the parameters of the differential equation (3.3) were determined by trial-and-error, giving: k_1=1, k_2=0.100046 and k_3=1456.7.

The relevant parameters are fed into the lamp-ballast system computer program, summarised by the flow diagram shown in Figure 3-3, to calculate the voltage and current waveforms generated by the combined non-linear system.

The results in Figure 3-5, show the measured and the calculated voltage-current characteristics of the lamp tube.

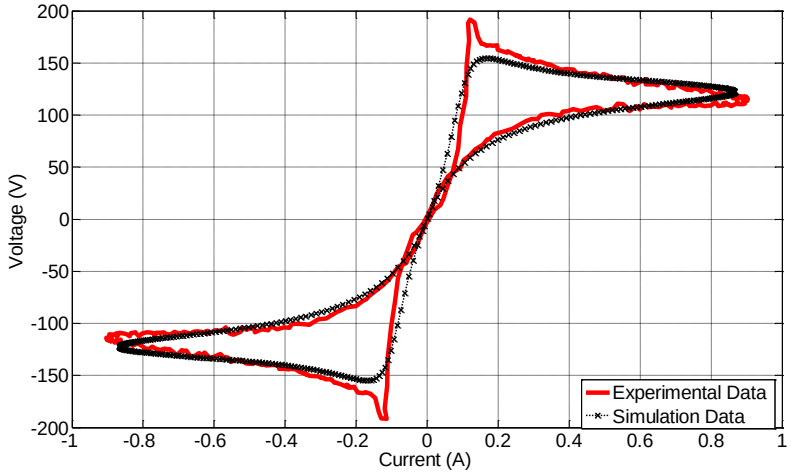

Figure 3-5 Experimental and simulated current-voltage characteristics of the lamp tube

For completeness, one full period of the arc voltage and current are shown in Figure 3-6 and

Figure 3-7 respectively, where experimental and measured current waveforms are shown to be in good agreement, with some differences observed between the two voltage waveforms, particularly in the "peaky" region of the measured voltage waveform.

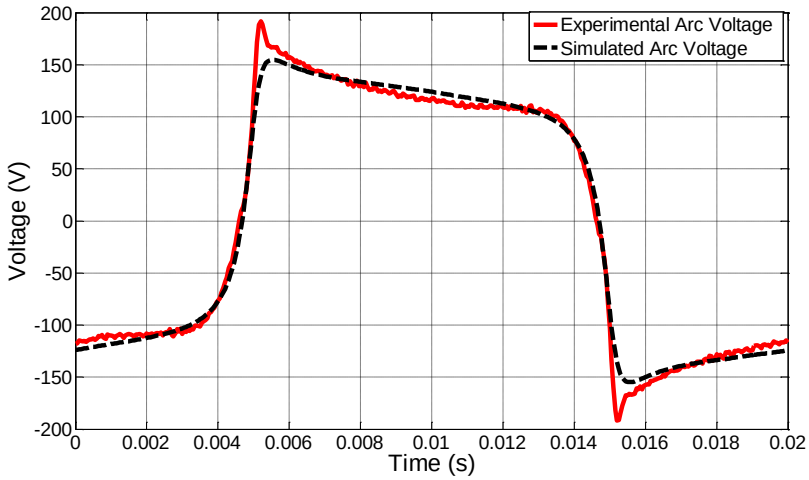

Figure 3-6 Measured and simulated voltage waveforms in the lamp tube

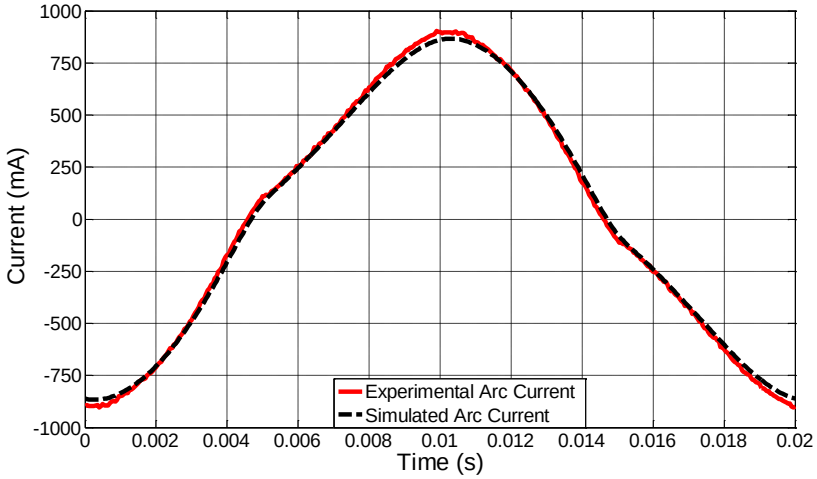

Figure 3-7 Measured and simulated current waveforms in the lamp tube

The harmonic contents of the experimental and simulated arc conductances are shown in Figure 3-8 It is timely to remember at this point that the lamp tube model used in this study uses the arc conductance as state variable and that the numerical solution takes place in the harmonic domain, where the values of the base conductance (G_0) and harmonic conductances (G_h) shown in Figure 3-8 are direct outputs from the simulation program. The "experimental" harmonic conductances, on the other hand, are derived from the experimental voltage and current waveforms and the use of a FFT. Both set of results are in close agreement.

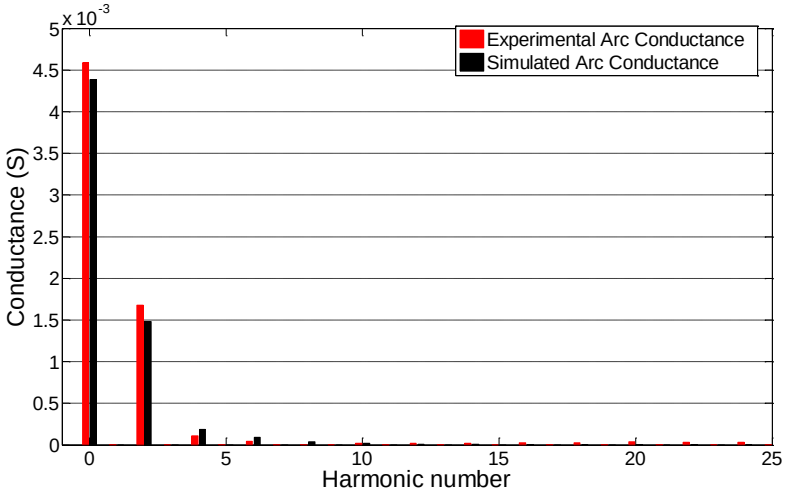

Figure 3-8 Harmonic arc conductance

Referring to flow diagram shown in Figure 3-3, a typical iterative solution of the lamp-ballast system converges in 34 external iterations, as is illustrated in Figure 3-9 to a current mismatch tolerance of 1×10^{-12}. The total number of internal iterations is 97.

Within one external iteration, the algorithm may take between five to one internal iterations to converge to a function mismatch tolerance of 1×10^{-12}, since the inner loop corresponds to a true Newton Raphson solution. The number of internal iterations required decreases as the number of external iterations progresses due to a better initialisation of the state variables in the Newton-Raphson solution.

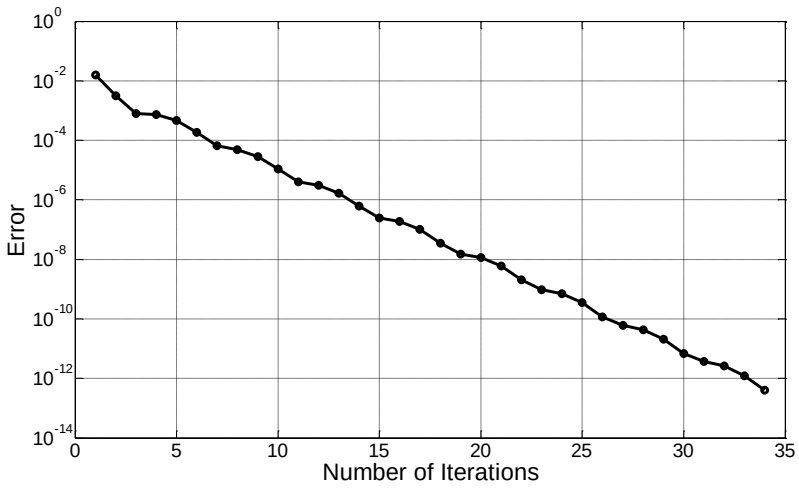

Figure 3-9 Error vs iteration number

Measurements and simulations for the complete lamp-ballast system, with the power factor correction capacitor included, were also carried out. By way of example, one full period of the current waveforms are shown in Figure 3-10.

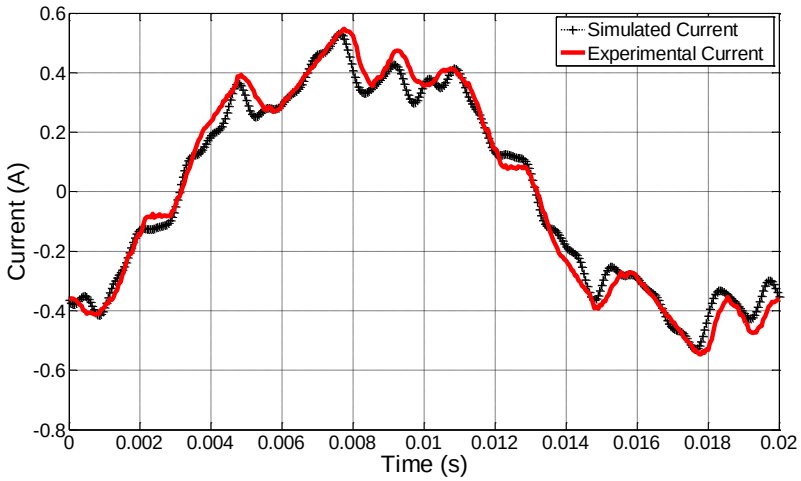

Figure 3-10 Currents in the lamp-ballast system with power factor correction capacitor fed from a distorted power supply

It is interesting to note that due to the interaction of the distorted supply voltage and the power factor correction capacitor the distortion in the lamp system current exacerbates. The circuit power factor improves to 0.8365 from a previous value of 0.4845 but this is

at the expense of an impoverished THD_I which worsens to 19.46% from a previous value of 8.95%. An equally important observation is the ability of the lamp system model, with the power factor correction capacitor included, to match reasonably well the experimental results.

3.5 The Aggregated Lamp Model

The use of individual arc discharge lamp models for simulation studies where several of these appliances are connected may be computationally expensive. In particular, when harmonic domain simulation methods are used since the size of the harmonic admittance matrix may grow excessively the use of aggregated models become attractive. To this end, the single lamp system model developed in section 3.2 may be expanded to become an aggregated model which represents several lamps of the arc discharge type. This model permits to represent *N* number of lamps to asses their effect in an electrical installation.

3.5.1 The aggregated arc lamp model

The main modification introduced with respect to the one-arc-lamp model is the use of a *ki* constant derived as the ratio of the nominal current of a measured and the nominal current of a non-measured lamp. From the solution of equation (3.3), solved using coefficients k_1, k_2 and k_3 which are lamp-specific parameters of the original lamp, V_{Arc} can be calculated using equation (3.4) which is akin to using equation (3.24), where I_{Arc1} and Gm_1 are the arc current and conductance of the original lamp respectively. This information is used as the basis to calculate the parameters of a non measured lamp, as follows:

$$V_{Arc1} = \left(Gm_1\right)^{-1} I_{Arc1} \tag{3.24}$$

$$V_{Arc2} = \left(Gm_2\right)^{-1} I_{Arc2} \tag{3.25}$$

If it is assumed that the current in both the original and new lamps contains little harmonic distortion then equation (3.26) defines a scalar number *ki* which is the ratio of currents values of the original lamp and new lamp.

$$ki = \frac{I_{Arc2rms}}{I_{Arc1rms}} \tag{3.26}$$

Since the voltages of both lamps, are assumed to be identical, an alternative form of the *ki* coefficient calculation can be carried out using the ratio of average power of the original lamp model and the average power of the new lamp

$$ki = \frac{P_2}{P_1} \tag{3.27}$$

3.5.2 The aggregated ballast model

The arc discharge lamp and the magnetic-ballast become one system, which cannot be separated in practice. If the arc voltages are equal, then the adjustment required for the new ballast model is the multiplication of the Norton current $\mathbf{I_{NB1}}$ and the Norton admittance $\mathbf{Y_{NB1}}$ by the factor *ki* given by (3.26)

$$\mathbf{Y_{NB2}} = ki\mathbf{Y_{NB1}} \tag{3.28}$$

$$\mathbf{I_{NB2}} = ki\mathbf{I_{NB1}} \tag{3.29}$$

3.5.3 The aggregated lamp-ballast model

One way to construct the aggregated lamp model of *N*-lamp-ballast installation with lamps of different capacities is for the constant *ki* to become *N.ki*. If a ballast is represented by a Norton equivalent (**In** and **Yb**) and the lamp by a conductance **Gm** then according to equations (3.30) and (3.31),

$$\mathbf{Yeq} = \left[\left(Nki\mathbf{Y}_{\mathbf{NB}} \right)^{-1} + \left(Nki\mathbf{Gm} \right)^{-1} \right]^{-1} = Nki \left[\left(\mathbf{Y}_{\mathbf{NB}} + \mathbf{Gm} \right)^{-1} \right]^{-1} \tag{3.30}$$

$$\mathbf{Ineq} = \left[\left(Nki\mathbf{Y}_{\mathbf{NB}} \right)^{-1} + \left(Nki\mathbf{Gm} \right)^{-1} \right]^{-1} \left[\left(N\mathbf{Y}_{\mathbf{NB}} \right)^{-1} N\mathbf{I}_{\mathbf{NB}} \right] = Nki \left[\left(\mathbf{Y}_{\mathbf{NB}} + \mathbf{Gm} \right)^{-1} \right]^{-1} \left[\mathbf{Y}_{\mathbf{NB}}{}^{-1}\mathbf{In} \right] \tag{3.31}$$

3.5.4 Aggregated lamp-ballast model system

The one-line diagram of Figure 3-11 comprising the voltage mains, an equivalent ballast Norton equivalent and an equivalent fluorescent lamp, is used to represent an installation consisting of N lamps of equal rating, where ki=1 if at least one of the lamps has been measured and $ki \neq 1$ if no lamp has been measured. The analysis is carried out using a harmonic system of equations where each nodal voltage and nodal current is a vector of $2h+1$ dimensions. Likewise each admittance entry into the overall nodal admittance matrix representing the circuit of Figure 3-11 is a matrix of $2h+1$ x $2h+1$ dimensions.

$$\begin{bmatrix} \mathbf{V}_1 \\ \mathbf{V}_2 \\ \mathbf{V}_3 \end{bmatrix} = \begin{bmatrix} \mathbf{Y}_{\mathbf{Mains}} & -\mathbf{Y}_{\mathbf{Mains}} & \mathbf{0} \\ -\mathbf{Y}_{\mathbf{Mains}} & \mathbf{Y}_{\mathbf{Mains}} + Nki\mathbf{Y}_{\mathbf{NB}} & -Nki\mathbf{Y}_{\mathbf{NB}} \\ \mathbf{0} & -Nki\mathbf{Y}_{\mathbf{NB}} & Nki\mathbf{Y}_{\mathbf{NB}} + Nki\mathbf{Gm} \end{bmatrix}^{-1} \begin{bmatrix} \mathbf{0} \\ -Nki\mathbf{I}_{\mathbf{NB}} \\ Nki\mathbf{I}_{\mathbf{NB}} \end{bmatrix} \tag{3.32}$$

Figure 3-12 represents the circuit of Figure 3-11 but with the supply system transformed into a Norton equivalent. The reduced system of equations is:

$$\begin{bmatrix} \mathbf{V}_2 \\ \mathbf{V}_3 \end{bmatrix} = \begin{bmatrix} \mathbf{Y}_{\mathbf{Mains}} + Nki\mathbf{Y}_{\mathbf{NB}} & -Nki\mathbf{Y}_{\mathbf{NB}} \\ -Nki\mathbf{Y}_{\mathbf{NB}} & \mathbf{Y}_{\mathbf{NB}} + Nki\mathbf{Gm} \end{bmatrix}^{-1} \begin{bmatrix} \mathbf{Y}_{\mathbf{Mains}}\mathbf{V}_1 - Nki\mathbf{I}_{\mathbf{NB}} \\ Nki\mathbf{I}_{\mathbf{NB}} \end{bmatrix} \tag{3.33}$$

This equation permits the calculation of the arc current:

$$\mathbf{I}_{\mathbf{Arc}} = Nki\mathbf{Y}_{\mathbf{NB}} \left[\mathbf{V}_2 - \mathbf{V}_1 \right] + Nki\mathbf{I}_{\mathbf{NB}} \tag{3.34}$$

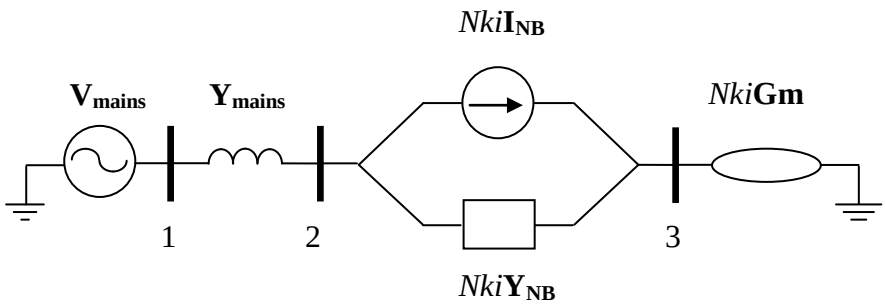

Figure 3-11 One-line diagram of the aggregated model

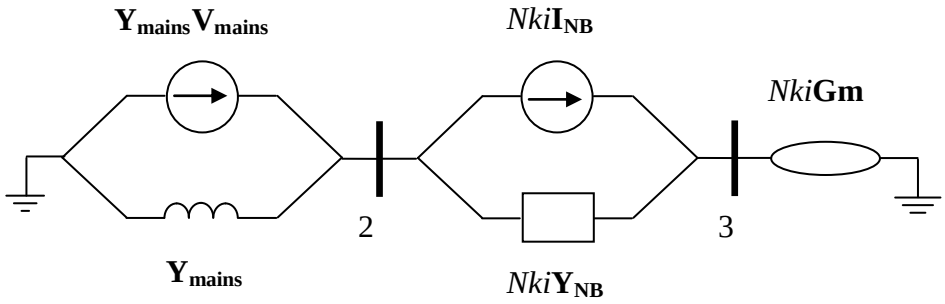

Figure 3-12 Equivalent circuit of the aggregated model

3.5.5 Algorithm of the aggregated lamp-ballast system

The procedure for the calculation of the system voltages and currents are similar to the one presented in the flowchart of Figure 3-3, but with some parameters adjusted.

The lamp coefficients of the original lamp: k_1, k_2 and k_3 and coefficients of the original ballast: *a*, *b* and *n* are provided together with the supply voltage *V*, equivalent impedance *R*, *X* and arc current nominal value *I*. The rating and number of the new lamp are specified by the *ki* coefficient and the number of lamps *N*. Second, the mismatch *mis01* is calculated if the mismatch *mis01* is not smaller than a specified tolerance then an iterative loop is entered where the lamp equation is solved for the original lamp models, then the conductance **Gm** is modified by the multiplication of *ki* coefficient.

In the third block, the Norton ballast model is solved for the original ballast (3.33) and then the Norton current $\mathbf{I}_{\mathbf{NB}}$ and Norton Admittance $\mathbf{Y}_{\mathbf{NB}}$ are modified by the *Nki* coefficient.

In the fourth block, nodal analysis is applied in the form of equation (3.43) and the new $\mathbf{I}_{\mathbf{Arc}}$ is calculated and then divided by the *ki* coefficient and the action is returned in the iterative loop. The zero frequency (dc) component of the calculated G is used as initial value in the iterative loop.

The *Nki* coefficient simplifies to *N* if the lamp corresponds to lamp of the same rating as the original lamp.

3.5.6 Simulation results

Groups of lamp-ballast systems with a different number of lamps but with the same characteristics as that used in section 3.4, are assumed to be connected to a single-phase dry transformer of 100 kilovolt-amperes with an impedance of 5 per cent. The number of lamps contained in each set will be 200, 400 and 600 lamps, with *ki* equal to 1. The current voltage characteristics for these lamp sets are shown in Figure 3-13

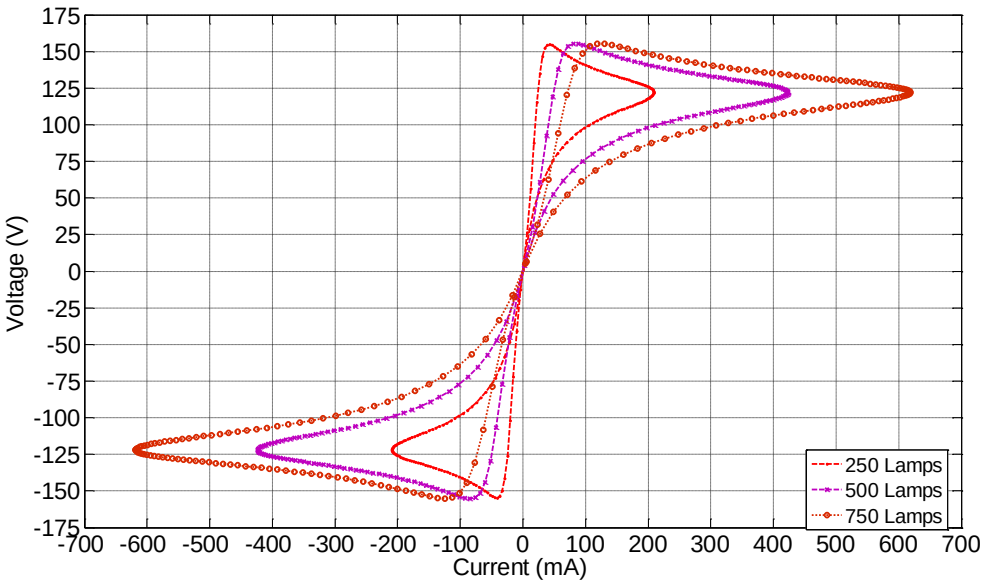

Figure 3-13 Current-voltage characteristics for different number of lamps

The root mean square of voltages and currents; Total Harmonic Distortions (THD) and Total Demand Distortion (TDD) for each set are given in

Table 3-1. This shows that this aggregated equivalent model is affected by system conditions and it is not a linear extrapolation of the results generated by a single-lamp system model.

N	V_{rms}	I_{rms}	THD_V	THD_I	TDD
250	236.26	142.87	0.4193 %	7.1854 %	2.4576 %
500	232.72	278.79	0.8272 %	7.1317 %	4.7598 %
750	229.36	408.35	1.2255 %	7.0907 %	6.9319 %

Table 3-1 Effect of lamp-balast groups on quality indexes using the aggregated model

The aggregated lamp-ballast model is used to carry out a further numerical example. A T8 lamp tube of 30 W, 240 V has parameters k_1=1, k_2= 0.116875 and k_3= 922.5092 with an electromagnetic ballasts with parameters a =0.5661301 b =0.0940873 and n =9 and a series resistance R =30.8568. It is assumed that 1056 lamps are connected to the same dry transformer of the previous example. This number of T8 lamps compare in terms of luminosity to approximately 500 lamps of 64 W. The

Table 3-2 shows the different parameters for the two set of lamps. The lamp average active power consumption nearly has the same value in both sets, but the active power delivered to T8 set is higher with a difference of 745 W attributed to losses. The current and the apparent power differ in great proportion in both set that produce a power factor of 0.5179 for the T12 set and 0.4017 for the T8 set. The power quality indexes THD_V and TDD hold similar values but the THD_I presents a big difference occasioned by the difference in current values. In consequence for this case the major difference between both sets is the non-active power consumption.

Lamp mod	N	P_{lamp}	V_{rms}	I_{rms}	THD_V	THD_I	TDD	P	S
	units	W	V	A	%	%	%	watts	vars
T12	500	30309	232.72	278.79	0.8272	7.1317	4.759	33605	64881
T8	1056	30304	229.75	372.12	0.7381	4.8692	4.343	34350	85497

Table 3-2 Comparison between the T12 and T8 lamp-ballast Models

3.6 Conclusions

In this work the theory of harmonic domain has been applied to model a full arc discharge lamp system comprising the electric arc tube, the reactor ballast and the power factor correction capacitor. The harmonic domain has been used previously to solve both the non-linear system of equations representing the arc plasma and the non-linear system of equations representing the ferromagnetic core. However, this is the first time that the combined models of the electric arc tube and the ballast's iron core have been solved in the harmonic domain. In the frame-of-reference afforded by the harmonic domain the periodic steady-state solution is calculated directly, with no need to calculate the transient response of the circuit. From the numerical point of view, the harmonic domain solution is essentially a harmonic balance technique where no time domain representation is involved for any of the participating variables; but only fundamental and harmonically related phasors. The harmonic balance is arrived at by iteration, using repeated linearisation. Simulation results for the lamp-ballast system are in good agreement with measurements carried out in the laboratory; including voltage and current waveforms, RMS values and average and apparent powers. Circuits with and with no power factor correction capacitor were studied. In the latter case, owing to a pre-existing distortion in the voltage power supply, the current becomes quite distorted, and although the capacitor does improve the power factor this is at the expense of an impoverished power quality.

In addition a simple aggregated model was derived from the single lamp-ballast system to include an N number of lamps; this permits the simulation of large electrical lighting installations in order to asses the impact of a large number of different lamps models in a three-phase electrical system and is neutral wire.

4 Electric Arc Furnace

4.1 Background on Electric Arc Furnace Installations

According to the International Iron and Steel Institute (IISI) report [2007] the quantity of world crude steel production reached 1,239.5 million metric tons for the year 2006, the highest level of crude steel output in history. In addition this was the third consecutive year that the mark of one billion tones had been superseded. The world steel production using electric arc furnaces (EAF) increased from 26.6 % to 33.6 % in the period 1988-1997, which means an annual average increase of 2.63 %. If the amount of energy to produce one metric ton of steel is between 300 and 500 kW-hr then it is not difficult to estimate the enormous quantity of electrical energy which goes into an electric arc furnaces process, as presented in Figure 4-1. This basic information throws some awareness as to how important the study and analysis of the electric arc furnace process really is, with the goal of finding guidelines for saving energy and resources.

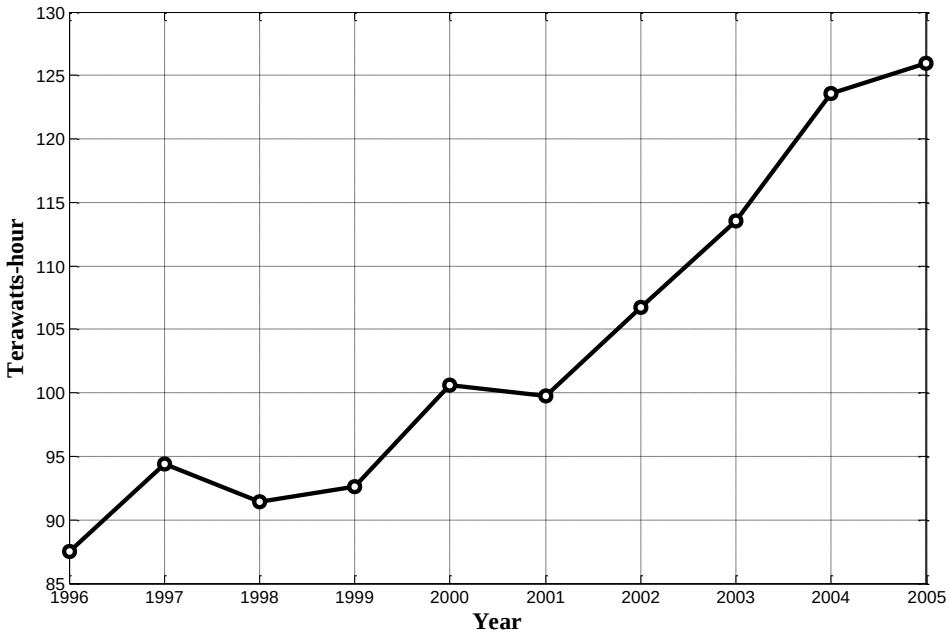

Figure 4-1 Global trend of electric energy consumption in electric arc furnace installations

The electric arc furnace design and operation has evolved over the years with improvements implemented in this kind of steel making process [B. Bowman 1997] part of this progress is directly related to electrical system improvements. Two examples

will be mentioned: the first one is the Ultra High Power (UHP) electric arc furnace, introduce in the USA in the sixties. This concept has its basis in the utilisation of a low reactance system that enables the delivery of high power. A low reactance design requires improving the secondary circuit comprising cables, buses, and lower impedance transformers. This led to the development of new designs of this kind of equipment, where modelling and simulation played an important role. The second example is a direct improvement of the electrical characteristic of electric arc furnace installations, which involves use of a high series reactance on the primary side of the furnace transformer. The goal is to increase arc stability and to operate with lower currents in conjunction with a high power delivery.

In the improvement path of the electrical arc furnace it was realised that not only the electric features of the electric arc furnace affected the electrical system but so did its philosophy of operation. The philosophy of operation differs from one region of the world to another, North America, Europe and Japan, where different goals are pursued in relation to the characteristics of power delivery; i.e. energy cost and existence of weak systems. The installation of new electric arc furnaces requires a comprehensive set of studies to assess the effect that the new installation or upgrade will have in the electrical network. Such studies can be carried out with appropriate models which permit the simulation of the complete system.

The large amount of energy required by the electric arc furnaces has further effects in the electrical power network. Chief among these is the lack that the electric arc is a non-linear phenomenon that affects the power quality. Several challenges have arisen through out the years in the elimination or attenuation of such adverse effects, and special recommendations and standards have been developed, i.e. [IEEE Standard 519 1992] for harmonics and [IEEE Std 1453 2004] for flicker.

In addition, the large quantities of electrical energy delivered to electric arc furnaces call for the compensation of non-active power, with the use of simple fixed banks of capacitors not really being an option due to the effect of harmonics and the dynamics of the load. Passive filters have proved useful for the cancellation of harmonics but they are unable to provide dynamic compensation. The development of high power, high current semiconductor devices has enable the construction of

equipment, such as the Static Var Compensator (SVC) and the STATCOM which can interact dynamically with the electrical power system, including electrical arc furnace installations. This kind of compensation equipment possesses non-linear characteristics and is well modelled in the harmonic domain as it will be addressed in the next chapter.

The case is made in this work that the integration of the arc model in the global representation of the electrical power network is of vital technical importance because of the many undesirable situations arising from the interaction of the electrical network with the non-linear behaviour of the electric arc. An advanced model of the electric arc and its integration with the electrical equipment and network models would enable comprehensive simulations studies which would give valuable information on the impact of impedance system changes, reactive compensation, transformer specifications and anomalous situations that may arise such as load unbalances. Other possible uses include the experimentation by simulation of the impact of new devices for the control and stabilization of the electric arc, filter design, and the effect that future utility expansions will have in the arc furnace installation.

4.2 Electric Arc Characterisation

Electric arcs have been the subject of multiple studies, owing to the importance that the accompanying non-linear phenomenon has in various applications. For example, progress made in the design of circuit breakers and electric arc furnaces had their basis on experimental and theoretical research of the electric arc, as documented by Philips [1967], who referenced the research that had been carried out by Cassie [1939] and Mayr [1943] in relation to circuit breaker design. In neither of these formulated models the radial variation of the arc was included. Further work by Philips [1967] resulted in a set of equations that provided a description of the energy transfer process within the electric arc; these are the well-established multi-component conservation equations. This approach was confirmed shortly afterwards by Lowke [1979]. An review and extended research work on this interesting phenomena is contained in the document "The Physics of High-power Arc" written by Jones and Fang [1980], where it is established that the behaviour of high-power arcs at high pressures ($\geq$ 1bar) is mainly governed by the physical properties of the plasma column. A general theory of the arc

column is presented where a separation is made between axisymmetric arcs and arcs in transverse flows and magnetic fields orthogonal to the arc axis. The former could be subdivided into the wall-stabilised arc, confined within a constant cross-section tube and the arc burning vertically with no additional constraints, termed axial convection-stabilised arcs. In the referred work [Jones and Fang 1980], a complete set of simplified equations derived from the general equations that describe the collision-dominated, partially ionised plasma are shown where conservation equations relating to mass, momentum and energy can be reduced in accordance with a particular arc classification.

In addition to the complex behaviour of the electric arc itself, the current-voltage characteristic of the electric arc furnace load has a strong dependence on how the plant is operated, a fact that has been amply documented [Ma *et al.* 1992]. Electric arc furnace load variability is determined by both arc behaviour and operating disturbances. There are four distinctive types of smelting electric arc furnaces, characterised by their main mode of operation-related to the mechanisms of energy conversion to heat and transference of heat to the furnace charge [Ma *et al.* 1992]. These types are termed open, shielded, submerged arc and immersed electrode. In the particular case of the open arc furnace, its operation stages are described in [Jones 1997] and [Acha and Madrigal, 2001], from where the following statement is paraphrased: "A typical heat cycle, termed tap to tap cycle, starts with the scrap charging stage, when this is finished, the operator start to control the descent of electrodes until the arc current is initiated and the electrodes bore through the scrap to start forming a pool of liquid metal, the materials to be reduced, i.e. scrap, are highly heterogeneous and produce sudden jolts in the electric arc. This stage is called the drilling period and the time duration is about 3 to 4 minutes. The next stage is called the melting period and is surrounded by melting scrap, the material is more homogeneous than in the former stage, and full voltage and power is used, lasting between 21 and 23 minutes. The last stage, when a metal pool is formed, completes the end of the melting process, and the process of injecting oxygen to oxidise the carbon in the steel (charge carbon) is called reheating. Shorter arcs are involving this stage which requires lower voltages and higher currents, with duration of around 5 minutes". By way of example, Figure 4-2 shows measurements of arc voltage and current waveforms pertaining to the operation of an industry-size electric arc furnace. The characteristics for different stages of the melting period are shown to

illustrate the high dynamics associated with the operation of the electric arc furnace [Von G. Schönfelder 1983]©.

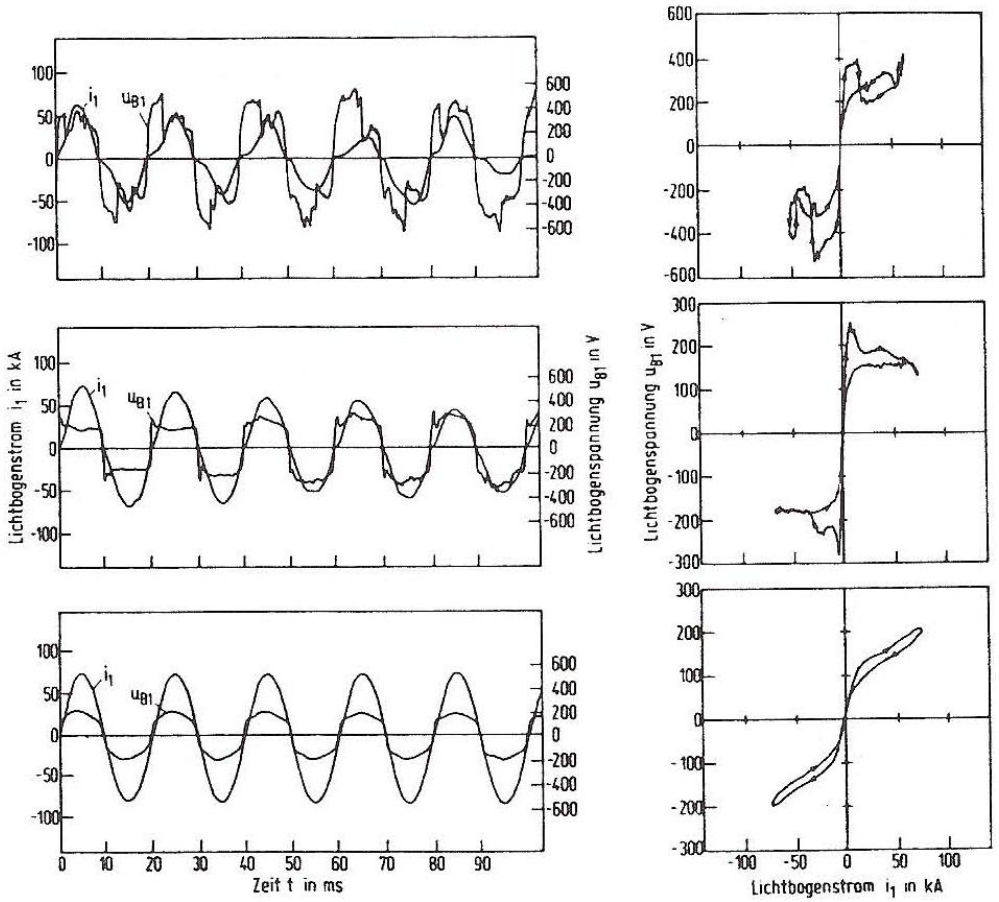

Figure 4-2 Arc voltages u_{g1} and arc current i_1 waveforms and arc characteristics $u_{g1}=f(i_1)$; measured about 9 minutes after start of meltdown of the first basket (top), about 7 minutes after start of meltdown of the second basket (centre) and about 40 minutes after start of meltdown of the second basket (bottom). [Von G. Schönfelder 1983] Eletrische Lichbogenöfen und ihr Einsatz in der eisenschaffenden Industrie, Elektrowarme international 41 (1983) B 5 Oktober ©

Various models of electric arc furnace characterisation have been used in the past. A recent review of models has been presented by [Tongxiu and Makram 2000] and by the Task Force on Harmonics Modelling and Simulation [2004]. The power balance model put forward by [Acha *et al.* 1990] is described as a new way of modelling arc furnaces. Contemporary works adopt this arc model but instead of solving the differential equation in the harmonic domain, as it has been done in the original work, it take a time domain approach [Ozgun and Omer 1999] and [Medina *et al.* 2005]. Additionally, this arc model has been implemented in an industrial software based on time domain solutions [Manitoba-HVDC research centre 2003], where the power

balance equation of the arc is used for an active interaction with the electric network. One of the main goals of this current research is to assess the interaction of the electric arc with the electrical power system, using harmonic domain techniques as opposed to time domain simulation. A key factor for the development of the overall harmonic model has been gaining an understanding of other electric arc phenomena such as the one taking place in electric arc discharge lamps where experimental and computational simulation work has been carried out and presented in Chapter 3 of this work, with a subset of this work presented in [Petit-Suarez *et al.* 2007].

The dynamic electric arc model is based on a power balance equation, as presented by [Acha *et al.* 1990], where it is shown that equation (4.1) is the sum of instantaneous powers

$$p_1 + p_2 = p_3 \tag{4.1}$$

where
p_1 represents the power transmitted in the form of heat
p_2 is the power responsible for increasing the internal energy in the arc
p_3 represents the total power developed in the arc

Then using specific arc installation constants k_1, k_2, and k_3, it is possible to achieve a match of the instantaneous powers with the radius of the electric arc r, which is taken to be the state variable.

The arc cooling is defined by equation (4.2), where the value of n=0 is for a hot environment around the arc, which corresponds to the end of the process; n=1, is for a long arc, where the cooling area is the lateral surface of the arc, a melting process, and n=2, corresponds to a very short arc when the cooling is proportional to the cross section area at the electrodes.

$$p_1 = k_1 r^n \tag{4.2}$$

$$p_2 = k_2 r \frac{dr}{dt} \tag{4.3}$$

$$p_3 = vi = \frac{k_3 / r^m}{r^2} i^2 \tag{4.4}$$

In equation (4.4), m=0…2, reflects the fact that for a larger radius the arc may be hotter in the interior. Substitution of (4.2)–(4.4) into (4.1) yields the next non-linear differential equation

$$k_1 r^n + k_2 r \frac{dr}{dt} = \frac{k_3 / r^m}{r^2} i^2 \tag{4.5}$$

Equation (4.5) may be rewritten as

$$f(r) = k_1 r^{m+n+2} + k_2 r^{m+3} \frac{dr}{dt} - k_3 i^2 \tag{4.6}$$

Equation (4.6) can be solved in time domain using any suitable integration method or, alternatively, it can be solved using harmonic domain, where the exponential operations can be calculated by discrete convolution operations using Toeplitz matrices, as documented by [Acha 1988]

$$\mathbf{F} = k_1 \mathbf{R}^{m+n+2} + k_2 \mathbf{R}^{m+3} \mathbf{D}\left(jh\omega_0 \right) \mathbf{R} - k_3 \mathbf{I}^2 = 0 \tag{4.7}$$

The solution of the non-linear algebraic equation (4.7) may be carried using Newton's method

$$\Delta \mathbf{R}^{(k+1)} = -\left[\frac{\partial \mathbf{F}}{\partial \mathbf{R}} \right]^{-1} \mathbf{F}^{(k)} \tag{4.8}$$

$$\mathbf{R}^{(k+1)} = \mathbf{R}^{(k)} + \Delta \mathbf{R}^{(k+1)} \tag{4.9}$$

where k is an iteration counter, and the Jacobian is:

$$\frac{\partial \mathbf{F}}{\partial \mathbf{R}} = \left(m+n+2 \right) k_1 \mathbf{R}^{m+n+1} + \left(m+3 \right) k_2 \mathbf{R}^{m+2} \mathbf{D}\left(jh\omega_0 \right) \frac{dr}{dt} + k_2 \mathbf{R}^{m+3} \mathbf{D}\left(jh\omega_0 \right) \frac{d\mathbf{R}}{d\mathbf{R}} \tag{4.10}$$

Following the iterative calculation of the radius using (4.7)-(4.10), the harmonic domain version of equation (4.4) is employed to determine the harmonic voltage vector, i.e.

$$\mathbf{V} = k_3 \left(\mathbf{R}^{m+2} \right)^{-1} \mathbf{I} \tag{4.11}$$

In order to make effective use of equation (4.7) in the study of actual electric arc furnace installations, such as the one shown in Figure 4-3, it is necessary to select the arc conductance as state variable as opposed to the arc radius. The conductance can be defined by equation (4.12),

$$g = \frac{r^{2+m}}{k_3} \tag{4.12}$$

which in harmonic domain becomes equation (4.13).

$$\mathbf{G} = \mathbf{R}^{m+2} / k_3 \tag{4.13}$$

This conductance represents the characteristic of a time variable function where convolutions are carried out in harmonic domain as opposed to simple multiplications. Furthermore, to combine the arc conductance with the model system of the rest of the electric arc furnace installation, using the nodal frame of reference, the arc conductance harmonic vector should be expressed in the form of a Toeplitz matrix,

$$\mathbf{G_m} = \begin{bmatrix} G_0 & G_{-1} & \cdots & G_{-h} & 0 & \cdots & 0 \\ G_1 & \ddots & \ddots & \ddots & \ddots & \ddots & \vdots \\ \vdots & \ddots & G_0 & G_{-1} & \ddots & \ddots & 0 \\ G_h & \ddots & G_1 & G_0 & G_{-1} & \ddots & G_{-h} \\ 0 & \ddots & \ddots & G_1 & G_0 & \ddots & \vdots \\ \vdots & \ddots & \ddots & \ddots & \ddots & \ddots & G_{-1} \\ 0 & \cdots & 0 & G_h & \cdots & G_1 & G_0 \end{bmatrix} \tag{4.14}$$

Use of sequence components to carry out the harmonic domain representation of the power network is unsuitable owning to the inherent balancing presumptions existing in

the derivation of the sequence components framework. [Arrillaga and Watson 2001]. Hence, the use of phase co-ordinates for modelling three-phase harmonic systems becomes standard.

4.2.1 Grounded star connection

There are different forms of representing the three-phase load of an electric arc furnace conductance, the simplest is a grounded star connection, equation (4.15). This representation is a straightforward extension of the positive sequence model of the arc to encompass a three-phase phase representation. However, such connection is seldom used in actual three-phase electric arc furnaces.

$$\mathbf{G}_{\mathbf{mabc}} = \begin{bmatrix} \mathbf{G}_{\mathbf{ma}} & \mathbf{0} & \mathbf{0} \\ \mathbf{0} & \mathbf{G}_{\mathbf{mb}} & \mathbf{0} \\ \mathbf{0} & \mathbf{0} & \mathbf{G}_{\mathbf{mc}} \end{bmatrix} \tag{4.15}$$

4.2.2 Ungrounded star connection

An alternative representation of the three phase load of an electric arc is the ungrounded star connection. One way to obtain this kind of circuit is to use three additional nodes in the electrode system where large conductances of value $\mathbf{G_{end}}$ are used, giving rise to the following delta-connection matrix:

$$\mathbf{G}_{\mathbf{endabc}} = \begin{bmatrix} \mathbf{G}_{\mathbf{end}} + \mathbf{G}_{\mathbf{end}} & -\mathbf{G}_{\mathbf{end}} & -\mathbf{G}_{\mathbf{end}} \\ -\mathbf{G}_{\mathbf{end}} & \mathbf{G}_{\mathbf{end}} + \mathbf{G}_{\mathbf{end}} & -\mathbf{G}_{\mathbf{end}} \\ -\mathbf{G}_{\mathbf{end}} & -\mathbf{G}_{\mathbf{end}} & \mathbf{G}_{\mathbf{end}} + \mathbf{G}_{\mathbf{end}} \end{bmatrix} \tag{4.16}$$

Matrices (4.15) and (4.16) are combined to form the two-node representation of the electrode system:

$$\mathbf{GY}_{\mathbf{mabc}} = \begin{bmatrix} \mathbf{G}_{\mathbf{mabc}} & -\mathbf{G}_{\mathbf{mabc}} \\ -\mathbf{G}_{\mathbf{mabc}} & \mathbf{G}_{\mathbf{mabc}} + \mathbf{G}_{\mathbf{endabc}} \end{bmatrix} \tag{4.17}$$

The additional mesh used in equation (4.17) is comprised by the common paths in the scrap or melting bath. This is a realistic approximation of the three-phase electric arc furnace and this model will be used in this work.

4.2.3 Delta connection

The delta connection admittance matrix of a three-phase arc furnace can be constructed using the arc current-voltage characteristics, corresponding to the measurements taken from line currents and phase voltages. Starting from a ungrounded star, a transformation is carried out to derive the vector elements of the equivalent delta connection representation

$$\mathbf{G}_{ab} = \left(\mathbf{G}_{ma} + \mathbf{G}_{mb} + \mathbf{G}_{mc}\right)^{-1} \mathbf{G}_{ma}\mathbf{G}_{b} \tag{4.18}$$

$$\mathbf{G}_{bc} = \left(\mathbf{G}_{ma} + \mathbf{G}_{mb} + \mathbf{G}_{mc}\right)^{-1} \mathbf{G}_{mb}\mathbf{G}_{c} \tag{4.19}$$

$$\mathbf{G}_{ca} = \left(\mathbf{G}_{ma} + \mathbf{G}_{mb} + \mathbf{G}_{mc}\right)^{-1} \mathbf{G}_{mc}\mathbf{G}_{a} \tag{4.20}$$

The subscript m means that the conductance vector is transformed in to a Toeplitz matrix to be able to carry out matrix algebra. The harmonic nodal admittance representing the equivalent delta circuit is:

$$\mathbf{GD}_{abc} = \begin{bmatrix} \mathbf{G}_{mab} + \mathbf{G}_{mca} & -\mathbf{G}_{mab} & -\mathbf{G}_{mca} \\ -\mathbf{G}_{mab} & \mathbf{G}_{mab} + \mathbf{G}_{mbc} & -\mathbf{G}_{mbc} \\ -\mathbf{G}_{mca} & -\mathbf{G}_{mbc} & \mathbf{G}_{mbc} + \mathbf{G}_{mca} \end{bmatrix} \tag{4.21}$$

As expected, the equivalent delta connection yields the same results as the ungrounded star connection.

4.3 Elements of the Electric Arc Furnace System

An electric arc furnace system is made up of various elements, as illustrated in Figure 4-3 page 83 by the one-line diagram of a typical electrical arc furnace installation. These elements, listed from the load to the power supply, are:

- Graphite Electrodes
- Flexible Cables
- Furnace Transformer
- Series Reactor
- Step-down Transformer

Circuit breakers are not listed but they do exist in the installation for the open-close operation of the electrical system. They can be of the types SF6 or vacuum technologies for an effective arc current extinction. They affect the electrical system quite substantially by switching in and out the very large non-linear load that the electric arc represents. However, their effects are outside the scope of this research.

4.3.1 Graphite electrodes

It has been documented in [Bowman 1985] and [Gorlani and Zavanella, 1993] that graphite electrode consumption represented the third largest cost of metal liquid production, around 8 %, after scrap and raw materials, 77 %, and electric energy, 10 %. It is mentioned too in these references that the specific consumption of graphite electrodes in Europe is typically 3 to 7 Kg/tonne of solid product. Graphite electrodes represent the last conductor used for the creation of the electric arc. Their main characteristics are low electrical resistivity, high mechanical strength, high resistance to thermal stresses and ease of manufacturability [Gorlani and Zavanella, 1993]. The physical characteristic used for the electrode model and its integration into the electric network circuit is the resistance or conductance. The technical specifications are connected with the electrode's physical dimensions; diameter and length are selected based on their electric arc furnace current capacity.

The specific electrical resistance can be obtained from Table 4-1, which is information taken from actual manufacturer data [SGL]. The data are in relation to the

electrode current capacity. Suitable physical dimensions, (diameter and length) can be used in equations (4.22) and (4.23) for the calculation of resistance and conductance, respectively.

Diameter mm	Nominal Length mm	Electrode Current Capacity kA	Specific Electrical Resistance Ωμm
350-450	1500-2400	20-60	5.0-7.5
500-650	1800-2700	60-80	4.5-6.5
700-800	2400-2700	80-100	4.0-5.5

Table 4-1 Graphite electrode characteristics

$$R = \rho \frac{l}{A} \tag{4.22}$$

$$G = \frac{1}{R} = \frac{A}{\rho l} \tag{4.23}$$

The diameter and length values are for new graphite electrodes, recently installed. In fact, a portion of the electrode is consumed each time that the furnace operates; electrode consumption affects directly its physical dimensions. The overall phenomenon has been considered to be the sum of tip and side consumption, [Gorlani and Zavanella 1993] the consumption due to tip loss and to under holder breakage. The first one classifies as continuous and the other two as intermittent consumption. The continuous consumption depends directly on the profile of the electric current or power absorbed by the electric arc furnace. Hence, continuous electrode consumption simulation can be carried out using the equations given by Gorlani [1993]. Values of continuous electrode consumption can be used for the calculation of variation of the physical dimensions of electrodes, which affect directly conductance values. An average value of total electrode consumption is around 3.48 Kg per metric ton of steel.

The graphite electrode can be modelled as a linear conductance (or resistance). Its inclusion in a harmonic domain nodal system is represented by a diagonal matrix of dimensions $2h+1$ by $2h+1$, as shown in equation (4.24), with elements of equal values in the main diagonal.

$$\mathbf{G_{Elec}} = \begin{bmatrix} G_{Elec} & 0 & \cdots & \cdots & 0 \\ 0 & \ddots & \ddots & \ddots & \vdots \\ \vdots & \ddots & G_{Elec} & \ddots & \vdots \\ \vdots & \ddots & \ddots & \ddots & 0 \\ 0 & \cdots & \cdots & 0 & G_{Elec} \end{bmatrix} \tag{4.24}$$

The assembly of the three-phase electrode conductance model is a fully diagonal matrix, as shown in equation (4.25),

$$\mathbf{G_{E}}_{abc} = \begin{bmatrix} \mathbf{G_{Elec}} & \mathbf{0} & \mathbf{0} \\ \mathbf{0} & \mathbf{G_{Elec}} & \mathbf{0} \\ \mathbf{0} & \mathbf{0} & \mathbf{G_{Elec}} \end{bmatrix} \tag{4.25}$$

4.3.2 Flexible cables, bus and connectors

The flexible cables, bus-bars and legs are commonly referred in the literature as secondary circuit. Reduction of the secondary reactance was one of the key goals in the developments of UHP furnaces. One of these secondary circuit elements, the flexible cables can contribute up to 75 % of the total reactance, as documented by [Kadar and Biringer 1990], where the impact of the cable swing movement in the voltage and current unbalances on the installation is analysed. The flexible cable can be represented as a series impedance made up of a resistance and an inductive reactance. The former has a constant value whereas the latter is directly proportional to the harmonic order. Its representation is shown in equation (4.13) as a diagonal matrix of dimension $2h+1$ by $2h+1$. The formation of the admittance matrix can be calculated as the inverse of the impedance matrix, where the entries can be calculated by using a classical representation of the cable impedance calculation as given by [Ciotti1986],

For a coplanar design

$$
\begin{aligned}
L_A &= L_S - L_{Bm} - L_{Cn} \\
L_B &= L_S - L_{Am} - L_{Cn} \\
L_C &= L_S - L_{Bm} - L_{An} \\
L_A &= L_C \\
L_B &< L_A
\end{aligned}
\tag{4.26}
$$

For a triangular design

$$
\begin{aligned}
L_A &= L_S - L_{Bn} - L_{Cn} \\
L_B &= L_S - L_{An} - L_{Cn} \\
L_C &= L_S - L_{An} - L_{Bn}
\end{aligned}
\tag{4.27}
$$

For the calculation of self and mutual inductance

$$
\begin{aligned}
L_S &= 2S\left[\ln\frac{2S}{ds} - 1\right]\times 10^{-9}\ \text{H} \\
L_M &= 2S\left[\ln\frac{2S}{ds} - 1 + \frac{d}{S}\right]\times 10^{-9}\ \text{H}
\end{aligned}
\tag{4.28}
$$

where:

S= Conductor length (cm)

ds=Geometric mean radius (cm)

d=Geometric mean distance between conductors (cm)

The inductance values are used for the calculation of reactance values. In accordance with [Ciotti 1986], the resistance values can be calculated assuming a ratio of X/R of 10 for the fundamental frequency. The cable sizing is using a theoretical current density of 4.5 A/mm^2 or their equivalence of 3000 A/inch^2.

An important element of the secondary circuit is the water-cooled bus, as documented by Soumitra and Ghosh [2005], where the sizing of a water-cooled bus for a single-phase arc furnace is carried out in a similar fashion as for a water-cooled cable.

Different sources where electric arc furnaces of different capacities are considered indicate that the secondary reactance values are in the range of 2.6 to 3.6 mΩ at frequency of 50/60 Hz, see for instance Bowman and Istria [1990] and Ciotti and Pelfrey [1986]. Moreover, the secondary circuit has been the subject of various studies,

including the impact of unbalanced effects in the installation [Cao and Biringer 1989], [Kadar and Biringer 1990].

4.3.3 Furnace transformer and step down transformer

The representation of a step down and furnace transformer are similar to that of a normal power transformer. The harmonic models of single-phase and three-phase banks of transformers presented by [Acha 1988] can be used. The differences between step down and furnace transformer are the type of connection and technical specifications.

The furnace transformer specification has great impact in the operation of the electric arc furnace installation [Akdağ, *et al.* 2000]. The megavolt-ampere capacity, number of taps and impedance affect the dynamics of the process. The selection of the transformer requires a good matching with the furnace specifications. Some flexibility can be introduced if a series reactor is used. The transformer tap mechanism requires a full identification of the different phases and stages of the melting operation process. Arc furnace transformers have stronger technical specifications than other transformers. During the melting process, the series impedance and tap changing of the furnace transformer have a very significant influence in the electric network. Less obvious facts is that between "tap to tap" cycles; the magnetising branch of the furnace transformer can, in conjunction with other system parameters, lead to adverse electrical phenomena. The resistance transformer can be calculated using a ratio X/R of 8 as recommended by [Ciotti and Pelfrey 1986].

4.3.4 Series reactor

The use of a series reactor was first employed in small electric arc furnace installations for the purpose of arc stabilisation, an idea which was later extended to larger furnaces [B. Bowman 1997]. The utilisation of series reactors, as is documented in [Mendis *et al*. 1995], improves the stability of the electric arc, diminishes electrode consumption, reduces heat times and may lead to voltage flicker elimination. The series reactor is used together with control of the furnace transformer secondary voltage, achieved by tap changing. The goal is to maintain a given amount of arc power with reduced electrode current using different combinations of the series reactor taps with the

furnace transformer taps. The slow response of the mechanical taps of the series reactor has motivated the development of series reactors with a faster dynamic. A power electronics-based controller, termed Solid State Predictive Line Controller (SPLC), has been installed in a electric arc furnace installation with good results [Ma and Mulcahy].

A table of series reactance values has been published in [Bowman 1993] where the range is 4 to 6 mΩ at 50/60 Hz and series reactance values in the range 0.209 to 0.418 p.u. have been used in [Prieto and Perez 2004].

4.3.5 Overhead line or cable

Transmission lines parameter calculations can be carried out for both lumped and distributed parameters [Acha and Madrigal 2001]. The former are obtained from the geometric configuration of the transmission line and take in account the effect of earth return and skin effects. The case of distributed parameters involve adds the long-line effects to be added in to the lumped parameters to generate an exact model of the transmission line. In this work the transmission line is modelled as linear series admittance.

4.4 Representation of the Electric Arc Furnace System

The integration of the various elements of the electric arc furnace installation shown in Figure 4-3 gives the total system. A series reactance for the arc stabilisation control has been added. The system can be represented by a set of nodal equations in the harmonic domain, comprised by admittance matrix, harmonic vectors of voltages and currents. For the representation of the three-phase electric furnace. The voltage and current vectors, (4.29) and (4.30), are composed of elements that represent vectors of dimensions $3(2h+1)$ and the admittance matrix in equation (4.31) is a matrix that contains matrix entries of $3(2h+1)$ by $3(2h+1)$.

$$\mathbf{V}_{Sys} = \begin{bmatrix} \mathbf{V}_{T1p} & \mathbf{V}_{SRp} & \mathbf{V}_{T2p} & \mathbf{V}_{CB} & \mathbf{V}_{Ge} & \mathbf{V}_{Ge} & \mathbf{V}_{End} \end{bmatrix} \tag{4.29}$$

$$\mathbf{I}_{Sys} = \begin{bmatrix} \left(\mathbf{Y}_{PS}\mathbf{V}_{PS} - \mathbf{I}_{N1}\right) & -\mathbf{I}_{N1} & -\mathbf{I}_{N2} & -\mathbf{I}_{N2} & \mathbf{0} & \mathbf{0} & \mathbf{0} \end{bmatrix} \tag{4.30}$$

$$\mathbf{Y}_{sys} = \begin{bmatrix} \mathbf{Y}_{PS} + \mathbf{Y}_{T1_{ABC}} & \mathbf{Y}_{T1_{ABCabc}} & \mathbf{0} & \mathbf{0} \\ \mathbf{Y}_{T1_{abcABC}} & \mathbf{Y}_{T1_{abc}} + \mathbf{Y}_{SR} & -\mathbf{Y}_{SR} & \mathbf{0} \\ \mathbf{0} & -\mathbf{Y}_{SR} & \mathbf{Y}_{SR} + \mathbf{Y}_{T2_{ABC}} & \mathbf{Y}_{T2_{ABCabc}} \\ \mathbf{0} & \mathbf{0} & \mathbf{Y}_{T2_{ABCabc}} & \mathbf{Y}_{T2_{abc}} + \mathbf{Y}_{CB} \\ \mathbf{0} & \mathbf{0} & \mathbf{0} & -\mathbf{Y}_{CB} \\ \mathbf{0} & \mathbf{0} & \mathbf{0} & \mathbf{0} \\ \mathbf{0} & \mathbf{0} & \mathbf{0} & \mathbf{0} \end{bmatrix} \begin{bmatrix} \mathbf{0} & \mathbf{0} & \mathbf{0} \\ \mathbf{0} & \mathbf{0} & \mathbf{0} \\ \mathbf{0} & \mathbf{0} & \mathbf{0} \\ -\mathbf{Y}_{CB} & \mathbf{0} & \mathbf{0} \\ \mathbf{Y}_{CB} + \mathbf{G}_{Ge} & -\mathbf{G}_{Ge} & \mathbf{0} \\ -\mathbf{G}_{Ge} & \mathbf{G}_{Ge} + \mathbf{G}_{m} & -\mathbf{G}_{m} \\ \mathbf{0} & -\mathbf{G}_{m} & \mathbf{G}_{m} + \mathbf{G}_{End} \end{bmatrix} \tag{4.31}$$

The numerical solution of the three-phase electric furnace system is carried out by properly accounting for the interaction taking place between the power balance equation that defines the arc conductance of each phase and the nodal system of equations that represents the electrical system. Figure 4-4 shows the flowchart of the algorithm used for the calculation of nodal voltages and line currents.

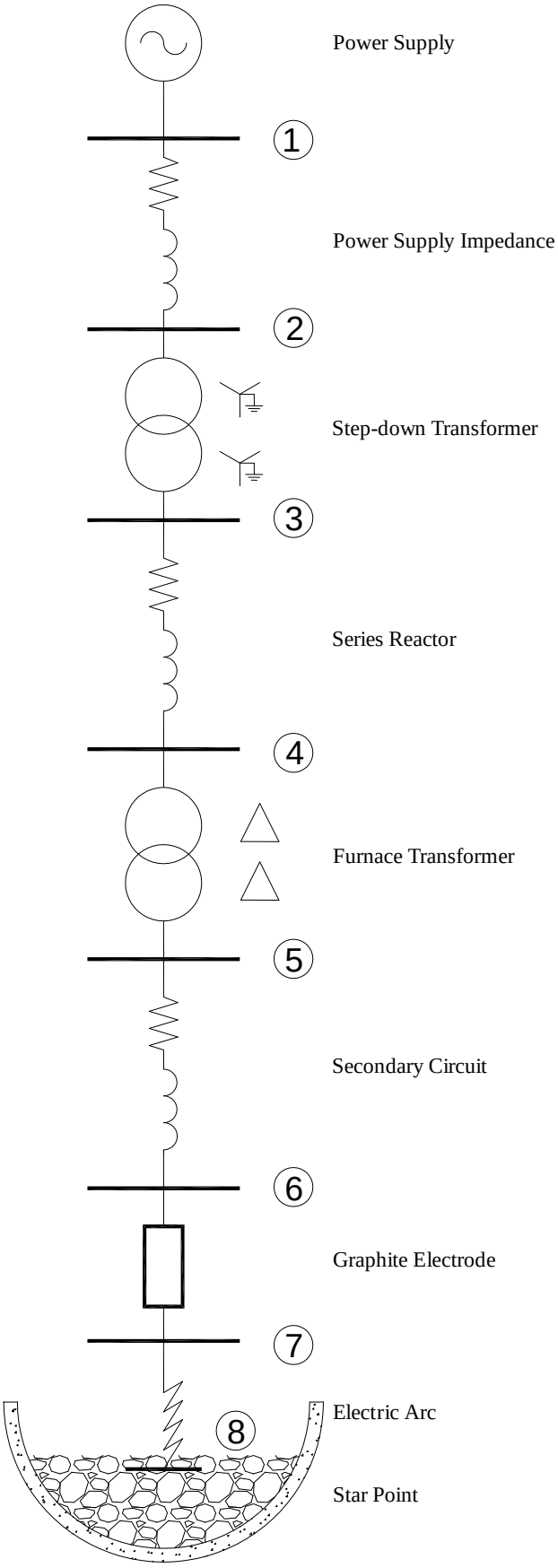

Figure 4-3 Electrical arc furnace system

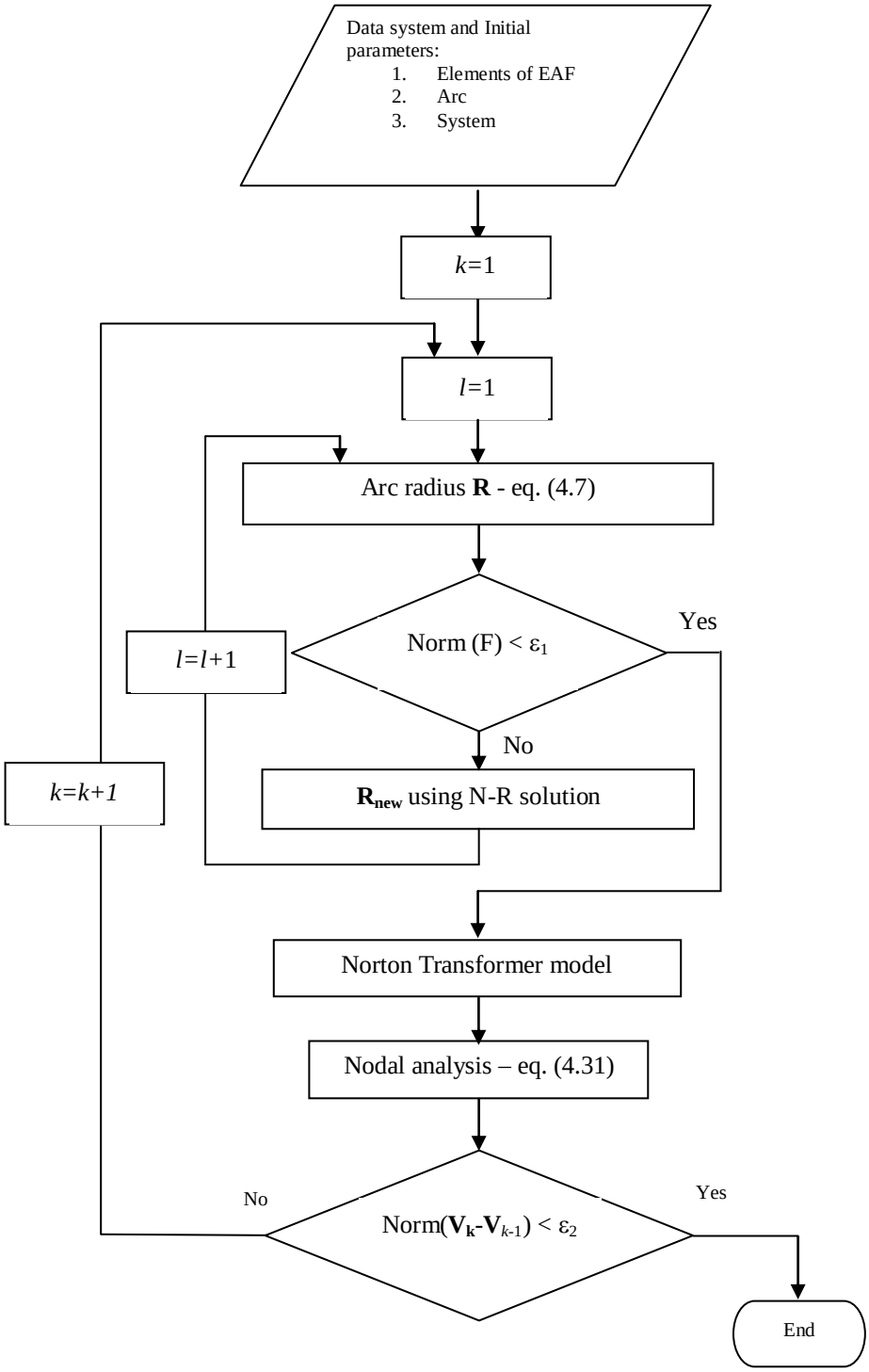

Figure 4-4 Flow chart of the algorithm

4.5 Harmonic Analysis of the Electric Arc Furnace System

Using the arc constants, system parameters and nominal values of voltage, current and power, the iterative solution is started. These values are transformed to per unit values where the base is the rms line-to-line voltage of the secondary voltage of the furnace transformer and, the three-phase apparent power of the arc furnace. Full data for the test case of the electric arc furnace installation is given in Table 4-2.

Utility	3000 MVA Short circuit capacity, 138 kV
Step down transformer	70 MVA, 138/34.5 kV, 8 % impedance
Distribution Line (or cable) and series reactor	R=0.28 mΩ X=2.80 mΩ
Furnace transformer	70 MVA, 34.5/0.700 kV, 5 % impedance
Flexible cable, bus and leads	R=0.28 mΩ X=2.80 mΩ
Graphite electrode	600 mm diameter, 1800 mm length an resistivity values between 4-5.5, Ω.μm

Table 4-2 Parameters of electric arc furnace equipment

4.5.1 Harmonic interactions of the electric arc furnace with the electric network

The algorithm presented in the flowchart of Figure 4-4 is implemented in Matlab code. The Newton-Raphson method in the complex harmonic domain is used to solve the power balance equation with the following constants: $k1$=3000, $k2$=1, $k3$=12.5, m=0 and n=2. These values yield the arc current-voltage characteristic documented in [Acha *et al.* 1990]. This characteristic is assumed to exist in the three branches of the ungrounded star connection.

The most significant harmonic components of the arc voltage are the first 25 odd harmonics, as documented by [King *et al.* 1994], however, the number of harmonic terms used in the simulation studies is 100, taking a voltage mismatch error of 1e-6 which represents a tight convergence criterion in the simulation study of electric arc furnace systems. Following convergence of the iterative solution, which is in the form

of harmonic complex nodal voltages, it is straightforward to calculate the currents, powers, rms THD of voltage and current. Moreover, voltage and current harmonic information may be transformed to determine time domain information in order to display waveforms.

The overall performance of the electric arc furnace system is dictated by the interaction of the electric arc, the electrical system parameters and the way the electric arc furnace is operated. The ideal case, where the electric arc furnace is completely balanced is probably very difficult to find in the real world. More often than not the electric arc at each phase will possess different arc conductance values and asymmetrical voltage and current waveforms will follow.

4.5.2 Impact of the arc load connection

As previously it was stated, different types of connections can be used in electrical arc furnace installations, they keep a strong relationship with the connection of the furnace transformer. Although rarely used a grounded star arc conductance connection requires a star-star grounded furnace transformer. On the other and an ungrounded star arc conductance connection regularly uses a delta-delta furnace connection

4.6 Balanced Load Modelled as an Ungrounded Star

An ungrounded star connection may be used to represent a three-phase electric arc conductance load. The constant and parameter values used for the computation of the electric arc furnace power balance equation are the same for each phase. The error, at each iterative step, is depicted in Figure 4-5 where it can be observed that convergence to a tolerance of 1e-6 is achieved in 22 global iterations, this tolerance it is selected in order to achieve a tolerance of 1e-12 with powers, this is a common tolerance in electrical power system analysis [Acha *et al.* 2004]. Starting from the fourth iteration, the linearity of convergence is self evident.

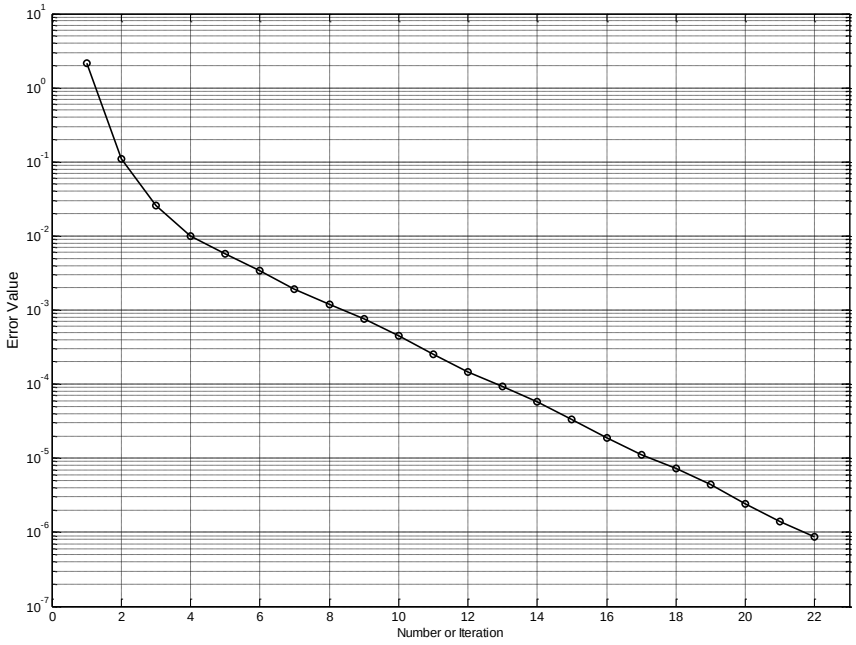

Figure 4-5 Error mismatch vs number of iteration

4.6.1 The electric arc load

The characterisation of the non-linear electric arc load is achieved with the calculated values of the electric arc conductance (state variable), resulting from the solution of the electric arc power balance equation, as explained Section 4.2. Figure 4-6 gives the harmonic conductance magnitudes per phase. In this particular case, the load is balanced and, as expected, the three conductances have identical values. The most significant harmonics are the second, fourth and sixth.

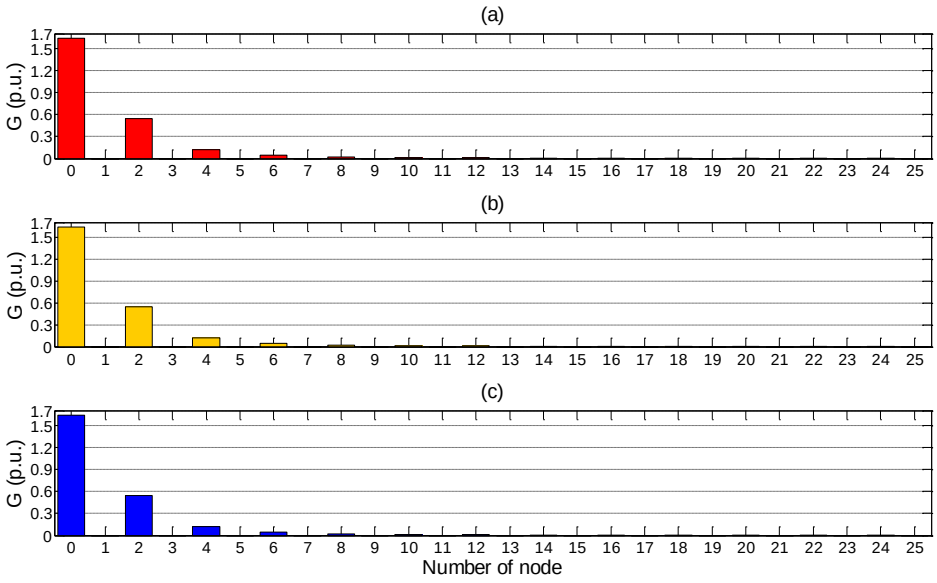

Figure 4-6 Harmonic magnitudes of the electric arc conductance (a) phase a (b) phase b (c) phase c

The current-voltage characteristic provides additional useful information in the representation of the electric arc phenomena. Using the calculated harmonic voltages and currents at the electric arc node, an Inverse Discrete Fourier Transformation (IDFT) is used to carry out a transformation from frequency domain into time domain, generating three different sets of current and voltage waveforms. The set of waveforms presented in Figure 4-7 correspond to phase voltages (with reference to ground) and line currents. As expected the three-phase current and voltage waveforms are balanced i.e. equal magnitudes and phase shifted by 120 degrees. The three-phase line voltage waveforms in conjunction with phase currents waveforms are shown in Figure 4-8. In similarity with the results shown in Figure 4-7 the current and voltage waveforms are balanced.

The arc voltages are those that exist across each one of the electric arcs whose equivalent three-phase conductances have a star point as common end. It should be noted that the current that passes through the electric arc and the line current of the corresponding phase coincide, as shown in Figure 4-7 and Figure 4-9

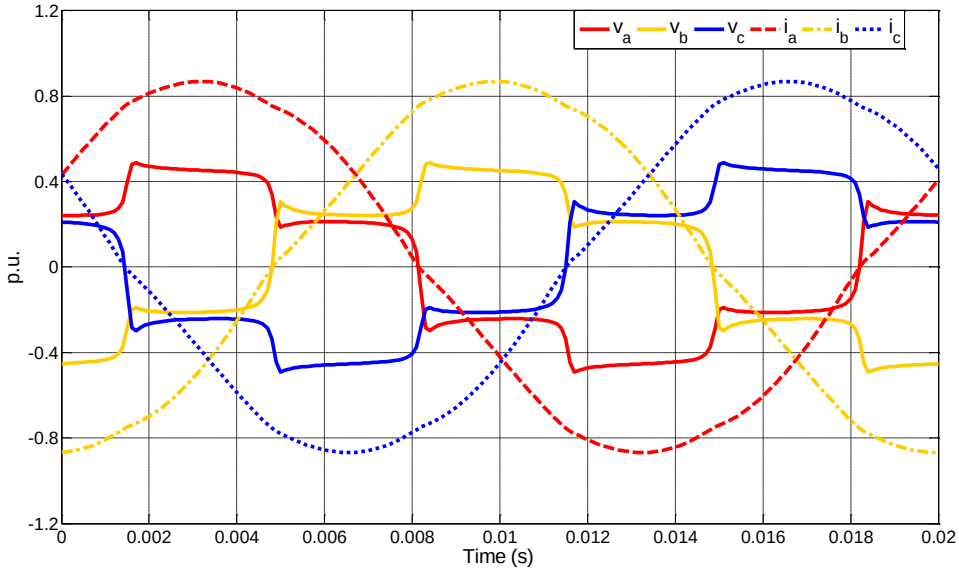

Figure 4-7 Anode phase voltage and line currents waveforms at the anode point

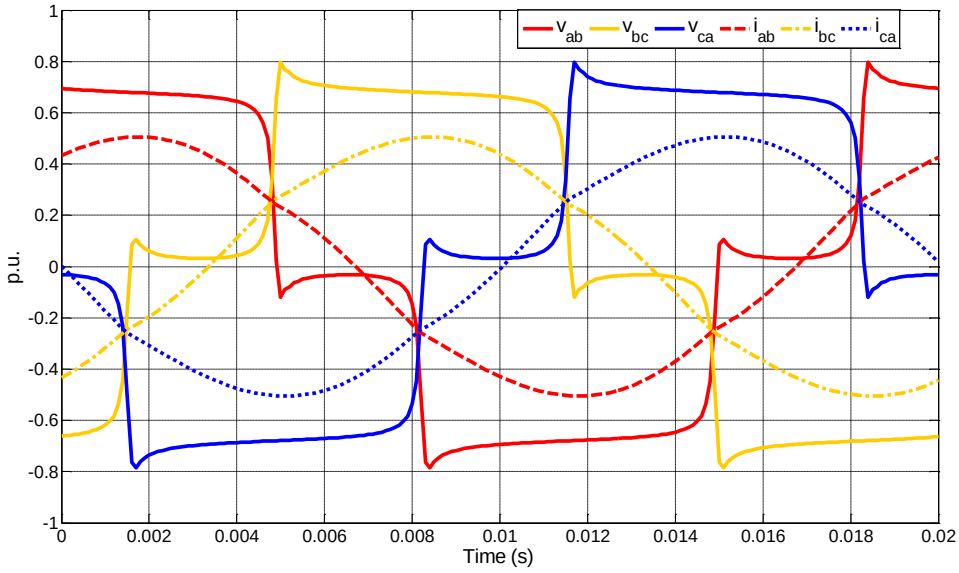

Figure 4-8 Anode line-to-line voltages and phase currents waveforms

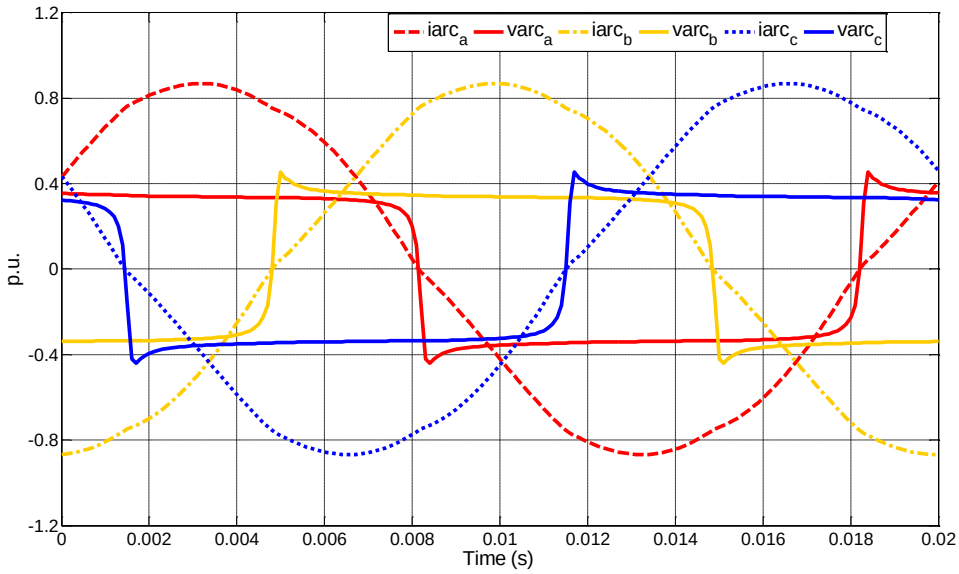

Figure 4-9 Arc voltage and current waveforms

The voltage and current waveforms may be used to generate sets of current-voltage characteristics, which are presented in Figure 4-10-Figure 4-12 respectively. Figure 4-10 gives the three characteristics formed with the line current and phase voltages where it is shown that all three characteristic are identical. As already elucidated this is an expected result in a balanced system, however, it should be borne in mind that the phase voltages are referred to the ground of the whole system and the load is in a three wire system. Figure 4-11 shows the characteristics created with phase currents and line-to-line voltages. Once again the three characteristics are identical. Figure 4-12 presents the three electric arc characteristics. These characteristics are the best well-known form of arc characteristic which happen to be identical because of the balanced condition of the load.

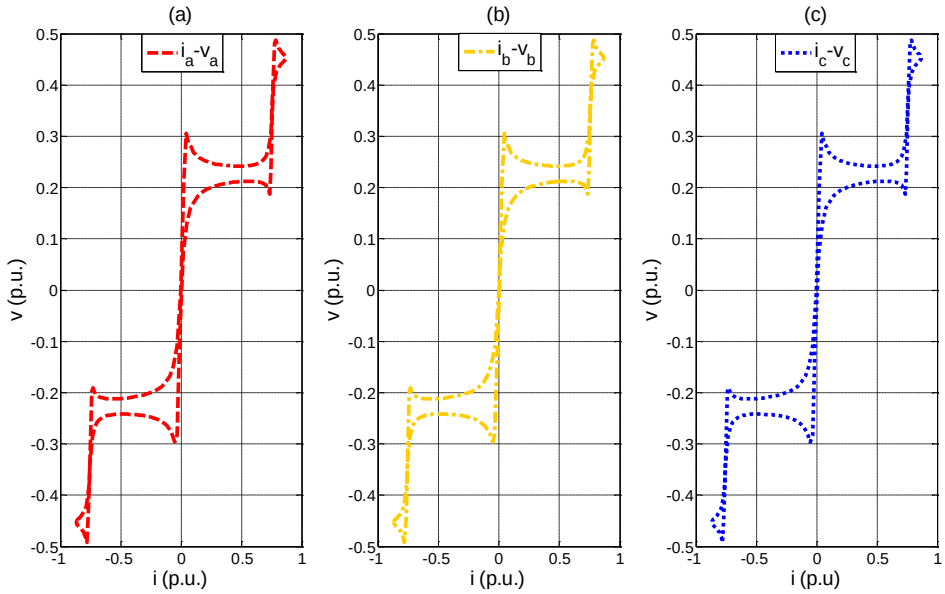

Figure 4-10 Line current-phase voltage characteristics

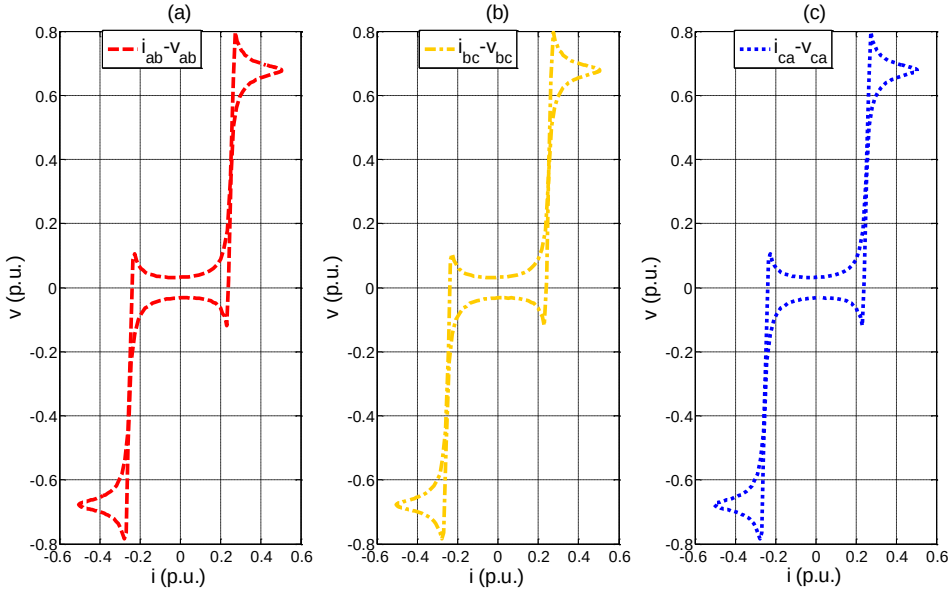

Figure 4-11 Phase current line voltage characteristics

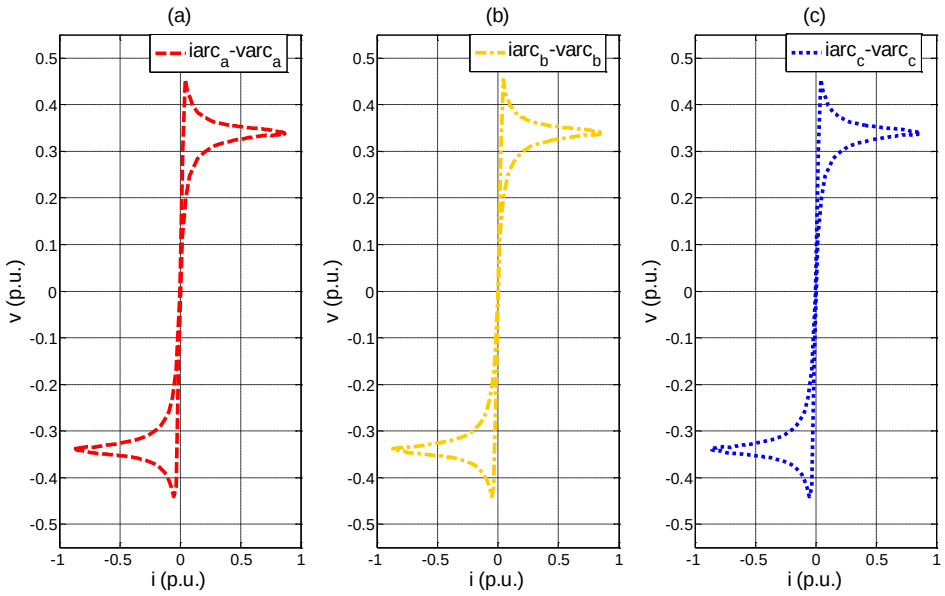

Figure 4-12 Current arc voltage characteristics

The instantaneous electric power of the arc load shown in Figure 4-13 is calculated using voltage and current information: The first set uses phase voltages and line currents; the second set uses line voltages and phase currents; the third set uses the current and voltages of the electric arc. In Figure 4-13(d) the three three-phase instantaneous powers are plotted with only one waveform becoming apparent since the three results are superimposed on top of each other. The three sets of results for the three-phase instantaneous powers have been obtained using Tellegen's theorem

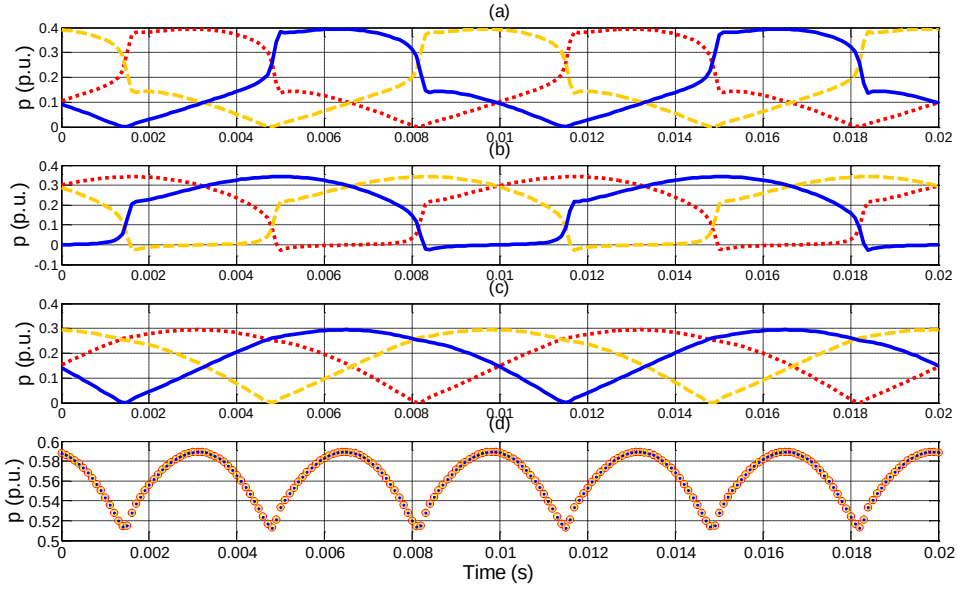

Figure 4-13 Instantaneous powers: (a) in the star-connected load; (b) in the equivalent delta-connected load; (c) in the arc; and (d) instantaneous three-phase power computed with the three sets of parameters

4.6.2 The star point of the ungrounded star

The star point of the ungrounded star is expected to contain distorted voltages as a consequence of the arc non-linearity. Computation of the voltage at the star point is essential for the calculation of the arc voltage, a computation carried out in Section 4.6.1. This parameter is of key relevance to the operation of the electric arc due to the strong relationship that exists between the arc voltage and the electric arc length, a physical property that is used for controlling of the electrodes position.

Figure 4-14(a) depicts the harmonic magnitudes of the voltage at the star point, where the third harmonic component is shown to be the most significant. Figure 4-14(b) shows shape of the distorted voltage waveform.

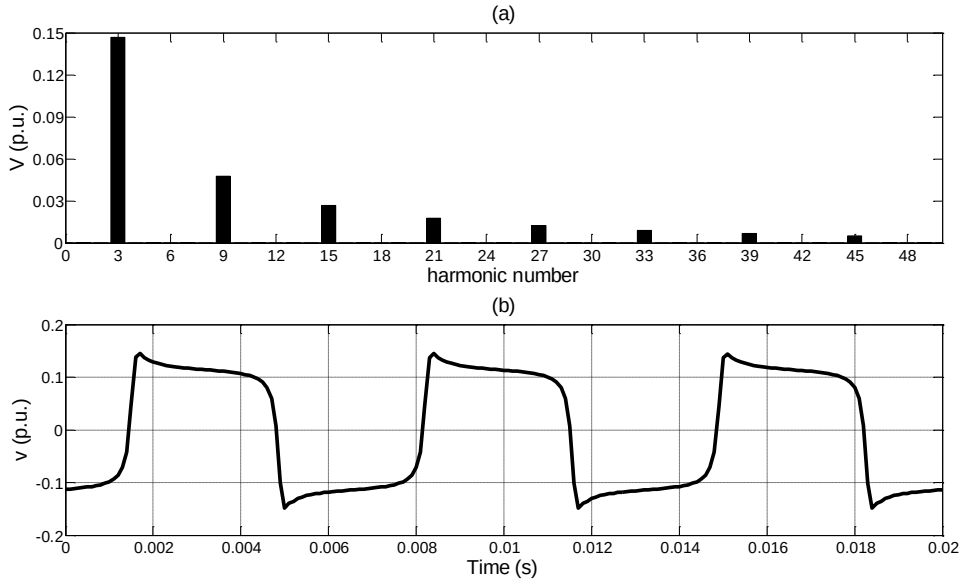

Figure 4-14 Voltage at the star point: (a) harmonic magnitudes; (b) waveforms

4.6.3 The magnetising branch of transformers

The non-linear effects introduced into the electrical circuit by the magnetising branch of the step-down and furnace transformers are assessed in this Section. To such end, the magnitudes of the harmonic magnetising current of the step-down transformer are depicted in Figure 4-15. The electrical system is balanced and hence the magnetising currents have equal magnitudes on the three phases. In this transformer connection the third harmonic is the largest but its magnitude is too small since this transformer is operating well below the knee point of the saturation characteristic. An alternative representation of the magnetising current is shown in Figure 4-16 where identical wave shapes are observed.

In the case of the furnace transformer, the magnetising currents per phase are shown in Figure 4-17 where the third harmonic is not shown due to the impact of the transformer delta connection. In this case the harmonic with higher magnitude is the fifth. The magnitudes of these magnetising currents are also small due to the absence of saturation.

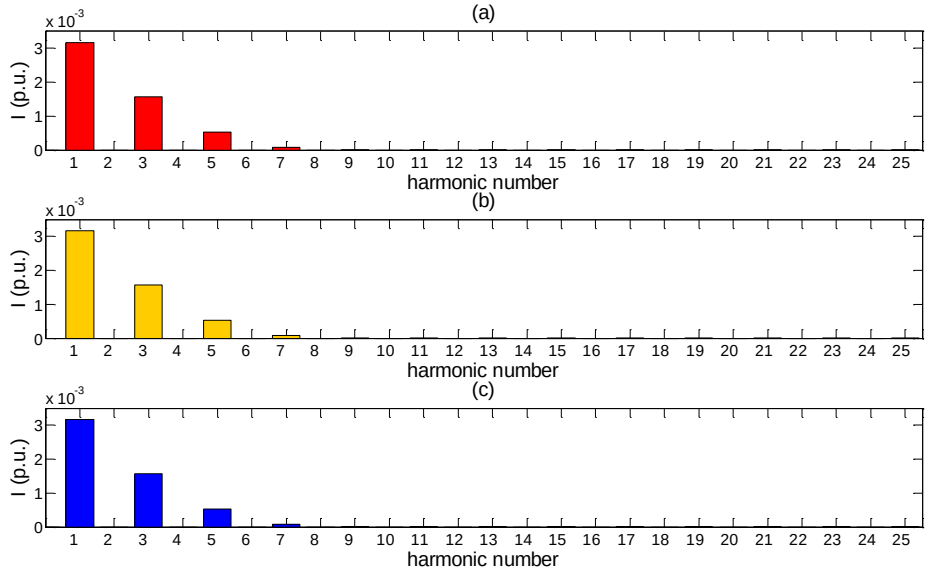

Figure 4-15 Harmonic current magnitudes of the magnetising branch of the step-down transformer

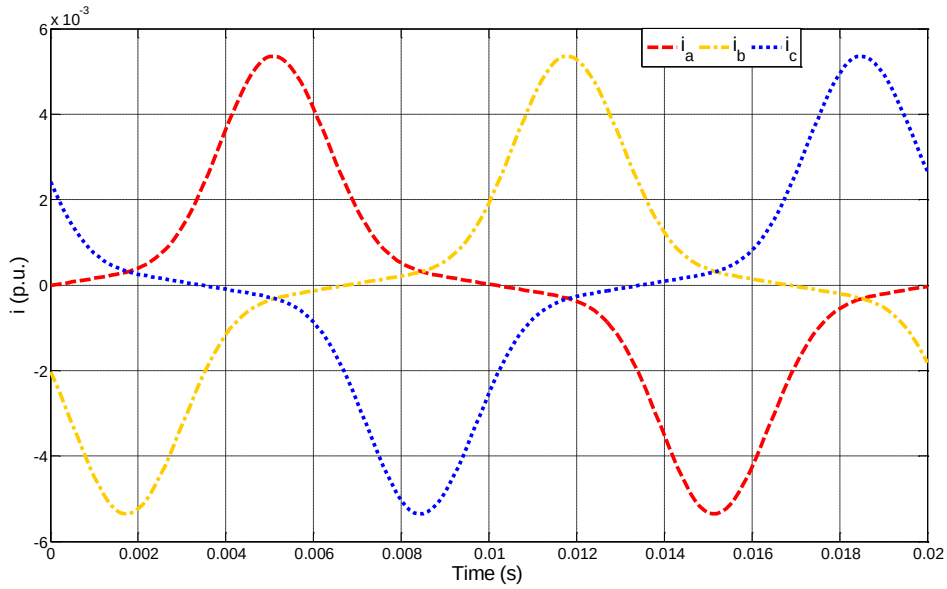

Figure 4-16 Current waveform of the magnetising branch of the step-down transformer

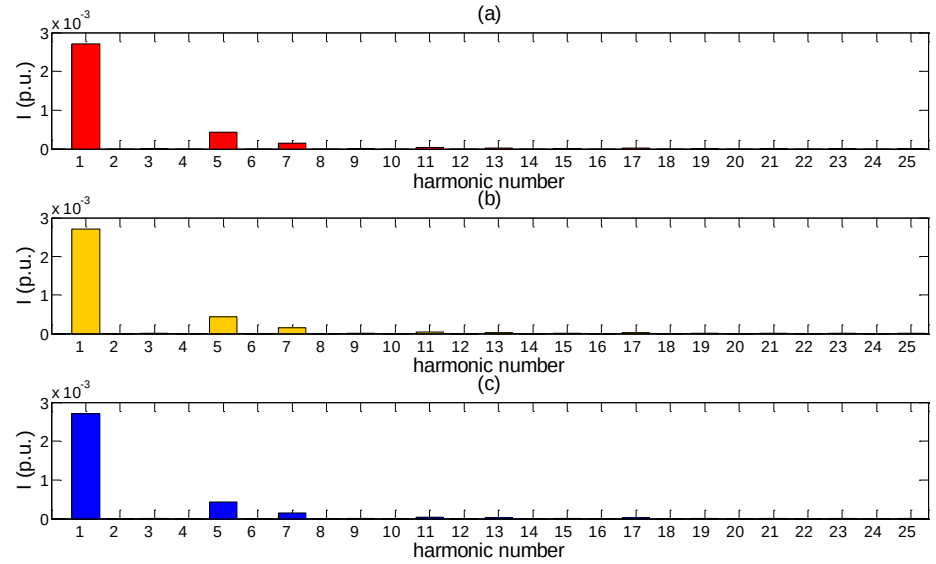

Figure 4-17 Harmonic current magnitudes of the magnetising branch of the furnace transformer

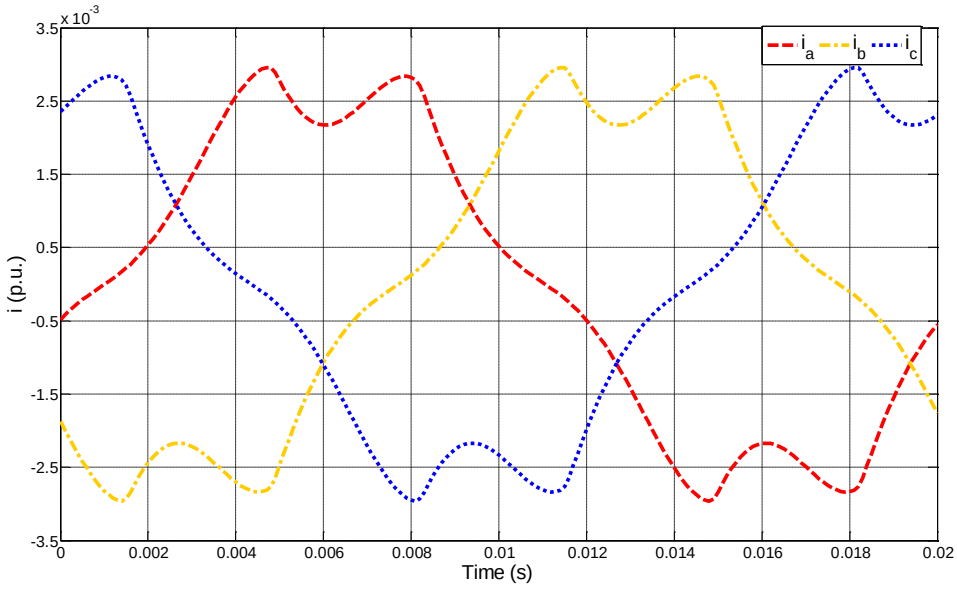

Figure 4-18 Current waveform of the magnetising branch of the furnace transformer

4.6.4 Harmonic analysis per node

The nodal harmonic voltage magnitudes of the test system of Figure 4-3 are shown in Figure 4-19. As expected, the voltage magnitudes are the same for each one of the three phases at each node. It can be observed that the magnitudes of the harmonics increase from the power supply (node 1) towards the arc furnace load (node 7). In contrast, the fundamental frequency voltage decreases from 1 p.u. magnitude at the supply point to values of 0.4 p.u. at the load point. The largest voltage drop takes place between nodes 3 and 4, where the series reactor is placed, and between nodes 5 and 6, across the furnace transformer. A full three-phase system analysis requires no only information of phase voltages but also information of line-to-line voltages, which are presented in Figure 4-20. The line-to-line voltages are also shown in a normalised fashion with respect to the base line-to-line voltage. Similarly to phase voltages, the line-to-line harmonic voltage magnitudes at each node, keep identical values at each phase.

The harmonic current magnitudes are presented in Figure 4-21. Changes in current magnitudes take place where shunt elements are located, which in this case are the magnetising branches of the step-down and furnace transformers. The small harmonic values show that the current is nearly sinusoidal. The fundamental frequency component has a value of around 0.87 p.u. Similarly to the voltages, only the current of

phase *a* is shown since currents in phase *b* and *c* hold identical harmonic magnitudes

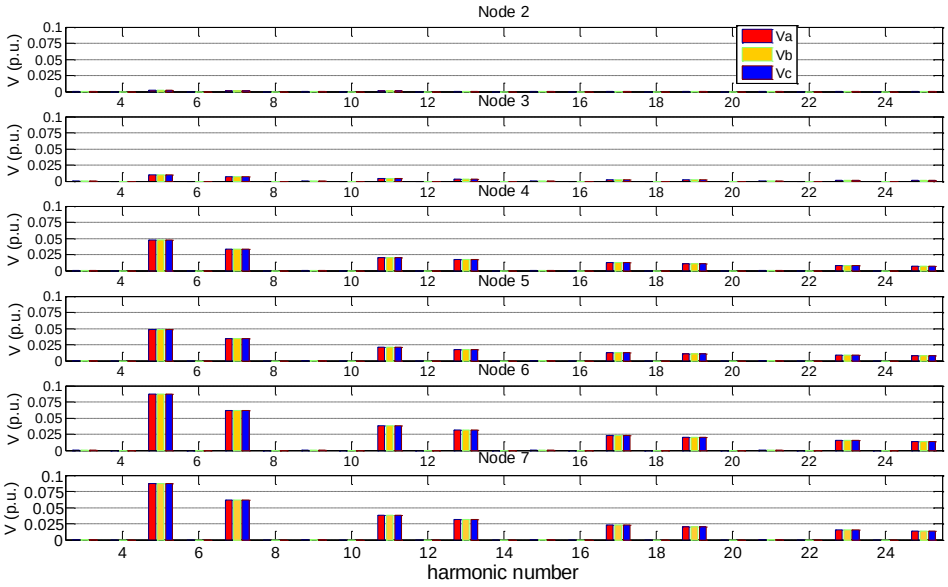

Figure 4-19 Harmonic voltage magnitudes *(a,b,c)*

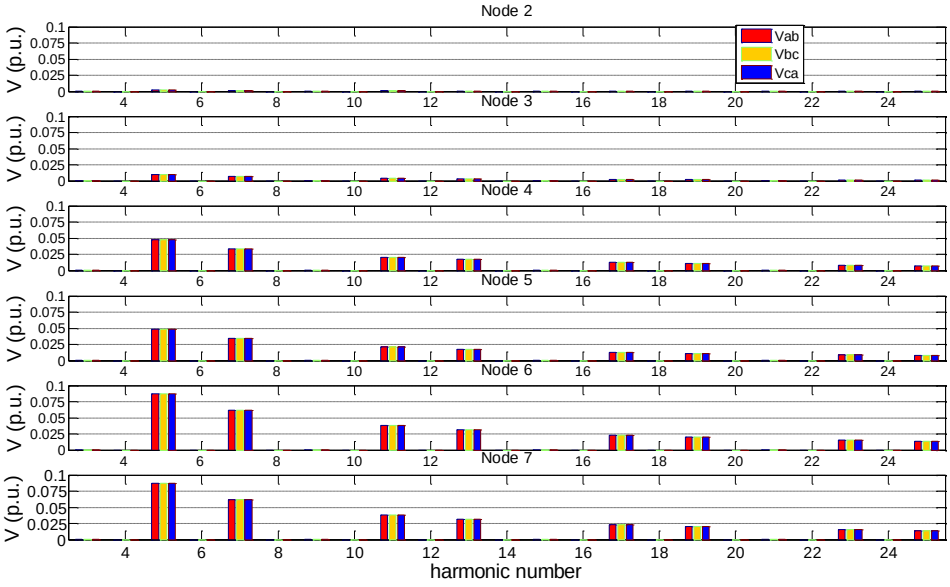

Figure 4-20 Harmonic voltage magnitudes *(ab, bc, ca)*

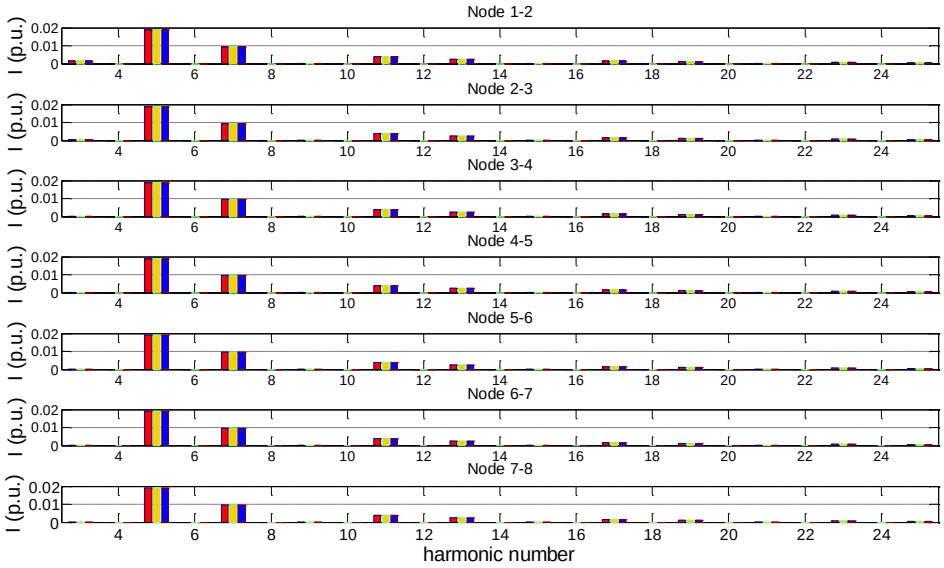

Figure 4-21 Harmonic current magnitudes

4.6.5 Root Mean Square values

The basis for the computation of apparent power and power quality indexes is the rms values of voltage and current. Figure 4-22 shows the results of the application of three different definitions for rms voltages given by the IEEE Standard 1459 [2000]. Figure 4-22 (a) shows the rms voltages at every node for phases a, b, c; Figure 4-22 (b) gives the rms line-to-line voltage, Figure 4-22 (c) shows the three-phase rms voltage values, termed effective voltages. It is clear that the largest drop is produced by the use of the series reactor, located between nodes three and four, causing a voltage difference of around 0.30 p. u. These results clearly indicate that they are for a balanced system.

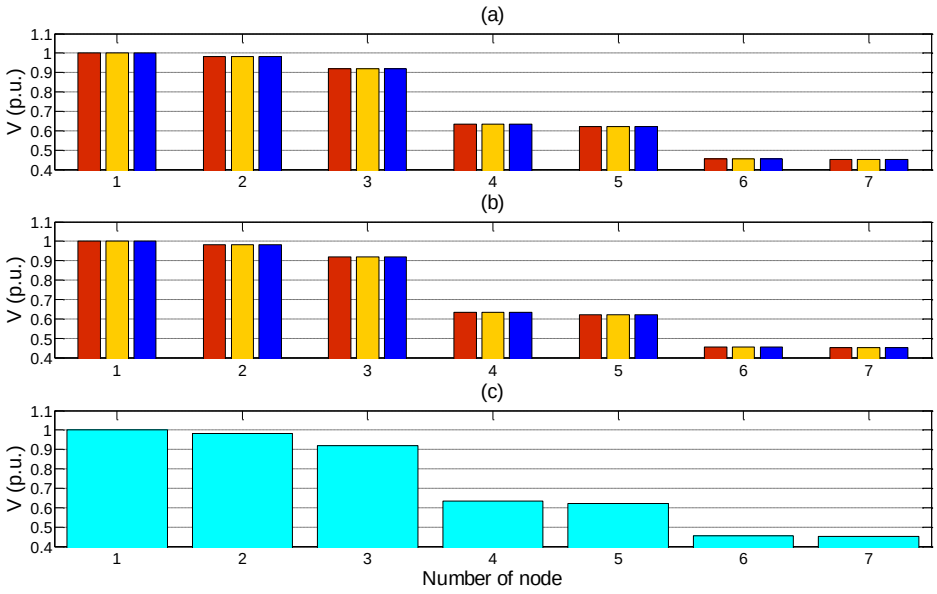

Figure 4-22 Root Mean Square voltages for nodes 1 to 7: (a) phase; (b) line-to –line; and (c) effective

The rms currents are plotted in Figure 4-23. For this example, small changes in current are observed starting from the supply and towards the load, i.e. from node one to eight. These changes due to the magnetising branch currents of the step-down and furnace transformer are below 1 % of the base current. The rms line currents are shown in the graph Figure 4-23 (a) for each phase and node. On the other hand, Figure 4-23 (b) shows the effective rms current [IEEE Standard 1459 2000].

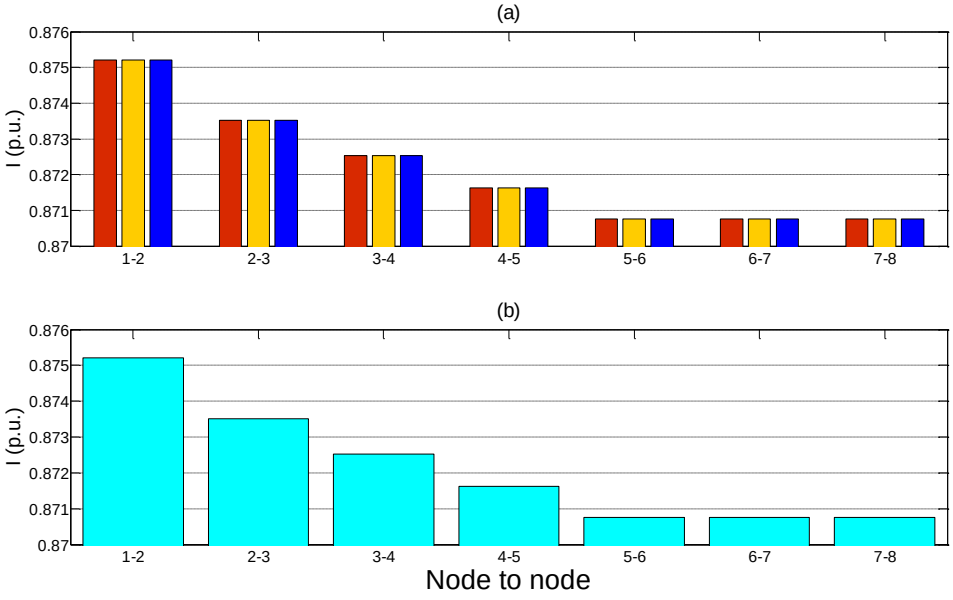

Figure 4-23 Root Mean Square current, (a) line and (b) effective

4.6.6 Voltage and current quality index terms

Separate rms definitions for fundamental and harmonic components are required for the calculation of total harmonic distortion THD of voltage and current or TDD according to [Standard 1459 IEEE 2000], [Standard 519 IEEE 1992] and [Bollen and Gu 2006].

In this work, TDD of current is used instead of THD of current, since it conveys current distortion information in a clearer way. Similarly, the THD of voltage will be replaced by an equivalent definition of TDD of voltage where the base voltage is the denominator instead of the fundamental component. Figure 4-24 shows the three indices of Total Demand Distortion of voltage, namely phase, line-to line and effective. The voltage at the supply point is taken to be sinusoidal. The highly distorted voltage at the load becomes more sinusoidal as it passes through the series impedance, which acts as a filter. The TDD current shown in Figure 4-25 presents changes in its values where the magnetising branches of the step-down and furnaces transformer exist; 1-2 to 3-4 and 3-4 to 5-6.

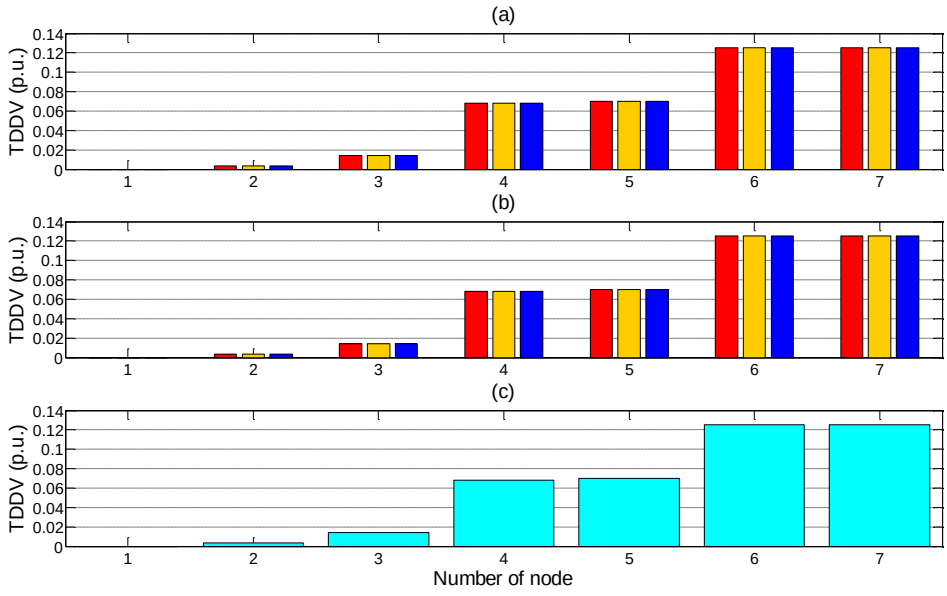

Figure 4-24 Total Demand Distortions of voltages; (a) per phase, (b) line-to-line and (c) effective

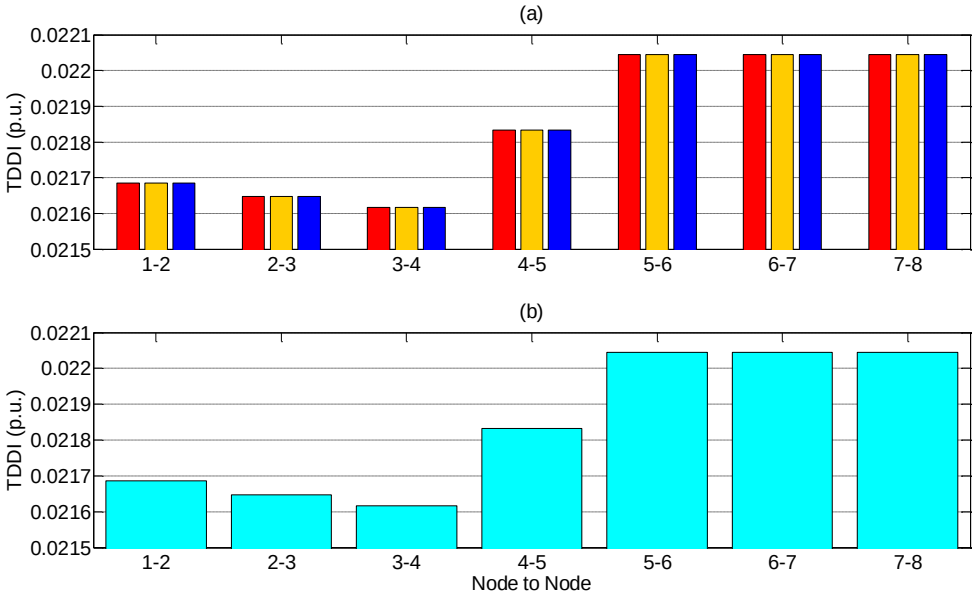

Figure 4-25 Total Demand Distortions of currents; (a) line and (b) effective

4.6.7 Active and non-active powers

The harmonic analysis results may be used in the calculation of additional electrical parameters such as powers, whose definitions can be found in the IEEE standards 1459 [2000] and 519 [1992]. Calculation of the average active power per phase may be carried out by discrete convolutions of harmonic voltage and current terms, as described in Chapter 2 of this work. The convolution operation yields a vector of harmonic components where the zero frequency component is the average active power. If the three-phase average power is required then the values of the three phases are summed up. These average powers are depicted for each phase and node in Figure 4-26 together with the total three-phase powers at each node of the system. These results reveal that slightly more than 0.37 p. u. is actually used in the steel production from the 0.45 p.u. total active power supplied to the system. This loss is attributed to the high currents used in the electric arc installation.

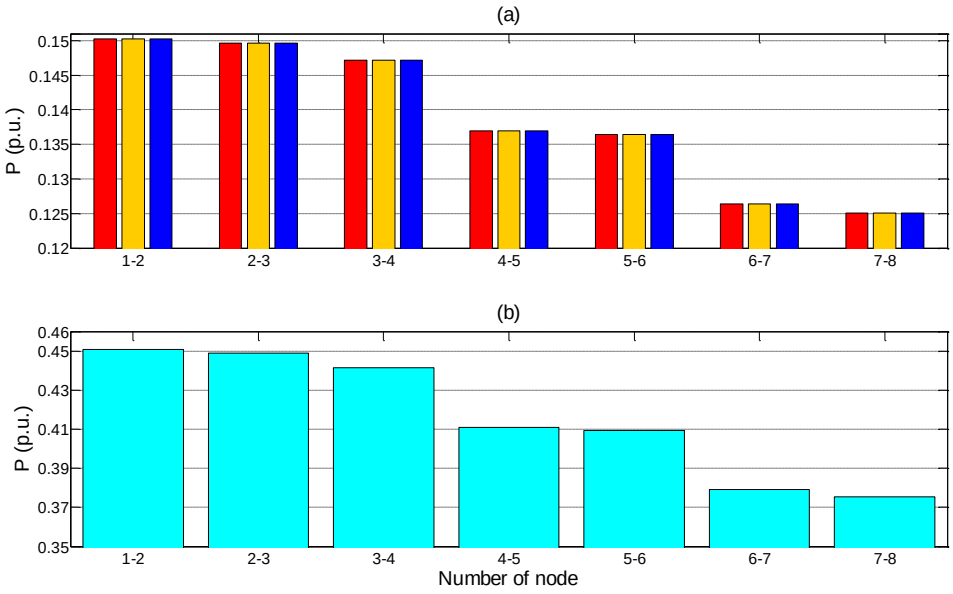

Figure 4-26 Average active powers at elements connected between nodes 1-2 to 7-8: (a) per phase (b) effective

Following the guidelines of IEEE Standard 1459 [2000] the results of three different definitions of apparent power are shown in Figure 4-27 at each node: (a) shows the apparent power per phase; (b) shows the arithmetic apparent power; (c) shows the effective apparent power. The apparent power is an important parameter which in the operation of the electric arc furnace is expected to have values below 1.0 p. u. because this is the nominal capacity of the equipment installed. The apparent power contrasts with the average active power since it has larger variations from node to node; variations which are due non-active powers consumption such as the variations presented between nodes 3 and 4 and nodes 5 and 6 where the series reactor and the secondary circuit are connected respectively. Figure 4-28 shows the average quadrature power which definition was presented in Chapter 2 and may be termed as reactive power. It is clear in this figure that both the series reactor and secondary circuit consume large quantities of reactive power.

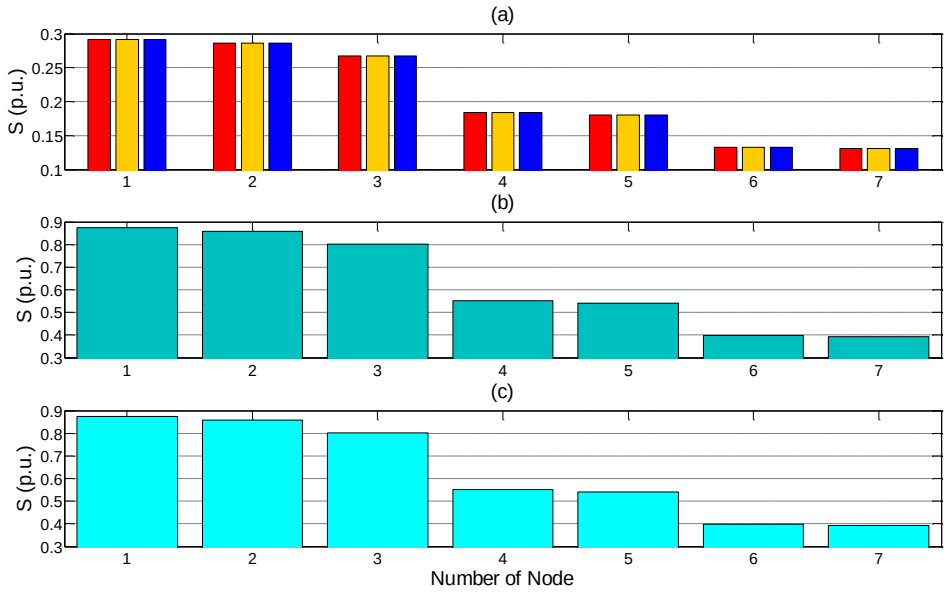

Figure 4-27 Apparent power at nodes 1 to 7: (a) per phase; (b) arithmetic; and (c) effective

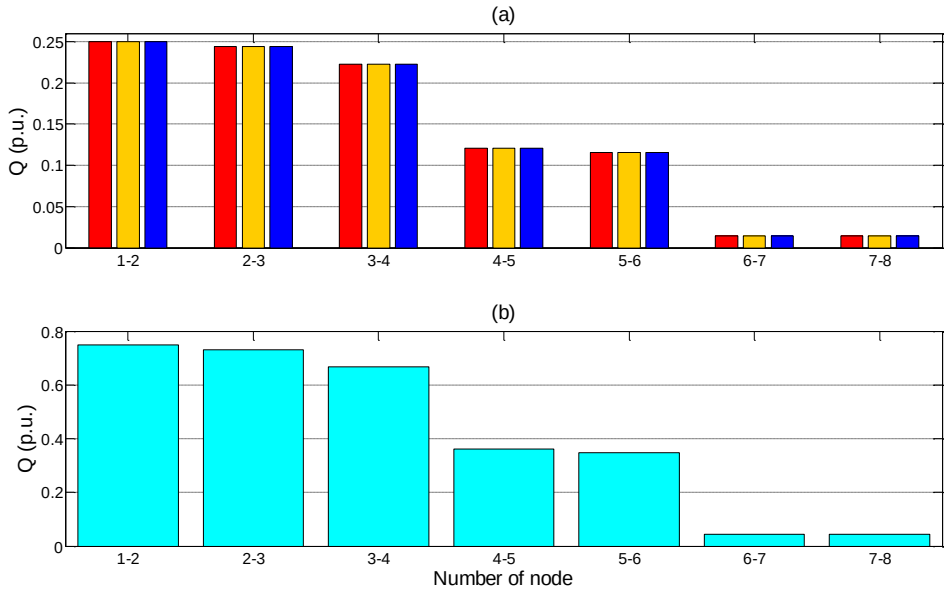

Figure 4-28 Reactive power at elements connected between nodes 1-2 to 7-8: (a) per phase and (b) effective

As defined in IEEE standard 1459 [2000], true power factor is defined, as the ratio of active power and apparent power. This definition applies to the computation of both the power factor per phase and the three-phase power factor using effective quantities. Results for the test case hand are shown in Figure 4-29 (b) and (c) respectively. In these two graphs the power factor is given per node. To contrast these results, which are both termed “true” power factors, are compared with those obtained

using the most restricted definition of power factor, involving the cosine of the angle displacement between voltage and current per phase. These are shown in Figure 4-29 (a). The most striking difference is found near the load point (nodes 6 and 7), where the calculated values using the angle displacement concept does not reflect the harmonic distortion that exist in the circuit at these points. At both nodes the value is unity and differs from the values given by the two other methods of calculating the power factor. It can be observed that the lower power factor values exist in the first three nodes of the system where inductive elements prevail.

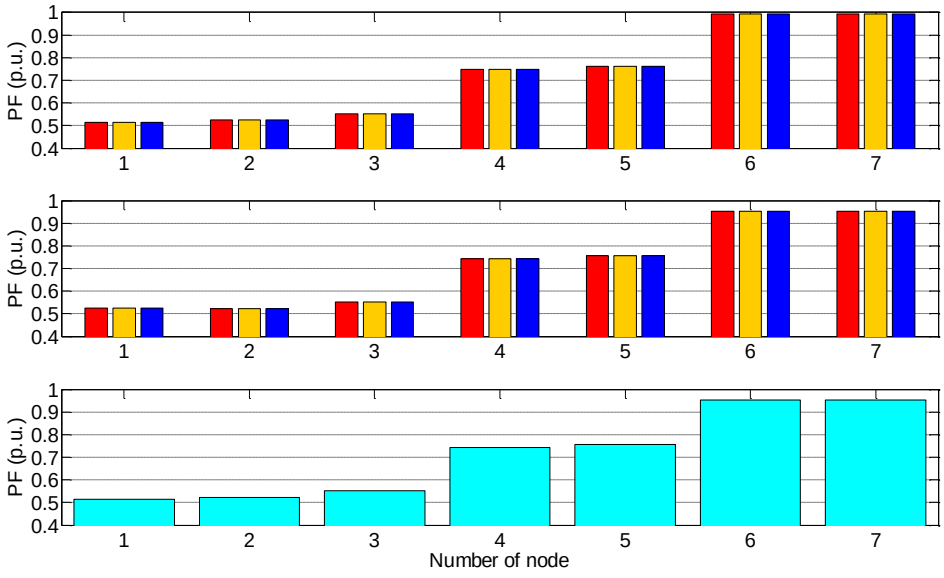

Figure 4-29 Power factor at nodes 1 to 7: (a) displacement; (b) arithmetic; (c) effective

The per unit values of voltage, current, average active power, effective apparent power and the power factor, per node, are given in Table 4-3. The Total harmonic distortion is also included for completeness. The entries in this table are given per phase and they may be compared with the effective values, which represent the full three-phase values shown in Table 4-4. It is noted that the per-phase values and the effective values are identical, at all nodes, for voltage, current, TDD and power factor. It is also noted that the effective active and apparent powers are the arithmetic sum of the powers per phase.

The voltage drops at nodes 1 to 7 is due to the high current used by the arc load which passes through a series reactor, the secondary circuit and two power transformers. The losses are just under 16.75 % of the average active power delivered by the power supply to the electric arc furnace installation; the losses will vary as a

function of the arc voltage length, the rating of the series reactor and number of transformer taps. These elements consume large amounts of reactive power which, in turn, have a direct impact on the apparent power in the primary side of the step-down transformer, which stands at 85.9 % of the transformer capacity. The power factor, which has a value of 0.5227, clearly indicates the need for some form of reactive power compensation. The TDDV at node 3, which is the secondary side of the step-down transformer, reaches a value of 1.4 %. Owing to its location, this value should be reduced since it may yield adverse effects in neighbouring sensitive loads.

Node	Phase	**V**	**I**	**P**	**S**	**PF**	**TDDV**	**TDDI**
1	*a*	1	0.8752	0.1503	0.2917	0.5151	0	0.0217
	b	1	0.8752	0.1503	0.2917	0.5151	0	0.0217
	c	1	0.8752	0.1503	0.2917	0.5151	0	0.0217
2	*a*	0.9815	0.8735	0.1497	0.2863	0.5227	0.0032	0.0216
	b	0.9815	0.8735	0.1497	0.2863	0.5227	0.0032	0.0216
	c	0.9815	0.8735	0.1497	0.2863	0.5227	0.0032	0.0216
3	*a*	0.918	0.8725	0.1471	0.267	0.5511	0.014	0.0216
	b	0.918	0.8725	0.1471	0.267	0.5511	0.014	0.0216
	c	0.918	0.8725	0.1471	0.267	0.5511	0.014	0.0216
4	*a*	0.6328	0.8716	0.137	0.184	0.7444	0.068	0.0218
	b	0.6328	0.8716	0.137	0.184	0.7444	0.068	0.0218
	c	0.6328	0.8716	0.137	0.184	0.7444	0.068	0.0218
5	*a*	0.6223	0.8708	0.1365	0.1806	0.7556	0.0703	0.022
	b	0.6223	0.8708	0.1365	0.1806	0.7556	0.0703	0.022
	c	0.6223	0.8708	0.1365	0.1806	0.7556	0.0703	0.022
6	*a*	0.4563	0.8708	0.1264	0.1324	0.9541	0.1252	0.022
	b	0.4563	0.8708	0.1264	0.1324	0.9541	0.1252	0.022
	c	0.4563	0.8708	0.1264	0.1324	0.9541	0.1252	0.022
7	*a*	0.4521	0.8708	0.1251	0.1312	0.9533	0.1252	0.022
	b	0.4521	0.8708	0.1251	0.1312	0.9533	0.1252	0.022
	c	0.4521	0.8708	0.1251	0.1312	0.9533	0.1252	0.022

Table 4-3 Per unit values of each phase using the base of 700 V, 75 MVA, the total harmonic distortion is presented in p.u.

Node	**V**	**I**	**P**	**Q**	**S**	**PF**	**TDDV**	**THDDI**
1	1	0.8752	0.4508	0.7498	0.8752	0.5151	0	0.0217
2	0.9815	0.8735	0.449	0.7319	0.859	0.5227	0.0032	0.0216
3	0.918	0.8725	0.4414	0.6677	0.801	0.5511	0.014	0.0216
4	0.6328	0.8716	0.411	0.3622	0.5521	0.7444	0.068	0.0218
5	0.6223	0.8708	0.4094	0.3479	0.5418	0.7556	0.0703	0.022
6	0.4563	0.8708	0.3791	0.0437	0.3973	0.9541	0.1252	0.022
7	0.4521	0.8708	0.3753	0.0437	0.3937	0.9533	0.1252	0.022

Table 4-4 Per unit effective values using the base of 700 V and 75 MVA, Total harmonic distortion is presented in p.u.

4.7 Unbalanced Load Modelled as an Ungrounded Star

The former case study has been carried out assuming idealised balanced three-phase electrical load which possesses a non-linear characteristic. However, in the case of an industrial three-phase electric arc furnace, the load representing the arc furnace load is not only non-linear but also unbalanced. The worst case of unbalance that will be considered in the electric arc furnace load will be the case when one of the three electric arcs is extinguished, either due to the dynamic interaction of the arc with the electrical system or due to an unexpected failure such as a graphite electrode breakdown. Notice that for the case of ungrounded arcs the case of two electrodes extinguished such condition does not exist because is not return path. This anomalous condition is simulated using the same parameter used in the balanced test case of Section 4.6, but with the electric arc conductance of phase *a*, assuming to have a zero value. One adverse effect observed when solving this particular case of unbalanced load condition is a slight degradation in the numerical properties of the algorithm as shown in Figure 4-30, the number of iterations is 32 for an error<1e-6. This contrasts with the 22 iterations of the balanced case.

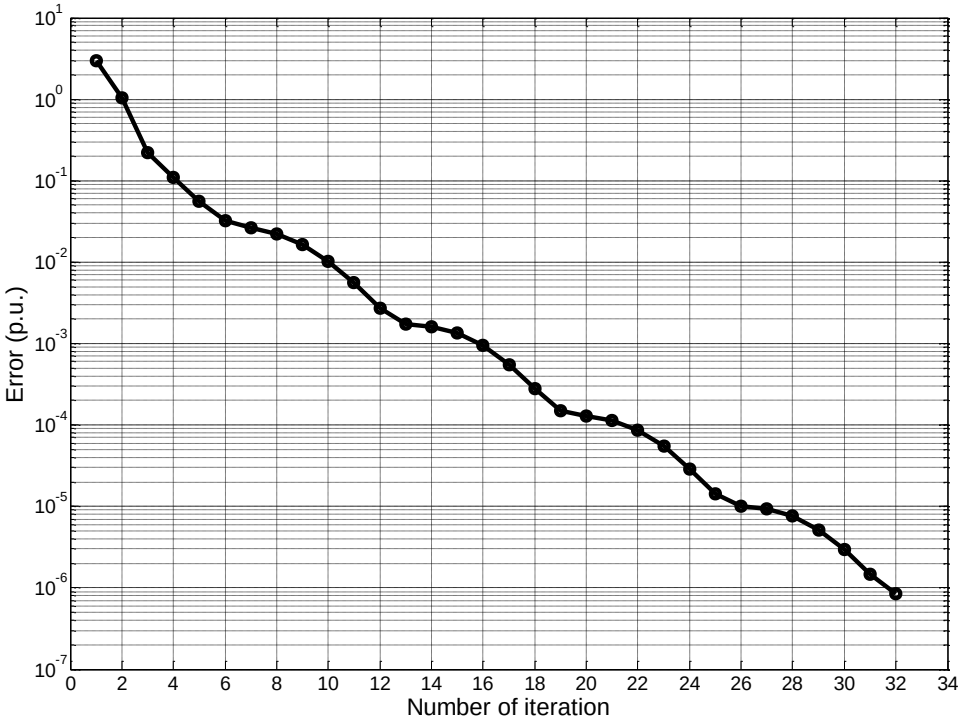

Figure 4-30 Error mismatch vs iteration number

4.7.1 Unbalanced electric arc load

Figure 4-31 shows no arc conductance value at phase *a* and equal conductance values at phases *b* and *c*. However, it should be noticed that these conductance values differ from these of the balanced load case.

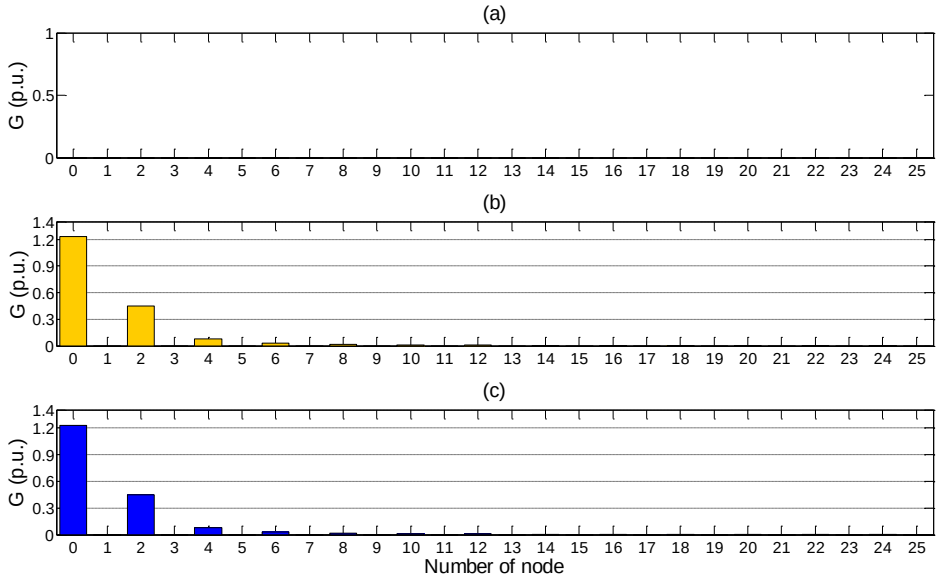

Figure 4-31Harmonic magnitudes of the electric arc conductance: (a) phase *a*; (b) phase *b*; and (c) phase *c*

Three sets of voltage and current waveforms are reproduced from the harmonic simulation results. Figure 4-32 depicts the first set, where the phase voltage waveforms present dissimilar shapes between them. The phase *a* voltage has a value close to one since no current is flowing in this phase on the contrary the phases *b* and *c* voltages have lower voltage values product of the voltage drop in the path of the current that close the unbalanced load. In the case of the line current waveforms, the current in phase *b* is identical to that of phase *c* but displaced by 180 degrees, which means that it is a loop current circulating in a closed loop and passing through both arc conductances. As already stated, the current in phase *a* is zero. Figure 4-33 shows the line-to-line voltages and phase currents that exist in the arc furnace installation, this is useful information that yield a good idea of the voltages values that the insulation of the cables is to withstand. Figure 4-34 shows the arc voltage waveforms of phase *b* and *c* which present a common shape but with a displacement of 180 degrees between them. The voltage waveforms of phase *a* does not exist.

Each set of current and voltage waveforms may be transformed in to corresponding sets of current-voltage characteristics. The first two sets yield unexpected shapes, as can be observed in Figure 4-35 and Figure 4-36. However, the set one, made up by arc currents and arc voltages, shown in Figure 4-37, conserve the familiar characteristic of the electric arc and correctly pickup the load unbalanced condition.

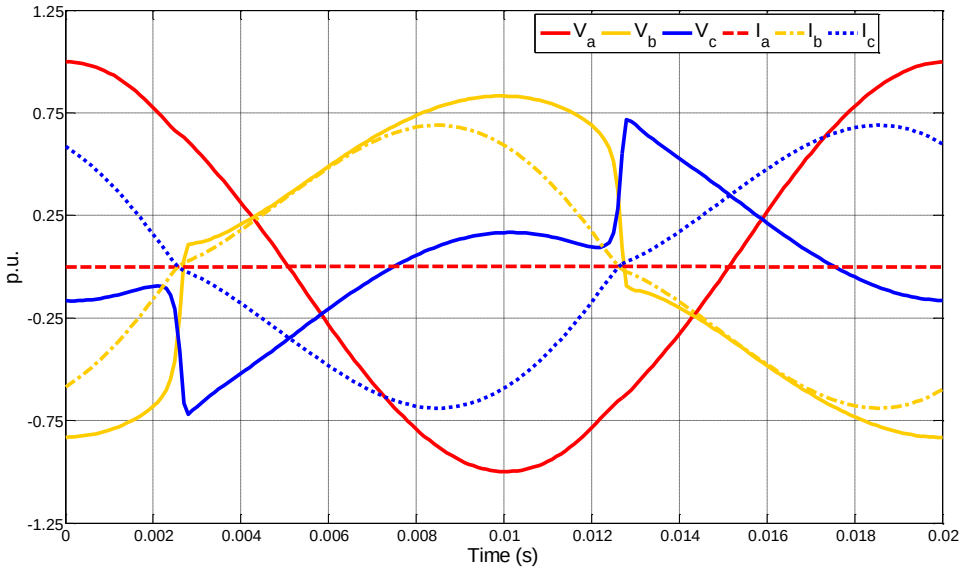

Figure 4-32 Phase voltages and line current waveforms

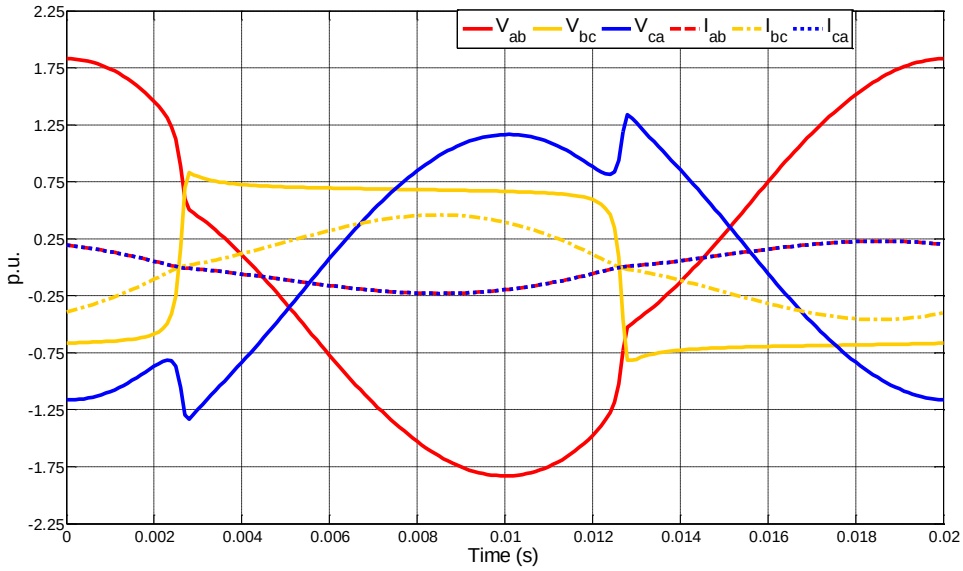

Figure 4-33 Line-to-line voltage and phase current waveforms

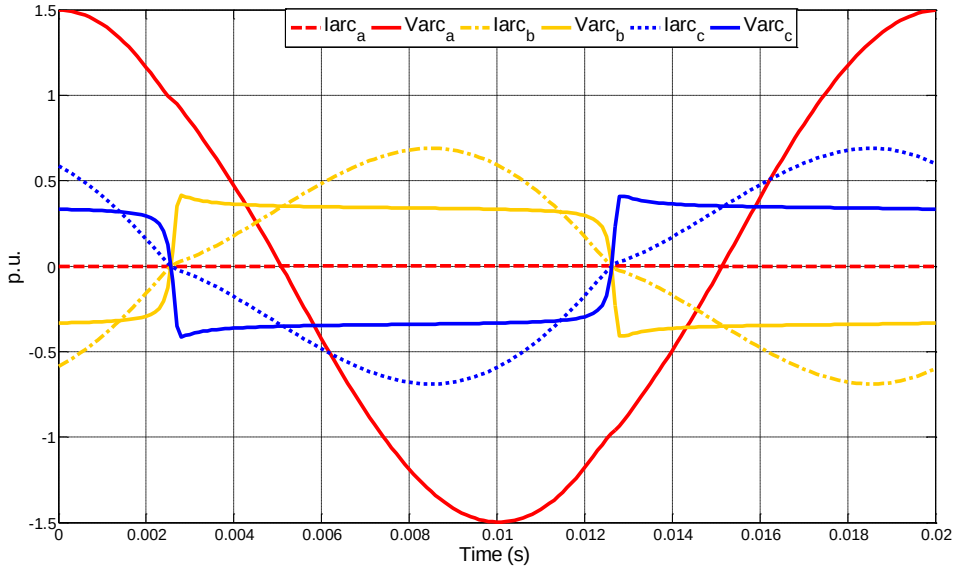

Figure 4-34 Arc voltage and arc current waveforms

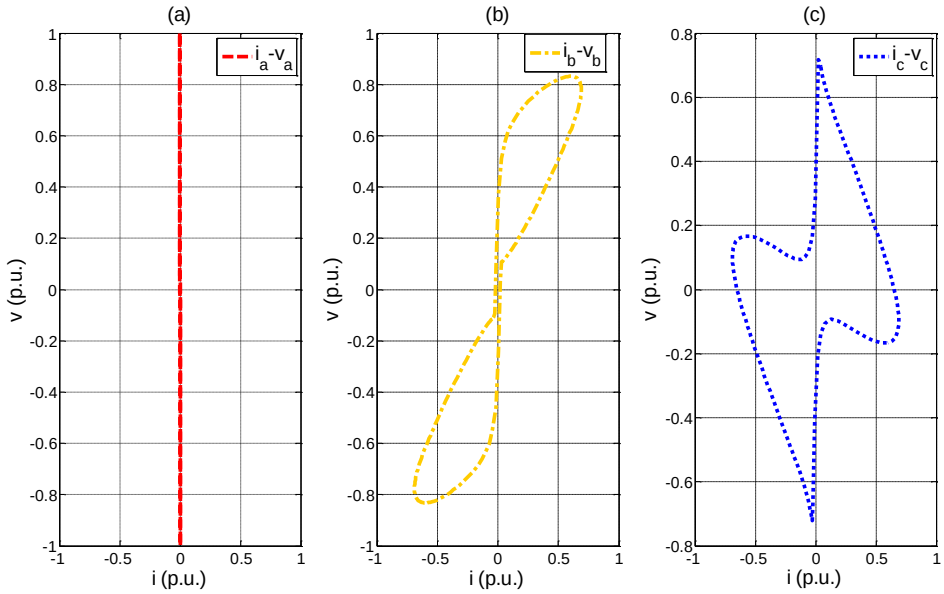

Figure 4-35 Phase voltage and line current characteristics

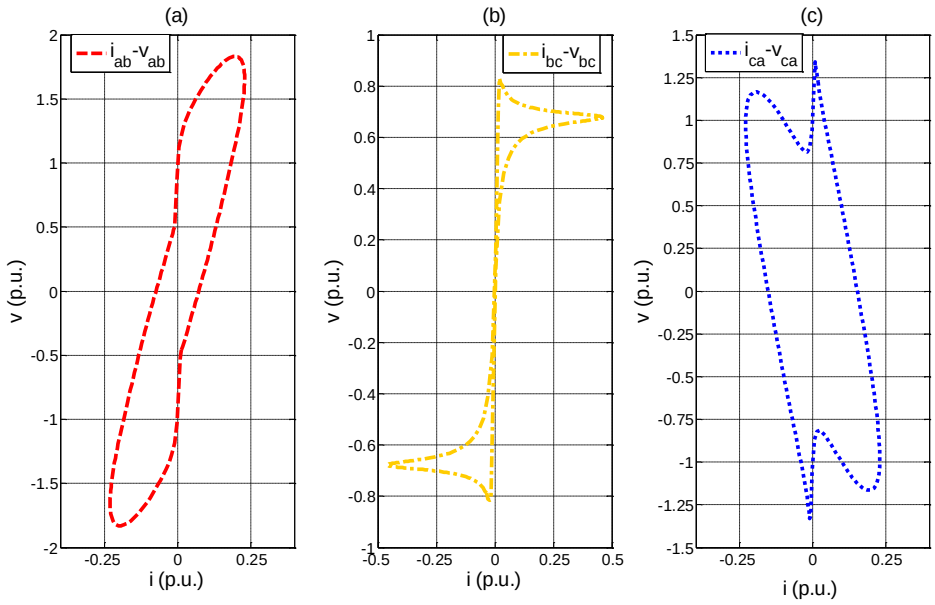

Figure 4-36 Line-to-line voltage and phase current characteristics of the equivalent delta

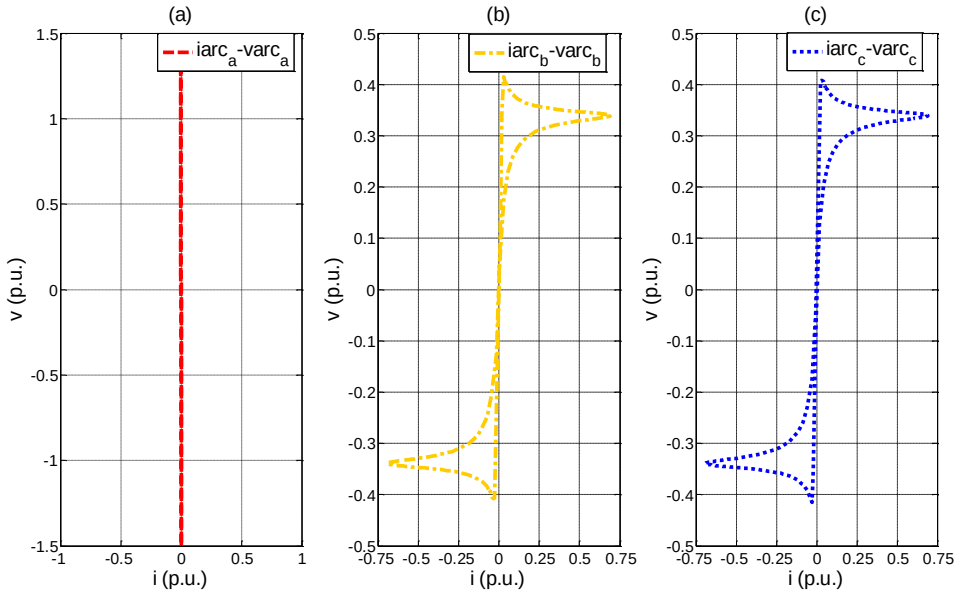

Figure 4-37 Arc voltage and arc current characteristics

Figure 4-38 depicts four graphs relating to arc powers; (a) shows the instantaneous power conformed by the product of phase voltage and line current. All waveforms have different shape, anticipating that the average power would be different at each phase. (b) shows the instantaneous power of a delta equivalent load, where the powers in each phase differ from each other. (c) shows the instantaneous power conformed by the product of arc voltage and arc current. This power consumption is equal in phases, *b* and *c*, as result the waveforms are superimposed and give the instantaneous power delivered by each arc to the load. The three-phase instantaneous power of each set presented in the graphs (a), (b), and (c) yields the same and the three waveforms are superimposed as is shown in (d).

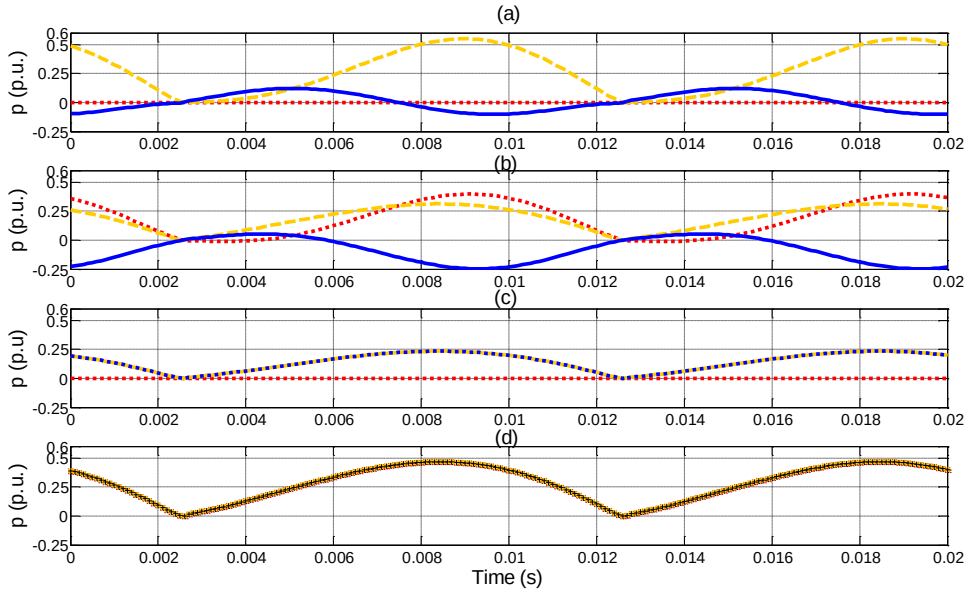

Figure 4-38 Instantaneous powers: (a) in the star-connected load ;(b) in the equivalent delta-connected load (c) in the arc; and (d) instantaneous three-phase power computed with the three set of parameters

4.7.2 Star point of the ungrounded star

Figure 4-39 shows the voltage at the star point of the star connection. This result corresponds to an unbalanced situation where the voltage has a high value of fundamental component with small contributions of third and fifth harmonic components compared with the balance case.

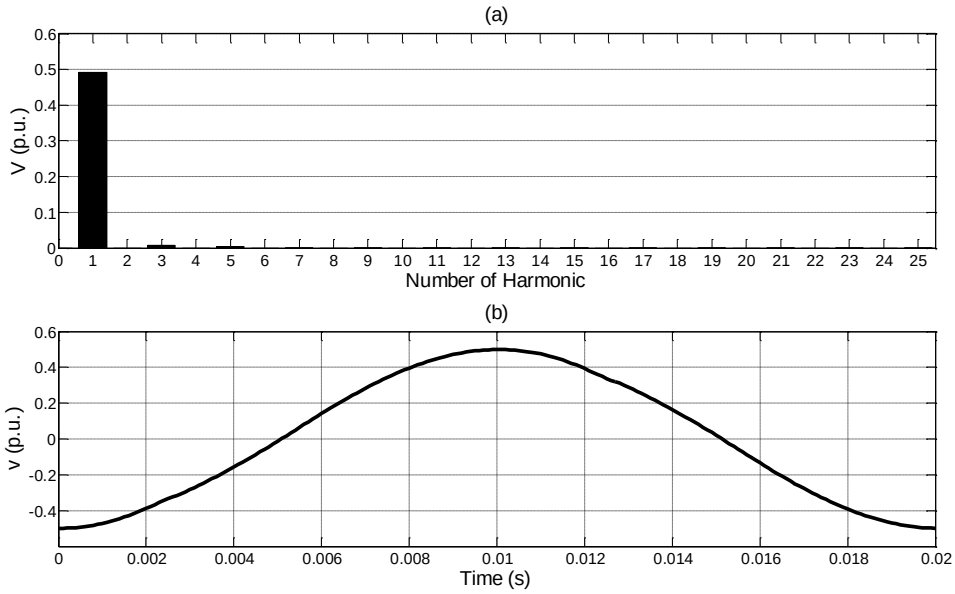

Figure 4-39 Harmonic magnitudes and waveform of the voltage at the star point

4.7.3 The impact of the transformer magnetising branch

The current delivered to the step-down transformers magnetising branch has similar values for each phase; these values are well below one percent of the base current and they are of no special concern. However, it is observed that the unbalanced load causes the transformer to have different current harmonic magnitudes in each phase, as shown in Figure 4-40. These differences can also be observed in the current waveforms depicted in Figure 4-41.

Quite a different situation exist in the furnace transformer where the magnetising branch produces higher harmonic distortion than in the step-down transformer, as shown in Figure 4-42 The third harmonic goes above 1 % of the base current in phase *a* and *b*. The currents are highly unbalanced as illustrated by the waveforms depicted in Figure 4-43.

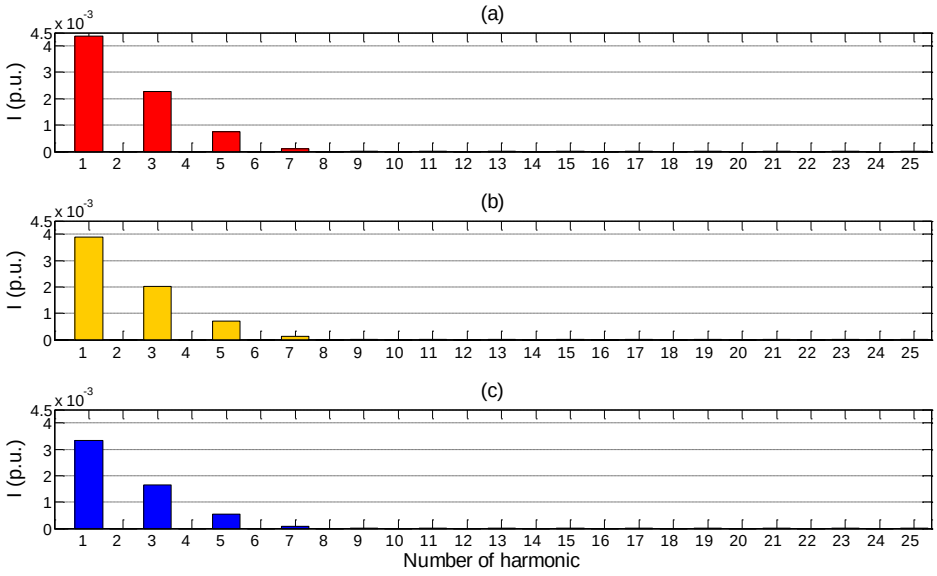

Figure 4-40 Harmonic current magnitudes of the step-down transformer magnetising branch

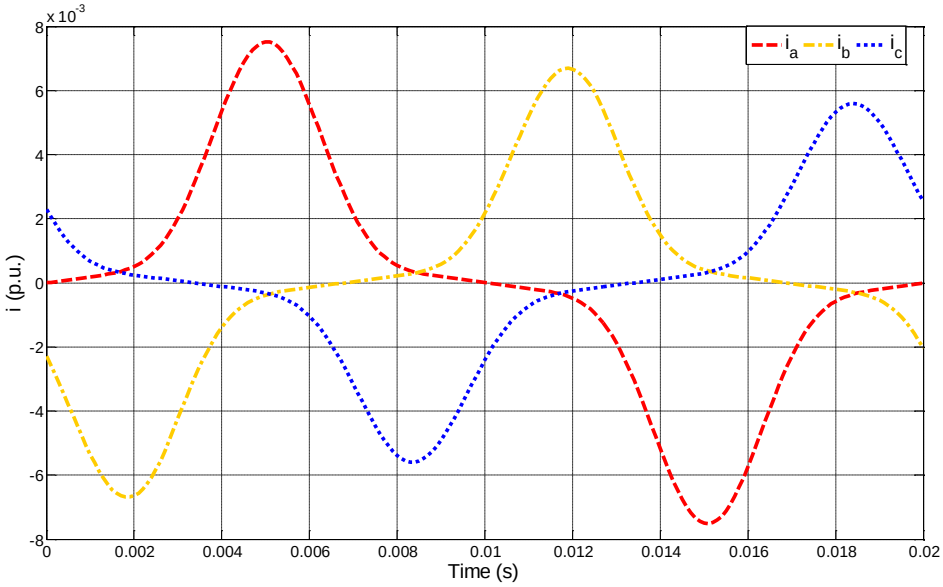

Figure 4-41 Current waveforms of the step-down transformer magnetising branch

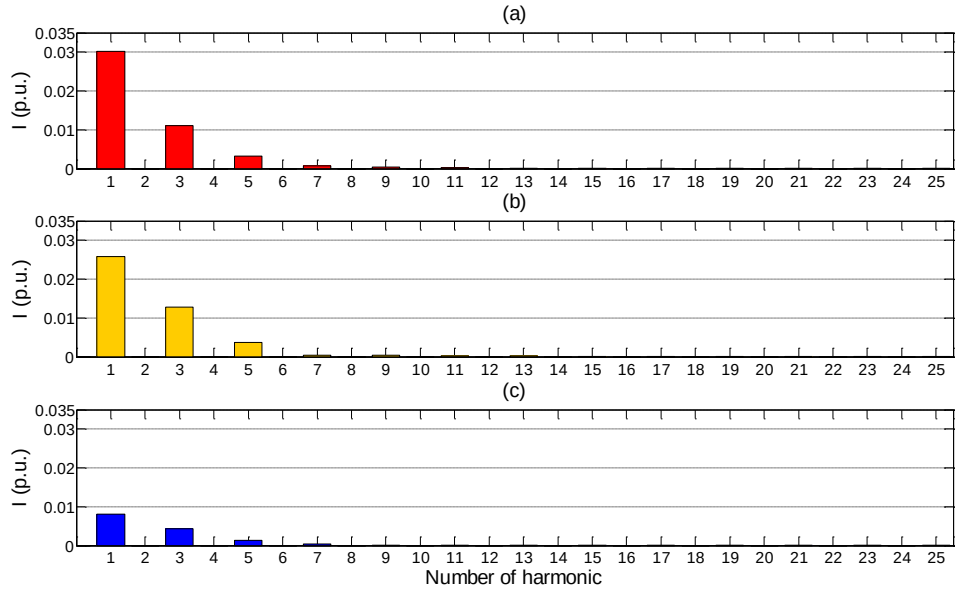

Figure 4-42 Harmonic current magnitudes of the furnace transformer magnetising branch

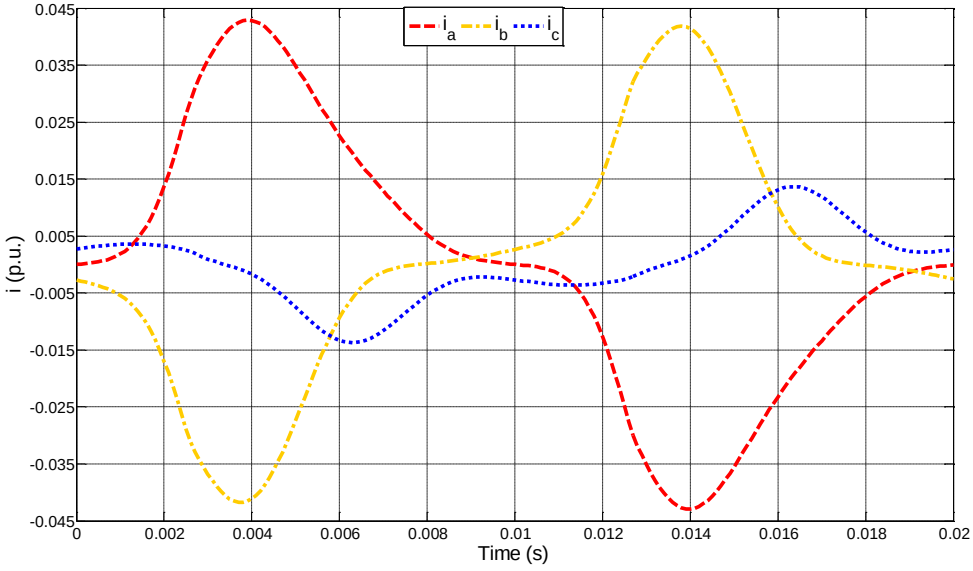

Figure 4-43 Current waveforms of the step-down transformer magnetising branch

4.7.4 Harmonic results

The per-phase harmonic voltages magnitudes are shown in Figure 4-44 for the seven-node test system. It is noticed that the voltages in phase *a* have similar fundamental and harmonic values at all nodes since this is an open phase and the step-down and furnace transformers cause only small voltage drops. In contrast, due to the loop current circulating in phases *b* and *c*, very significant voltage drops and rises for

the fundamental and harmonic frequencies, respectively, are noted for phases *b* and *c*, at nodes 5 and 7. It is observed that for phases *b* and *c* the values of third harmonic are 8% and 15% at nodes 5 and 7, respectively. Likewise, the values of fifth harmonic are 5% and 9%. This is in marked contrast to the case of balanced operation, where the zero sequence harmonics have very low values - the third and fifth harmonics are both 1%.

The line-to-line voltages shown in Figure 4-45 offer additional information on the harmonic voltages which are delivered to line-to-line connected loads. It should be noticed that the line-to-line harmonic voltages in the unbalance case, in contrast to the balanced case, exhibit third harmonic voltages and their multiples.

The harmonic line currents flowing in the elements connected between nodes 1-2 to 7-8 are shown in Figure 4-46. The open condition in phase *a* causes a zero current flow in this phase in the elements connected between nodes 5-6 to 7-8. However, owing to the transformer connection, some current appears in phase *a* in the elements connected between nodes 1-2 to 4-5 is product of the line to line connected branches. The unbalanced load condition is responsible for the existence of zero sequence harmonic currents at all the nodes. In particular, it is noted that the magnitude of the third harmonic current increases with the unbalance to values of around 5% in phases *b* and *c*.

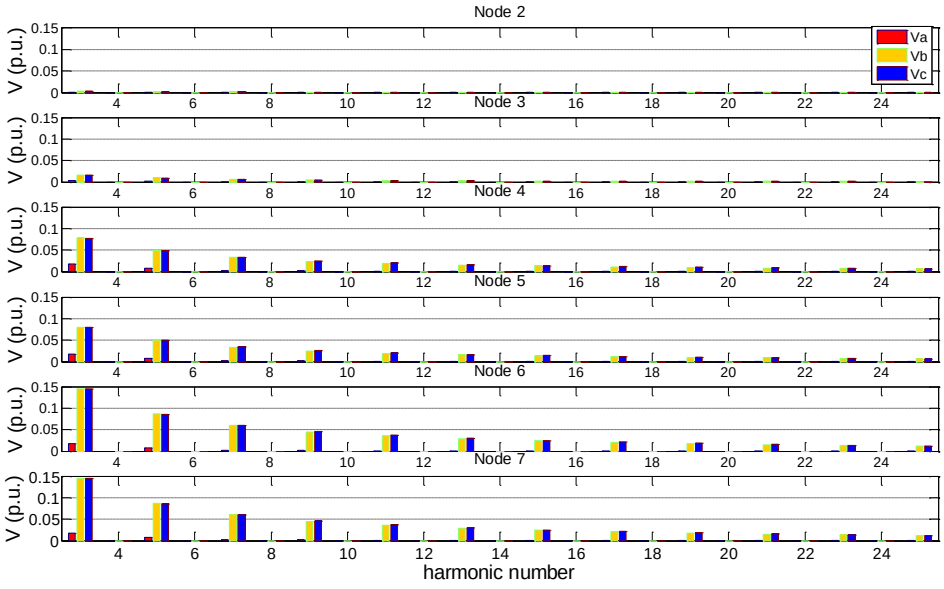

Figure 4-44 Harmonic magnitudes of phase voltages at nodes 1-7

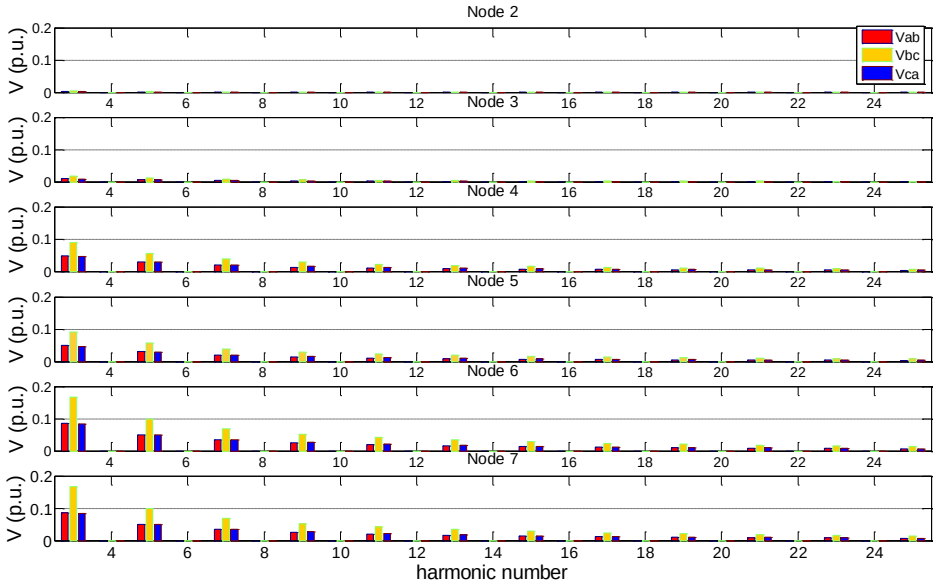

Figure 4-45 Harmonic magnitudes of line-to-line voltages at nodes 1-7

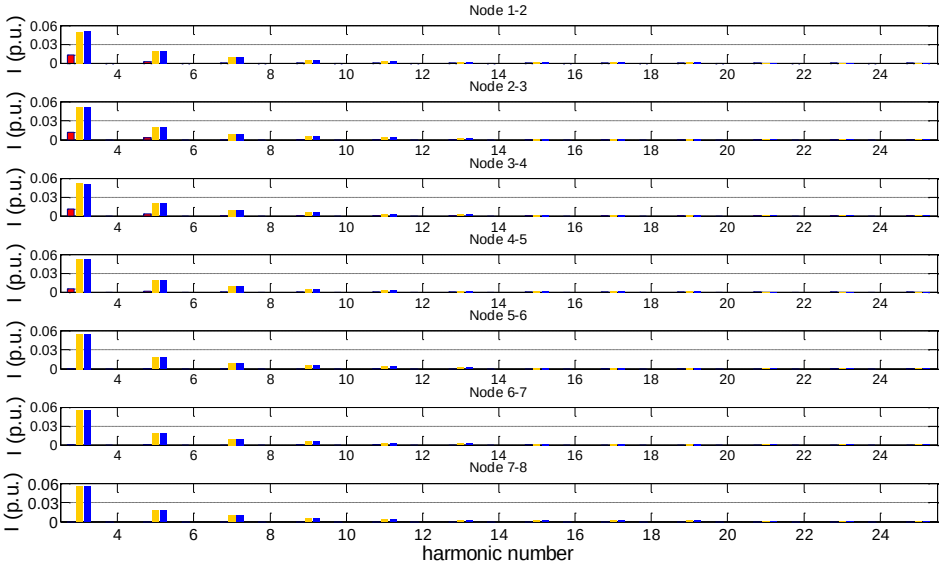

Figure 4-46 Harmonic magnitudes of currents at elements connected between nodes 1-2 to 7-8

4.7.5 Root Mean Square values

In the same form than balanced case the root mean square voltages, per phase, line-to-line and effective are calculated. These are depicted in Figure 4-47, the unbalanced is reflected in them but it is difficult to conclude that the unbalanced is effect of an open phase, but with additional information such as the rms current values,

shown in Figure 4-48 a complete image of the unbalanced situation of the system is clear.

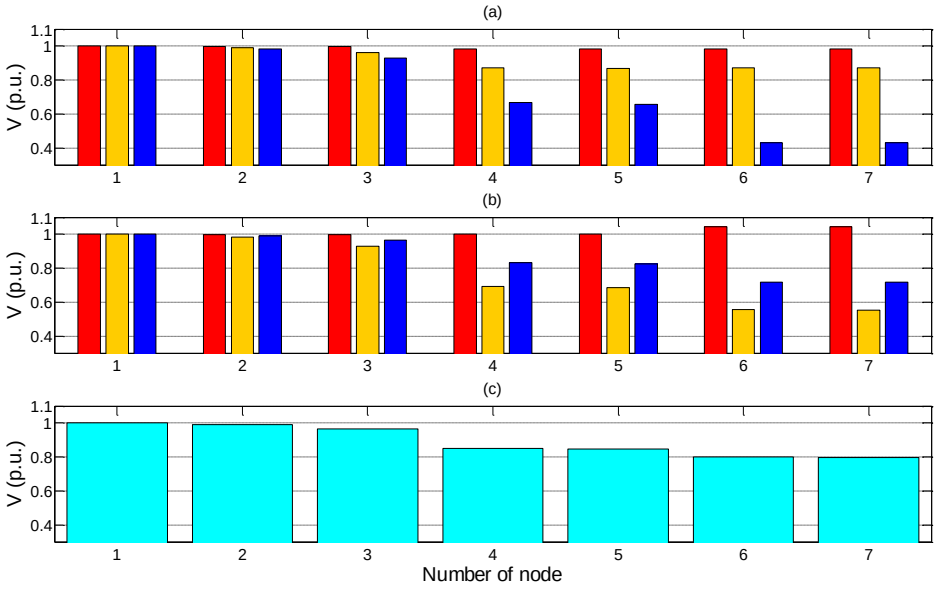

Figure 4-47 Root Mean Square voltages at nodes 1 to 7; per phase, line-to-line and effective

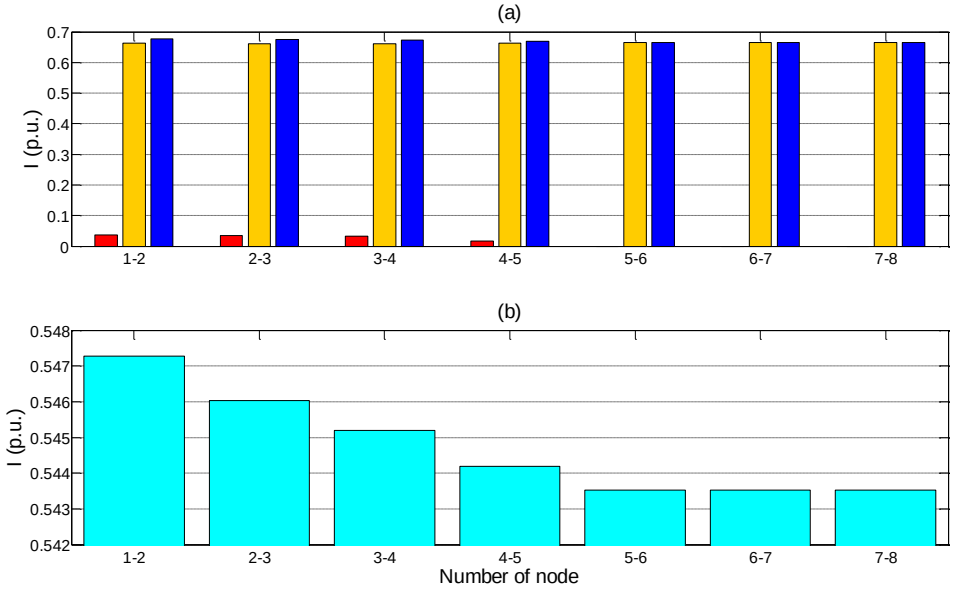

Figure 4-48 Root Mean Square currents at elements connected between nodes 1-2 to 7-8: (a) line and (b) effective

4.7.6 Harmonic distortion indices

In contrast to the case of balanced load presented in Section 4.6, the unbalanced case presents increased values of the total harmonic distortion of voltage and current as shown in Figure 4-49 and Figure 4-50. Harmonics that are not present in the balanced case do appear in the unbalanced case, such as third harmonic. The total demand distortion of voltage shown in Figure 4-49 reveals values at the primary side of the step-down transformer (PCC), near to the maximum limits recommended in IEEE Standard 519. It can also be observed that TDD voltage values at node 3, which is the secondary side of the step-down transformer, the values are above 1.82 % which can impact negatively on the steel-making process. The total demand distortion of current varies between 3.31 and 4.73 % which are accepted values in the Std 519 and are cause of no concern.

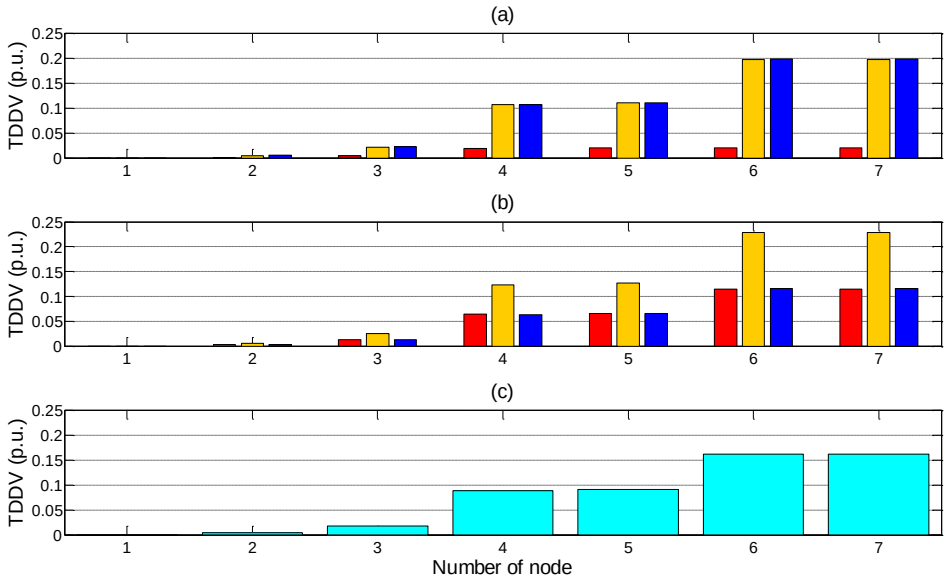

Figure 4-49 Total Demand Distortion of voltage at each nodes 1 to 7: (a) per phase; (b) line-to-line; and (c) effective

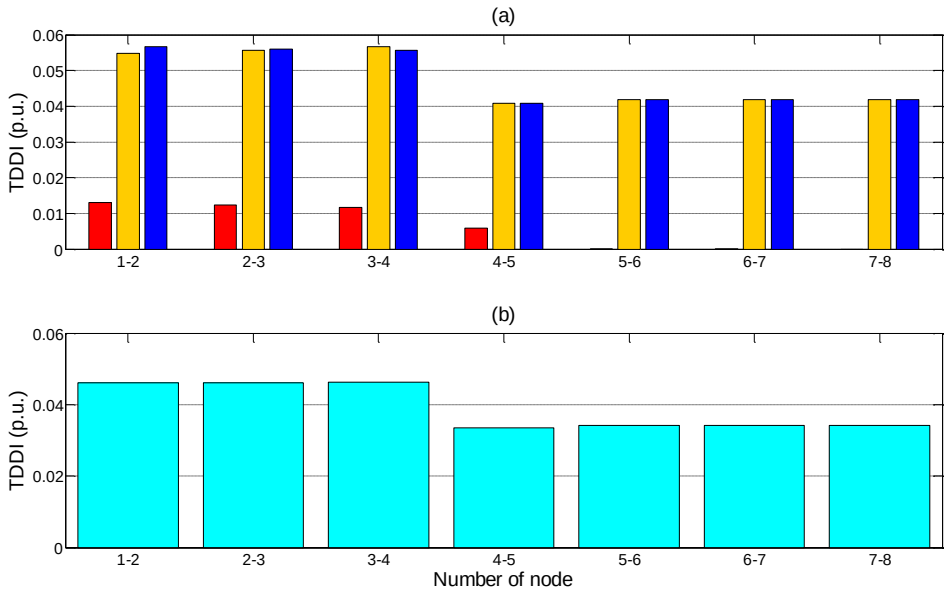

Figure 4-50 Total Demand Distortion of current at elements connected between nodes 1-2 to 7-8: (a) line and (b) effective

4.7.7 Active and non-active powers

The interpretation of results of active power per phase can be misleading, as it was the case in the results presented in Figure 4-38 where it was shown that only the three-phase instantaneous active powers yield a consistent set of results. The Figure 4-51 (a) shows the average active power per phase where the major amount of power is delivered by phase *a*. Figure 4-51 (b) shows the three-phase average active power, which compared to the balanced case presented in Figure 4-26, shows drops in active power consumption of more than half.

Figure 4-52 (a) shows the apparent power per phase, where it is clear that the apparent powers of phase *a* at the lowest values where the arc load is not connected. Apparent power of phase *a* and *b* in similar form that the active power can be misleading. The effective apparent power shown in Figure 4-52 (b), with node 7 is holding a value slightly higher than in the balanced case result shown in Figure 4-27 (b).

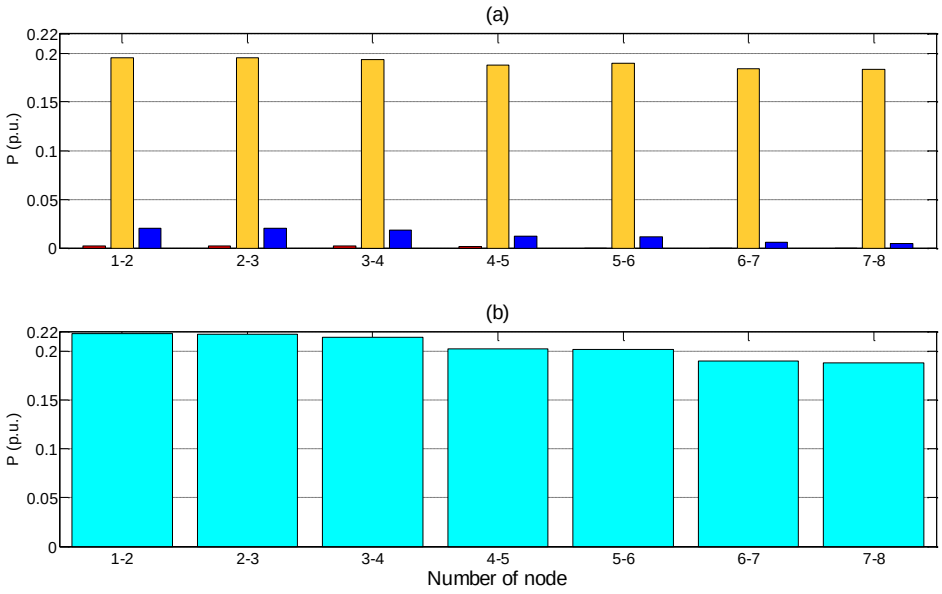

Figure 4-51 Average active power at elements connected between nodes 1-2 to 7-8: (a) per phase and (b) three-phase

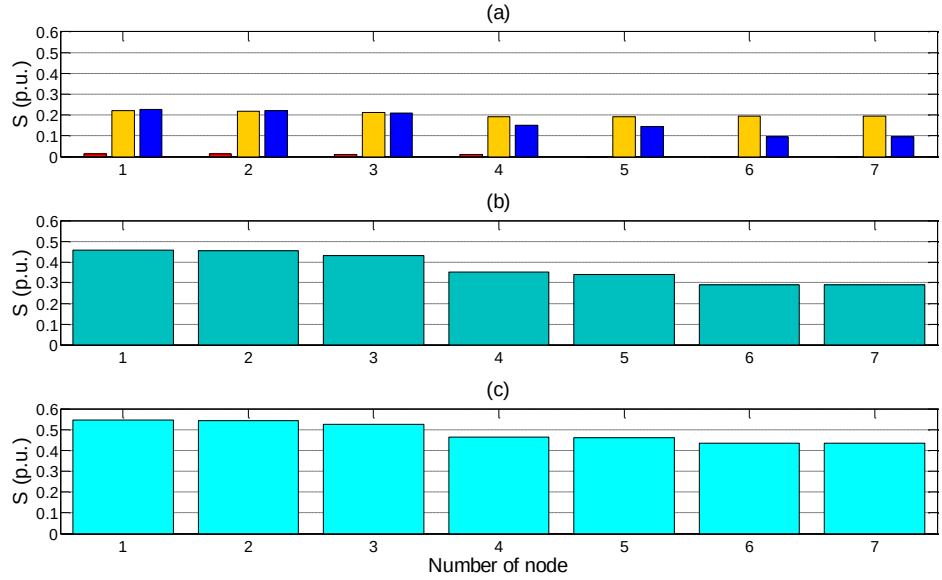

Figure 4-52 Apparent powers at nodes 1 to 7: (a) per phase, (b) arithmetic and (c) effective

For completeness, the information presented in Figure 4-47 to Figure 4-52 is also presented in numeric form in Table 4-5 and Table 4-6. The per-unit voltages are derived with a base line-to-line voltage of 700 V. The base power is the three-phase apparent power with a value of 70 MVA.

In Table 4-5, it is significant the difference that exists between the rms phase voltage of phases *b* and *c* at node 7. It has been established that this is due to the current loop that the unbalanced load condition establishes between the two healthy phases. The rms currents in phases *b* and *c* keep identical values between nodes 5 to 7 but have some perceptible changes between nodes 1 to 4, which are attributed to the magnetizing branches of the two power transformers and their winding connections. The per-phase values of the average active power shown in this table indicate that phase *b* contributes the most active power. The TDDV of phase *b* and *c* have values above 2% at the node 3 (secondary side of step-down transformer), which represents a point where some sensitive loads could be connected to.

Node	**Phase**	**V**	**I**	**P**	**S**	**PF**	**TDDV**	**TDDI**
1	**a**	1	0.0369	0.0019	0.0123	0.1532	0	0.0131
1	**b**	1	0.6629	0.1954	0.221	0.8842	0	0.0548
1	**c**	1	0.6766	0.0204	0.2255	0.0903	0	0.0566
2	**a**	0.9992	0.0346	0.0019	0.0123	0.1533	0.001	0.0123
2	**b**	0.9916	0.662	0.195	0.2191	0.8901	0.0049	0.0557
2	**c**	0.9842	0.6745	0.02	0.222	0.0901	0.005	0.056
3	**a**	0.9966	0.0323	0.0019	0.0107	0.1749	0.0041	0.0116
3	**b**	0.9634	0.6614	0.1936	0.2124	0.9114	0.0217	0.0566
3	**c**	0.9303	0.6732	0.0185	0.2088	0.0885	0.0221	0.0557
4	**a**	0.9847	0.0162	0.0019	0.0106	0.1757	0.0192	0.0058
4	**b**	0.8706	0.6634	0.1877	0.1919	0.9781	0.1069	0.0409
4	**c**	0.669	0.6694	0.0124	0.1501	0.0829	0.1071	0.0408
5	**a**	0.9845	0	0	0	-0.3318	0.0195	0
5	**b**	0.8684	0.6657	0.1899	0.1927	0.9853	0.1105	0.0418
5	**c**	0.6586	0.6657	0.0115	0.1461	0.079	0.1107	0.0418
6	**a**	0.9845	0	0	0	-0.3162	0.0195	0
6	**b**	0.8738	0.6657	0.184	0.1939	0.9487	0.1975	0.0418
6	**c**	0.4312	0.6657	0.0056	0.0957	0.059	0.1985	0.0418
7	**a**	0.9845	0	0	0	Na	0.0195	0
7	**b**	0.8707	0.6657	0.1832	0.1932	0.9483	0.1974	0.0418
7	**c**	0.431	0.6657	0.0049	0.0956	0.0513	0.1985	0.0418

Table 4-5 Per unit values of each phase using the base of 700 V, 75 MVA, the total harmonic distortion is presented in p.u.

The effective values shown in Table 4-6 give general information about the system. The rms voltage and current effective values at node 7 no give information about the severe unbalanced condition, but the low power factor in the same node indicates an anomalous situation that can not be attached to the low reactive power values. Another important sign is the small variation of power factor at node 1 to 7 in contraposition with Table 4-4 which are the numerical results of balanced condition.

Node	V	I	P	Q	S	PF	TDDV	TDDI
1	1	0.5473	0.2176	0.3367	0.5473	0.3976	0	0
2	0.9917	0.546	0.2169	0.3296	0.5427	0.3997	0.0041	0.0041
3	0.9638	0.5452	0.2139	0.3016	0.5255	0.4071	0.0186	0.018
4	0.8515	0.5442	0.202	0.1805	0.4642	0.4352	0.104	0.0881
5	0.848	0.5435	0.2014	0.157	0.4609	0.437	0.1079	0.091
6	0.7997	0.5435	0.1896	0.0365	0.4347	0.4362	0.2069	0.162
7	0.7985	0.5435	0.1881	0.0365	0.434	0.4334	0.2072	0.162

Table 4-6 Per unit effective values using the base of 700 V and 75 MVA, Total harmonic distortion is presented in p.u.

4.8 Conclusion

A non-linear power balance differential equation that characterises the electric arc has been expressed in the complex conjugate harmonic domain and used to develop a full three-phase model of an arc furnace installation. The overall model is in the harmonic domain and combines the representation of non-linear elements such as the magnetising branches of the step-down and the furnace transformers, where saturation is incorporated, and other plant components such as a series reactor, cables and electrodes. This model enables comprehensive harmonic assessments of the electric arc furnace installation and yields physical understanding of the harmonic interactions taking place between the various non-linearities that exist in different parts of the installation.

The overall model was coded in Matlab and solved using up to the 100^{th} harmonic. The numerical performance of the overall model presents good convergence characteristics, taking 22 and 32 iterations to converge for the balanced and unbalanced case respectively, with an error mismatch of 1e-06.
The case of balanced operation of the electric arc furnace installation is addressed first, providing a starting point in the understanding the non-linear effects introduced by the load in rest of the electrical system. A comprehensive set of power quality parameters are generated for each node of the system such as harmonic spectrum, root mean square, powers and TDD indexes. These data reveal the complex interaction that exists between the non-linear electric arc loads and their impact in the electrical network. In this case the magnetising branch of step-down and furnace transformer does not contribute to notorious harmonic pollution to the system.

The case of unbalanced operation of the electric arc furnace installation gives credence to the robustness of the algorithm, where quite severe conditions exist. It is observed that in this case the unbalanced load is responsible for increasing further the harmonic content of the voltage and current waveforms. In the arc, only the arc current and voltage characteristics hold coherent information about the arc load. One further negative effect cause by the unbalance in the furnace transformer is an increase in magnetisation current at both the fundamental and harmonic frequencies. The comprehensive set of power quality indices carried out for this study is useful to asses

whether or not the electric arc furnace installation operated within power quality recommendations and standards. The integrated model of the electrical furnace installation is further expanded in the next Chapter to study the impact of power electronic-based compensation in the operation of the installation.

5 Harmonic Interaction of Electric Arc Furnace Installations with Ancillary Power Electronics Equipment

5.1 Background on Power Electronics Compensation in Electric Arc Furnace Installations

Electric arc furnace installations demand large amounts of non-active power compensation owing to the very pronounced non-linear characteristic of the electric arc load which yields highly distorted voltage and current waveforms and hence non-active powers. Moreover, the stability of the arc requires the use of equipment that demands reactive power compensation such as the furnace transformer and the series reactor. A less well-know fact is that the behaviour of the three-phase electric arc furnace is intrinsically an unbalanced one, and that this phenomenon in itself is a sink of non-active power.

In early electric arc furnace installations, reactive power compensation was carried out using fixed banks of capacitors, with sections being switched in and out according to requirements. However, the behaviour of the electric arc furnace is dynamic in nature and marked variations exist not only for different stages of the melting cycle but also within stage itself. One solution was to use electromechanical switching capacitors which adapt their reactive power provision to different stages of the electric arc furnace operation but their response time was deemed too slow.

The development of power electronic valves such as the Thyristor enable the construction of VAR compensation equipment with a finely regulated and much faster dynamic response; the Static Var Compensator is one of such equipment. From the outset the main concern in SVC application was reactive power compensation aimed at eliminating the angle displacement between the voltages and current waveforms. However, the issue of the harmonic generation soon became a matter of study when the SVC is used to provide VAR compensation. As stated by Miller [1982] electronic power devices produce distortion in both voltage and current waveforms in the electrical network. Hence when the primary goal of reactive power compensation is reached, it then becomes necessary to carry out a harmonic assessment to try to eliminate the waveform pollution produced by the compensator. Miller [1982] remarks

that electrical arc furnace installations contain a unique combination of problems which need to be solved for an efficient operation of the installation. The most pressing are; reactive power compensation, harmonic filtering and voltage stability control.

More recently, as the power electronics technology has advanced, Larsson and Poumarède [1999] have pointed out that the SVC switches at the fundamental frequency and that this yields long response times with compensation limited to respond to events on a cycle by cycle basis. It is argued that this limits the capability of the SVC to react to the voltage variations responsible for flicker emissions. Moreover, the SVC harmonic elimination needs to be carried out using tuned filters. These authors argue that such limitations of the SVC have been surpassed with the introduction of a new generation of VAR compensation equipment such as the Static Compensator (STATCOM). This device comprised a voltage source converter and an interfacing transformer with the converter using IGBT valves and PWM switching control. They have the ability to deliver reactive power with a faster response than the SVC and are better able to cancel out flicker effects. However, STATCOMS have a higher price tag than SVCS with comparable rating and questions remain about their harmonic performance and switching losses. In contrast, the SVC technology is very mature and many electric arc furnace installations use this technology. This provides the motivation for modelling the SVC within the overall representation of the electric arc furnace plant. The integration of a STATCOM model will be part of a future research.

Power electronics is not only used for the purpose of compensation in electric arc furnace installations. Stabilisation of the electric arc depends on a series reactor, which according to [Cardoso and Cardoso 2006] and [Ma and Mulkahy], could be replaced by a Thyristor Switched Reactor for a faster response with improved stability and flicker control as opposed to the traditional series reactor with on-load tap changers which are mechanically controlled. In the power electronic variant the Thyristor valves are used as on-off valves.

The interaction between the arc furnace and the power electronic devices is the full electric arc furnace installation used in Chapter 4 in this study.

5.2 Modelling of Three-phase Static Var Compensators

The SVC is made up of a Thyristor Controlled Reactor, a capacitor bank and harmonic filters. It serves the purpose of either supplying or absorbing reactive power from the AC power network at the point of connection. Apart from HVDC transmission the Static Var Compensator was first power electronics application in electrical power networks. In industrial applications, the SVC was used at a very early stage to provide reactive power compensation in electrical arc furnace installations.

5.2.1 Modelling of the three-phase thyristor controlled reactor

The Thyristor controlled reactor is a key component of several power electronic converters. Researchers such as Yacamini and J.W. Resende J [1986] and W. Xu *et al.* [1988] have modelled the TCR using the frequency domain. Furthermore, L. J. Bohmann and RH Lasseter [1989] and E. Acha [1991] have modelled the TCR using the harmonic domain as frame of reference, where all the harmonics and cross-couplings between harmonics are explicitly shown. Each single-phase unit of the three-phase TCR is modelled as a voltage-dependent harmonic Norton equivalent, realized by extracting the harmonic content of non-linear characteristic using FFT procedures. This model is enhanced by [Rico *et al*. 1996] where a three-phase TCR model is based on the use of switching vectors and discrete convolutions instead of using the FFT. This model is suitable for incorporation into the harmonic domain frame of reference and will be utilised in this work.

Borrowing from [Rico *et al*. 1996], the TCR will be modelled in the harmonic domain using switching functions and convolutions. The admittance is calculated using equation (5.1), where $\mathbf{S_w}$ is a matrix witch represents a switching function evaluated at a given Thyristor firing angle:

$$\mathbf{Y_{TCR}} = \frac{1}{L}\mathbf{D}^{-1}\left(jh\omega_0\right)\mathbf{S_w} \tag{5.1}$$

In this equation, L is the nominal inductance of the TCR linear reactor and D is a diagonal admittance matrix with entries $jh\omega_0$. It should be remarked that the admittance matrix $\mathbf{Y_{TCR}}$ is the representation of the TCR during the periodic steady state. For a

three-phase TCR, the admittance matrices are calculated for each phase and then a delta connection is carried out to represent the three-phase circuit,

$$\mathbf{Y}_{\mathbf{TCR}3\phi} = \begin{bmatrix} \mathbf{Y}_{\mathbf{TCR}}^{ab} + \mathbf{Y}_{\mathbf{TCR}}^{ca} & -\mathbf{Y}_{\mathbf{TCR}}^{ab} & -\mathbf{Y}_{\mathbf{TCR}}^{ca} \\ -\mathbf{Y}_{\mathbf{TCR}}^{ab} & \mathbf{Y}_{\mathbf{TCR}}^{bc} + \mathbf{Y}_{\mathbf{TCR}}^{ab} & -\mathbf{Y}_{\mathbf{TCR}}^{bc} \\ -\mathbf{Y}_{\mathbf{TCR}}^{ca} & -\mathbf{Y}_{\mathbf{TCR}}^{bc} & \mathbf{Y}_{\mathbf{TCR}}^{ca} + \mathbf{Y}_{\mathbf{TCR}}^{bc} \end{bmatrix} \tag{5.2}$$

5.2.2 Modelling of the three-phase capacitor bank

A healthy capacitor is taken to be a linear device and in such circumstances a single-phase capacitor admittance is represented in harmonic domain by the admittance which is a diagonal matrix calculated by equation (5.3):

$$\mathbf{Y}_{\mathbf{C}} = C\mathbf{D}\left(\mathrm{j}h\omega_0\right) \tag{5.3}$$

with entries $\mathrm{j}h\omega_0$ and C is the nominal capacitance of the bank. In this application the three-phase bank of capacitors is not really connected in star but for modelling purposes an equivalent delta connection will be used. The transformation from star to delta is carried out using equations (5.4) to (5.6)

$$\mathbf{Y}_{\mathbf{Cab}} = \left(\mathbf{Y}_{\mathbf{Ca}} + \mathbf{Y}_{\mathbf{Cb}} + \mathbf{Y}_{\mathbf{Cc}}\right)^{-1} \mathbf{Y}_{\mathbf{Ca}} \mathbf{Y}_{\mathbf{Cb}} \tag{5.4}$$

$$\mathbf{Y}_{\mathbf{Cbc}} = \left(\mathbf{Y}_{\mathbf{Ca}} + \mathbf{Y}_{\mathbf{Cb}} + \mathbf{Y}_{\mathbf{Cc}}\right)^{-1} \mathbf{Y}_{\mathbf{Cb}} \mathbf{Y}_{\mathbf{Cc}} \tag{5.5}$$

$$\mathbf{Y}_{\mathbf{Cca}} = \left(\mathbf{Y}_{\mathbf{Ca}} + \mathbf{Y}_{\mathbf{Cb}} + \mathbf{Y}_{\mathbf{Cc}}\right)^{-1} \mathbf{Y}_{\mathbf{Cc}} \mathbf{Y}_{\mathbf{Ca}} \tag{5.6}$$

The resulting model for the three-phase bank of capacitors is

$$\mathbf{Y}_{\mathbf{C}3\phi} = \begin{bmatrix} \mathbf{Y}_{\mathbf{Cab}} + \mathbf{Y}_{\mathbf{Cca}} & -\mathbf{Y}_{\mathbf{Cab}} & -\mathbf{Y}_{\mathbf{Cca}} \\ -\mathbf{Y}_{\mathbf{Cab}} & \mathbf{Y}_{\mathbf{Cab}} + \mathbf{Y}_{\mathbf{Cbc}} & -\mathbf{Y}_{\mathbf{Cbc}} \\ -\mathbf{Y}_{\mathbf{Cca}} & -\mathbf{Y}_{\mathbf{Cbc}} & \mathbf{Y}_{\mathbf{Cbc}} + \mathbf{Y}_{\mathbf{Cca}} \end{bmatrix} \tag{5.7}$$

Using (5.2) and (5.7) the three-phase admittance representation of the SVC can be expressed by the addition of both matrices.

$$\mathbf{Y}_{\mathbf{SVC}3\phi} = \mathbf{Y}_{\mathbf{TCR}3\phi} + \mathbf{Y}_{\mathbf{C}3\phi} \tag{5.8}$$

In this study the SVC is placed on the secondary side of the step-down transformer which is the node 3 as is shown in Figure 5-1 page 132. This means that the admittance representation of the SVC of equation (5.8) will be added to the admittance representation of the system.

5.2.3 Modelling of the three-phase passive filters

It is common practice in existing electric arc furnace installations to use passive filters to eliminate the harmonics produced by the utilisation of power electronics and the electric arc load. Passive filters are made up of inductive reactors, capacitor banks and resistors. A suitable combination of such elements provides a low impedance path at specific harmonic frequencies [Akagi 2006]. They may be classified into tuned and high pass filters. The former can be further classified into single and double tuned filters while the later may be classified as first, second and third order high-pass filters.

For the case of a single tuned filter, the tuned frequency f_{tuned} and corresponding harmonic h_{tuned} can be calculated using equations (5.9) and (5.10), where L and C are the inductance and capacitance of the filter respectively,

$$f_{tuned} = \frac{1}{2\pi\sqrt{LC}} \tag{5.9}$$

$$h_{tuned} = \frac{f_{tuned}}{f_{system}} = \frac{1}{2\pi\left(f_{system}\right)\sqrt{LC}} \tag{5.10}$$

With information of the tuned capacitive reactance and the tuned harmonic frequency, the inductive reactor value can be calculated,

$$X_{Lfilter} = \frac{X_{Cfilter}}{\left(h_{tuned}\right)^2} \tag{5.11}$$

Calculation of the tuned capacitive reactance $X_{Cfilter}$ is carried out using (5.12) where the effective reactance of the filter X_{Eff} is related to the effective reactive power Q_{eff} that is required for compensation and to the filter nominal voltage, as given by (5.13),

$$X_{Cfilter} = \left(\frac{\left(h_{tuned}\right)^2}{\left(h_{tuned}\right)^2 - 1} \right) \tag{5.12}$$

$$X_{Eff} = \left(\frac{\left(Kvolts_{LLSys}\right)^2}{Q_{eff}(M\,var)} \right) X_{Eff} \tag{5.13}$$

The single-phase filter may be represented in the harmonic domain as the series combination of the capacitive and reactive admittances matrix algebra, using the following procedure:

$$\mathbf{Y}_{\mathbf{C}filter} = C_{filter}\mathbf{D}\left(jh\omega_0\right) \tag{5.14}$$

$$\mathbf{Y}_{\mathbf{L}filter} = \frac{1}{L}\mathbf{D}^{-1}\left(jh\omega_0\right) \tag{5.15}$$

$$\mathbf{Y}_{\mathbf{Filter}} = \left(\mathbf{Y}_{\mathbf{L}filter}\mathbf{Y}_{\mathbf{C}filter}\right)^{-1}\left(\mathbf{Y}_{\mathbf{L}filter} + \mathbf{Y}_{\mathbf{C}filter}\right) \tag{5.16}$$

For harmonic filters connected in either ungrounded star or delta configurations, identical harmonic cancellation results are expected [IEEE Std 1531 2003]; In both cases, the harmonic filter model can be expressed as either an equivalent delta or as an actual delta representation,

$$\mathbf{Y}_{\mathbf{Filterab}} = \left(\mathbf{Y}_{\mathbf{Filtera}} + \mathbf{Y}_{\mathbf{Filterb}} + \mathbf{Y}_{\mathbf{Filterc}}\right)^{-1}\mathbf{Y}_{\mathbf{Filtera}}\mathbf{Y}_{\mathbf{Filterb}} \tag{5.17}$$

$$\mathbf{Y}_{\mathbf{Filterbc}} = \left(\mathbf{Y}_{\mathbf{Filtera}} + \mathbf{Y}_{\mathbf{Filterb}} + \mathbf{Y}_{\mathbf{Filterc}}\right)^{-1}\mathbf{Y}_{\mathbf{Filterb}}\mathbf{Y}_{\mathbf{Filterc}} \tag{5.18}$$

$$\mathbf{Y}_{\mathbf{Filterca}} = \left(\mathbf{Y}_{\mathbf{Filtera}} + \mathbf{Y}_{\mathbf{Filterb}} + \mathbf{Y}_{\mathbf{Filterc}}\right)^{-1}\mathbf{Y}_{\mathbf{Filterc}}\mathbf{Y}_{\mathbf{Filtera}} \tag{5.19}$$

Then, the model for the three-phase tuned filter is

$$\mathbf{Y}_{\mathbf{Filter}3\phi} = \begin{bmatrix} \mathbf{Y}_{\mathbf{Filter}ab} + \mathbf{Y}_{\mathbf{Filter}ca} & -\mathbf{Y}_{\mathbf{Filter}ab} & -\mathbf{Y}_{\mathbf{Filter}ca} \\ -\mathbf{Y}_{\mathbf{Filter}ab} & \mathbf{Y}_{\mathbf{Filter}ab} + \mathbf{Y}_{\mathbf{Filter}bc} & -\mathbf{Y}_{\mathbf{Filter}bc} \\ -\mathbf{Y}_{\mathbf{Filter}ca} & -\mathbf{Y}_{\mathbf{Filter}bc} & \mathbf{Y}_{\mathbf{Filter}bc} + \mathbf{Y}_{\mathbf{Filter}ca} \end{bmatrix} \tag{5.20}$$

5.2.4 Modelling of the Static Var Compensator

The overall SVC admittance comprised the sum of the following admittances: the TCR, the capacitor banks and as many harmonic filters as it is necessary. For instance, for the case when the 3_{rd} and 5_{th} harmonic filters as is shown in Figure 5-2 are required the equation is:

$$\mathbf{Y}_{\mathbf{SVC}3\phi} = \mathbf{Y}_{\mathbf{TCR}3\phi} + \mathbf{Y}_{\mathbf{C}3\phi} + \mathbf{Y}_{3rd\mathbf{Filter}3\phi} + \mathbf{Y}_{5th\mathbf{Filter}3\phi} \tag{5.21}$$

If only the SVC requires representation then the last two terms yield zero values.

5.3 Modelling of the Three-phase Thyristor Controlled Series Reactor

The use of a series reactor with several taps is common practice in electric arc furnaces installations, as documented in [Montanari *et al*. 1994], with the goal of achieving better control over the dynamic response of electric arc load. More recently application of power electronics in the form of a series reactor controlled by Thyristors has been proposed [Cardoso and Cardoso 2006] and [Ma and Mulcahy] as an alternative to the tapped series reactor. The component of this device is the TCR, but in this application it is connected in parallel with a fixed reactor. The device is connected between the step-down transformer and the furnace transformer. The model comprises the admittances of the TCR and the parallel reactor:

$$\mathbf{Y}_{\mathbf{TCSR}3\phi} = \mathbf{Y}_{\mathbf{TCR}3\phi} + \mathbf{Y}_{L3\phi} \tag{5.22}$$

This admittance replaces the admittance of the conventional series reactor in the overall model of the electric arc furnace installation as is shown in Figure 5-3.

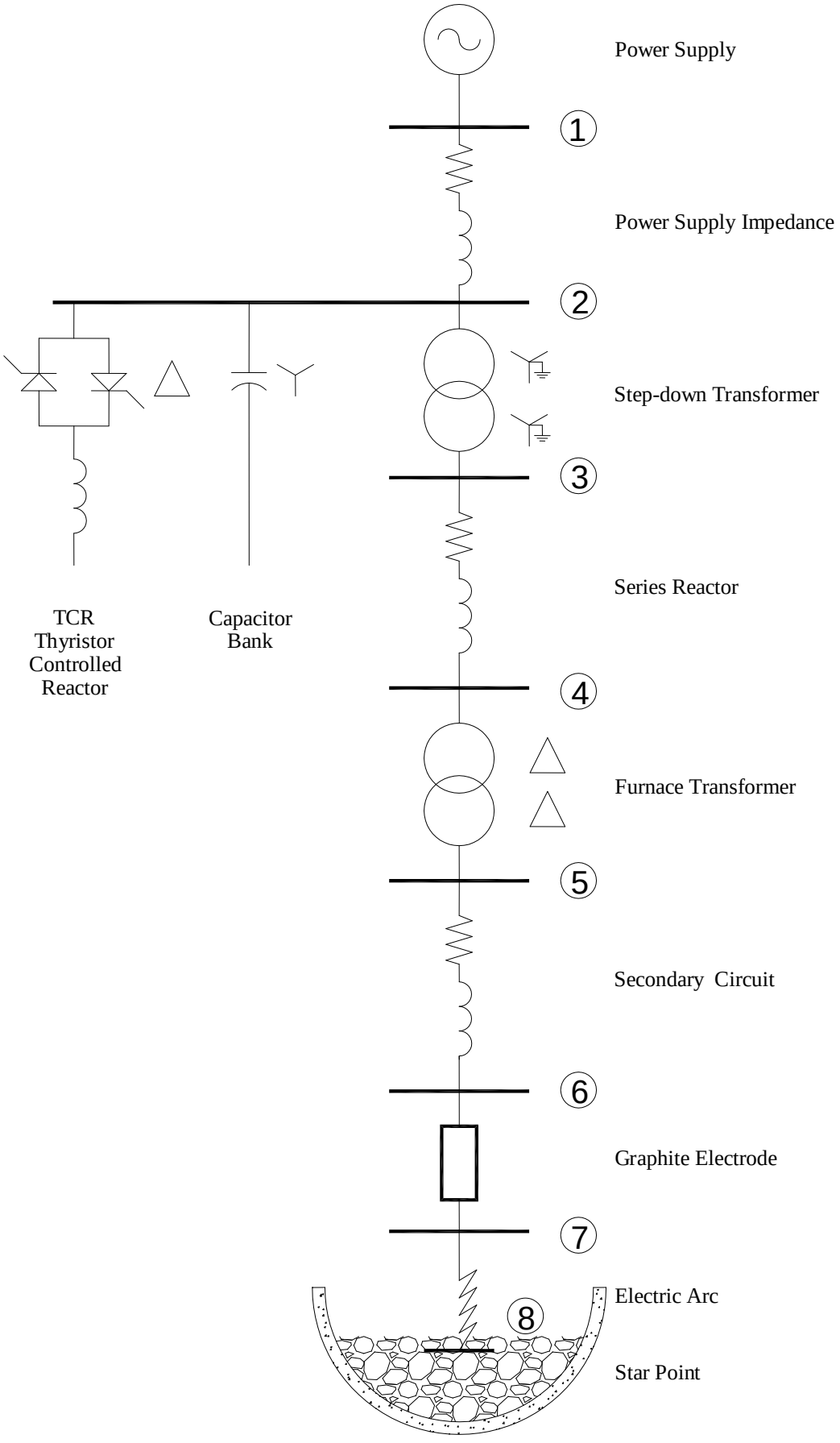

Figure 5-1 Electric arc furnace installation with SVC

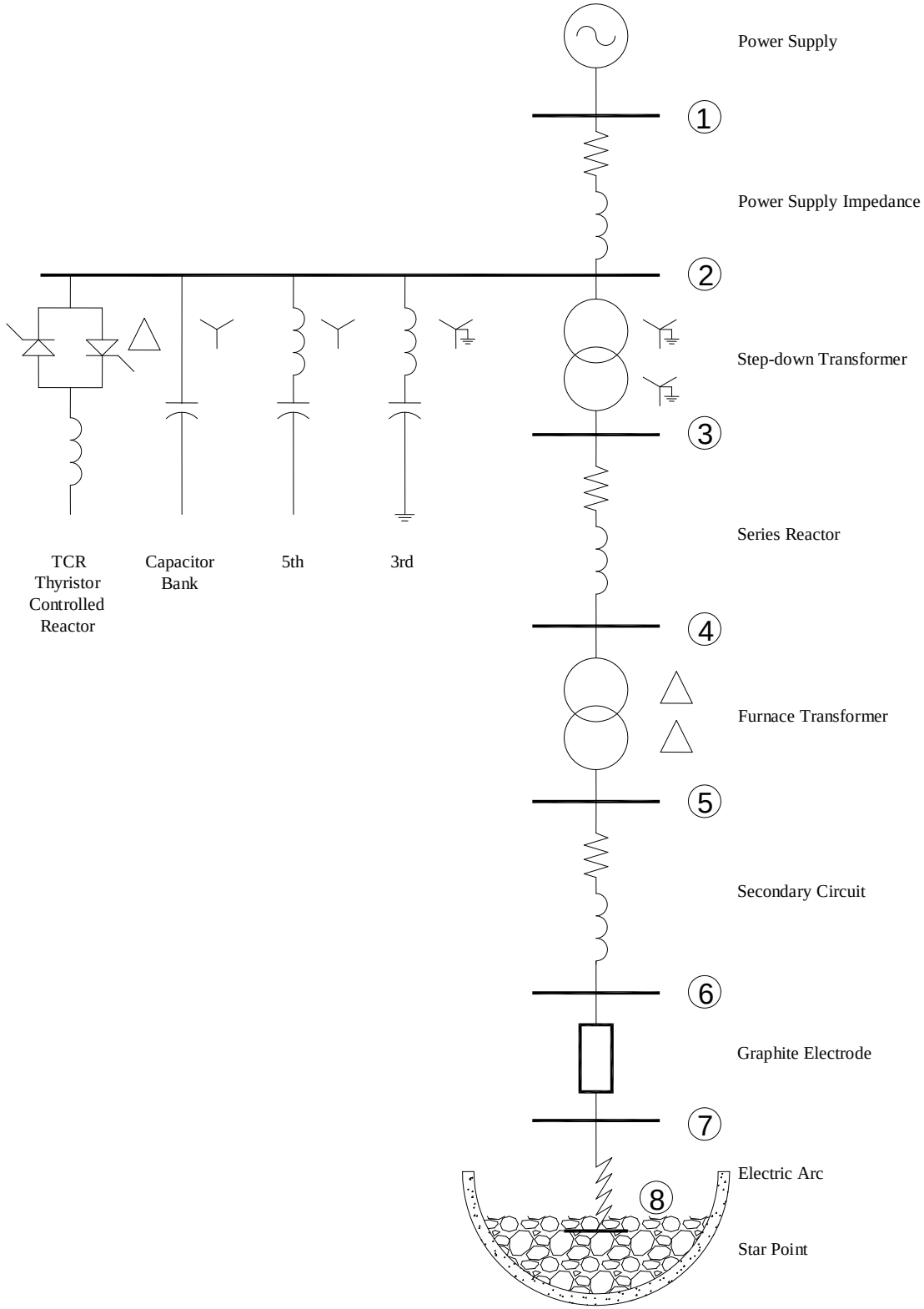

Figure 5-2 Electric arc furnace installation with SVC and filters

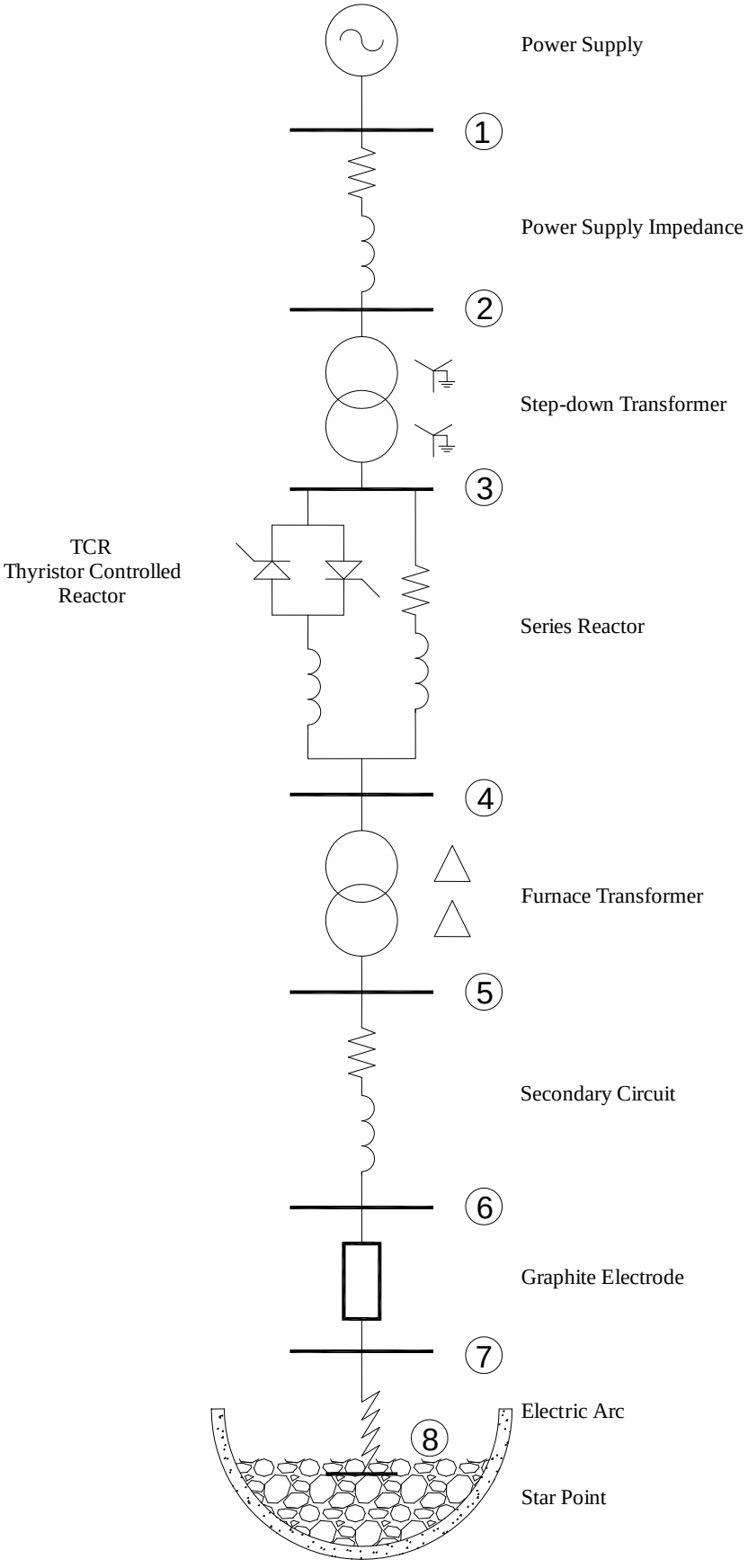

Figure 5-3 Electric arc furnace installation with TCSR

5.4 The Case of a Three-phase Electric Arc Furnace System with a Static Var Compensator

The harmonic domain model of the enhanced electric arc furnace installation with SVC enables comprehensive studies of the harmonic interaction of three distinct non-linear elements; the non-linearity associated with the plasma of the electric arc, the non-linearity introduced by saturation of the transformers iron cores and the non-linear characteristic introduced by the TCR switches. The first stage is to assess their harmonic interaction assuming balanced conditions. This study yields quantitative information on the impact of the Thyristor firing angle on reactive power compensation. This study is carried out assuming both balanced and unbalanced operating conditions. This study with the imbalance assumed to take place in only one of the three load arcs progresses from a small degree of imbalance to the extreme case represented by the extinction of the electric arc in that phase. A comprehensive set of simulation results such as the ones provided by the computer model developed may be used for enhanced design of filters, transformers and reactors in the arc furnace installation. The standard IEEE 531 [2003] dedicated to harmonic filter design deals with issues such as no-load operation, beginning of the melting cycle and the inrush current caused by the furnace transformer energisation. Nevertheless, the effect of imbalances is not addressed in a comprehensive manner, a characteristic that is recurrent in an electric arc furnace installation. The following cases of operation are considered in this section:

- balanced operation of the electric arc furnace installation, with a SVC,
- unbalanced operation of the electric arc furnace with SVC angle variation
- unbalance operation of the electric arc furnace, with TCR angle variation and tune filters
- Effect of the magnetising branch of step-down and furnace transformers

5.4.1 Balanced operation of the three-phase electric arc furnace system with Static Var Compensator without harmonic passive filters

The case of an electric arc furnace installation operating under balanced conditions more often than not is an ideal case. However, important observations and

conclusion can be drawn which enables a clear understanding of the impact of VAR compensation using power electronic control. To such end, the integration of a SVC in the electric arc furnace installation is carried out; this is connected to secondary side of the step-down transformer as is shown in Figure 5-1. The SVC is composed of a three-phase TCR of 70 MVA's connected in delta and a three-phase capacitor bank of 70 MVA's connected in star with ungrounded star point. The rating of the SVC is based in the apparent power specification of the step down transformer that with a ideal power factor value of one deliver the maximum active power available to the load. A set of simulations is carried out with different TCR firing angles in the range 90 to 180 degrees, with steps of 10 degrees. The last step which would correspond to 180 degrees is fact carried out with an angle of 179 degrees because 180 degrees corresponds to the open phase condition. The results provided by the harmonic iterative solution are the harmonic voltages at each node of the system and they are used to calculate the effective root men square values, power quality indices and powers through the installation.

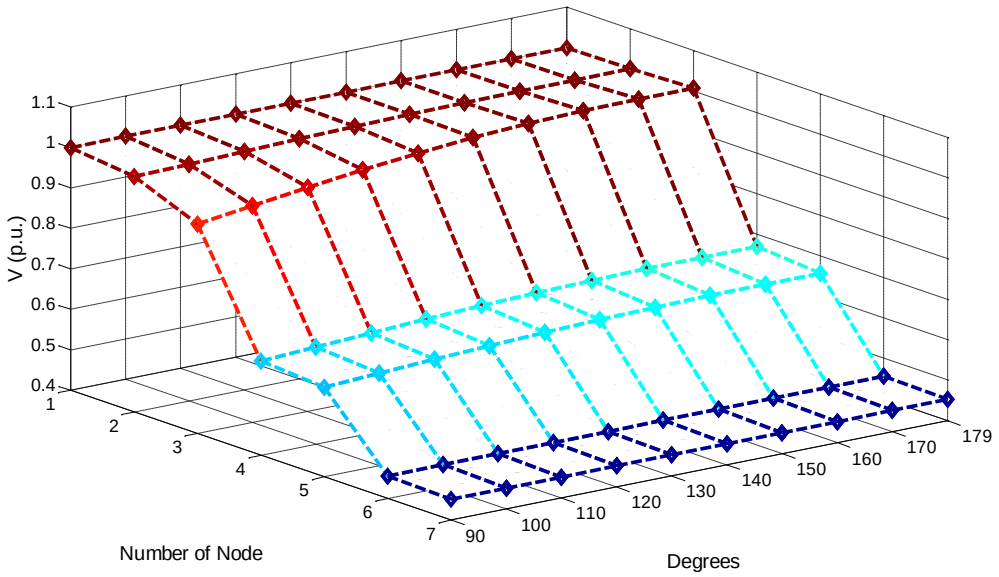

Figure 5-4 Effective voltages vs TCR firing angles, at node 1 to 7

Figure 5-4 shows that the TCR firing angle changes have their main impact in the effective voltages of nodes 2 and 3 for values above 140 degrees. The later node is in fact the connecting node of the SVC and the effective voltages rise over 1.0 per unit values, suggesting and overcompensated condition.

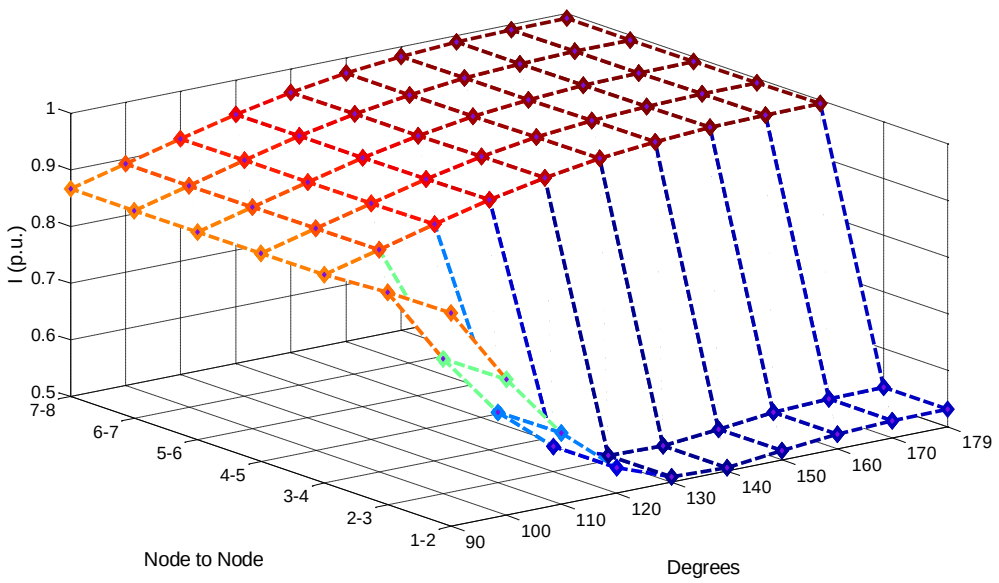

Figure 5-5 Effective currents vs TCR firing angles, at elements connected between nodes 1-2 to 7-8

Very pronounced changes in effective currents take place those flowing from node 1 to 2 and those flowing from node 2 to 3. This is attributed to the reactive power injected by the SVC at node 3; the current supplied by the SVC reduces considerably the effective current that otherwise would have to be delivered by the power supply. For example, the currents flowing from node 3 to 4 which have values of around 0.9 per unit decrease to around 0.5 per unit in the branch connected between nodes 2 to 3, as shown in the graph of Figure 5-5. Another interesting observation is that increases in TCR firing angles from 90 to 179 degrees yield increases of effective current from below 0.9 to almost 1 per unit values. This is a direct result of effective voltage increases at node 3 caused by SVC VAR compensation.

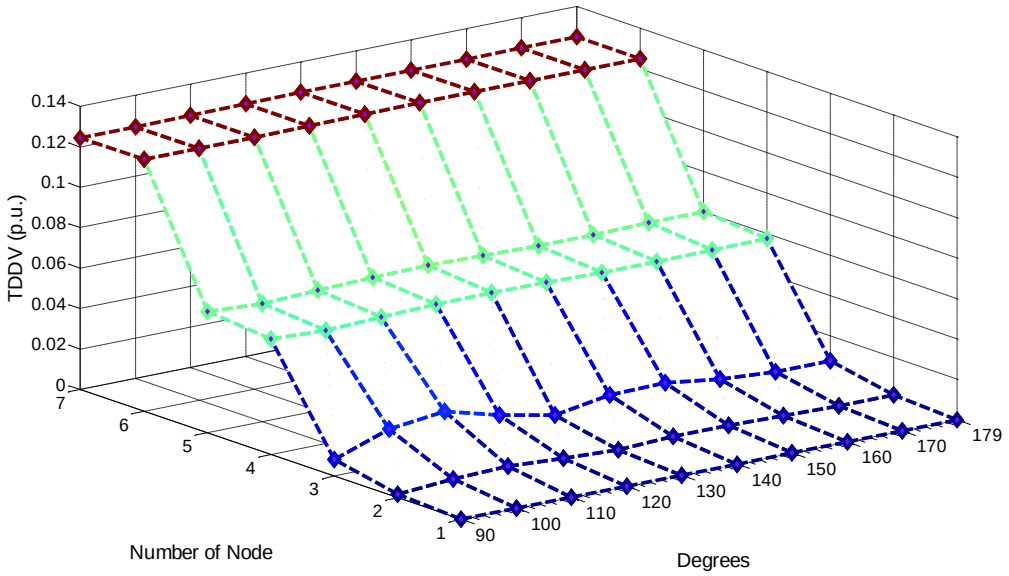

Figure 5-6 Effective voltage TDD vs TCR firing angles, at nodes 1 to 7

Another key effect of TCR firing angles increases is in the voltage and current quality indices; Figure 5-6 shows that the higher values of effective TDD voltage are near the electric arc load at nodes 6 and 7 where the effect of the TCR firing angle is minimum. The two nodes near the power supply (2 and 3) have low TDD voltage values but exhibit important variations with TCR firing angle changes. For example, node 2 has a maximum THD voltage of 0.47 % and node 3 has a maximum value of 2.1%. These values correspond to a firing angle of 110 degrees. In some electric arc furnace installation, node 3 is in practice a point of common coupling (PCC) where it is of paramount importance to keep harmonic pollution under control, since other end users may be connected at this bus. Figure 5-7 shows the effective TDD current where a value of just over 2.5 % is observed for all values of firing angle and at all branches except for branches 1-2 and 2-3 where variations do exist with a maximum value of 2.66 % at a firing angle of 110 degrees.

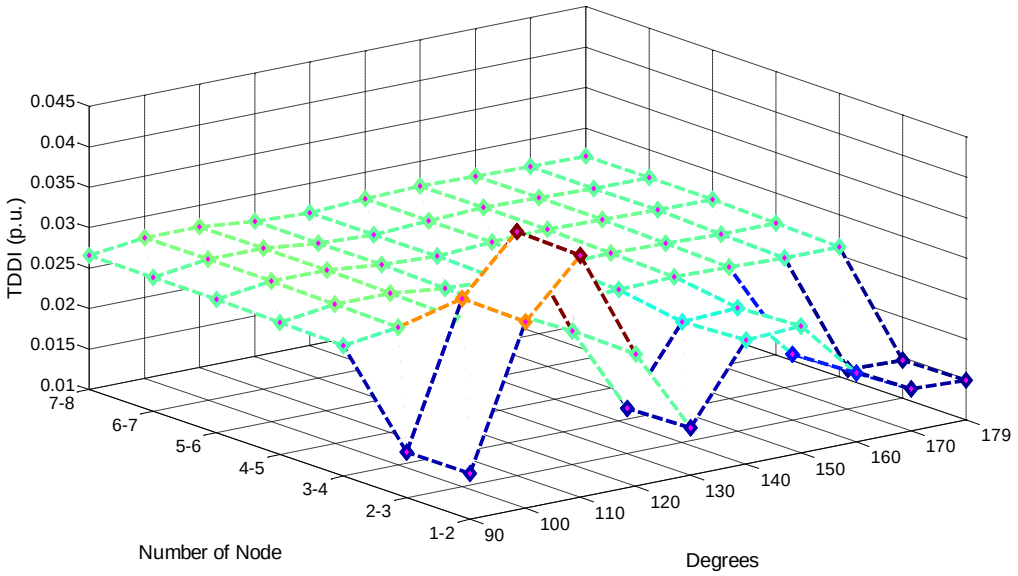

Figure 5-7 Effective current TDD vs TCR firing angles, at elements connected between nodes 1-2 to 7-8

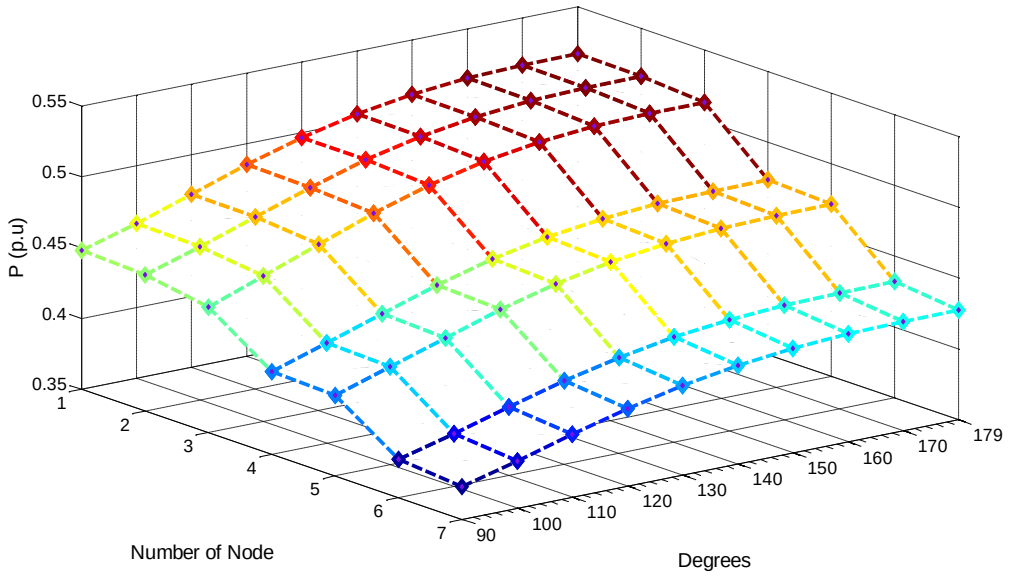

Figure 5-8 Average Active Power vs TCR firing angles, at elements connected between nodes 1-2 to 7-8

The three-phase average active power rises in with the TCR firing angle values, as show in Figure 5-8, increasing the electric power delivery to the arc load. It is observed that all nodes of the system are affected by the changes in the firing angle in different proportion. This is an important observation since the operator's first goal is to deliver maximum active power to the electric arc load, reducing operation times and increasing production. Figure 5-8 also shows that increased in reactive power

compensation enables an increase in the power delivered to the load in node 7 from 0.3731 per unit with a firing angle of 90 degrees to 0.427 per unit with the firing angle of 180 degrees.

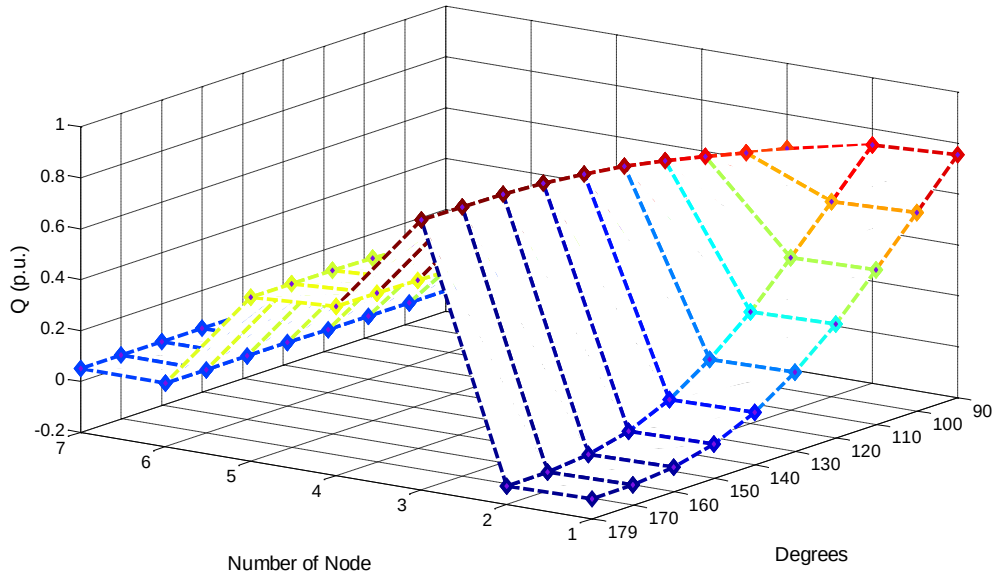

Figure 5-9 Average reactive power vs TCR firing angles, at elements connected between nodes 1-2 to 7-8

The definition of three-phase average reactive power used in this chapter is the average value over one period of the instantaneous quadrature power presented in Chapter 2. Such a definition gives a clear indication of when reactive power changes direction; a change in sign in the average reactive power is linked to a change in the direction of reactive power. Figure 5-9 shows that for TCR firing angles between 140 and 150 degrees, where a change of sign occurs for both nodes 1 and 2, means that The SVC is supplying reactive power to the Supply Company. In nodes 3 to 7 the larger reactive variations occurs between nodes 5 and 6 and between nodes 3 and 4 corresponding to the points where the secondary circuit and the series reactor are located respectively.

The effective apparent power yields accurate information on the actual utilisation of each plant company in relation to the installed capacity of the complete system. In this case where the base apparent power was selected to be rated power of the step-down transformers, this marking the maximum operation limits of the arc furnace installation. Figure 5-10 shows that the lower values of apparent power presented in nodes 1 and 2 correspond to compensated and overcompensated systems.

The latter is achieved when the TCR firing angles are higher than 130 degrees with apparent power keeping an almost constant value. It should be remarked that the apparent power direction can not be determined because no sign is attached to it (it is an absolute value) and fails to have conservative properties. Nevertheless is advantageous to decrease the values of apparent power at PCC resorting to reactive power compensation thus avoiding this reactive power to be drown from the power supply.

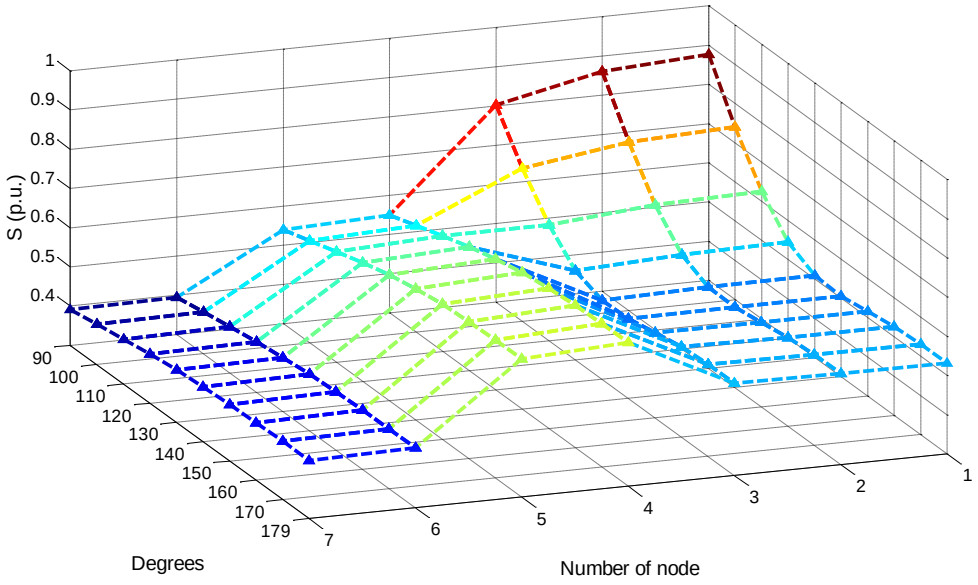

Figure 5-10 Effective apparent power vs TCR firing angles, at nodes 1 to 7

The behaviour of the effective power factor which is defined as the ratio of average active power and effective apparent power is shown in Figure 5-11. Perfect power factor compensation takes place when the compensator keeps the power factor to a value of 1. TCR firing angles between 130 and 140 degrees were found to yield values of power factor of 1. Figure 5-11 shows that the effective power factor at the load point located in (node 7) is very good, it takes values around 0.95. The major consumption of reactive and non-active powers takes place at node points where the power factor changes in value; it is not difficult to pinpoint that this is in the secondary circuit which is connected between nodes 5 and 6 and in the series reactor which is connected between nodes 3 and 4.

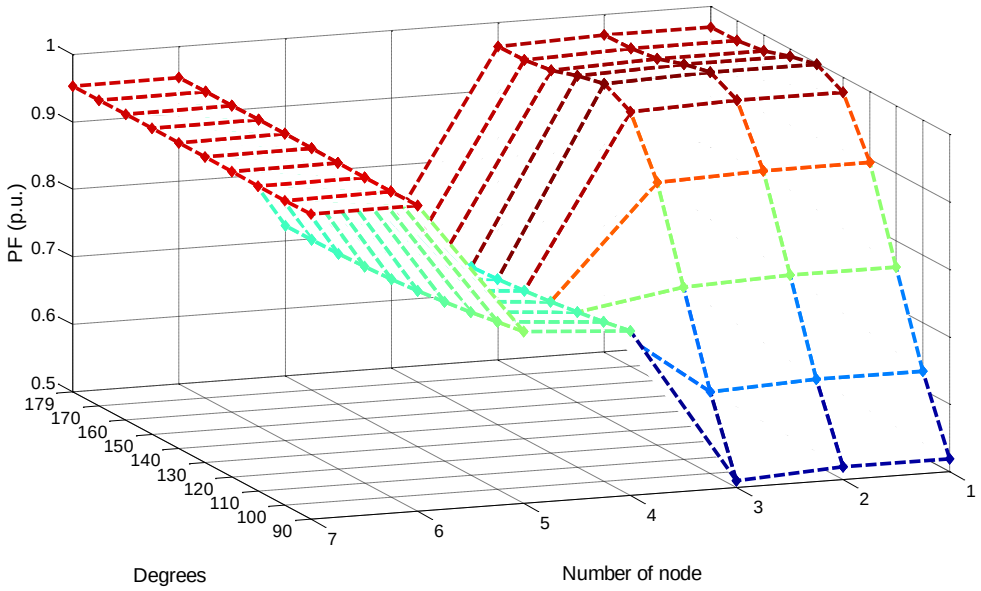

Figure 5-11 Effective power factor vs TCR firing angles, at nodes 1 to 7

From this study it becomes clear that simulation studies for a wide set of TCR angles is the way forward for assessing the behaviour of electric arc furnace installations with VAR compensation using a SVC; even though this was carried for a constant balanced load. Gathering information for a wide range of power quality definitions enables comprehensive analyses. One set of power quality parameters does not give enough information for the evaluation of the full system.

5.4.2 Unbalanced operation of the three-phase electric arc furnace systems with Static Var Compensator

Imbalance is common feature in electric arc furnace installations; a condition that increases non-active power consumption [Miller 1982] and harmonic voltages and current distortion [Acha 2001]. To assess the impact of unbalanced effects in an electric arc furnace installation with VAR compesation using a SVC, the system is submitted to progressive imbalances in the electric arc load. This is carried out by using square factor *u* which is proportional to the electric arc voltage and directly affects non-linear equation of the electric arc presented in the chapter 2. The square factor *u* is set to affect the constant *k3* of the equation corresponding to phase *a*. To set up simulations, this square factor *u* will take step increments of 0.25, from 0.25 to 2, with a square factor of

1.0 corresponding to a balanced load condition. Figure 5-12 shows the three-phase current-voltage characteristic for the case when u =0.25 for phase a with the other two phases having u =1. To try to gain a basic understanding of the effect that the imbalance has in the spectra of the electric arc furnace installation, an analysis of power is carried out. The instantaneous power is calculated using several equivalents forms. Figure 5-13 shows the instantaneous power for each phase: (a) using electric arc voltages and currents, (b) using phase voltages and line currents, (c) using line voltages and phase currents. In (d) the three-phase instantaneous powers using the three different forms are plotted. The results match each other identically and the waveform shows the effects of harmonics (ripple) and imbalance (asymmetry). In addition to this progressive set of imbalances introduced by means of the square factor u, a more severe unbalanced condition is introduced termed **EA,** achieved by giving the electric arc conductance a value of zero in phase a, which would represent an extinguished arc.

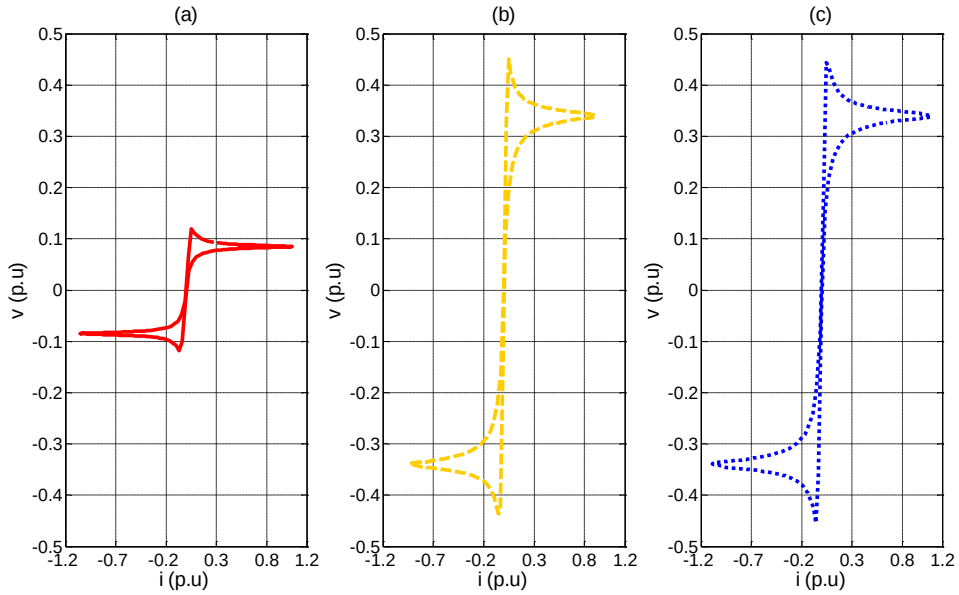

Figure 5-12 Arc current-voltage characteristics with the following u factor (a) 0.25 (b) 1 (c) 1

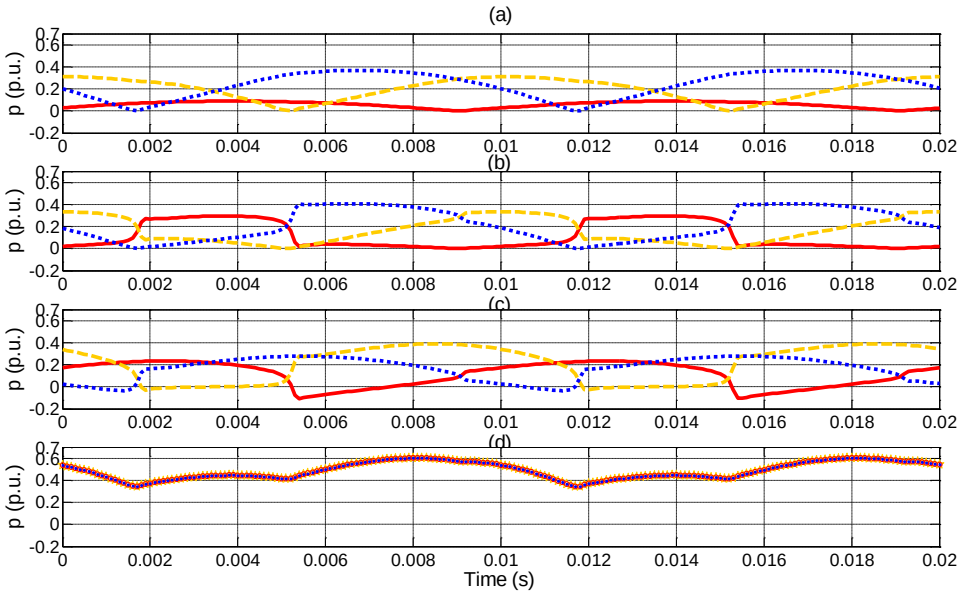

Figure 5-13 Instantaneous powers at the arc load: (a) arc voltages and currents; (b) phase voltages and line currents (c) Line voltages and phase currents (d) instantaneous three-phase power computed with the three set of parameters

A measure of imbalance is the difference between the characteristic of phase *a* and those of phases *b* and *c*. The usefulness of this factor becomes clearer when used in conjunction the fundamental frequency symmetrical components, calculated at each node. Figure 5-14 depicts the negative sequence values of voltages, in per unit. It is observed that voltage imbalances are small in nodes 2 and 3, below 1 %. However in node 4 it takes values of 21 % for the condition of extinguished arc, a situation which will affect directly the furnace transformer. At the arc load point, which is directly affected by the *u* factor, the correlation between *u* and the negative sequence is proportional.

Additional complementary information is given by the fundamental frequency negative sequence of current, whose values raise in direct proportion to *u*. In this particular case, these values reach 42 % for the condition of extinguished arc in phase *a*, as shown in Figure 5-15

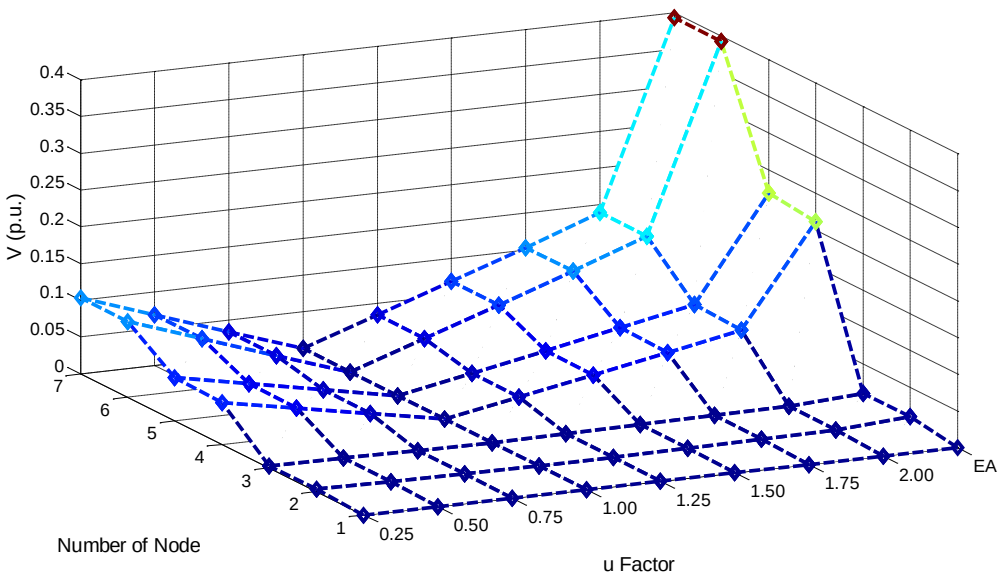

Figure 5-14 Negative sequence, fundamental frequency voltage vs *u* factor, at nodes 1 to 7

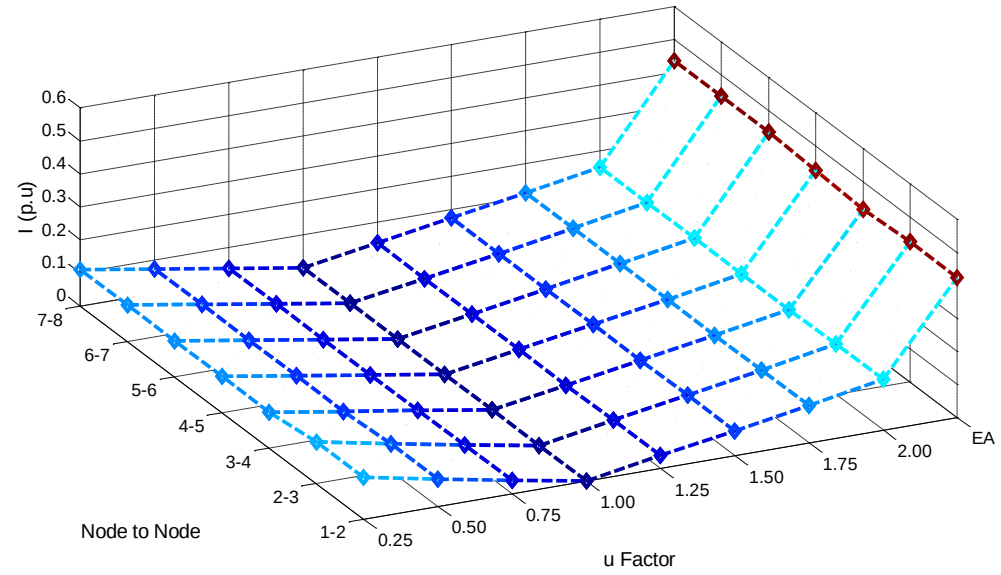

Figure 5-15 Negative sequence fundamental frequency current vs *u* factor, at elements connected between nodes 1-2 to 7-8

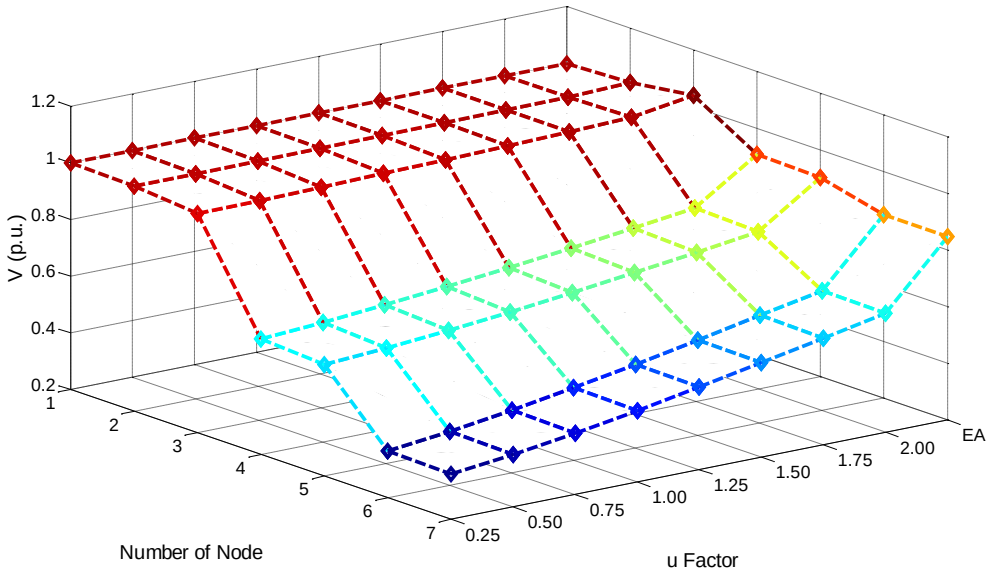

Figure 5-16 Effective voltages vs u factor, at nodes 1 to 7

Figure 5-16 shows the rms voltages at nodes 1 to 7, with *u* values in the range 0.25 to 2. It should be borne in mind that *u*=1.00 means that the system is operating under balanced conditions. The rms effective voltages are correlated to unbalanced factor *u* since the arc voltages increase its value with it.

Figure 5-17 shows the behaviour of the rms currents subject to progressive step changes of *u*. Starting in branch 3-4 the changes taking place in the currents are in inverse proportion to changes in the *u* factor, this is as a consequence of increases in electric arc voltages. This trend is in contrast to the currents flowing in the branches connected between nodes 1-2 and 2-3 which are in inverse proportion to increases in *u*. This is a clear indication that the SVC, which is connected at node 3, has strong bearing on unbalance system.

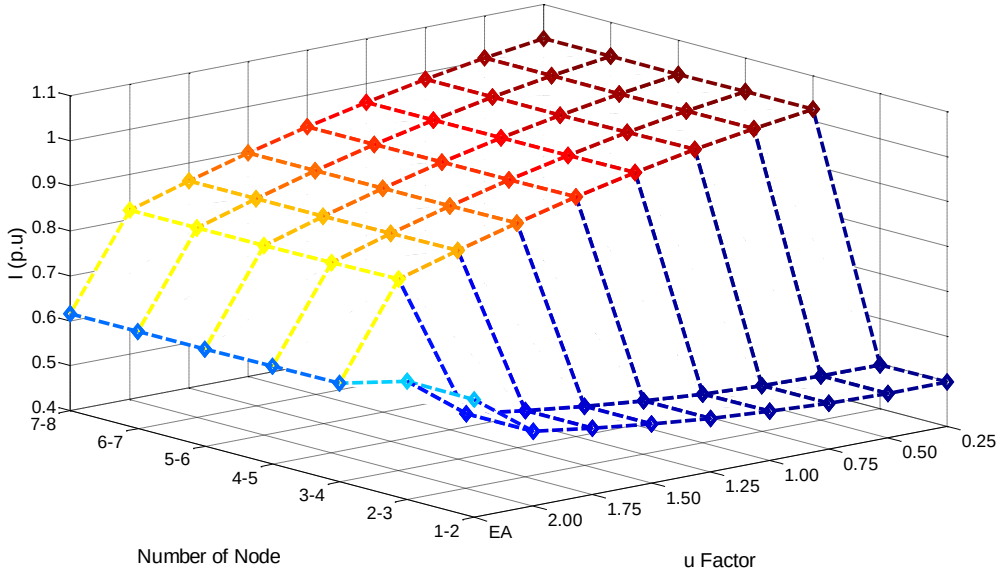

Figure 5-17 Effective current vs *u* factor, at elements connected between nodes 1-2 to 7-8

Figure 5-18 shows the average active powers which tend to rise with the length of the electric arc in the unbalanced phase. They rise with the *u* factor, because the effective arc voltage rises with this factor which in turns translates into increases of active power delivered to the load. However, the extreme case of an extinguished arc shows a very marked decrease in power supplied to the arc load.

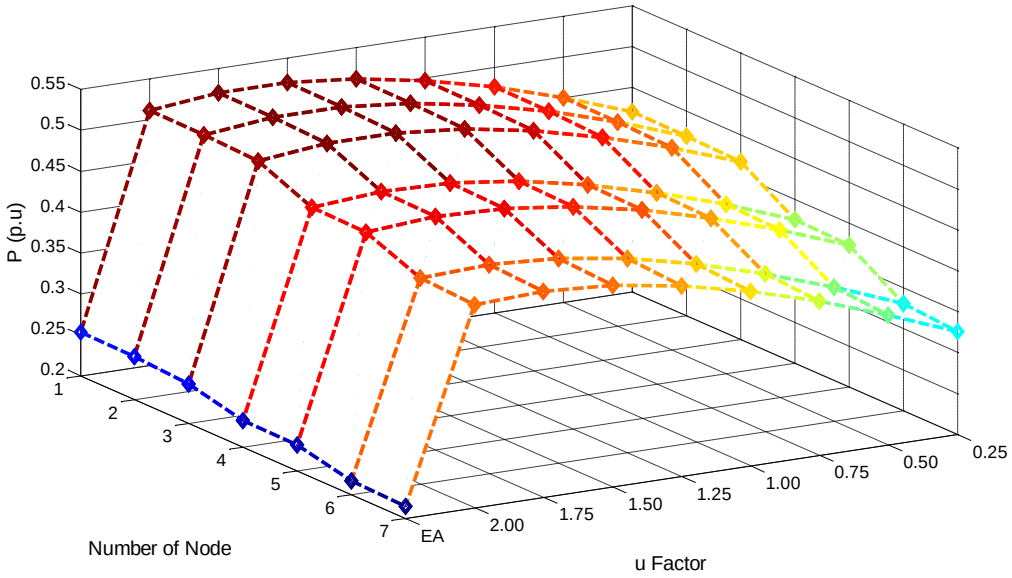

Figure 5-18 Average active power vs u factor, at elements connected between nodes 1-2 to 7-8

The reactive power at each node of the system and for the various unbalances is presented in Figure 5-19 nodes 6 and 7 keeping almost constant values of zero reactive power at all values of *u*. This is in contrast to the behaviour of the reactive power in nodes 1 to 5. Whose values are well above zero, particularly at node 3. The case of one extinguished arc clearly gives rise to an export of reactive power from the SVC to the supply source, evidenced by the change in sign in the value of reactive power.

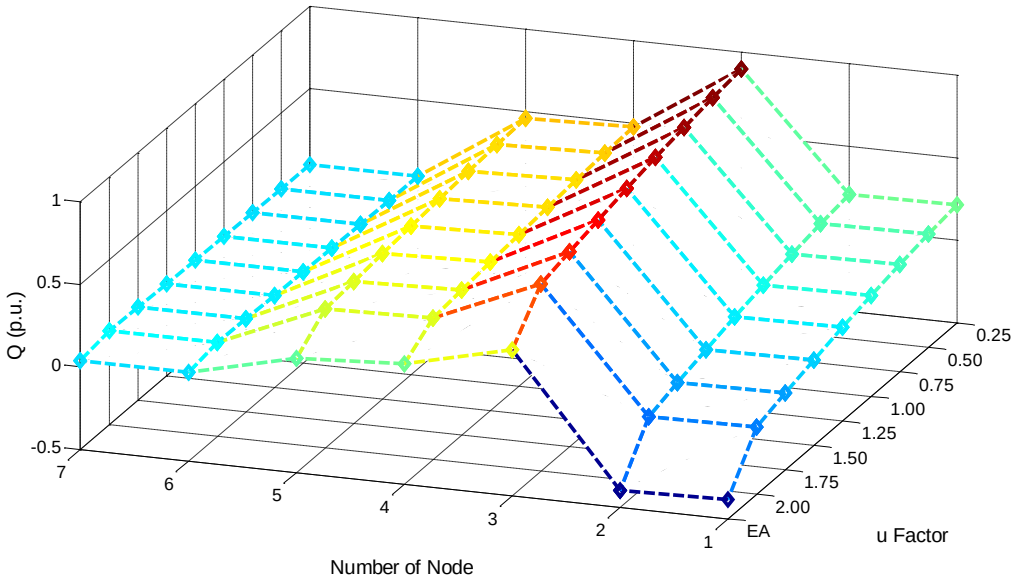

Figure 5-19 Average reactive power vs *u* factor, at elements connected between nodes 1-2 to 7-8

Figure 5-20 shows that as expected, the effective apparent power presents a different trend than that of the reactive power. In node 7 the apparent power increases with the value of *u*, an effect that is linked to increases in both active and non-active powers. On the other hand, at node 3, the apparent power decreases its value as *u* rises which means that the SVC is delivering higher values of non-active power, as a result of higher harmonic generation.

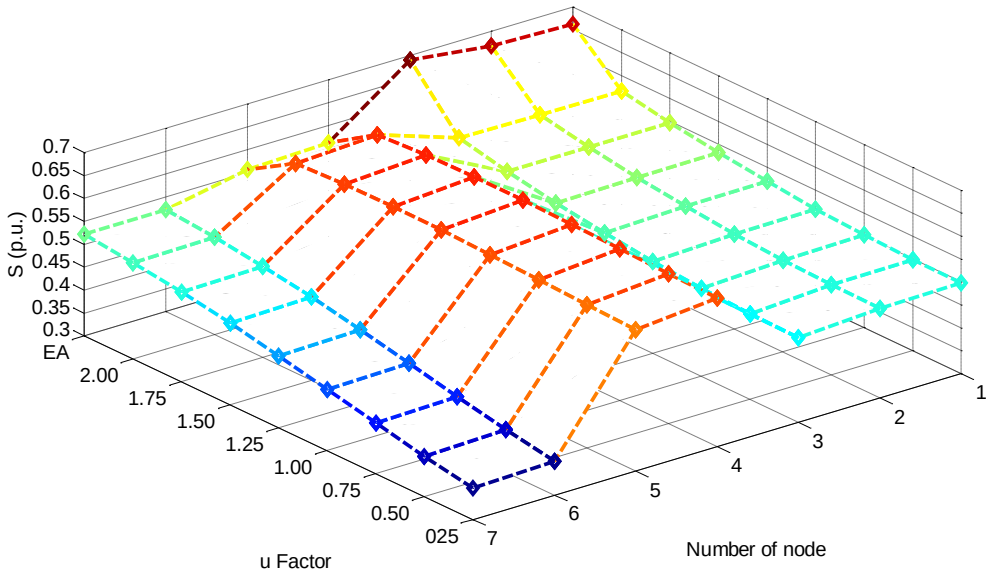

Figure 5-20 Effective apparent power vs *u* factor, at nodes 1 to7

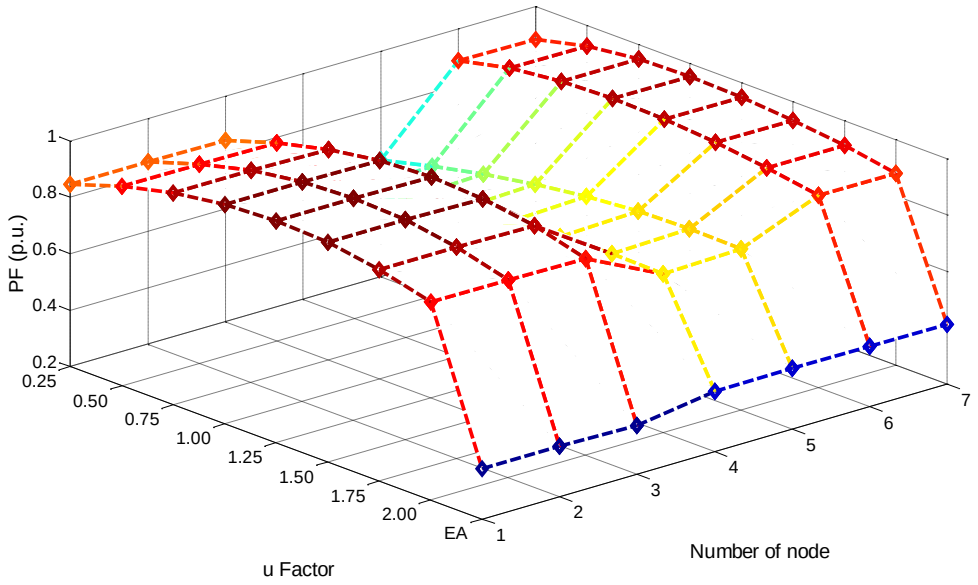

Figure 5-21 Effective power factor vs u factor, at nodes 1 to 7

The effective power factor is presented in Figure 5-21. It is interesting to note that nodes 1, 2 and 3 hold similar power factor values as those in nodes 6 and 7. The reactive compensation delivered by the SVC is responsible for the market improvement on power factor at nodes 3, 2 and 1, whereas the good power factor in nodes 6 and 7 is due to the fact that the graphite and electric arc do not demand reactive power. It is clear that the operating condition that yields the worst power factor values at all the nodes is

the case of extinguished arc, a fact that justifies every effort to try to prevent such condition from happening in an electric arc furnace installation.

When the electric arc furnace installation and its accompanying SVC are connected to a strong electric network and operating under balanced operating conditions, the effective voltage TDD has shown to exhibit values below 1 % at nodes 2 and 3. However, the unbalanced condition, as shown in Figure 5-22, causes at the voltage TDD to rise well above the 1 % mark in proportion to the unbalance. In node 2, the voltage TDD has a maximum of 1.5 % when the extinguished arc presents itself and in node 3 it rises to 6.6 %. Such harmonic pollution in voltage may have adverse effects and inside the electric arc furnace installation but also in neighbouring en user installation. Moreover, the high voltage TDD values, which rise to 11 % at the node 4, will have negative effects in the of furnace transformer.

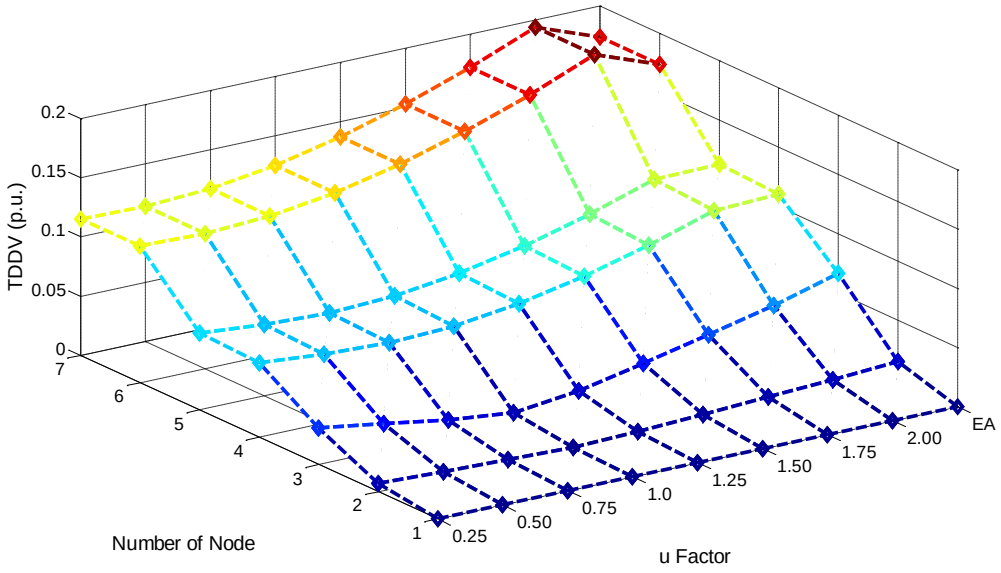

Figure 5-22 Effective voltage TDD vs u factor, at nodes 1 to 7

Contrary to the voltage TDD, where the largest values are in nodes 6 and 7, the current TDD has its largest values in the branches connected between nodes 1 and 2 and 2 and 3, as shown in Figure 5-23. The current TDD at all others nodes have relatively small values. This suggests that such a behaviour is governed by the SVC, which is connected at node 3 and injecting harmonic currents into the electrical network. The maximum value takes place in the branches connected between nodes 1-2 and 2-3 for the case of extinguished arc condition which rise to 21%. This value is prohibitively high and it is exported directly to the supply point which would be the utility network.

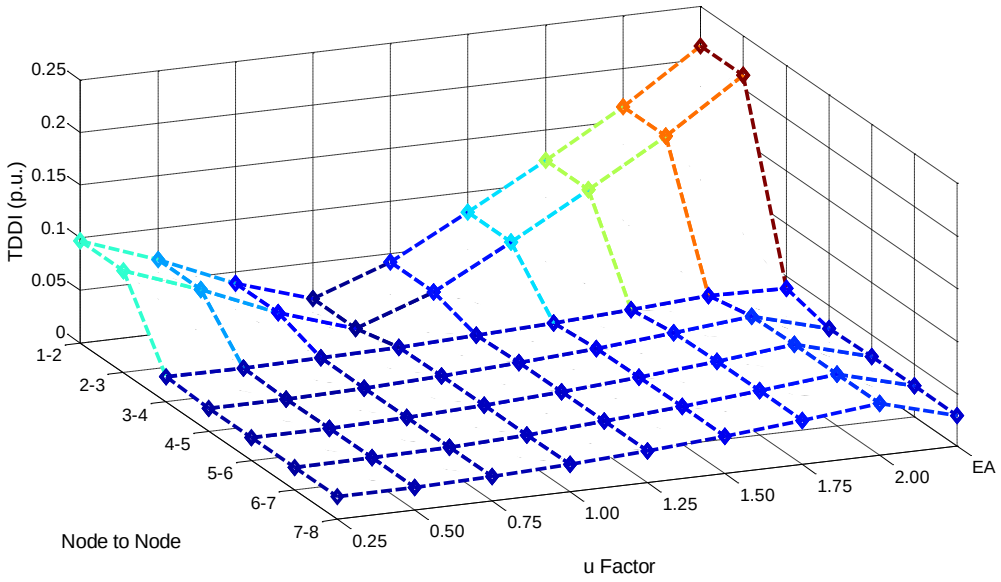

Figure 5-23 Effective current TDD vs u factor, at elements connected between nodes 1-2 to 7-8

It should be remarked that unbalanced operation is the norm in electrical arc furnaces and that most severe unbalanced condition presents itself when the electric arc extinguishes due to an excessive separation between one electrode and the scrap or due to the rupture of one of the graphite electrodes. Such as unbalanced situation may persist some cycles until an automatic detection system override this; if such a control mechanism exists. Similarly a severe unbalance can also be produced by a sudden change in the load. For instance, the case when the TCR operates with a firing angle of 130 degrees and u= 2 is single out for a more detailed analysis with reference to node 3, which is where the Static Var Compensator is connected.

Figure 5-24 shows the harmonic current magnitudes from node 1 to 2, with node 2 being the input to the step-down transformer. Results are processed for each phase where the unbalance is shown. These results are compared with those of the current flowing from nodes 3 to 4, presented in Figure 5-25. It is noticed that lower magnitudes of the third harmonic currents flow towards the supply then towards the arc load. For completeness, the current waveforms are depicted in Figure 5-26.

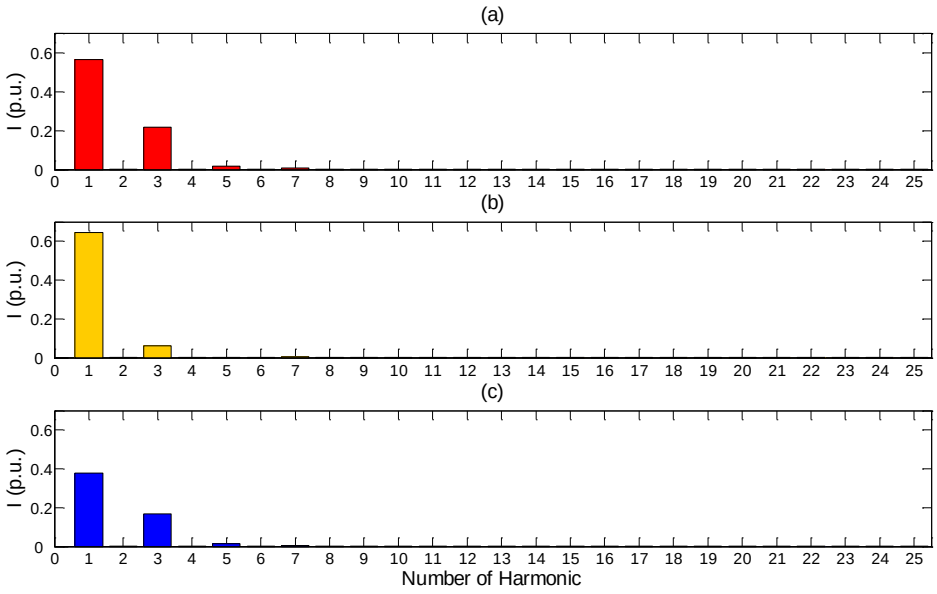

Figure 5-24 Harmonic current magnitudes in branch connected between nodes 1 and 2, for a factor *u*=2

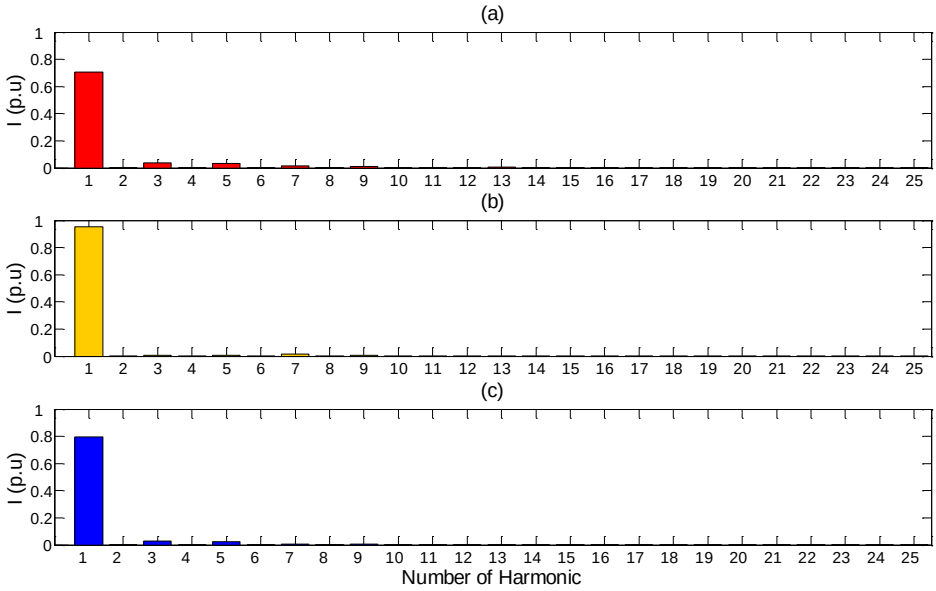

Figure 5-25 Harmonic current magnitudes in branch connected between nodes 3 and 4, for a factor *u*=2

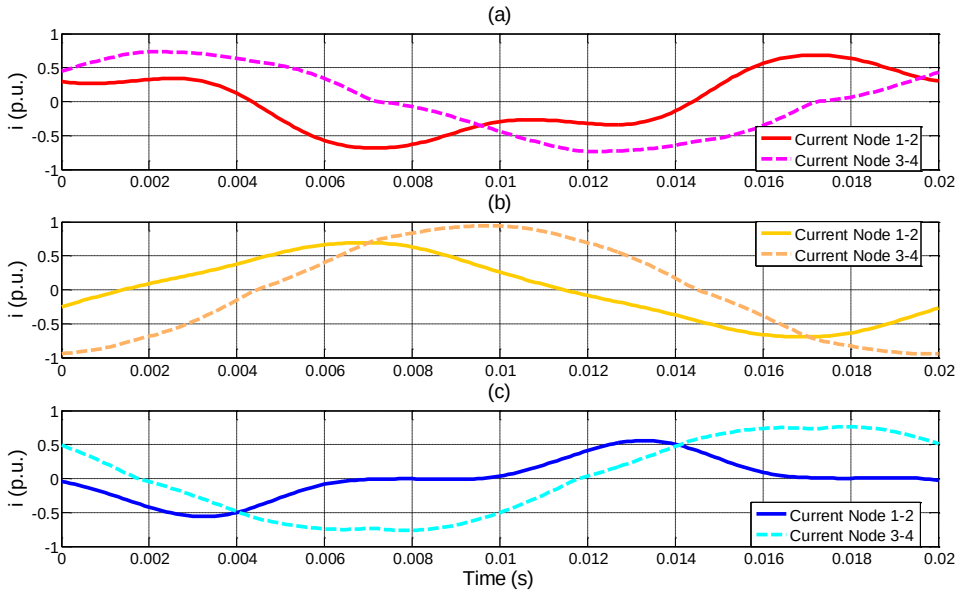

Figure 5-26 Three-phase current waveforms in branches connected between nodes 1 and 2 and between nodes 3 to and 4 for a factor u=2

The current changes taking place in node 3, where the SVC is connected to, calls for a more detailed analysis of the SVC currents. Figure 5-27 depicts the currents delivered by the SVC, shown in Figure 5-27 (a), which are in fact a summation of TCR current; capacitor bank currents shown in Figure 5-27 (b) and (c) respectively. It should be noticed that both unbalances and harmonics are present in these waveforms. The total effect of this device is shown in the SVC harmonic current composition which is depicted in Figure 5-28 where it can be observed that third harmonic component of phase (a) it is just under 20%. The other device connected to node 3 is the step-down transformer; the current contribution of this element is low as is shown in Figure 5-29 but a large contribution to harmonic distortion is the magnetising branch of the furnace transformer, shown in Figure 5-30.

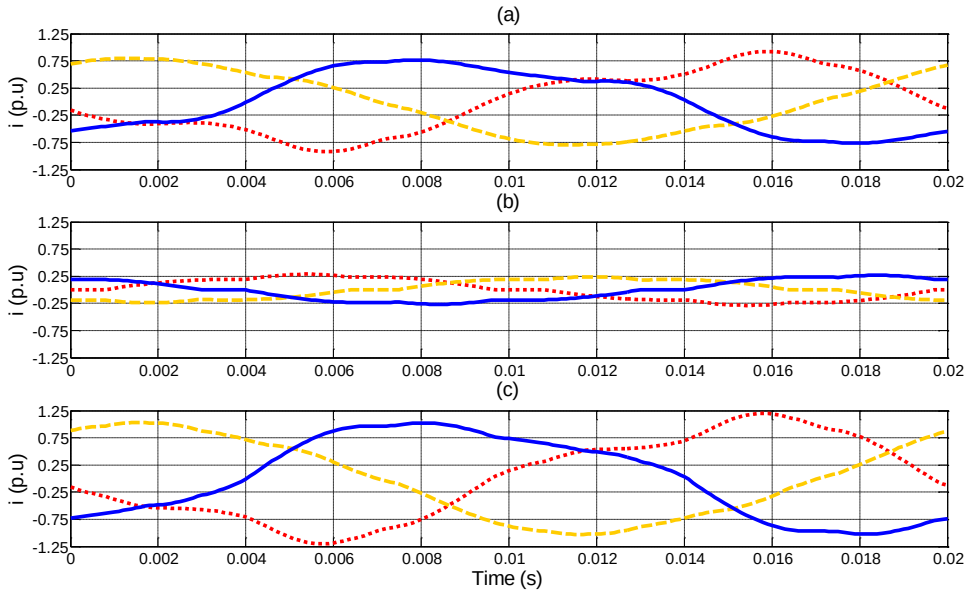

Figure 5-27 Three-phase current waveforms for a factor of u=2 in: (a) SVC; (b) TCR; and (c) capacitor bank

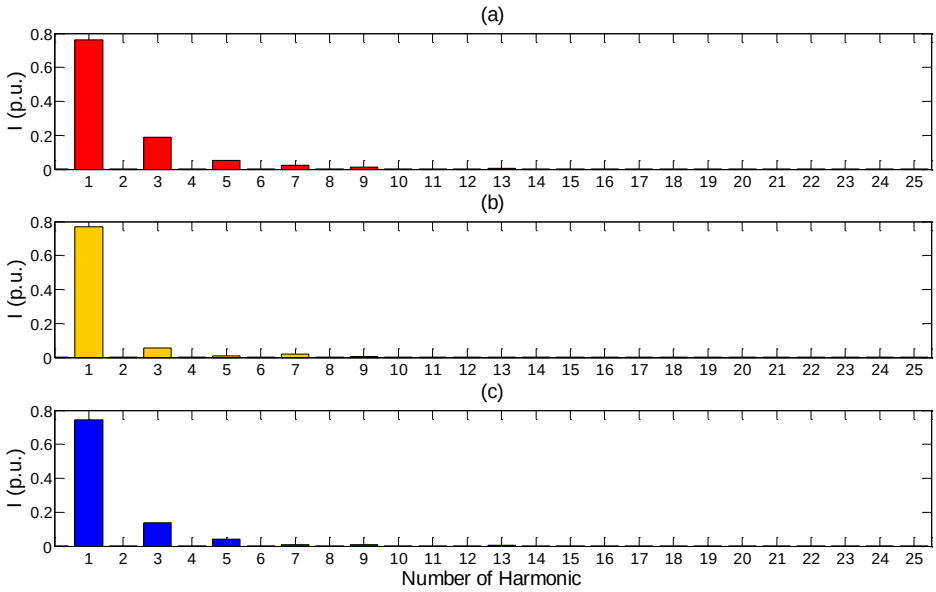

Figure 5-28 Harmonic current magnitudes for a factor of *u*=2 in the SVC

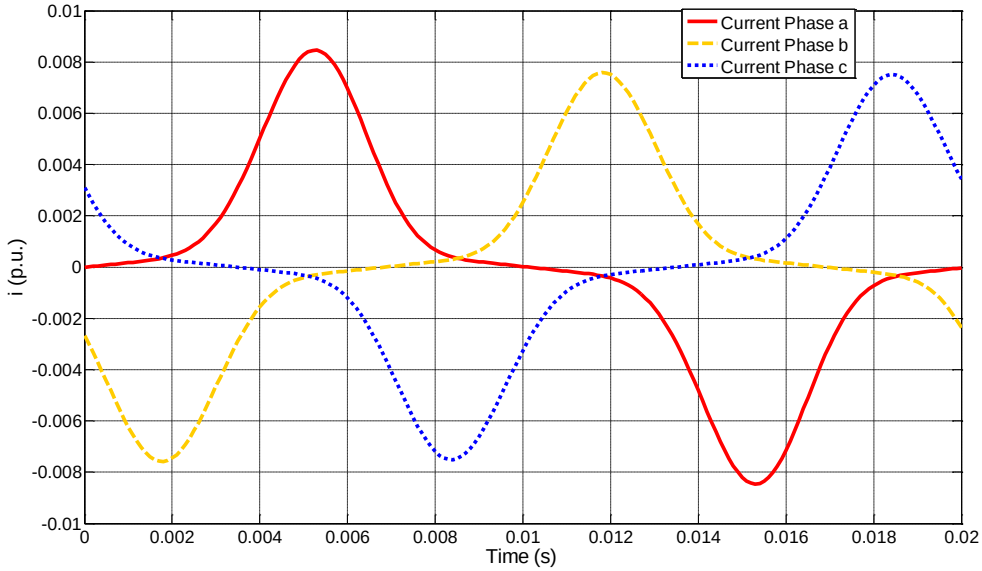

Figure 5-29 Three-phase current waveforms for a factor of u=2 in the step-down transformer

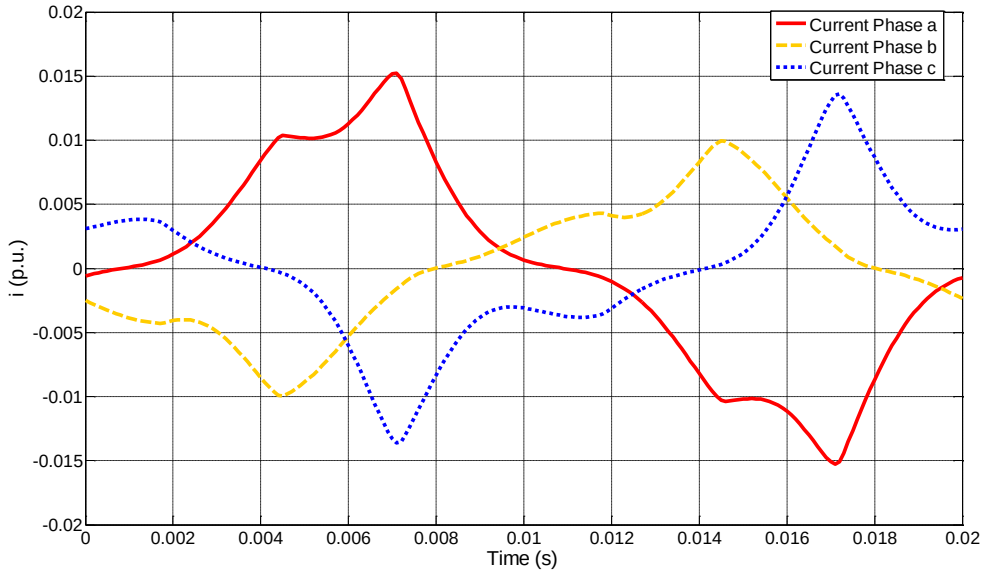

Figure 5-30 Three-phase current waveforms for a factor of u=2 in the furnace transformer

5.4.3 Unbalanced operation of the three-phase electric arc furnace system with Static Var Compensator and harmonic filters

Filters normally exist in electric arc furnace installations and their effect is incorporated in the simulations carried out in this work. Harmonic filters contribute reactive power at the fundamental frequency hence, the three-phase capacitor bank which conform the SVC is reduced from 70 MVA to 40 MVA. Two harmonic filters will be used to filter out the 3rd and 5th harmonic currents each of 15 MVA. A comparison is made of the simulation results obtained for the electric arc furnace installation with harmonic filter and without them.

The voltage TDD has an improved performance with the inclusion of filters as indicated by the results shown in Figure 5-31. For instance node 3 which reach a maximum value of 6.6% in Figure 5-22 with no harmonic filters, decreases to around 3% when filters are used. At the node 4, it decreases from a maximum value of 11% with no filters to around 9%. It is noted that there is not improvement in the arc load because this is the point where actually unbalance takes place and the voltage waveform keeps the same wave shape. In general, it is observed that the inclusion of filters do help to decrease the values of voltage TDD in the electric arc furnace installation.

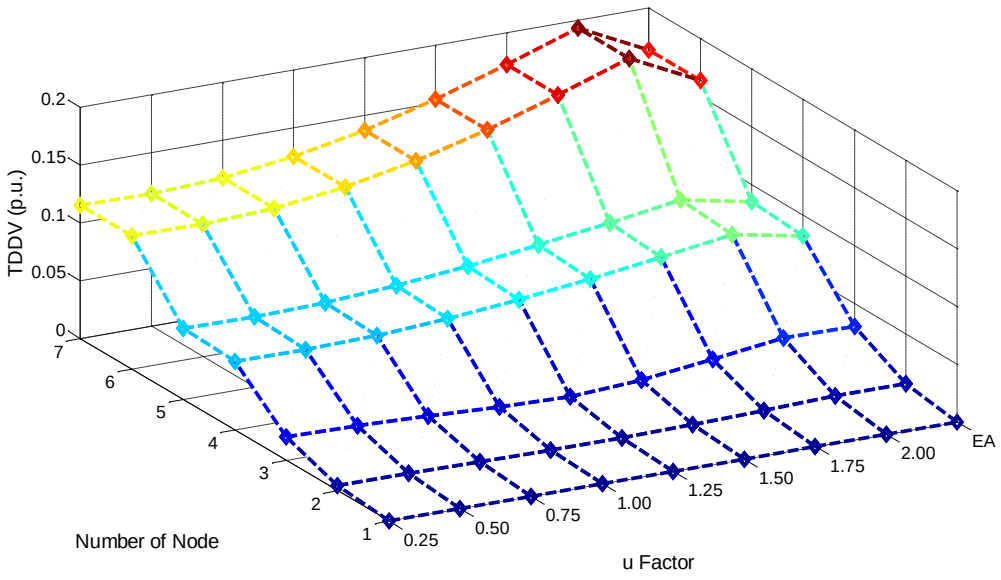

Figure 5-31 Effective voltage TDD vs *u* factor at nodes 1 to 7, with harmonic filters

It is observed that the harmonic filters are more effective in improving the TDD. For instance, before the inclusion of harmonic filters the current TDD in branch between nodes 1 and 2 reached values of around 21% for the case of the extinguished arc condition, as can be observed in Figure 5-23. In contrast when filters are used the maximum values decrease to just under 7%, can be observed in Figure 5-32. The two power quality indices receive the major impact in their values in relation with the connection of filters, the other quantities as power and sequence fundamental components no show significant variations.

To better appreciated the benefit of adding the harmonic filters to the system, the case of u= 2 is single out for further analysis. Figure 5-33 shows three-phase waveforms of the currents flowing from nodes 1 to 2 and from nodes 3 to 4. A direct comparison with the results of Figure 5-26 shows a perceptible reduction in waveform distortion. This is further confirmed by comparing the harmonic spectrum shown in Figure 5-34 with that is shown in Figure 5-24, where the third harmonic current has virtually disappeared.

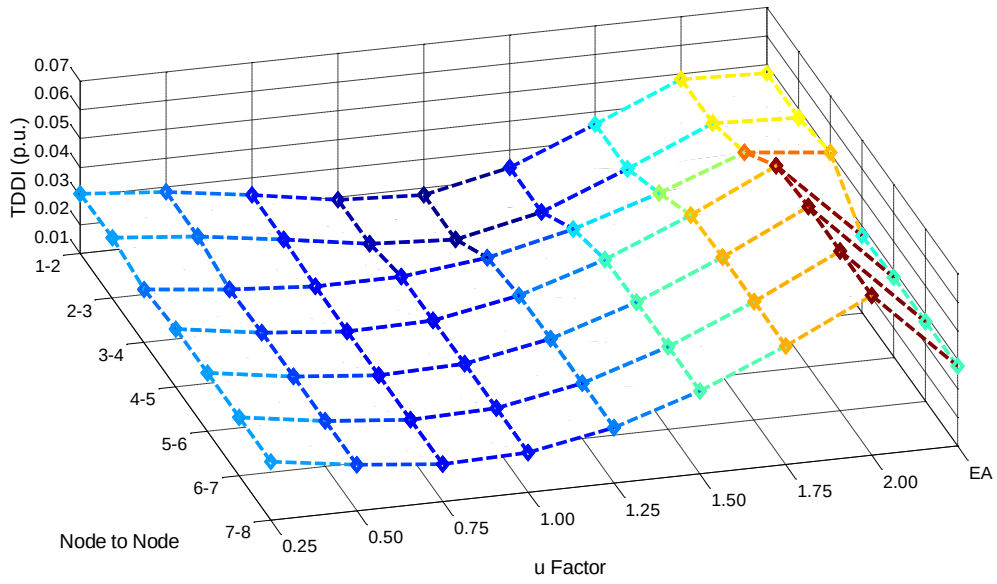

Figure 5-32 Effective current TDD vs u factor, at elements connected between nodes 1-2 to 7-8

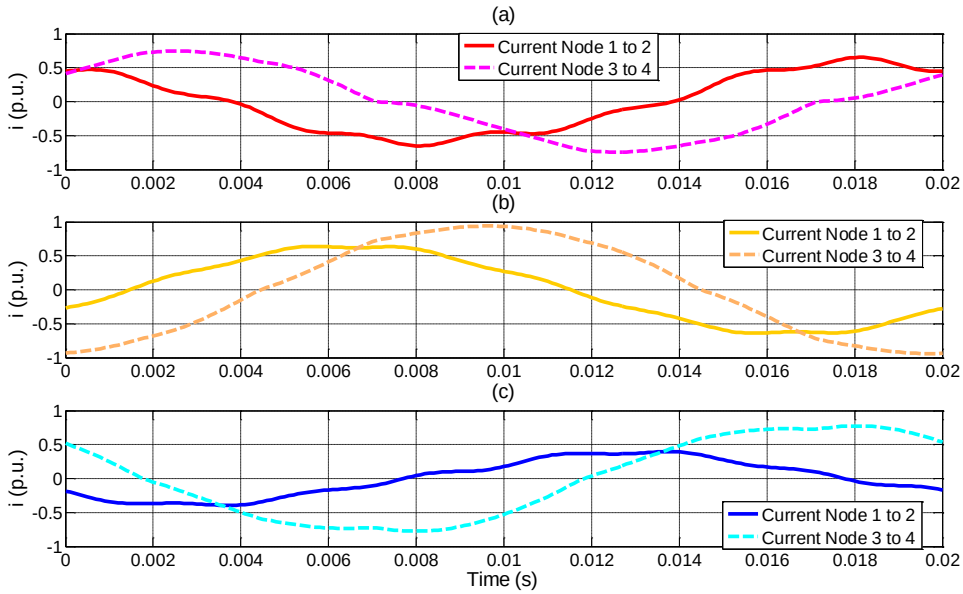

Figure 5-33 Three-phase current waveforms for a factor u=2, at branches connected between nodes 1 and 2 and between nodes 3 and 4, with SVC and filters

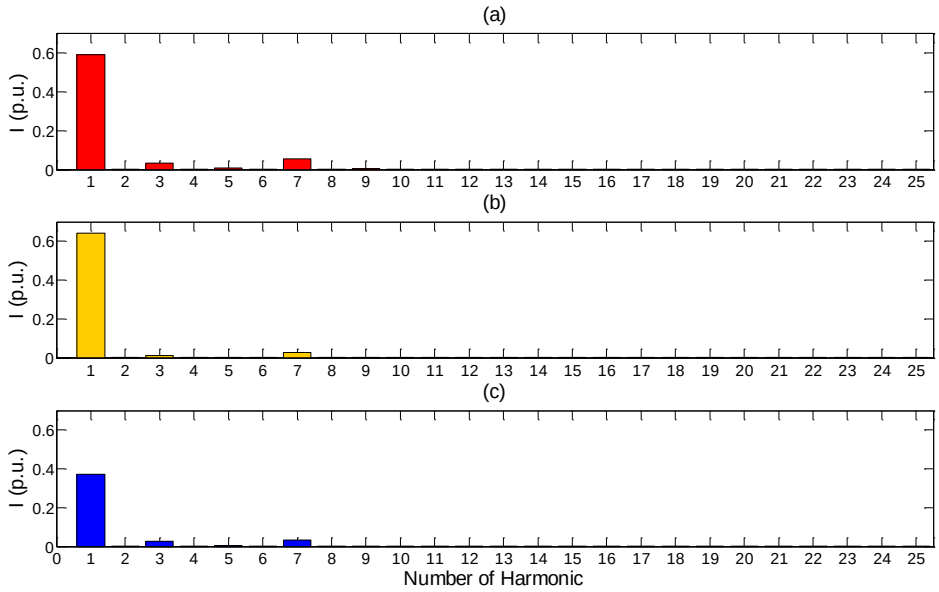

Figure 5-34 Magnitudes of harmonic currents for a factor of u=2, in the branch connected between nodes 1 to 2, with SVC and filters

The changes produced in the current flowing from node 1 to node 2, is attributed to the harmonic filters. As shown in Figure 5-35 the waveforms of current in the TCR, capacitor bank and SVC show a marked improvement in comparison with the current waveforms presented in Figure 5-27.

It is noted that the harmonic filters is beneficial not only at the node which they are connected (in node 3) but its influence extend to other nodes of the electric arc furnace installation. A case in point is the magnetising branch of the furnace transformer with its current waveform showing a slight difference in Figure 5-36 compared with the current waveform shown in Figure 5-30. This is more noticeable for phase *a* an *b*

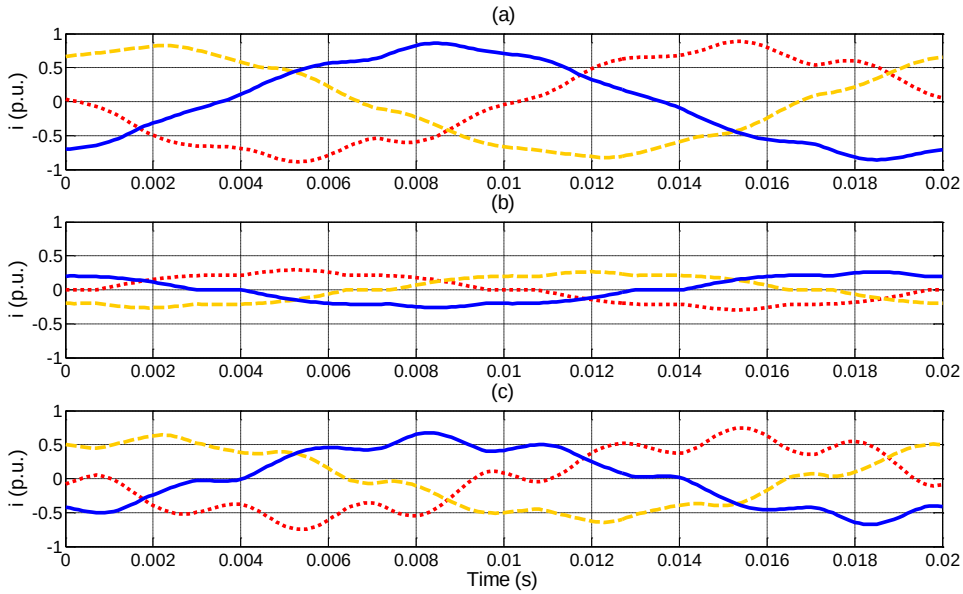

Figure 5-35 Three-phase current waveforms for a factor *u*=2, in: (a) SVC; (b) TCR; and (c) capacitor bank, with SVC and filters

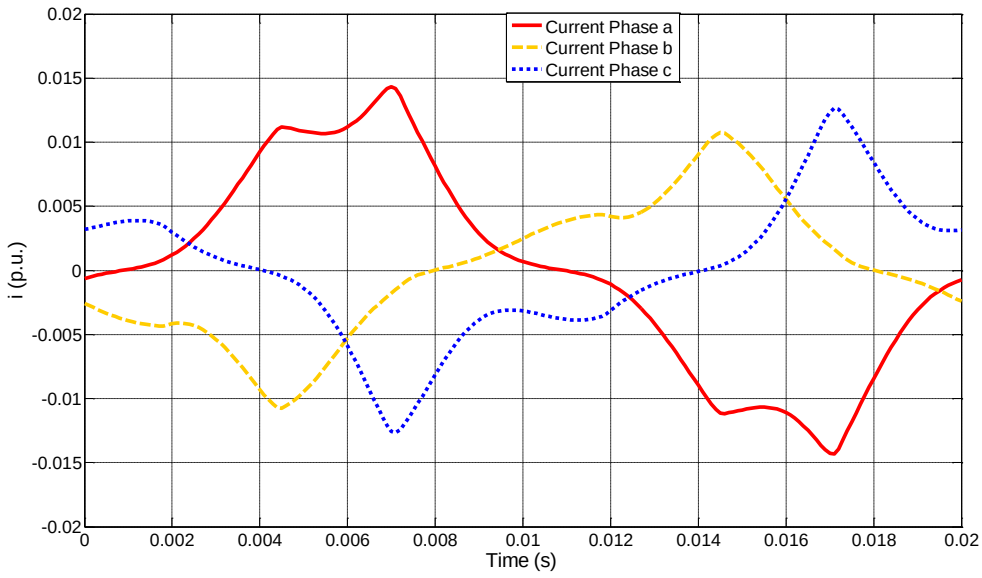

Figure 5-36 Three-phase current waveforms for a factor *u*=2, in the furnace transformer, with SVC and filters

5.5 Balanced Operation of the Three-phase Electric Arc Furnace System with a Thyristor Series Reactor Compensator

The use of a series reactor increases current stability in the electric arc furnace, amply discussed in reference [Montanari *et al.* 1994]. An improvement switched on this basic current stability may be achieved by using a power electronics solution with devices such as the Thyristor Switched Series Reactor [Cardoso and Cardoso 2006] and the Smart Predictive Control [Ma and Mulcahy] two examples in this category. The work reported in those references give assurance that the use of power electronics enables response to the variations observed in electric arc furnace load, with the TCR being used as an improved dynamic switch, i.e. with values of firing angles of 90^o and 180^o. In this work the applicability of a TCR, at the level of simulation is investigated. It is assumed to be connected between nodes 3 and 4 as is presented in Figure 5-3, comprising an impedance of 1.5 times the value of the original series reactor in parallel with a reactor of equal value. The equivalent impedance of this device rises with the TCR firing angle. Therefore, a set of simulations is carried out with different values of the TCR firing angle. Similarly to the other results presented in this Chapter when the TCR firing angles has been varied, simulations are carried out for angle variations in the range 90 to 180 (179) degrees at 10 degree intervals. However, it has been found that the algorithm failed to converge in a range of values around 120 degrees, hence, numerical results are presented for a value of the firing angle of 115 degrees.

The effective voltage values at nodes 2 and 3 rises slightly with the firing angle, as shown in Figure 5-37. For instance at node 3 the increase is from 0.90 to 0.93 per unit at values of TCR firing angles of 90 and 179 degrees, respectively; this contrast with the behaviour of the effective voltages at nodes 4 and 5. For instance, where the values decrease from 0.66 to 058 per unit values for the same firing angles. In node 7 where the electric arc load is connected, variations in this firing angle have even less of an impact.

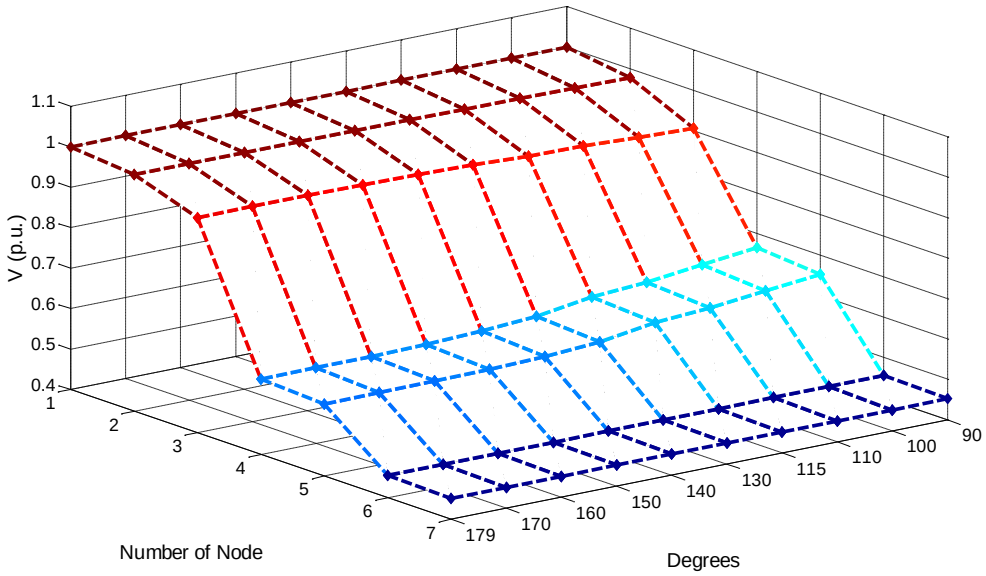

Figure 5-37 Effective voltages vs TCR firing angles, at nodes 1 to 7, with TCSR

The TCSR shows a good control of the effective current, with values varying inversely with the TCR firing angle values, as shown in Figure 5-38. For example, the current flow from node 1 to node 2 goes from 0.99 to 0.71 per unit for firing angles of 90 and 179 degrees, respectively. Such a control over the effective current is attributed to the TCSR.

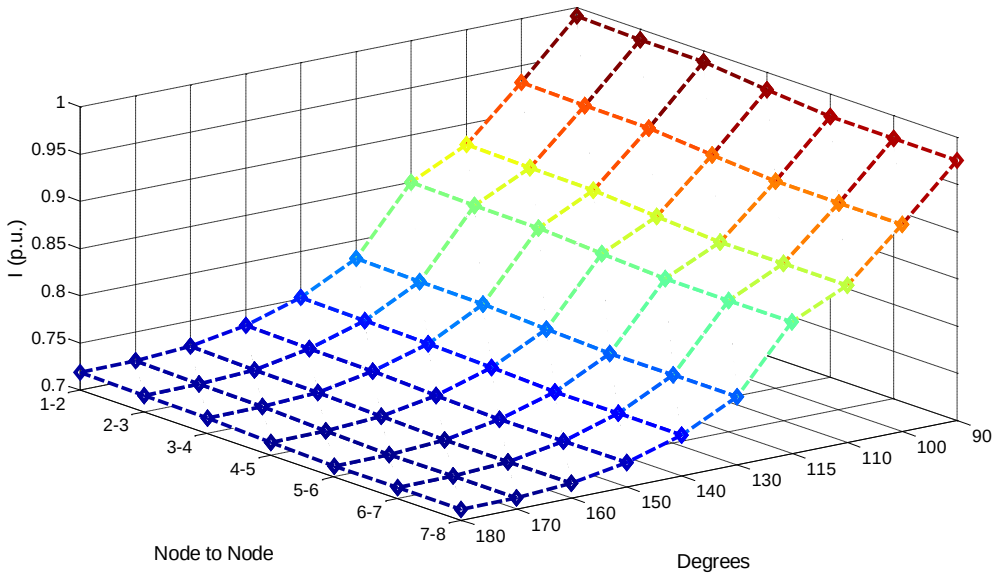

Figure 5-38 Effective currents vs TCR firing angles, at elements connected between nodes 1-2 to 7-8, with TCSR

Similarly to the effective current, the average active power also varies inversely with the TCR firing angle as observed in Figure 5-39, but with the respective power losses clearly shows as the power flows from the equivalent supply source (node 1) towards the arc load (node 7). The electric arc load power consumption varies from 0.42 to 0.30 per unit for values of TCR firing angles of 90 and 179 degrees, respectively. It is clear that with such current control, the delivery of active power to the arc load may be carried out in a controlled manner.

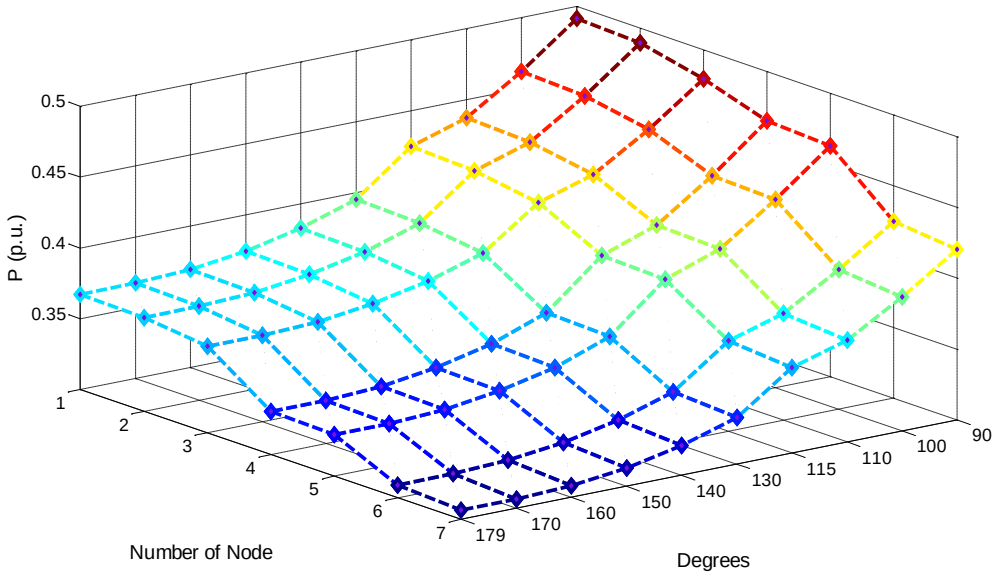

Figure 5-39 Average active powers vs TCR firing angles, at elements connected between nodes 1-2 to 7-8, with TCSR

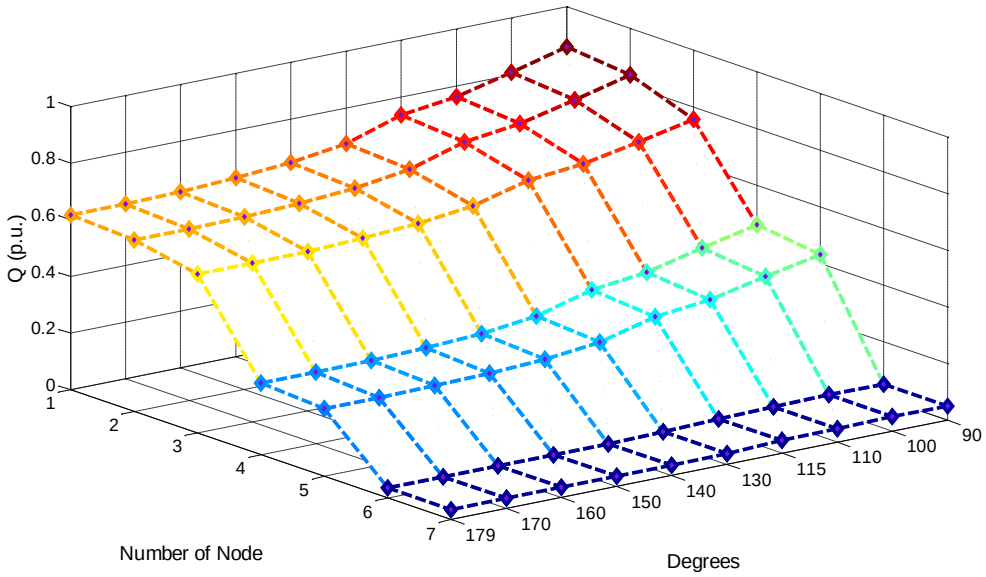

Figure 5-40 Average reactive powers vs TCR firing angles, at elements connected between nodes 1-2 to 7-8, with TCSR

The reactive power at the various nodes of the electric arc furnace installation follows a similar behaviour to the active power flow, with their values varying inversely with TCR firing angle values, as shown in Figure 5-40. It is observed that the largest changes take place when the firing angle is 90 degrees and that these large variations reduce with increases of the firing angle. Concerning the consumption of reactive power, it is observed that this takes place between nodes 3 and 4, and between nodes 5 and 6, which are the place where the TCSR and the secondary circuit, are respectively. It is clear that these series devices consume the largest amount of reactive power.

The apparent power shown in Figure 5-41 has the same general shape as those of active power and reactive power. The effective apparent power is related to the electrical capability of the equipment in the electrical furnace installation. The maximum apparent power value is of 0.99 per unit, which takes place in node 1 with a firing angle of 90 degrees, which is a value close to the limits of the system capacity. The TCSR exerts control over the apparent power by controlling the effective current.

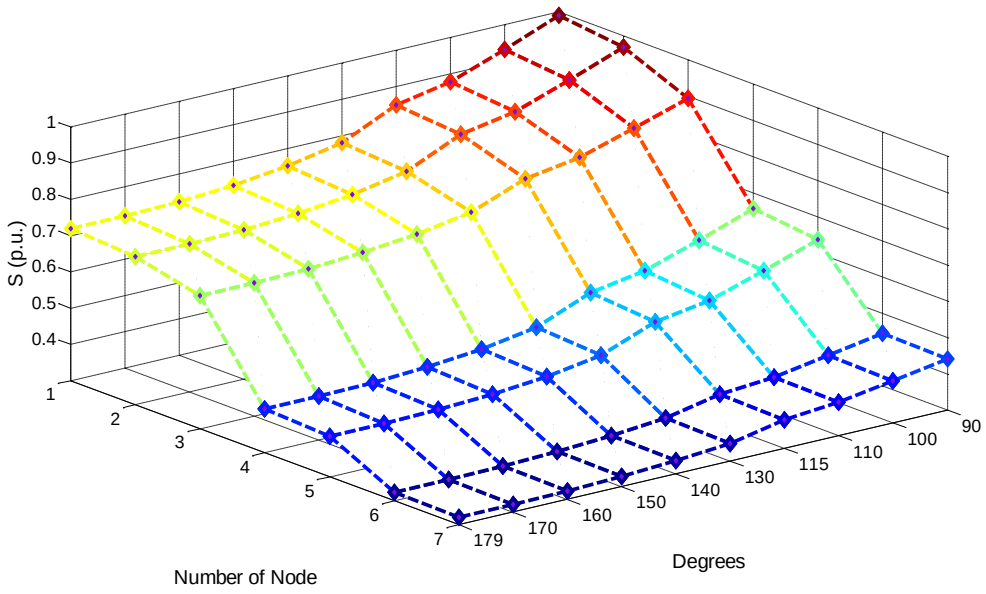

Figure 5-41 Effective apparent powers vs TCR firing angles, at nodes 1 to 7, with TCSR

The effective power factor values increases slightly with the TCR firing angles, with the exception of node 3 where it decreases at angle of 100 degrees. The largest changes take place at nodes 5 and 4 where differences of around 7% exist between the TCR firing angles of 90 and 179 degrees.

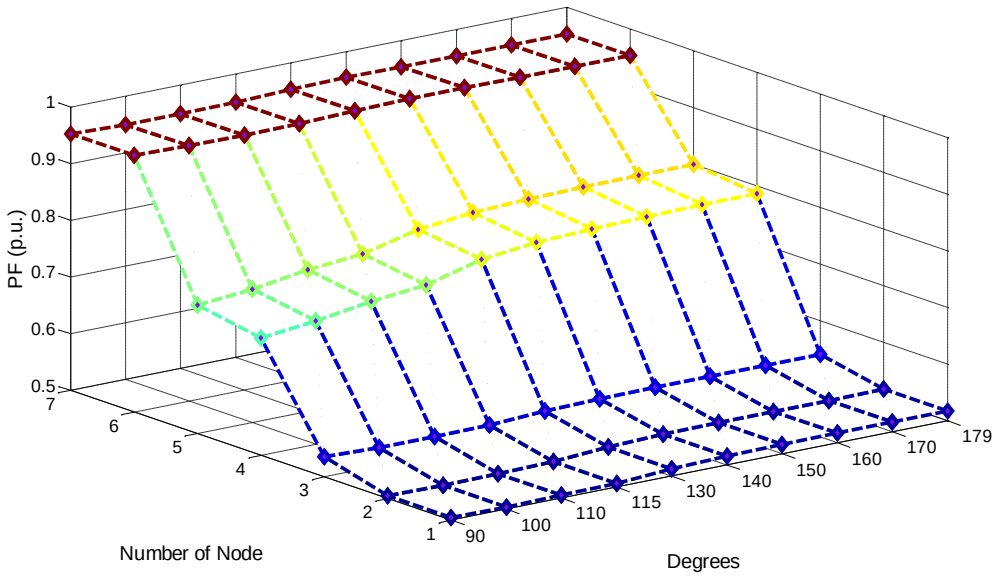

Figure 5-42 Effective power factors vs TCR firing angles, at nodes 1 to 7, with TCSR

The largest effect that the TCR firing angles has on voltage TDD is in nodes 3 to 5, as shown in Figure 5-43. It reaches a value of around 2% at node 3, with firing angles of 100 and 110 degrees. However in nodes 4 and 5 it rises to values above 8%t with firing angles of 140 and 150 degrees. At the arc load it hold values above 12% at all values of firing angle.

The effective current TDD has highest values in the firing angle range of 90 to 130 degrees. They rise above 3.5%, as shown in Figure 5-44. Outside the range 0-130 degrees the effective current TDD is relatively small causing no concern.

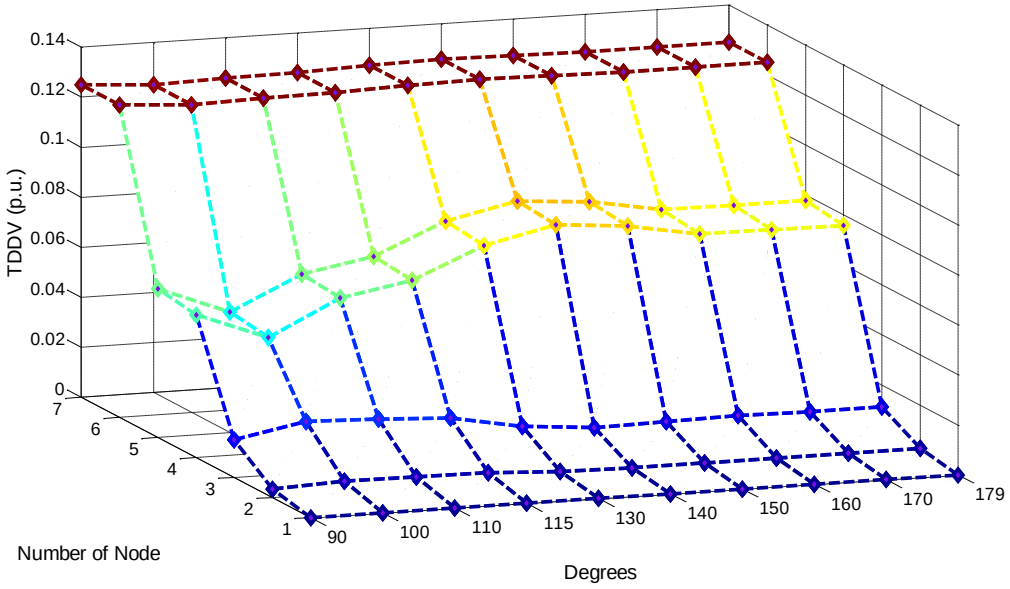

Figure 5-43 Effective voltage TDD vs TCR firing angles, at nodes 1 to 7, with TCSR

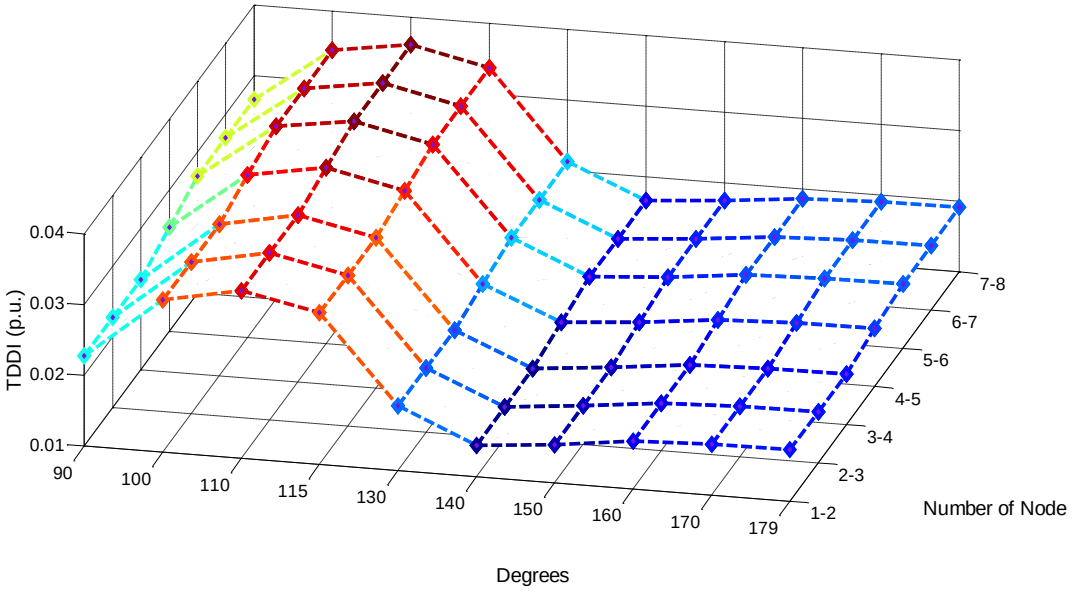

Figure 5-44 Effective current TDD vs TCR firing angles, at elements connected between nodes 1-2 to 7-8, with TCSR

5.6 Conclusion

Observations derived from the comprehensive simulation results carried out in this Chapter using harmonic domain techniques lend further credence to the claim made elsewhere that the installation of electronic power devices within the installation has a positive impact in the operation of the electric arc furnace.

In this chapter, the model of a SVC was included to the harmonic domain model of an electric arc furnace installation. To begin with, to gain a basic understanding of the SVC impact in the installation idealised balanced conditions are assumed, for a fix arc load and a wide range of TCR firing angles. The simulation results show that the SVC has a good response to a wide range of reactive power compensation characteristics, reflecting in an improved power factor in different points of the installation. This observation applies to both balanced and unbalanced conditions. Furthermore, the inclusion of a Thyristor Controlled Series Reactor in the electric arc furnace installation has shown to have a very beneficial effect. Comprehensive simulations have been carried out to establish the best operation range of the TCR firing angles. The device yields an effective control over the current that flows to the arc load. This is a powerful characteristic of the equipment that maximizes the utilisation of the electric arc furnace installation. The research was extended to consider a wide range of a set of unbalanced arc load conditions, coming to a conclusion that harmonic voltage and current pollution increases with the unbalanced condition. The results also point out that the inclusion of harmonic filter is desirable because, in general, they help to decrease voltage and current TDD under the same situation. Further research is required to integrate the models of SVC and the TCSR in to the model of the electric arc furnace installation.

6 Conclusions

6.1 General Conclusions

It has been found in this research that Tellegen's theorem is a useful tool to classify various forms of electrical power into conservative and non-conservative. Conservative powers as defined by the use of the Hilbert Transform and analytic functions are useful to develop power-based models of electrical power equipment and systems. Moreover, such conservative powers in conjunction with the IEEE 1459 Standard [2000] enable the periodic, steady-state analysis of three-phase electrical power systems where any number and types of non-linearity is present, including electrical power networks with severe design and operational imbalances. The frame-of-reference used for carrying out the periodic, steady-state calculations is the harmonic domain, a direct frequency representation where all the harmonics and cross-couplings between harmonics are explicitly shown.

In this research work, integration of two kinds of non-linearities, the electric arc and the magnetic ballast, have been successfully modelled in the harmonic domain. The model of the arc discharge tube is quite generic and can be made to represent other types of electric arc discharge lamps, with ease. Its integration with the harmonic Norton equivalent representing the ballast should only be treated as the starting point for integrating the arc discharge tube with other more detailed models of magnetic ballasts, such as laminated iron core ballasts for loss minimization. Indeed, developing models of electronic ballasts in harmonic domain should be looked at as a natural extension of the research work reported in this thesis. An extension of the single lamp-ballast system to model the more general case of aggregated lamp-ballast systems has been started, with potential applications in the assessment of lighting installations comprising hundreds of arc discharge lamps, on the electrical supply company.

The integration of the lamp-ballast model in harmonic domain is a new development in electrical engineering which incorporates with a high degree of fidelity, the dynamic behaviour of the plasma. The overall solution algorithm is a blend of the Newton-Raphson method and the Gauss-Seidel method, which iteration mismatch values exhibit linear convergence characteristics. Typically, a numerical solution is carried out in 32

iterations to a mismatch tolerance of 1e-12. In this kind of harmonic domain applications it has been found convenient to include up to the 100^{th} harmonic due to the square-wise nature of the arc voltage. This gives rise to a non-linear system of equations of large dimensions where the admittance matrix has 1206 rows and 1206 columns, but contains a high-degree of sparsity. It should be emphasised that the simulation results have been compared with experimental measurements and that they agree with each other.

The aggregated lamp-ballast model in the harmonic domain is also a new development which inherits the physical attributes of the single lamp-ballast system. The solution algorithm is equally robust towards the convergence, achieving solutions to a tight convergence of 1e-12 in a linear fashion. The model groups together any number of lamps having the same characteristic. It can be used equally well single-phase lighting installations or three-phase ones.

It has been found in this research that high-power electric arcs, such as those found in electric arc furnace installations, are more challenging to abstract mathematically and to solve than those found in arc discharge lamps. The reason is that the non-linear characteristic of the electric arc in an electric arc furnace installation interacts with several other non-linear elements, such as the magnetizing characteristics of two power transformers and the non-linear characteristics high-power, high-current semiconductor equipment. Moreover, the electric arc furnace installation is a three-phase circuit and the melting of the scrap is a highly irregular process that induces very severe imbalances in the operation of the installation. The combined adverse affects introduced by the non-linear characteristics in the form of harmonic generation and operational imbalances call for highly robust iterative algorithms in the harmonic domain. Nevertheless, having achieved a solid understanding of how best to characterize and solve the non-linear differential equation of the arc discharge lamp, in harmonic domain has yielded invaluable information and experience for solving the most demanding case of the electric arc furnace installation.

The model of the three-phase electric arc furnace installation, in the harmonic domain frame-of-reference has a power balance equation of the electric arc, at its core. It is a non-linear differential equation that yields physical meaning – it is fundamentally

different from other alternative representations which are based on heuristic considerations. The power balance equation which incorporates the dynamics of the high-current, high-power electric arc, with high fidelity is well represented in the harmonic domain where all harmonics and cross-couplings between harmonics are explicitly shown. Such a representation enables a seamless integration of the three-phase model representing the three arcs and, indeed, the complete electric arc furnace representation which comprises the power supply, supply impedance, step-down transformer, series reactor, furnace transformer, secondary circuit, graphite electrodes and the electric arc. Either of the two three-phase models of the arc that have been developed, can be used since they are fully equivalent and the harmonic domain frame-of-reference can accommodate either of them quite naturally. It should be emphasised that this is the first time that the harmonic interaction of the electric arc furnace load, the magnetic saturation of power transformers and the switching characteristics of power electronics equipment is being modelled and assessed using direct harmonic domain calculations. The algorithm, which blends the Newton-Raphson method and the Gauss-Seidel method, possesses linear convergence characteristics. It has been found that owing to the three-phase nature of the model, the representation of numerical unbalances and the large number of non-linearities involved and their location in the test network, the algorithm's convergence is dented slightly compared to the case of the arc discharged lamp, and the tolerance criterion has been set to 1e-6 as opposed to 1e-12. In this case as well the number of harmonics used in the solution is 100, giving rise to a sparse harmonic admittance matrix of 4221 rows and 4221 columns. A fact of perhaps greater relevance is that the algorithm converges even for cases which exhibit extreme imbalances, e.g. one open phase.

The three-phase model of the electric arc furnace installation with high-power, high current semiconductor devices in the harmonic domain of reference is a new development in electrical engineering. As far as this author is aware, a harmonic model with the following features is not available anywhere:

- A Static Var Compensator made up by a Thyristor Controlled Reactor and a capacitor bank has been incorporated in the harmonic domain model of the electric arc furnace installation. The integration is carried out using the harmonic

nodal admittance where all nodes of the system, phases, harmonics and cross-couplings between harmonic are explicitly represented.

- Comprehensive models of the electric arc load, transformers with core saturation, and switching semiconductor-based equipment are all integrated and solved together.
- The harmonic algorithm, which blends seamlessly the best characteristics of the Newton-Raphson method and the Gauss-Seidel method, is used to carry out reliable iterative solutions up to a tight tolerance of 1e-6.
- The algorithm converges very reliable whether for balanced or unbalanced operating conditions.

6.2 Applications

The model of the arc discharge lamp and its accompanying ballast system is well placed to carry out assessments of harmonic distortion and resonances of the lamp-ballast circuit with the power factor correction capacitor for different capacities of arc discharge lamps and magnetic ballasts. Similarly, the aggregated model of the electric lamp-ballast system can be used to quantify the impact of different kinds of arc discharge lamps of varying capacities for a better selection of lamps for lighting installations comprising a room or an entire building; yielding information of power efficiency, reactive power consumption, harmonic distortion and values of neutral currents.

A reduced equivalent model of the three-phase electric arc furnace load in the form of a harmonic Thevenin equivalent or a harmonic Norton equivalent would be very useful for integration with the model of a larger electrical power systems, this enabling detailed assessments of the impact of the electric arc furnace installation on the external electrical power system.

Besides applications of the model of electric arc furnace installations in planning studies, the model has a key potential role in improving the operation of actual installations by producing diagrams of currents versus power for different values of arc lengths, different transformer tap positions for voltage control and different series reactor tap positions for current control. This information would be presented in

operational charts as an aid to the electric arc furnace operator aiming at achieving safer and more efficient operations of the electrical arc furnace installation. An application that would be perhaps restricted to balanced operation and one where the use of positive sequence models would be preferred over the full three-phase models presented in this thesis.

Concerning planning studies, the electric arc furnace installation model would be useful to assess the effect of re-sizing equipment in the electric arc furnace installation such as step-down and furnace transformers or series reactors. The analysis would also include graphite electrode consumption. The model would be useful to carry out preliminary studies of harmonic interaction and resonance effects caused by the incorporation of high-power, high current semiconductor devices in to the installation and the harmonic filter deployment.

6.3 Future Work

As part of future research in this area of development, the harmonic domain model of the arc discharge lamp tube should be improved by using an iterative method to find out the constants from the current-voltage characteristic for different capacities and types of discharge lamp tubes.

The harmonic domain model of the saturated magnetic core and its losses should be improved by using models conformed by technical information such as physical dimensions, saturation characteristics of magnetic cores and wiring data.

The algorithm for the solution of the single discharge lamp-ballast model should be improved by using a full Newton-Raphson method or a Quasi-Newton method instead of the hybrid Newton-Raphson and Gauss-Seidel method, aiming at enhancing convergence characteristic. Moreover, use of sparsity techniques and a more efficient computer language such as FORTRAN or C++ instead of Matlab would lead to more expedient solutions.

Concerning future research on electric arc furnace modelling, similarly to the arc discharge lamp model, the algorithm should be improved by using a full Newton-

Raphson method or a Quasi-Newton method. Aiming at numerical efficiency, sparsity techniques should be used and the algorithm coded using a computer language such as FORTRAN or C++.

The use of Unified Magnetic Equivalent Circuit (UMEC) models to represent three and five leg transformer models as part of the model of the electric arc furnace installation should be developed.

Additional models of power electronics equipment should be developed, in particular, models of the new generation of power electronic converters based on voltage source converters such as the STATCOM and series active filter.

It is clear that the model of the electric arc furnace installation should benefit from the integration of the following harmonic domain models: (i) an actual synchronous generator model instead of the model of an idealised power supply; (ii) a detailed cable model instead of a series impedance; (iii) a Variable Frequency Transformer (VFT) model to assess the viability of this technology as a competitor of a power electronic solution such as the TCSR.

The range of analysis in this application area would be extended very considerably using Extended Harmonic Domain (EHD) methods to represent the electric arc furnace installation; enabling dynamic analysis of the installation.

I would like to conclude by stating that the research on harmonic domain models of electric arc loads has been a challenging but fruitful research exercise, and even more so when integrated with the study of magnetic core saturation in power transformers and high-power, high current semiconductor devices. I feel that in fact this research only touches the surface of a wealth of applications that the harmonic domain has to offer in commercial and industrial applications, as well as its proven applicability in the analysis of traditional electrical power networks but perhaps more important in Flexible AC Transmission Systems, Custom Power and distributed generation with renewable energy sources.

References

[Acha 1988] E. Acha, Modelling of Power System Transformers in the Complex Conjugate Harmonic Space, PhD Thesis, University of Canterbury, New Zealand, 1988.

[Acha *et al.* 1990] E. Acha, A. Semlyen and N. Rajakovic, A Harmonic Domain Computational Package for Non-Linear Problems an Its Applications to Electric Arcs, IEEE Transactions on Power Delivery, Vol. 5, No. 3, July 1990, pp. 1390-1397.

[Acha, 1991] E. Acha, Harmonic Domain Representation of Thyristor Controlled Reactors, International Conference on AC and DC Power Transmission, 1991, 17-20 Sep 1991, pp. 404-406.

[Acha *et al.* 1997] E. Acha, J. J. Rico, S. Acha, M. Madrigal, Harmonic Modelling in Hartley's Domain with Particular Reference to Three Phase Thyristor-Controlled Reactors, IEEE Transactions on Power Delivery, Vol. 12 No. 4, Oct. 1997.

[Acha and Madrigal 2001] E. Acha, M. Madrigal, Power System Harmonics: Computer Modelling and Analysis, John Wiley and Sons, 2001.

[Acha *et al.* 2004] E. Acha, C.R. Fuerte-Esquivel, H. Ambriz-Pérez, C. Angeles-Camacho, FACTS: Modelling and Simulation in Power Networks, John Wiley and Sons, 2004.

[Akagi *et al.* 1984] H. Akagi, Y. Kanazawa, A. Nabae, Instantaneous Reactive Power Compensators Comprising Switching Devices Without Energy Storage Components, IEEE Transactions on Industry Applications, Vol. IA-20, No. 3, May/June 1984.

[Akagi, 2006] H. Akagi, Modern Active Filters and Traditional Passive Filters, Bulletin of Polish Academy of Sciences, Technical Sciences, 31 January - 4 February 1999, Vol. 54, No. 3, 2006.

[Aller and Bueno 2002] J.M. Aller, A. Bueno, T. Paga, Power System Analysis Using Space-Vector Transformation, IEEE Transactions on Power Systems, Vol. 17, No.4, Nov. 2002, pp. 957-965.

[Arrillaga and Watson 2003] J. Arrillaga, N.R. Watson, Power System Harmonics, 2nd Ed., John Wiley & Sons, Inc., 2003.

[Bakken *et al.* 1997] J. A. Bakken, L. Gu, H. L. Larsen and V. G. Sevastyanenko, Numerical Modeling of Electric Arcs, Journal of Engineering Physics and Termophysics, Vol. 70, No. 4, 1997.

[Beites et al. 2001] L.F. Beites, J.G. Mayordomo, A. Hernandez, R. Asensi, Harmonics, Interharmonics and Unbalances of Arc furnaces: a New Frequency Domain Approach, IEEE Transactions on Power Delivery, Oct. 2001, Vol. 16, Issue: 4 pp. 661-668.

[Bo and Masumi 1976] H. Bo and K. Masumi, Analysis and Operating Circuits for Discharge Lamps by the Simulation method, Journal of the Illuminating Engineering Society, Vol. 5, No, 1, Jan. 1976, pp. 92-98.

[Bollen and Gu 2006] M.H.J. Bollen, Y. H. Gu, Signal Processing of Power Quality Disturbances, IEEE Press series in Power Engineering, John Wiley & Sons, 2006.

[Bowman and F. Istria 1990] B. Bowman, F. Istria, Critical Factor Determining The Choice of Equipment for Electric Steelmaking, Southeast Asia Iron and Steel (SEAISI) Conference, Jakarta, Indonesia, Nov. 5-6 1990.

[Bowman 1992] B. Bowman, Development of the AC Arc Furnace, Xi'an Symposium on Electric Steelmaking Installations, Sep. 1993.

[Bowman 1997] B. Bowman, Major Developments in Arc Furnace Technology Over The Last Four Decades, Instituto Argentino de Siderurgia, Seminario, Nov 26-28, 1997.

[Brown 1985] H.E. Brown, Solution of Large Networks by Matrix Methods, John Wiley and Sons, Inc., 1985.

[Campbell *et al.* 1953] J.H. Campbell, H.E. Schultz, D.D. Kershaw, Characteristics and Applications of High Frequency Fluorescent Lighting, Illuminating Engineering (North America), Vol. 48, No. 2, Feb. 1953, pp. 95-103.

[Carrillo *et al.* 1996] C. Carrillo, J. Cidras, J. Arrillaga, An Iterative Algorithm For The Analysis of The Harmonic Currents Produced by Fluorescent Lamp, IEEE Proceedings 7th International Conference on Harmonics and Quality of Power (ICHQP), 1996, pp. 1211-1217.

[Carrillo and Cidras 1998] C. Carrillo, J. Cidras, Harmonic Model for the Fluorescent Lamp, IEEE Proceedings 8th International Conference on Harmonics and Quality of Power (ICHQP), 14-18 Oct 1998, Vol. 2, pp. 1211-1217.

[Carrillo and Cidras 2001] C. Carrillo, J. Cidras, Fluorescent Lamp Modelling for Voltage Fluctuations, European Transactions on Electrical Power ETEP, Vol. 11, No. 2, pp. 119-127, March/April 2001.

[CELMA 2000] Guide for the application of Directive 2000/55/EC on Energy Efficiency Requirements for Ballast for Fluorescent Lighting, 2000.

[Chang 2003] G.W. Chang, Characterizing Harmonic Currents Generated by Fluorescent Lamps in Harmonic Domain, IEEE Trans. on Power Delivery, Vol. 18, No. 4, Oct. 2003, pp. 1583- 1585.

[Chung *et al.* 2007] S.H. Chung, N.M. Ho, W. Yan, P.W. Tam, S.Y. Hui, Comparison of Dimmable Electromagnetic and Electronic Ballast Systems An Assessment on Energy Efficiency and Lifetime, IEEE Transactions on Industrial Electronics, Dec. 2007, Vol. 54, No. 6, pp. 3145-3154

[Ciotti and Pelfrey 1986] Jon A. Ciotti and Donald L. Pelfrey, Electrical Equipment and Operating Power Characteristics, Electric Furnace Steelmaking, Chapter 3, Iron and Steel Society.

[Curtis and Silsbee 1935] H.L. Curtis, F.B. Silsbee, Definitions of Power and Related Quantities, AIEE, April 1935, pp. 394-404.

[Clarke 1943] E. Clarke, Circuit Analysis of A-C Power Systems. Volume 1 - Symmetrical and Related Components, John Wiley and Sons, Inc., 1943.

[Czarnecki 1987] L.S. Czarnecki, What is Wrong with the Budeanu Concept of Reactive and Distortion Power and Why It Should Be Abandoned, IEEE Transactions on Instrumentation and Measurement, Vol. IM-36, No. 3, Sep. 1987, pp. 834-837.

[Czarnecki 1996] L.S. Czarnecki, Instantaneous Reactive Power p-q Theory and Power Properties of Three-Phase Systems, IEEE Transactions on Power Delivery, Vol. 21, No. 1, Jan. 2006, pp. 362-367.

[Das 2004] J. C. Das, Passive Filters Potentialities and Limitations, IEEE Transaction on Industry Applications, Vol. 40, No. 1, Jan./Feb. 2004, pp. 232- 241

[Depenbrock and Wrede 2003] M. Depenbrock, H. Wrede, A Theoretical Investigation of Original and Modified Instantaneous Power Theory Applied to Four-Wire Systems, IEEE Transactions on Industry Applications, Vol. 39, No. 4, July/Aug. 2003, pp. 1160-1167.

[Edels and Fenlon 1965] H. Edels and F. H. Fenlon, Theory of a Filled-tube Thermal Arc Column, British Journal of Applied Physics, 1965, Vol. 16, pp. 219-230.

[Ferraci 1998] P. Ferracci, Ferroresonance, Cahier Technique No. 190, Groupe Schneider, 1998.

[Filipski 1980] P. Filipski, A New Approach to Reactive Current and Reactive Power Measurement in Nonsinusoidal Systems, IEEE Transactions on Instrumentation and Measurement, Vol. IM-29. No. 4, Dec. 1980, pp. 423-425.

[Francis 1948] V.J. Francis, Fundamentals of Discharge Tube Systems, John Wiley & Sons, Inc. New York, NY, 1948.

[Gorlani and Zavanella, 1993] C. Gorlani and L. Zavanella Continuous Simulation and Industrial processes: Electrode Consumption in Arc Furnaces, International Journal of production, Vol. 31, Issue 8 August 1993, pages 1873-1889.

[Gluskin 1999] E. Gluskin, “The Fluorescent Lamp Circuit”, IEEE Transactions on Circuits and Systems – I: Fundamental Theory and Applications, Vol. 46, No. 5, May 1999, pp. 529-544.

[Hernandez *et al.* 2003] A. Hernandez, J.G. Mayordomo, R. Asensi, L.F. Beites, A New Frequency Domain Approach for Flicker Evaluation of Arc Furnaces, IEEE Transactions on Power Delivery, April 2003, Vol. 18, Issue: 2, pp. 631- 638.

[Heydt 1986] G. T. Heydt, Computer Analysis Methods for Power Systems, Macmillan Publishing company, 1986.

[IEEE Standard 519, 1992] 519 IEEE Recommended Practices and Requirements for Harmonic Control in Electrical Power Systems, June 1992.

[IEEE Standard 1459, 2000] 1459 IEEE Power Engineering Society, IEEE Trial-Used Standard Definitions for the Measurement of Electric Power Quantities Under Sinusoidal, Nonsinusoidal, Balanced, or Unbalanced Conditions, 30 Jan. 2000.

[IEEE Std 1531, 2003] 1531 IEEE Guide for Application and Specification of Harmonic Filters, Transmission and Distribution Committee, IEEE Power Engineering Society, IEEE, 24 Nov. 2003.

[IEEE Standard 1453, 2004] 1453 IEEE Power Engineering Society, IEEE Recommended Practice for Measurement and Limits of Voltage Fluctuations and Associated Light Flicker on AC Power Systems, 31 March 2005.

[IEEE Working Group 2000] Slow transient Task Force of the IEEE Working Group, Modelling and Analysis Guidelines for Slow Transients- Part III: The Study of Ferroresonance, IEEE Transactions on Power Delivery, Vol. 15, No. 1, Jan. 2000, pp. 255-265.

[Ilic and Zaborsky 2000] M. Ilic, J. Zaborsky, Dynamics and Control of Large Electric Power Systems, John Wiley & Sons, 2000.

[Jones and Fang 1980] G.R. Jones and M.T.C. Fang, The Physics of High-power Arcs, Reports on Progress in Physics, 43, pp.1415-1465, Dec. 1980.

[Jones 1997] J. Jones, Understanding Electric Arc Furnace Operations, Techcomentary/TC-107714 6, Published by The EPRI Center for Materials Production, 1997.

[Kadar and Biringer, 1990] L.I. Kadar and P.P. Biringer, The influence of Cable Swings on the Electrical Parameters of Flexible Cables, Conference Record of the 1990 IEEE Industry Applications Society Annual Meeting, 7-12 Oct 1990, Vol. 2, pp. 2031-2035.

[King, *et al.* 1994] P.E. King, T.L. Ochs, A.D. Hartman, Chaotic Responses in Electric Arc Furnaces, Journal of Applied Physics vol. 76, no. 4, pp. 2059-2065, Aug. 1994.

[Kim and Nam 1998] H.S. Kim, T.J. Nam, Saving Power by Discharge Lamps with High Efficient Magnetic Ballast, IEEE Proceedings 1998 International Conference on Power Electronic Drives and Energy Systems for Industrial Growth, 1-3 Dec. 1998.

[Kojori 1999] H.A. Kojori, Smart Predictive Line Controller For AC and DC Electric Arc Furnace, US 6,603,795 B2, August 5, 2003.

[Kusters and Moore 1980] N.L. Kusters and W.J.N. Moore, On the definition of Reactive Power Under Non-Sinusoidal Conditions, IEEE Transactions on Power Apparatus and Systems, Vol. PAS-99, No. 5, pp. 1845–1854, Sep./Oct. 1980.

[Lavers *et al.* 1985] J.D. Lavers, B. Danai, P.P. Biringer, J. Chee-Hing, A Method of Examining in Detail Electric Arc Furnace Performance, IEEE Transactions on Industry Applications Vol-IA-21, No. 1, pp. 137-146, Jan./Feb. 1985.

[Larsson and Poumarède 1999] T. Larsson, C. Poumarède, Statcom an Efficient Means for Flicker Mitigation, Power Engineering Society 1999 Winter Meeting, IEEE, 31 Jan-4 Feb 1999.

[Lavers and Danai 1985] J.D. Lavers and B. Danai, Statistical Analysis of Electric Arc Furnace Parameter Variations, IEE Proceedings, Vol. 132, Pt. C. No. 2, pp. 82–93, March 1985.

[Lavers and Biringer 1986] J.D. Lavers, P.P. Biringer, Real-Time measurement of Electric Arc-Furnace Disturbances and Parameter Variations, IEEE Transactions on Industry Applications Vol-IA-22 No. 4, pp. 568-577, July/Aug. 1986.

[Lei 2005] Y. Lei, A Power Electronics-controlled Resistor for Mitigating Ferroresonance in Single-phase and Three-Phase Power System Transformers, MSc Thesis, University of Glasgow, Scotland, United Kingdom, 2005.

[Leon *et al.* 2000] L.F.M. Tolbert, T.G. Habetler, Comparison of Time-Based Non-Active Power Definitions for Active Filtering, IEEE CIEP 2000, Acapulco Mexico, pp. 73-79.

[Liew 1989] A.C. Liew, Excessive Neutral Currents in Three-Phase Fluorescent Lighting Circuits, IEEE Transactions on Industry Applications, Vol. 25, No. 4, pp. 776-782, July/Aug. 1989.

[Lister *et al.* 2004] G. G. Lister, J. E. Lawler, W. P. Lapatovich, V. A. Godyak, The Physics of Discharge Lamps, Reviews of Modern Physiccs, Volume 76, Issue 2, pp. 541-598, April 2004.

[Lowke and Zollweg, 1975] J.J. Lowke and R.J. Zollweg, Theoretical Predictions of AC Characteristics of Mercury Arc Lamps, Journal of the Illuminating Engineering Society, Vol. 4, No, 7, July 1975, pp. 253-259.

[Lowke 1979] J.J. Lowke, Simple Theory of Free-burning Arcs, Journal Physics Applied Physics, Volume 12, pp. 1873-1886, 1979.

[Lyon 1935] W.V. Lyon, Discussion of Definitions of Power and Related Quantities, AIEE, Oct. 1935, pp. 1121.

[Lyon 1954] W.V. Lyon, Transient Analysis of Alternating–Current Machinery an Application of the Method of Symmetrical Components, The technology Press of Massachusetts Institute of Technology and John Wiley and Sons, 1954.

[Ma *et al.* 1992] T. Ma, G. J. Bendzsak, M. Perkins, Power System Design for High Power Electric Smelting and Melting Furnaces, The Proceedings of the International Symposium on Non-Ferrous Pyrometallurgy: Trace Metals, Furnace Practices and Energy Efficiency, Edmonton, Alberta Canada, Aug. 23-27, 1992.

[Ma and Armstrong 2003] T.L.W. Ma, B. Armstrong, Control System and Method for Voltage Stabilization in Electric power Systems, Patent US 6,573,691 B2, June 2003.

[Ma and Sedighy 2003] T.L.W. Ma and M. Sedighy, Power Control System for AC Electric Arc Furnace, US 6,603,795 B2, August 5, 2003.

[Madrigal 2001] M. Madrigal-Martinez, Modelling of Power Electronics Controllers For Harmonic Analysis in Power System, PhD Thesis, University of Glasgow, , Scotland, United Kingdom, 2001.

[Madrigal and Acha 2002] M. Madrigal, E. Acha, A New Harmonic Power Flow based on the Instantaneous Power Balance, 10th International Conference on Harmonics and Quality of Power, 2002. 6-9 Oct. 2002, Vol.2, pp. 655-662.

[Mayordomo *et al.* 1997] J.G. Mayordomo, L.F. Beites, R. Asensi, M. Izzeddine, L. Zabala, J. Amantegui, A New Frequency Domain Arc Furnace Model for Iterative Harmonic Analysis, IEEE Transactions on Power Delivery, Oct. 1997 Vol. 12, Issue 4, p.p. 1771-1778.

[Mayordomo 2000] J.G. Mayordomo, E. Prieto, A. Hernandez, L.F. Beites, Arc Furnace Characterization From an Off-Line Analysis of Measurements, IEEE, Proceedings Ninth International Conference on Harmonics and Quality of Power, 2000 Vol. 3, pp. 1073-1078.

[Mendis *et al.* 1995] S. R. Mendis, M. T. Bishop, T. R. Day, D. M. Boyd, Evaluation of Supplementary Series Reactors To Optimize Electric Arc Furnace Operations, Conference Record of the 1995 IEEE Industry Applications Conference, Thirtieth IAS Annual Meeting, IAS '95, 8-12 Oct 1995, Vol. 3, pp. 2154-2161

[Micu *et al.* 1973] E. Micu, W. Shepherd, P. Zakikhani, Discussion of Power-Factor Compensation of Thyristor-Controlled Single-Phase Load, Proc. IEE, Vol. 120, No. 7, July 1973, pp. 796-798.

[Milanez and Emanuel 2003] D.L. Milanez, A.E. Emanuel, The instantaneous – Space-Phasor a Powerful Diagnosis Tool, IEEE Transactions on Instrumentation and Measurement, Vol. 52, No. 1, pp.143- 148, February 2003.

[Miller 1982] T.J.E. Miller, Reactive Power Control in Electric Systems, John Wiley and Sons, 1982.

[Ozgun and Omer, 1999] O. Ozgun, A. Abur, Development of an Arc Furnace Model for Power Quality Studies, Power Engineering Society Summer Meeting, 1999. IEEE**,** 18-22 Jul 1999, Vol. 1, pp. 507-511.

[Page 1980] C.H. Page, Reactive Power in Nonsinusoidal Situations, IEEE Transactions on Instrumentation and Measurement, Vol. IM-29. No. 4, Dec. 1980, pp. 420-423.

[Park 1929] R.H. Park, Two-Reaction Theory of Synchronous Machines, Generalized Method of Analysis - Part I, AIEE Transactions, Vol. 48, No.2 July 1929 pp. 716-730.

[Peak and Spencer 1968] S.C. Peak, D.E. Spencer, A Differential Equation for the Fluorescent Lamp, Illuminating Engineering (North America), Vol. 63, No. 4, April 1968, pp. 157-162.

[Penfield 1970] P. Penfield Jr., R. Spence, S. Duinker, Tellegen's Theorem and Electrical Networks, Research Monograph No. 58, The M.I.T. Press, Cambridge, Massachusetts and London, England, 1970.

[Phillips 1967] R.L, Phillips, Theory of Non-stationary Arc Column, British Journal Applied Physics, Vol. 18. 65-78, January 1967.

[Prieto and Perez, 2004] M.A. Prieto-Alonso, M. Perez-Donsion, An Improved Time Domain Arc Furnace Model for Harmonic Analysis, IEEE Transactions on power Delivery, Vol. 19, No. 1, pp. 367- 373 Jan. 2004.

[Rico *et al.* 1996] J.J. Rico, E. Acha, T.J.E. Miller, Harmonic Domain Modelling of Three Phase Thyristor-Controlled Reactors by Means of Switching Vectors and Discrete Convolutions, IEEE Transactions on Power Delivery, Vol. 11 No. 3, pp. 1678-1684, July 1996.

[Rico and E. Acha 1998] J.J. Rico, E. Acha, The use of Switching Functions and Walsh Series to Calculate Waveform Distortion in Thyristor Controlled Compensated Power Circuits, IEEE Transactions on Power Delivery, Vol. 13 No. 4, pp. 1370-1377, Oct. 1998.

[Sasson and Jaimes 1967] A.M. Sasson, F.J. Jaimes, Digital Methods Applied to Power Flow Studies, IEEE Transactions on Power Apparatus and Systems, Vol. PAS-86, No. 7 July 1967, pp. 860-867.

[Semlyen, *et al.* 1987] A. Semlyen, E. Acha, J. Arrillaga, Harmonic Norton Equivalent for the Magnetising Branch of a Transformer, IEE Proceedings, Vol. 134, Pt. C. No.2, pp.162-169, March 1987.

[Semlyen *et al.* 1988] A. Semlyen, E. Acha, and J. Arrillaga, Newton-Type Algorithms for the Harmonic Phasor Analysis of Nonlinear Power Circuits in Periodical Steady State with Special Reference to Magnetic Nonlinearities, IEEE Transactions on Power Delivery, Vol. 3, No. 3, July 1988, pp. 1090-1098.

[SGL] Graphite Electrodes - Ultrahigh-Performance Electrodes - A New Dimension in Productivity http://www.sglcarbon.com/cg/custsup/index.php4

[Shepherd and Zakikhani 1972] W. Shepherd, P. Zakikhani, Suggested Definition of Reactive Power for Nonsinusoidal Systems, Proc. IEE, Vol. 119, No. 9, Sep. 1972, pp. 1361-1362.

[Shepherd and Zakikhani 1973] W. Shepherd, P. Zakikhani, Power-Factor Compensation of Thyristor-Controlled Single-Phase Load, Proceedings of IEE, Vol. 120, No. 2, Feb. 1973, pp. 245-246.

[Shepherd and Zand 1979] W. Shepherd, P. Zand, Energy Flow and Power Factor in Nonsinusoidal Circuits, Cambridge University Press, 1979.
[Steinmetz 1900] C.P. Steinmetz, Theory and Calculation of Alternating Current Phenomena, Electrical World and Engineering, Third Edition 1900.

[Stott 1974] B. Stott, Review of Load-Flow Calculation Methods, Proceedings of the IEEE, vol. 62, No. 7, July 1974, pp. 916-929.

[Sharon 1973] D. Sharon, Reactive-Power Definitions and Power-Factor Improvement in Nonlinear Systems, Proc. IEE, Vol. 120, No. 6, June 1973, pp. 704-706.

[Task Force on Harmonics Modeling and Simulation 1996] Task Force on Harmonics Modeling and Simulation, Modeling and Simulation of the Propagation of Harmonics in Electric Power Networks, Part I: Concepts, Models, and Simulation Techniques, IEEE Transactions on Power Delivery, Vol. 11, No. 1, 452-465, Jan. 1996.

[Task Force on Harmonics Modeling and Simulation 2001] Task Force on Harmonics Modeling and Simulation, Modeling of Components With Nonlinear Voltage Current Characteristics For Harmonic Studies, IEEE Power Engineering Society General Meeting, 2004, June 2004, Vol.1, pp. 769- 772.

[Task Force on Harmonics Modeling and Simulation 2004] Chang, G. Hatziadoniu, C. Xu, W. Ribeiro, P. Burch, R. Grady, W.M. Halpin, M. Liu, Y. Ranade, S. Ruthman, D. Watson, N. Ortmeyer, T. Wikston, J. Medina, A. Testa, A. Gardinier, R. Dinavahi, V. Acram, F. Lehn, P., Modeling Devices With Nonlinear Voltage-Current Characteristics For Harmonic Studies, IEEE Transactions on Power Delivery, on Oct. 2004 Vol. 19, Issue: 4, pp. 1802- 1811.

[Tongxin, *et al.* 1998] T. Zheng, E.B. Makram, A.A. Girgis, Effect of Different Arc Furnace Models on Voltage Distortion, IEEE 8th Conference on Harmonics and Quality of Power ICHQP, October 14-16 1998.

[Tsao and Tsai 2004] T.P. Tsao, J.I. Tsai, Torsional Interactions Between an Electrical Arc Furnace Load and a Turbine-generator Set, IEEE Proceedings of the 2004 International Conference on Electric Utility Deregulation, Restructuring and Power Technologies, 2004.

[Václavík *et al.* 2004] J. Vaclavik, M. Novak, A. Richter, Aspects of Energy Consumption in Large Lighting Systems, Record of the IEEE 39th Conference on Industry Applications (IAS) Annual Meeting, 3-7 Oct. 2004, Vol. 2, pp. 1373- 1378.

[Willems 1992] J.L. Willems, A New Interpretation of the Akagi-Nabae Power Components for Nonsinusoidal Three-Phase Situations, IEEE Transactions on Instrumentation and Measurement, Vol. 41. No. 4, Aug. 1992, pp. 523-527.

[Xia and Heydt 1982] D. Xia, G.T. Heydt, Harmonic Power Flow Studies Part I – Formulation and Solution, IEEE Transactions on Power Apparatus and Systems, Vol. PAS-101, No. 6 June 1982, pp. 1257-1265.

[Xia and Heydt 1982] D. Xia, G.T. Heydt, Harmonic Power Flow Studies Part II – Implementation and Practical Application, IEEE Transactions on Power Apparatus and Systems, Vol. PAS-101, No. 6 June 1982, pp. 1265-1270.

[Xu *et al.* 1991] W. Xu, J.R. Marti, H.W. Dommel, Harmonic analysis of systems with static compensators, IEEE Transaction on Power Systems, Vol. 6, No. 1, February 1991, pp. 183-190

[Zheng Peng and Lai 1996] F. Zheng-Peng. J.S. Lai, Generalized Instantaneous Reactive Power Theory for Three-Phase Power Systems, IEEE Transactions on Instrumentation and Measurement, Vol. 45. No. 1, Feb. 1996, pp. 293-297.

[Zheng Peng *et al.* 1998] F. Zheng-Peng, G.W. Ott Jr., D.J. Adams, Harmonic and Reactive Power Compensation Based on the Generalized Instantaneous Reactive Power Theory for Three-Phase Four-Wire Systems, IEEE Transactions on Power Electronics, Vol. 13, No. 6, Nov. 1998, pp. 1174-1181.